

Crystal Engineering of Palladium Terpyridine Complexes

By
Razan Alshgari

Thesis submitted to the University of Nottingham for the Degree of Doctor of Philosophy

July 2017

For my family

Declaration

Except where specific reference is made to other sources, the work presented in this thesis is the original work of the author. It has not been submitted, either in whole or in part, for any other degree.

Signed: Razan Alshgari

Date:

Acknowledgements

The first acknowledgement is for my supervisor: Professor Neil Champness for his advice, support and encouragement. His guidance helped me in all the time of research and writing of this thesis.

Massive thanks must particularly go to Dr. William Lewis and Dr. Connie Pfeiffer for their help with crystallography sections of this work.

I would like to thank the expert post-docs of the group: Dr. Stephen Argent and Dr. Lixu Yang. My greatest appreciation to all the technical staff at Nottingham: Shazad Aslam, Kevin Butler, Mick Cooper, Graham Coxill, and Ben Pointer-Gleadhill.

I would like to thank all the people in Champness group for making B52 such an excellent place to work.

A lot of credit is due to my parents in Saudi Arabia, who despite being far away always stay in a great contact and are just as amusing from a distance. My deep and sincere gratitude to my husband for his continuous and unparalleled love, help and support. Finally, there are my children, who have given me much happiness. I hope I have been a good mother and that I have not lost too much during the tenure of my study. To my family, you should know that your support and encouragement was worth more than I can express on paper.

List of Abbreviations

°	Degree
Å	Ångstrom
mmol	Millimole
h	Hour
ppm	Part per million
mg	Milligram
ml	Millilitre
MALDI	Matrix Assisted Laser Desorption Ionisation
TOF	Time of Flight
MS	Mass Spectrometry
ESI	Electrospray Ionisation
HRMS	High Resolution Mass Spectrometry
NMR	Nuclear Magnetic Resonance
λ	Wavelength
GOF	Goodness Of Fit
DMSO	Dimethylsulfoxide
MeCN	Acetonitrile

Abstract

The ability of 2,2':6',2''-terpyridine (terpy) to chelate to a wide variety of metal ions has led to the synthesis of different metal-terpyridine complexes. In addition, there are different synthetic strategies have been improved, allowing 2,2':6',2''-terpyridine and its derivatives to find a wide range of applications as sensors and catalysts.

This thesis concerns the synthesis of a series of Pd(terpy) complexes with different *para*- and *meta*-substituted pyridine ligands and their properties are studied by X-ray crystallography. In order to extend the experimental observations and the range of applicability of the proposed interpretation, another system involving the tridentate aromatic nitrogen donor 4,4',4''-tri-*tert*-butyl-2,2':6',2''-terpyridine (*t*Bu$_3$-terpy) has been examined.

A range of *N,N*-bidentate ligands are introduced in next section. These can be potentially used to bridge two metal centres. The reactivity of [Pd(terpy)(NCCH$_3$)](CF$_3$SO$_3$)$_2$ was investigated with a wide range of *N,N*-bidentate ligands. Substitution of the acetonitrile ligand of [P(terpy)(NCCH$_3$)](CF$_3$SO$_3$)$_2$ with these ligands was found to be efficient and facile with reactions occurring at room temperature. Extension of this reaction to *meso*-tetra(4-pyridyl)porphyrin results in tetranuclear Pd(terpy) complex and affords [{Pd(terpy)}$_4$(H$_2$T(4-Py)P)](CF$_3$SO$_3$)$_8$.

In Chapter 6, similarly to terpyridine, 2-phenyl-4,6-bis(2-pyridyl)-1,3,5-triazine (pbptz) is coordinated to palladium as a tridentate ligand and no complex was seen to adopt any of the other potential binding modes for this molecule.

Contents

Chapter 1 Introduction 1

1.1. Supramolecular Chemistry 2

1.2 Crystal engineering 4

1.3 Coordination chemistry 6

1.4 2,2':6',2''-Terpyridine 8

1.4.1 2,2':6',2''-Terpyridine conformation 9

1.4.2 Unusual binding modes to terpyridine 9

1.4.3 Basic Synthetic Strategies 10

1.4.4 Synthesis of 2,2':6',2''-terpyridine derivatives 13

1.4.5 Crystal structure of terpyridine 16

1.4.6 Terpyridine metal complexes 17

1.4.7 Applications of terpyridine complexes 21

1.5 Thesis overview 25

1.6 References 26

Chapter 2 Mono Palladium (2,2':6',2''-Terpyridine) Complexes with *Para*-Substituted Pyridine Derivatives 35

2.1 Introduction 36

2.1.1 Crystal structures of Pd(terpy) complexes 37

2.2 Results and Discussion 39

2.2.1 Synthesis of a series of mononuclear palladium (2,2':6',2''-terpyridine) triflate complexes 39

2.2.2 X-ray crystallography 40

2.3 Conclusions 84

2.4 Materials and Methods 85

2.4.1 Synthesis of 2,2':6',2''-terpyridine (4-cyanopyridine) palladium triflate [Pd(terpy)(4-cyanopyridine)]$(CF_3SO_3)_2$ (2-1). 86

2.4.2 Synthesis of 2,2':6',2''-terpyridine (4-methylpyridine) palladium triflate [Pd(terpy)(4-methylpyridine)]$(CF_3SO_3)_2$ (2-2). 87

2.4.3 Synthesis of 2,2':6',2''-terpyridine (4-iodopyridine) palladium triflate [Pd(terpy)(4-iodopyridine)]$(CF_3SO_3)_2$ (2-3). 88

2.4.4 Synthesis of 2,2':6',2''-terpyridine (4-dimethylaminopyridine) palladium triflate [Pd(terpy)(4-dimethylaminopyridine)]$(CF_3SO_3)_2$ (2-4). 88

2.4.5 Synthesis of 2,2':6',2''-terpyridine (4-pyridinecarboxaldehyde) palladium triflate [Pd(terpy)(4-pyridinecarboxaldehyde)]$(CF_3SO_3)_2$ (2-5). 89

2.4.6 Synthesis of 2,2':6',2''-terpyridine (4-aminopyridine) palladium triflate [Pd(terpy)(4-aminopyridine)]$(CF_3SO_3)_2$ (2-6). 90

2.4.7 Synthesis of 2,2':6',2''-terpyridine (4-pyridineboronic acid) palladium triflate [Pd(terpy)(4-pyridineboronic acid)]$(CF_3SO_3)_2$ (2-7). 90

2.4.8 Synthesis of 2,2':6',2''-terpyridine (4-methylpyridine) palladium hexafluorophosphate [Pd(terpy)(4-methylpyridine)]$(PF_6)_2$ (2-8). 91

2.4.9 Synthesis of 2,2':6',2''-terpyridine (4-dimethylaminopyridine) palladium hexafluorophosphate [Pd(terpy)(4-dimethylaminopyridine)]$(PF_6)_2$ (2-9)…… 92

2.4.10 Synthesis of 2,2':6',2''-terpyridine (4-cyanopyridine) palladium tetrafluoroborate [Pd(terpy)(4-cyanopyridine)]$(BF_4)_2$ (2-10). 92

2.4.11 Crystal data 93

2.5 References 95

Chapter 3 Mono Palladium (4,4',4''-Tri-*tert*-butyl-2,2':6',2''-terpyridine) Complexes with *Para*-Substituted Pyridine Derivatives **99**

3.1 Introduction 100

3.2 Results and Discussion 100

3.2.1 Synthesis of a series of mononuclear palladium (4,4',4''-tri-*tert*-butyl-2,2':6',2''-terpyridine) triflate complexes 100

3.2.2. X-ray crystallography 101

3.3 Conclusions 130

3.4 Materials and Methods 131

3.4.1 Synthesis of 4,4',4''-tri-*tert*-butyl-2,2':6',2''-terpyridine (4-cyanopyridine) palladium triflate [Pd(*t*Bu_3-terpy)(4-cyanopyridine)]$(CF_3SO_3)_2$. 132

3.4.2 Synthesis of 4,4',4''-tri-*tert*-butyl-2,2':6',2''-terpyridine (4-methylpyridine) palladium triflate [Pd(*t*Bu$_3$-terpy)(4-methylpyridine)](CF$_3$SO$_3$)$_2$. 132

3.4.3 Synthesis of 4,4',4''-tri-*tert*-butyl-2,2':6',2''-terpyridine (4-iodopyridine) palladium triflate [Pd(*t*Bu$_3$-terpy)(4-iodopyridine)](CF$_3$SO$_3$)$_2$. 133

3.4.4 Synthesis of 4,4',4''-tri-*tert*-butyl-2,2':6',2''-terpyridine (4-dimethylaminopyridine) palladium triflate [Pd(*t*Bu$_3$-terpy)(4-dimethylaminopyridine)](CF$_3$SO$_3$)$_2$. 134

3.4.5 Synthesis of 4,4',4''-tri-*tert*-butyl-2,2':6',2''-terpyridine (4-pyridinecarboxaldehyde) palladium triflate[Pd(*t*Bu$_3$-terpy)(4-pyridinecarboxaldehyde)](CF$_3$SO$_3$)$_2$. 134

3.4.6 Synthesis of 4,4',4''-tri-*tert*-butyl-2,2':6',2''-terpyridine (4-aminopyridine) palladium triflate [Pd(*t*Bu$_3$-terpy)(4-aminopyridine)](CF$_3$SO$_3$)$_2$. 135

3.4.7 Synthesis of 4,4',4''-tri-*tert*-butyl-2,2':6',2''-terpyridine (4-pyridineboronic acid) palladium triflate[Pd(*t*Bu$_3$-terpy)(4-pyridineboronic acid)](CF$_3$SO$_3$)$_2$. 136

3.4.8 Synthesis of 4,4',4''-tri-*tert*-butyl-2,2':6',2''-terpyridine (4-hydroxypyridine) palladium triflate[Pd(*t*Bu$_3$-terpy)(4-hyrdoxypyridine)](CF$_3$SO$_3$)$_2$. 136

3.4.9 Crystal data 137

3.5 References 139

Chapter 4 Mono Palladium (2,2':6',2''-Terpyridine) Complexes with *Meta*-Substituted Pyridine Derivatives 141

4.1. Introduction.....142

4.2. Results and Discussion.....142

4.2.1. Synthesis of a series of mononuclear Pd(Yterpy) (Y = H or *t*Bu$_3$) triflate complexes with *meta*-substituted pyridine derivatives 142

4.2.2. X-ray crystallography.....143

4.2 Conclusions 171

4.3 Materials and Methods 173

4.3.1 Synthesis of 2,2':6',2''-terpyridine (3-cyanopyridine) palladium triflate [Pd(terpy)(3-cyanopyridine)](CF$_3$SO$_3$)$_2$. 173

4.3.2 Synthesis of 2,2':6',2''-terpyridine (3-methylpyridine) palladium triflate [Pd(terpy)(3-methylpyridine)](CF$_3$SO$_3$)$_2$. 174

4.3.3 Synthesis of 2,2':6',2''-terpyridine (3-iodopyridine) palladium triflate [Pd(terpy)(3-iodopyridine)](CF$_3$SO$_3$)$_2$......175

4.3.4 Synthesis of 2,2':6',2''-terpyridine (3-pyridinecarboxaldehyde) palladium triflate [Pd(terpy)(3-pyridinecarboxaldehyde)](CF$_3$SO$_3$)$_2$......175

4.3.5 Synthesis of 4,4',4''-tri-*tert*-butyl-2,2':6',2''-terpyridine (3-aminopyridine) palladium triflate [Pd(*t*Bu$_3$-terpy)(3-aminopyridine)](CF$_3$SO$_3$)$_2$. 176

4.3.6 Synthesis of 4,4',4''-tri-*tert*-butyl-2,2':6',2''-terpyridine (3-hydroxypyridine) palladium triflate [Pd(*t*Bu$_3$-terpy)(3-hydroxypyridine)](CF$_3$SO$_3$)$_2$. 177

4.3.7 Synthesis of 4,4',4''-tri-*tert*-butyl-2,2':6',2''-terpyridine (3-iodopyridine) palladium triflate and paladium(3-iodoopyridine)$_4$ triflate [Pd(*t*Bu$_3$-terpy)(3-iodopyridine)].[Pd(3-iodopyridine)$_4$](CF$_3$SO$_3$)$_4$. 177

4.3.8 Crystal data 178

4.4 References 180

Chapter 5 Dinuclear Palladium (2,2':6',2''-Terpyridine) Complexes 181

5.1 Introduction 182

5.2 Results and discussion 186

5.2.1 Synthesis of the precursor palladium terpyridine acetonitrile [Pd(terpy)NCCH$_3$](CF$_3$SO$_3$)$_2$ and palladium *t*Bu$_3$-terpyridine acetonitrile [Pd(*t*Bu$_3$-terpy)NCCH$_3$](CF$_3$SO$_3$)$_2$ complexes. 186

5.2.2 Synthesis of the ligands 188

5.2.3 Synthesis of dinuclear palladium terpyridine complexes 195

5.2.4 Synthesis of tetranuclear palladium terpyridine complex 195

5.2.5 X-ray crystallography 197

5.3 Conclusions 235

5.4 Materials and Methods 237

5.4.1 Synthesis of [Pd(terpy)(CH$_3$CN)](CF$_3$SO$_3$)$_2$ 237

5.4.2 Synthesis of the ligands 238

5.4.3 Synthesis of dinuclear palladium terpyridine complexes 240

5.4.4 Synthesis of tetranucealr palladium terpyridine complex 244

5.4.5 Crystal data 245

5.5 References 247

Chapter 6 Palladium 2-Phenyl-4,6-bis(2-pyridyl)-1,3,5-Triazine Complexes 251

6.1 Introduction 252

6.1.1 Melamine derivatives as synthons for the preparation of H-bonded self-assemblies 253

6.1.2 1,3,5-Triazine derivatives as ligands for the preparation of coordination self-assemblies 255

6.1.3 The 2-phenyl-4,6-bis(2-pyridyl)-1,3,5-triazine ligands 256

6.2 Results and Discussion 257

6.2.1 Synthesis of 2-phenyl-4,6-bis(2-pyridyl)-1,3,5-triazine(pbptz). 257

6.2.2 Synthesis of palladium (2-phenyl-4,6-bis(2-pyridyl)-1,3,5-triazine) triflate complexes. 258

6.2.3 X-ray Crystallography 259

6.3 Conclusions 267

6.4 Materials and Methods 268

6.4.1 Synthesis of 2-phenyl-4,6-bis(2-pyridyl)-1,3,5-triazine(pbptz) 268

6.4.2 Synthesis of 2-phenyl-1,4,6-bis(2-pyridyl)-1,3,5-triazine(4-cyanopyridine) palladium triflate complex [Pd(pbptz)(4-cyanopyridine)]$(CF_3SO_3)_2$. 269

6.4.3 Synthesis of 2-phenyl-1,4,6-bis(2-pyridyl)-1,3,5-triazine(4-mwthylpyridine) palladium triflate complex [Pd(pbptz)(4-methylpyridine)]$(CF_3SO_3)_2$. 270

6.4.4 Crystal data....270

6.5 References....271

Chapter 7 Conclusions 274

7.1 Conclusions....275

Chapter 1

Introduction

1.1. Supramolecular Chemistry

Much effort has been made by scientists to synthesise molecules in a sophisticated and efficient manner [1-4]. However, it is required to fully understand how the small components (e.g., nucleotides) act to create more complex structures (e.g., DNA) with unique properties and structures beyond the capability of the individual molecules. In biological systems, it is known that the noncovalent interactions are responsible for most of the interactions occurring between the individual components [5]. With time, noncovalent interactions have been recognised as an important influence in reorganising small molecules into complex structures (i.e., supermolecules). The use of noncovalent interactions to construct supermolecules has led to a novel chemical discipline known as supramolecular chemistry.

Supramolecular chemistry has played a fundamental role in modern chemistry. In 1987, J.-M. Lehn, C. J. Pederson and D. J. Cram received the Nobel Prize in recognition of their results in this field [6–8]. The improvement of selective "host-guest" complexes was considered as a crucial contribution. The concept of supramolecular chemistry was defined by Lehn: as 'chemistry beyond the molecule' [9]. Recently, supramolecular chemistry has been developed to include not just host-guest system, but also all aspects of self-assembly. It involves crystallization at all scales, noncovalent polymers, supramolecular devices and "bottom-up" nanotechnology [10-17]. Supramolecular chemistry aims to construct highly complex chemical structures from the association of two or more chemical species components that are held together by noncovalent intermolecular forces [18-21]. Compared to covalent interactions, noncovalent interactions are reversible, weaker and more sensitive to external stimuli. These properties lead to the formation of supramolecular systems with unique and attractive properties [22-28]. The reversibility offers the ability to self-correction of any defects

produced during the assembly process. The noncovalent interactions include a wide variety of attractive and repulsive interactions, such as hydrogen bonding, van der Waals and π· · ·π interactions.

In supramolecular chemistry, there are two steps: first the building blocks (*e.g.,* molecules, ions) are synthesised and second, the building blocks are arranged in a desired way to achieve and control the properties of the supermolecule [29]. The evolution of supramolecular chemistry can be outlined in Figure 1.1. The group of solid state *inclusion compounds* form host-guest complexes as crystalline solids (clathrates) (Figure 1.1a). On the other hand, a large host molecule is synthesised covalently and the four binding sites bind to a central guest molecule (Figure 1.1b). Where there is no host or guest molecules and the molecular components have similar size, the non-covalent joining of two or more components is called self-assembly.

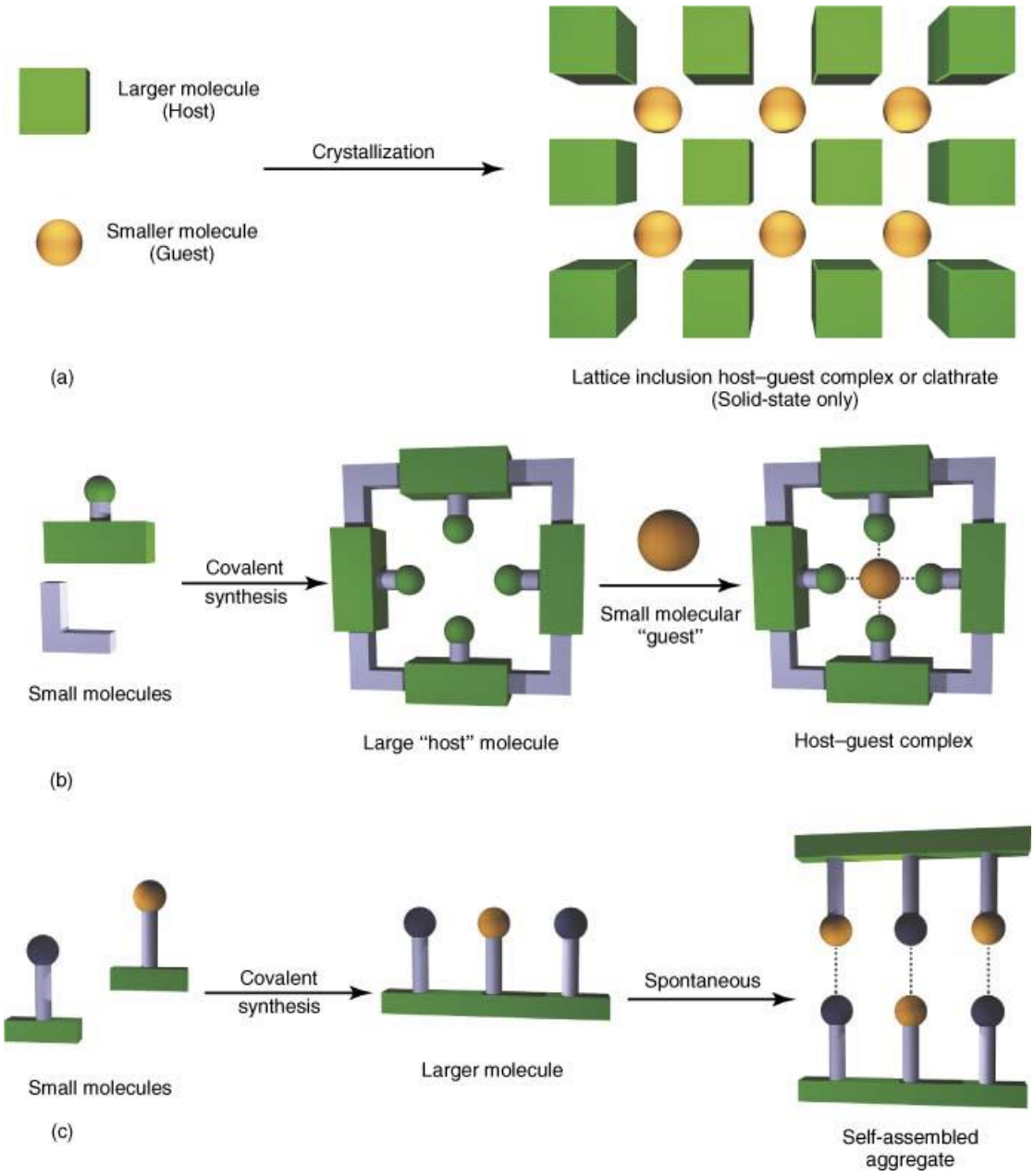


Figure 1.1: The improvement of supramolecular chemistry from molecular building blocks. (a) Solid-state clathrate, (b) host-guest complexation, (c) self-assembly [30,31].

1.2 Crystal engineering

Over the past 55 years, the field of crystal engineering has improved as an expected consequence of the cooperation between crystallography and chemistry [32-45]. The term crystal engineering was first mentioned by Pepinsky in 1955 [46]. However, the

contributions of Schmidt led to the foundation of this term [47]. Crystal engineering was defined by Desiraju in 1989: "Crystal engineering is the understanding of intermolecular interactions in the context of crystal packing and the utilization of such understanding in design of new solids with desired physical and chemical properties" [48]. This definition involves three stages: (1) the analysis of intermolecular interactions, (2) the analysis of crystal packing to design appropriate strategies for crystal construction and (3) the analysis of crystal properties.

Supramolecular synthon is the smallest unit within crystal and it is assembled by known operations including intermolecular interactions [37]. Supramolecular synthons are structural units that express the main properties of a crystal structure. The structure of benzoic acid dimer is one of the most significantly studied supramolecular synthons. As shown in Figure 1.2, two 1,4-benzenedicarboxylic acid molecules interact via O–H···O hydrogen bonds to form a cyclic array.

A wide range of intermolecular interactions have been used in crystal engineering. Due to the strength and directionality of hydrogen bonding, it is the most studied interaction in crystal engineering. The hydrogen bond can be considered as a special kind of dipole-dipole interaction in which a hydrogen atom attached to an electronegative atom is attracted to a neighbouring dipole on another molecule. Hydrogen bonds are usually written D−H···A and involve a hydrogen atom bonded to strongly electronegative atom such as oxygen or nitrogen as the donor (D) and another electronegative atom with a lone pair of electrons as the acceptor (A). In addition, a wide range of hydrogen bonding interactions occurs when a hydrogen atom bonded to carbon rather than electronegative atoms (electronegativities: H 2.20, C 2.55, N 3.04, O 3.44). Hydrogen bonds can be strong or weak, depends on their length and geometries (Table 1.1). The existence of hydrogen bonds between nucleobases is crucial to form the most famous double helical

structure DNA. π· · ·π Interaction is one of the most important non-covalent interactions occur in supramolecular chemistry. These interactions occur between aromatic rings, where one is electron rich and another is electron poor. There are different geometries for π· · ·π interactions, such as face-to-face and edge-to-face interactions. The former is responsible for the interaction between the aryl rings for nucleobase pairs and helps to stabilise the DNA double helix. The edge-to-face interactions are responsible for the herringbone packing in the crystal structures for a wide range of small aromatic hydrocarbons.

Table 1.1: Some properties of strong, medium and weak hydrogen bonds.

	Strong	Medium	Weak
Bond energy (Kcal/mol)	14-40	4-14	0-4
Interaction type	Mostly covalent	Mostly electrostatic	Electrostatic
Bond lengths (Å)	A---H = H…B	A---H < H…B	A---H << H…B
A---B H…B	2.2-2.5 1.2-1.5	2.5-3.2 1.5-2.2	3.2-4.0 2.2-3.2
Bond angle (°)	175-180	130-180	90-150
Examples	Proton sponges HF complexes	Carboxylic acid biomolecules	C-H…O/N O/N-H…π

1.3 Coordination chemistry

Coordination chemistry is one of the most important fields in supramolecular chemistry. In this area, chelate complexes derived from N-heteroaromatic compounds, mainly based on 2,2'-bipyridine (bpy), 1,10-phenanthroline (phen), and 2,2':6',2''-terpyridine (terpy), have been intensively investigated (Figure 1.3). 2,2'-Bipyridine is the most utilised ligand

in coordination chemistry, with Fritz Blau first synthesising a bipyridine-iron complex in 1888 [49].

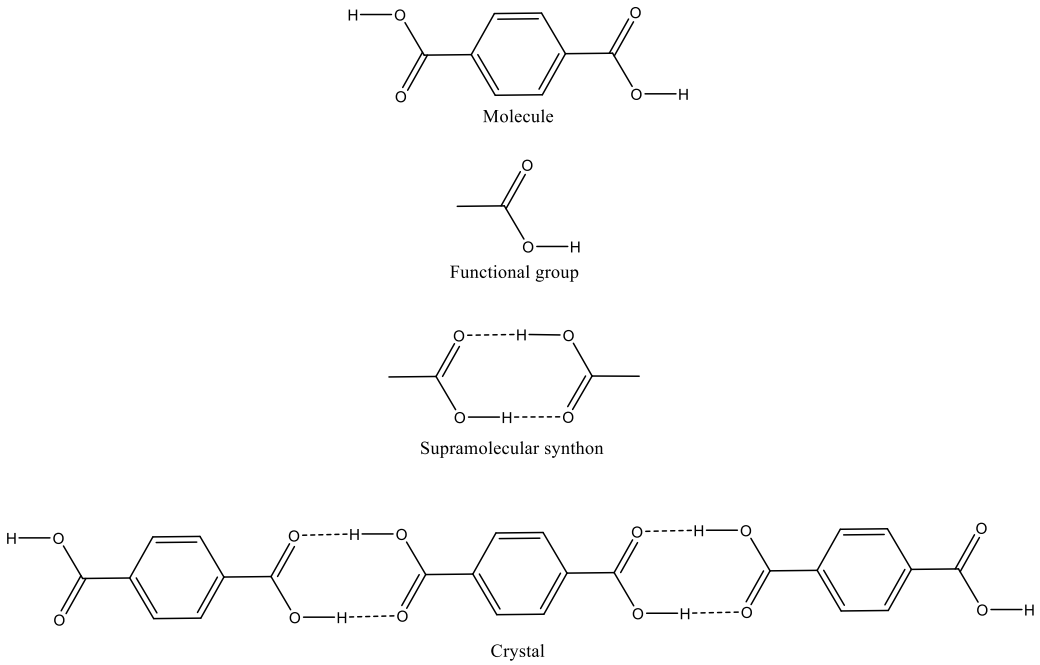


Figure 1.2: Supramolecular synthons.

There are many comprehensive reviews on bipyridines [50-54]. These reviews highlight different synthetic methodologies for the preparation of bipyridine and its derivatives, its important role in supramolecular chemistry and its use in the complexation of metal ions.

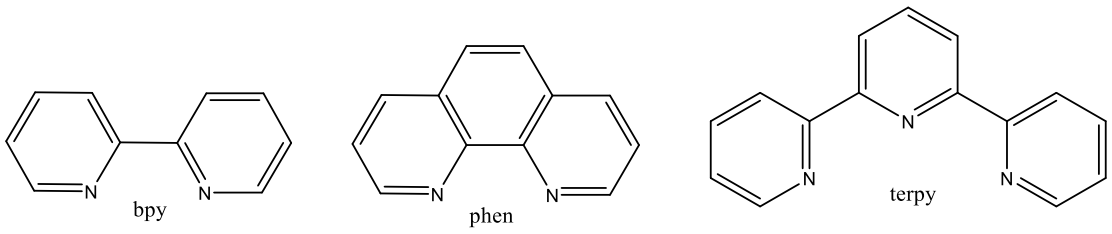


Figure 1.3: Structures of the most commonly used N-heteroaromatic compounds, bpy, phen and terpy.

1.4 2,2':6',2''-Terpyridine

The chemistry of 2,2':6',2''-terpyridine (termed as simply terpyridine or terpy) is much newer than that of 2,2'-bipyridines. Terpyridine was produced for the first time by Morgan and Burstall by heating pyridine with anhydrous ferric chloride as a catalyst [55]. The synthesis of terpyridine was an accident, as it was a side product of a bipyridine synthesis. Later, it was found that the solution of terpyridine compound turned to a purple colour after the addition of iron (II) ions, presenting the first indication for the synthesis of a metal-terpyridine complex [56].

The ability of 2,2':6',2''-terpyridine to chelate to a wide variety of metal ions has led to the synthesis of different metal-terpyridine complexes such as Co(II), Os(II), Ru(II), Ir(II), Pd(II), Pt(II), and Au(III) complexes and supramolecular complexes [57–65]. In addition, alternative synthetic strategies have been improved, allowing 2,2':6',2''-terpyridine and its derivatives to find a wide range of applications as sensors and catalysts [66-68].

2,2':6',2''-Terpyridine normally acts as a tridentate donor either in octahedral or square-planar geometry [69-71]. However, there are few examples of the terpyridine acting as a bidentate or monodentate donor [72-76] (discussed later). Terpyridine conventional numbering system is shown in (Figure 1.4).

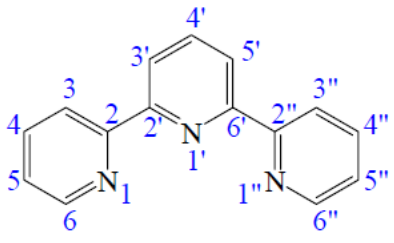


Figure 1.4: Terpyridine conventional numbering system.

1.4.1 2,2':6',2''-Terpyridine conformation

Free terpy adopts a *trans-trans* conformation, as confirmed by many crystal structures, such as unsubstituted terpyridine and also the 4'-phenyl, 4-aniline and 4'-NMe_2 derivatives [77-82]. This conformation minimizes the repulsion between the nitrogen atom lone pairs and also minimizes the repulsion between the two *ortho* hydrogen atoms [83]. When terpyridine coordinates to a metal, it isomerizes to a *cis*-configuration, though preferably to a *cis*–*cis*-configuration (Figure 1.5).

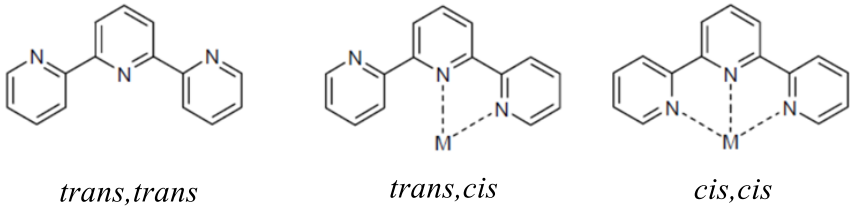


Figure 1.5: The three possible conformations of terpyridine.

1.4.2 Unusual binding modes to terpyridine

There are rare examples of terpyridine adopting unusual binding modes. As shown in (Figure 1.6), the X-ray crystallographic structure for the Pd(II) complex $[Pd(C_6F_5)_2(terpy)]$ confirms the bidentate coordination of the terpyridine [84]. The pendant pyridine ring adopts an orientation of 48° out of the PdNN plane. The obvious distortion in the square-planar geometry around Pd results from the small 'bite-angle' of terpyridine N1–Pd–N2 = 77.9°. Moreover, the Pd-N distances are not the same with Pd–N1 = 2.064 and Pd–N2 = 2.131 Å. This geometrical feature is comparable to those observed in the related terpyridine complexes $[ReBr(CO)_3(terpy)]$ and $[PtIMe_3(terpy)]$ [85,86].

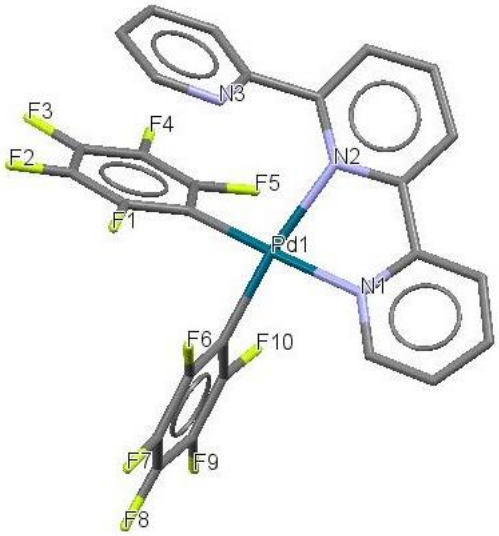


Figure 1.6: The crystal structure of $[Pd(C_6F_5)_2(terpy)]$ [84].

On the other hand, the crystal structure of $[Pd(terpy)(py)](ClO_4)_2$ indicates that when terpy is co-ordinated in a tridentate fashion, the Pd–N bond length to the central atom of terpy is significantly shorter than any of the other Pd–N distances [87].

The metal ions usually coordinate to terpy via nitrogen atoms. However, there is a cyclometallated complex synthesised by Minghetti and co-workers (Figure 1.7) [74]. The reaction between terpy and cis-$[Pt(DMSO)_2Me_2]$ leads to the C–H activation and produces dinuclear complex $[(terpy)\{Pt(DMSO)(CH_3)\}_2]$. Each platinum atom is coordinated to a nitrogen atom of the outer pyridine ring and to a *meta*-carbon atom of the central pyridine ring. The DMSO can be easily replaced by acetonitrile or carbon monoxide.

1.4.3 Basic Synthetic Strategies

The main synthetic strategies used to synthesise terpyridines are either central ring assembly or coupling methodologies.

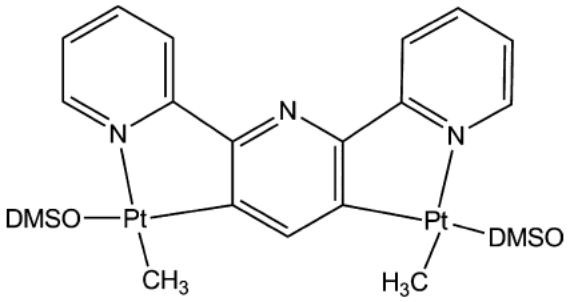
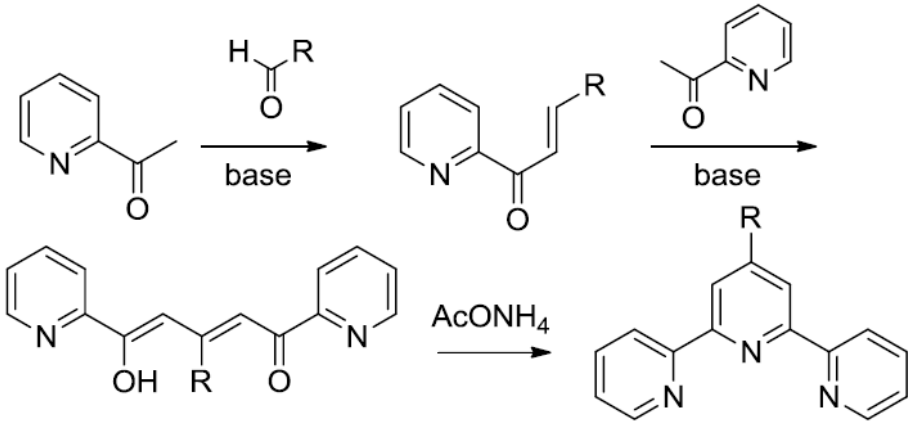


Figure 1.7: C–H activation of terpyridine.

1.4.3.1 Ring assembly

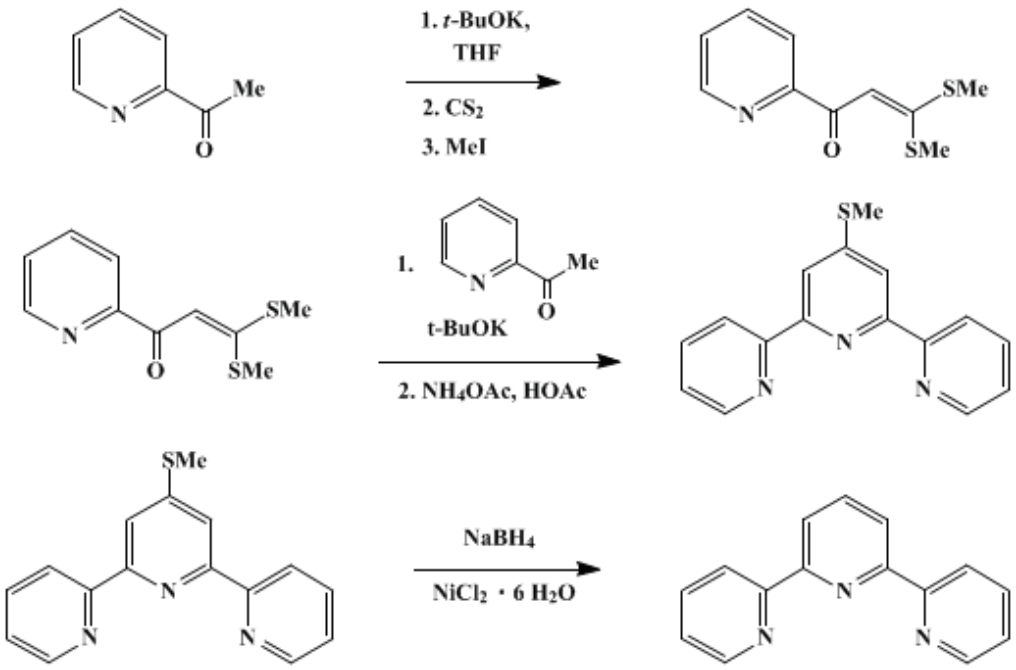
The most common strategy for the synthesis of terpyridines was reported by Kröhnke [88]. The reaction between 2-acetylpyridine and an aldehyde affords α,β-unsaturated ketone. Then, the reaction between the intermediate and another 2-acetylpyridine forms 1,5-diketone and that can undergo ring closure with an ammonia source such as $AcONH_4$ (Scheme 1.1).



Scheme 1.1: Example of the Kröhnke strategy.

Potts methodology is an effective procedure with good yields. The desired terpyridine was obtained by a three-step procedure starting from the commercially available 2-

acetylpyridine to produce an α-oxoketene dithioacetal. The reaction between this intermediate and another 2-acetylpyridine affords 4'-(methylthio)-2,2':6',2''-terpyridine after in situ ring closure with ammonium acetate in glacial acetic acid at reflux (Scheme 1.2) [89].

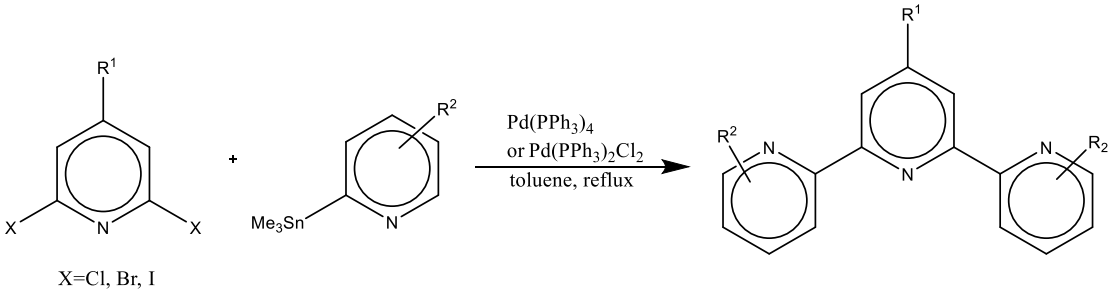


Scheme 1.2: Ring assembly procedure using Potts methodology.

In order to improve the yield and develop a more efficient synthetic protocol, a series of modifications to Kröhnke strategy have been made. Many terpyridines have been synthesized in a one-pot procedure using "green solvents" such as poly(ethylene glycol) solvent-free conditions [90-96]. Clean Kröhnke procedures have been developed in aqueous media under either conventional heating conditions or microwave irradiation (in order to reduce the reaction time) [97-100].

1.4.3.2 Cross coupling

Cross-coupling procedures have widely been used for the construction of the terpyridine core. Pd(0)-catalysed coupling reactions such as Suzuki, Negishi, and Stille couplings are simple and effective. In addition, it is easy to control substitution possibilities [101-103]. In particular, Stille cross-coupling has become the most common pathway to terpyridines. The advantages of this method are that many functionalities can be introduced at any position and the desired terpyridine can be produced on multi-gram scale [104-107]. Terpyridine with functional groups at central ring or/and outer rings can be synthesised using suitable 2,6-dihalopyridines as central building blocks, which can be reacted with 2-trialkylstannylpyridines in the presence of Pd(0) as a catalyst in toluene at reflux.

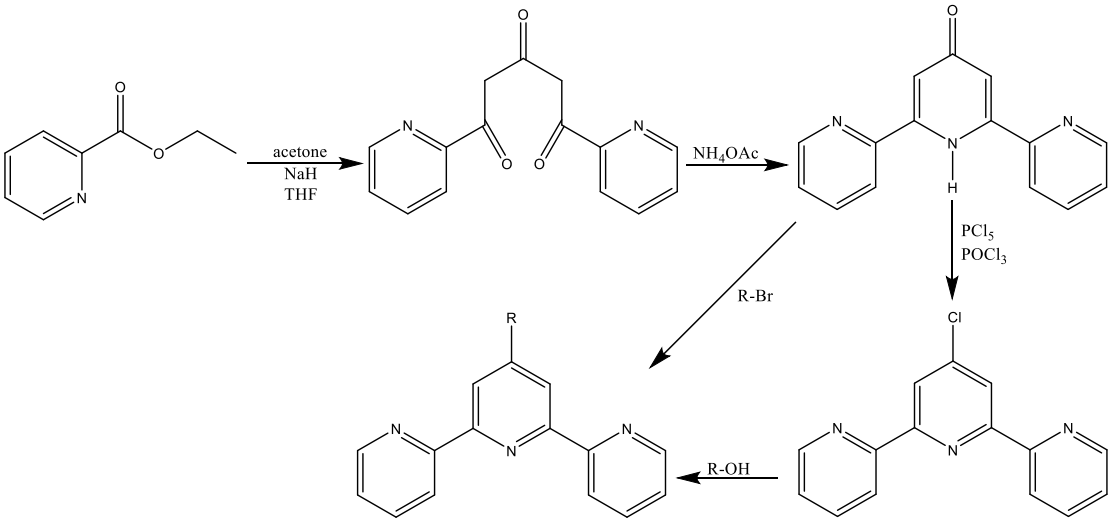


Scheme 1.3: Stille-coupling 2,6-dihalopyridine and 2-trimethylstannylpyridine.

1.4.4 Synthesis of 2,2':6',2''-terpyridine derivatives

Many terpyridine derivatives have been prepared by introducing different substituents at both the central and the terminal rings. Thus, the appropriate functional groups need to be incorporated into substituted starting compounds via ring-assembly or cross-coupling procedures.

4'-Substituted-2,2':6',2"-terpyridinoxy derivatives are a dominant class of terpyridine derivatives. These compounds can be synthesised easily from either nucleophilic aromatic substitution of 4'-haloterpyridines by any primary alcohols or condensation reactions with 4'-hydroxyterpyridines (Scheme 1.4). As a consequence, a wide range of functional terpyridinyl ethers has been synthesised [108-117].



Scheme 1.4: Synthetic routes to terpyridinoxy derivatives.

A wide range of 4'-aryl-substituted 2,2':6',2"-terpyridines has been synthesised because of their convenient accessibility via central ring assembly. 4'-(4-*Tert*-butylphenyl)terpyridine was synthesised as an oligopyridine with enhanced solubility properties. It was synthesised by a two-step ring closure with 2-acetylpyridine and 4-*tert*-butylbenzaldehyde as the starting materials [118-119].

Different N-donor pyridyl substituents attached to the C(4`) position of a terpyridine play an important role in the assembly of coordination complexes. This can be attributed to their various coordination modes and bridging ability (Figure 1.8) [120]. It was noted that 4'-pyridyl substituent on C(4`) position of a terpyridine is very weakly electron

withdrawing and the extended conjugation makes 4'-pyridyl terpyridine a better π-acceptor than unsubstituted terpyridine [121].

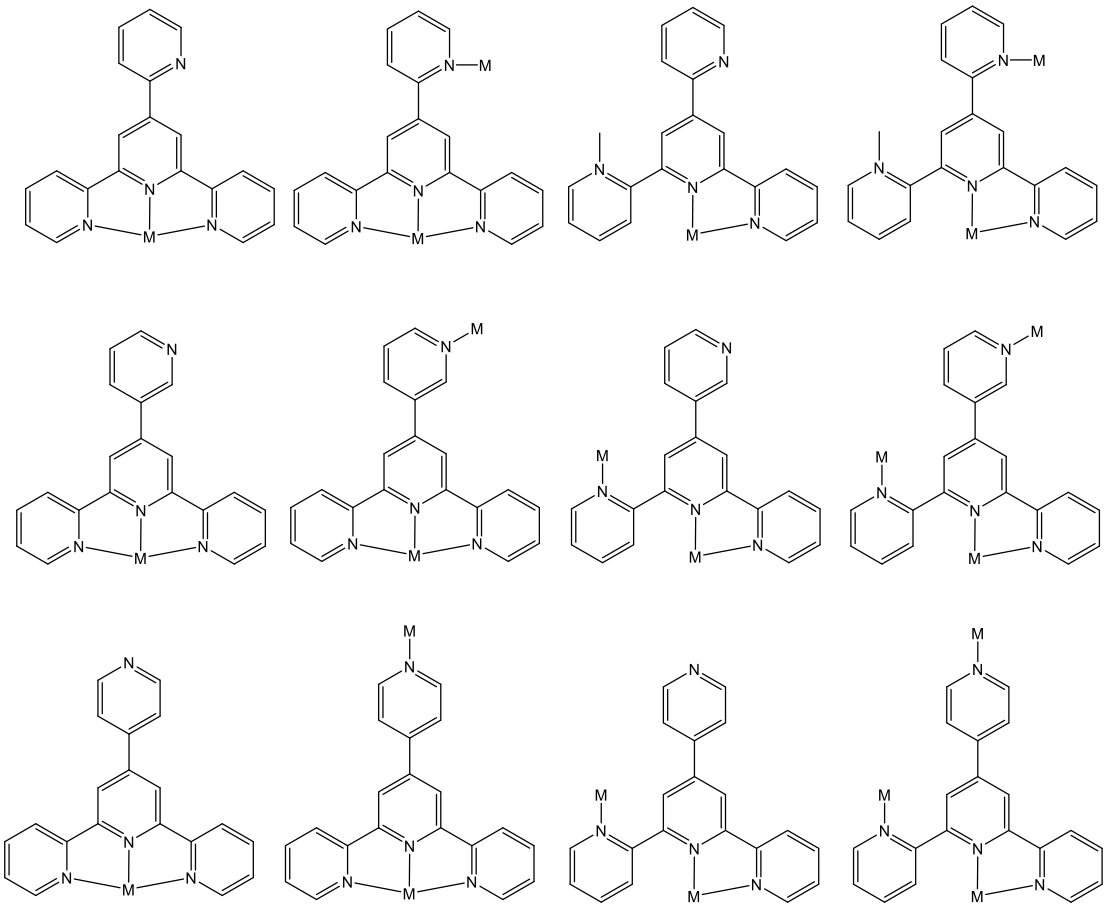


Figure 1.8: Different coordination modes of 4'-pyridyl terpyridines [120].

Constable and co-workers synthesised a wide range of terpyridine derivatives with various substituent groups at the 4'-position, including ferrocene, anthracene, fluoro-substituted aryl groups, and C_{60}-functionalized alkyl chains [122-127].

Ligands containing two or more terpyridine moieties joined by a spacer can bind to metals to create macrocycles or polymers. The ligand containing the multiple terpyridine moieties is used to form dendritic cores (Figure 1.9). This design allows for the chelation of various metal ions to create metallodendrimers [128].

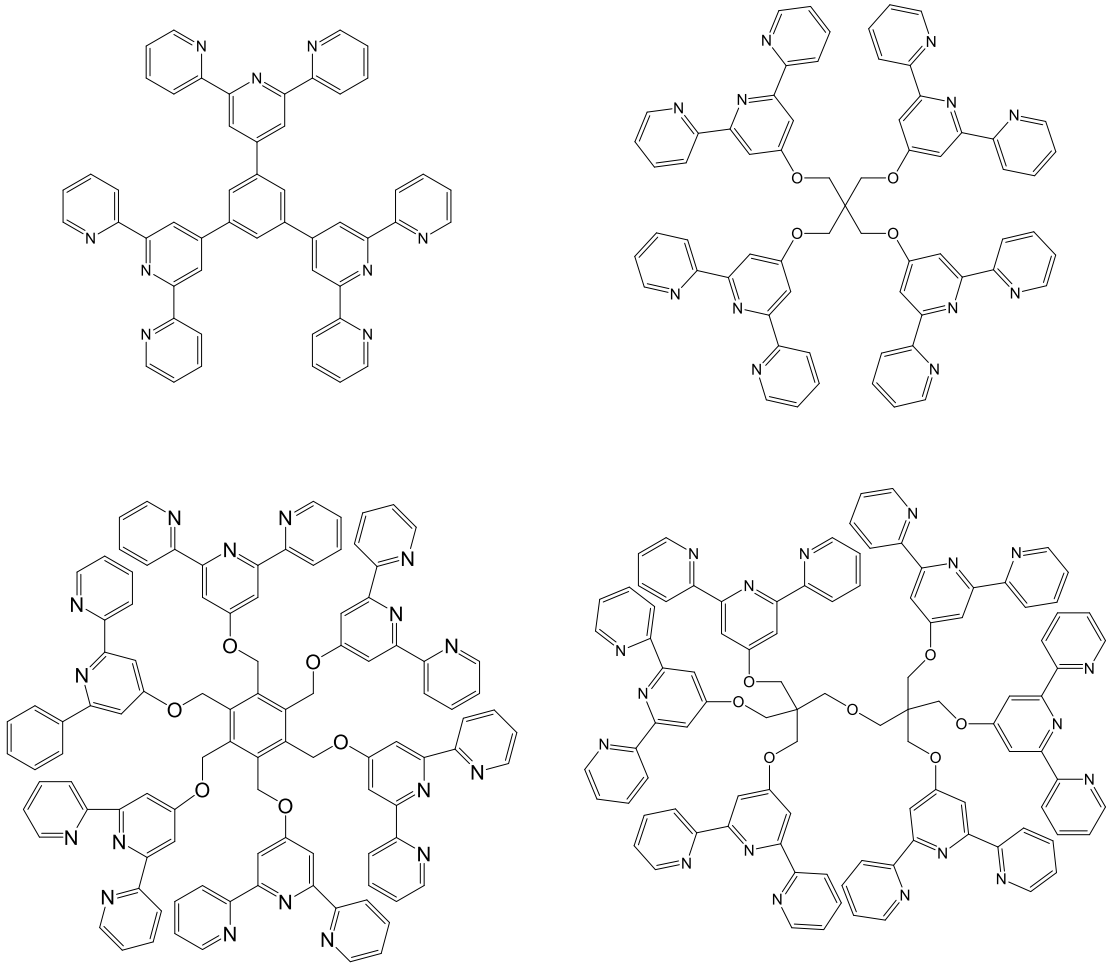


Figure 1.9: Multiple terpyridine moieties form dendritic cores.

1.4.5 Crystal structure of terpyridine

In 1992, the crystal structures of the tridentate ligand 2,2':6',2''-terpyridine was determined by single-crystal diffraction studies (Figure 1.10) [122]. Terpyridine crystallises in orthorhombic space group $P2_12_12_1$. The C–C bonds that link pyridine rings are C(12)–C(22) 1.488(8) Å and C(26)–C(32) 1.493(8) Å. Inside the ring systems, the C–C bond

lengths average 1.378 Å and the C–N bond lengths average 1.342 Å. In terms of angles, there are two sets: the angles involve nitrogen atoms [N–C–C] (average 116.2°) and the angles involve only carbon atoms [C–C–C] (average 120.9°). All three rings are almost coplanar with the torsion angles between the central ring and terminal rings involving N(11) and N(31) being 5.1° and 7.2°, respectively.

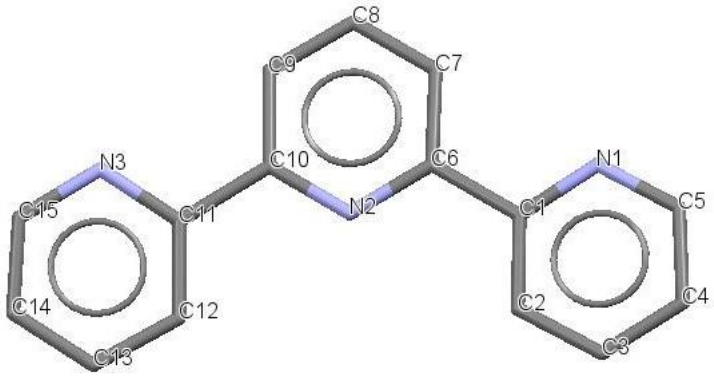


Figure 1.10: Crystal structure of terpyridine[122].

1.4.6 Terpyridine metal complexes

Terpyridine and its derivatives are widely used as building units in supramolecular chemistry due to their ability to coordinate to a wide range of transition metal ions. A distorted octahedral geometry is the common geometry of terpyridine complexes with transition metal ions such as Fe(II), Ru(II) and Zn(II). Figure 1.11 represents the crystal structure of a distorted octahedral geometry of $[Ru(tpy)_2]^{2+}$ complex [129]. Terpyridine complexes with Ru(II) can be synthesised in a two-step reaction. The Ru(III) intermediate is reacted with a second ligand of the same or different terpyridine under reductive conditions to form the symmetric or asymmetric Ru(II) complex, respectively (Scheme 1.5) [81]. Firstly, ruthenium(III) trichloride hydrate is added to an ethanolic or a methanolic solution of the first terpyridine ligand. The intermediate mono-complex is

insoluble in most cases and it can be filtered. In the second step, the intermediate is suspended in methanol with the second equivalent of terpyridine in the presence of *N*-ethylmorpholine [130]. The solvent can act as a reductive agent for the Ru(III) → Ru(II) conversion.

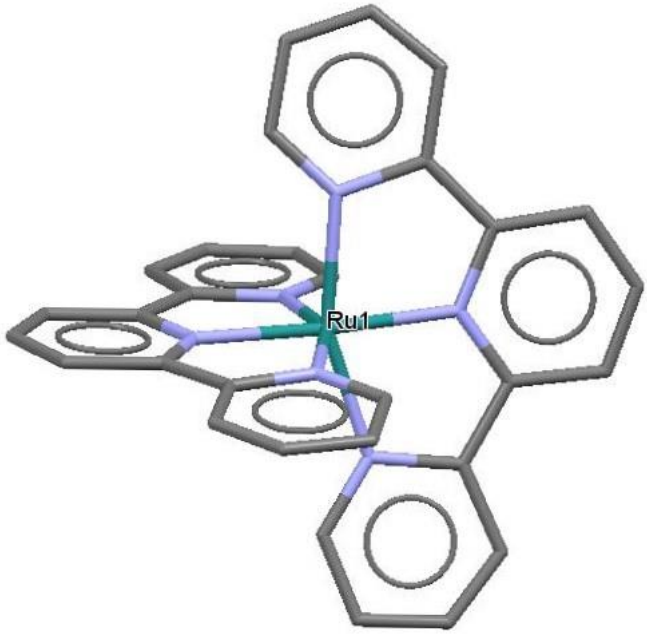
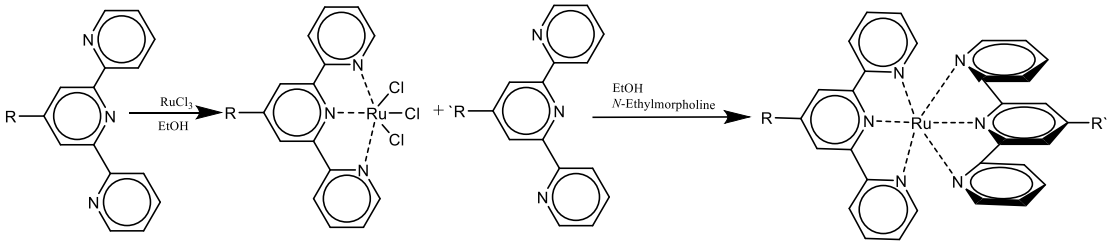


Figure 1.11: Crystal structure of a typical $[Ru(terpy)_2]^{2+}$ complex [129].



Scheme 1.5: Synthetic procedure towards asymmetric terpyridine complexes.

The use of terpyridine instead of bipyridine avoids the formation of a mixture of isomers with differing spatial arrangements of the metal centres and different physical and chemical properties [64].

It is possible to construct extended complex architectures by combining two or more terpyridine moieties with shared nitrogen atoms. The linear ligand with two binding sites of terpyridines coordinates to $Ru(terpy)^{2+}$ centres (Figure 1.12 a) [131]. The structure showed that the ligand axis is bent because of the distorted octahedral geometry for each Ru centre. The existence of the 9-anthryl substituent incorporated in the 5-position of the pyrimidine ring decreases this bend because of the steric repulsion between this central aryl unit and terpyridine moieties (Figure 1.12 b).

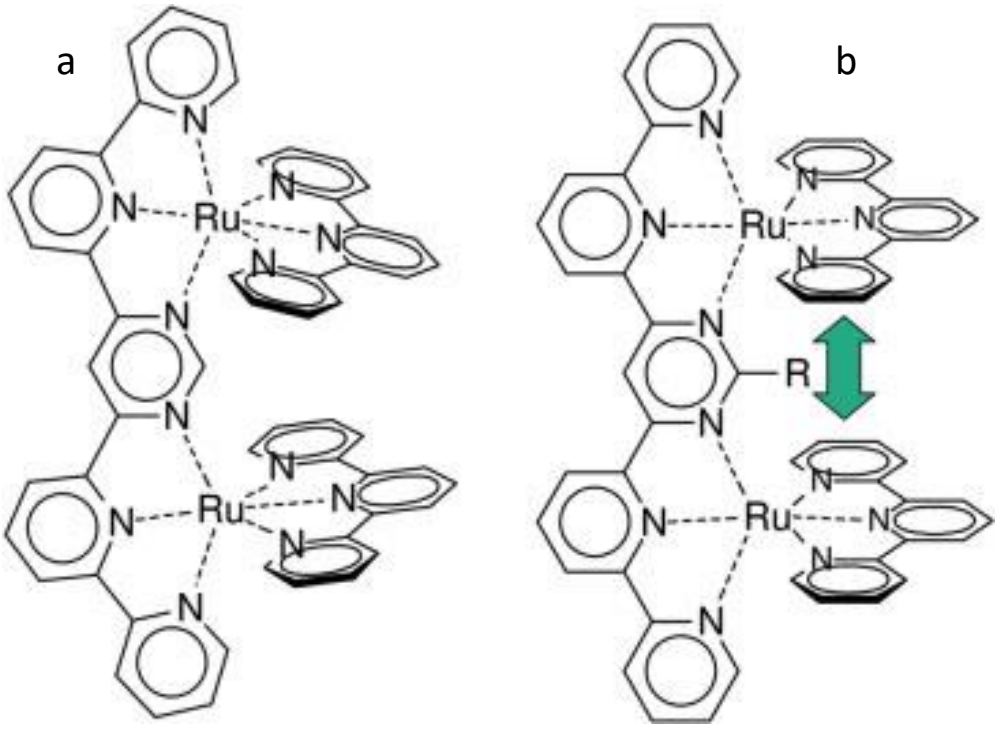


Figure 1.12: (a) Distorted geometry of dinuclear rack-type Ru(II) complex. (b) Molecular structure of dinuclear rack-type Ru(II) complex using (R = 9-anthryl) substituent in the 5-position of the pyrimidine ring [131].

Terpyridine moieties have been intensely studied for their square-planar complexes with various transition metals, for example, Pt(II), Pd(II), and Au(III). These square-planar complexes have found a great many potential applications in luminescence, chemosensor for solvent and metal ions, biological activities, such as DNA intercalation and antitumor agents [132-143].

The terpyridine complexes with Pt(II) and Pd(II) have first been synthesized by Morgen and Burstall [56]. [Pd(4'-R-terpy)(Cl)][Cl], R = H, $CH_3(CH_2)_2O$, $Ph(CH_2)_3O$, complexes were synthesised in reasonable yield by different routes. [Pd(terpy)(Cl)][Cl] was synthesised in quantitative yield, in which a suspension of $PdCl_2$ with an equivalent amount of terpyridine in $MeNO_2$ or concentrated HCl [144,145]. Other synthetic approaches were developed to afford [Pd(4'-R-terpy)(Cl)][Cl] using *cis*-[$Pd(DMSO)_2Cl_2$] in MeOH or [$Pd(MeCN)_2Cl_2$] in THF [145,146]. The chloro complex can be considered as the "parent" complex of a wide range of Pd(II) terpy complexes. The Cl co-ligand of the [Pd(terpy)(Cl)][Cl] complex can be replaced with different functional groups, for example pyridine, 3,4-dimethylphenol, H_2O, OH, and biomolecules, such as L-cysteine and 1-Me-cytosine [87,146-150]. In terms of terpyridine complexes with platinum $[Pt(terpy)X]^{n+}$, there are many synthetic procedures and they differ in their starting materials, reaction conditions and yield [152-156].

Single crystal X-ray structures of the structure of the "parent" complex cation $[Pd(terpy)Cl]^+$ has been determined by Intille (Figure 1.12) [157].

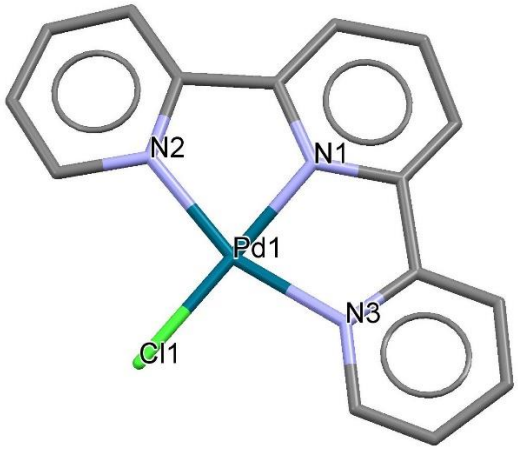


Figure 1.13: Solid state structure of the complex cation in the crystal of $[Pd(terpy)Cl]^+$ [157].

The structure of $[Pd(terpy)Cl]^+$ exhibits features common to nearly all other $[Pd(terpy)X]^{n+}$ systems (discussed in detail later). $[PdCl(terpy)]^+$ are approximately 10^3–10^4 times more reactive than its aliphatic analogue $[PdCl(dien)]^+$ (dien = diethylenetriamine) toward various ligands [158,159]. The existence of three aromatic pyridine rings in the coordination plane leads to an increase in the electrophilicity of the metal centre, as a result of electron density delocalization [160,161].

1.4.7 Applications of terpyridine complexes

The properties of square-planar terpyridine complexes depend on the structure of terpyridine moiety. As a consequence, any substituent introduced to the terpyridine can tune the photophysical, electrochemical, and optical properties of the complex, thereby encouraging new applications in optical limiting, molecular sensing, and construction of supramolecular architectures.

Luminescent and coloured Pt(II) terpyridine complexes have been used extensively as sensors for pH, ions, and solvents. Nicotinamide Pt(II) terpyridine complex [Pt(Nttpy)-Cl]$(PF_6)_2$ (Nttpy = 4'-(*p*-nicotinamide-N-methylphenyl)-2,2':6',2''-terpyridine) indicates a reversible vapochromic behaviour [135]. After exposure to methanol vapour, the complex shows a shift in the emission band to higher energy and the colour of the complex changes from red to orange (Figure 1.14). Before exposure to methanol, the emission maximum of red form occurs at 660 nm at room temperature. After exposure of the red form to methanol vapour, a fast vapochromic response is detected in which the colour changes from red to orange colour with a shift of λ_{em}^{max} to 630 nm (Figure 1.15). Analysis of the packing diagram indicates that the red form has significant metal-metal interactions with Pt atoms arranged in a nearly linear arrangement (shown by a Pt···Pt···Pt angle of 171.9°). On the other hand, the orange form's crystal packing reveals a zigzag arrangement (shown by a Pt···Pt···Pt angle of 126.7°) between nearest neighbour Pt atoms (Figure 1.16). The analysis of the solid-state packing explains the colour change between the two forms and the their photophysical properties. This vapochromic behaviour can be exploited as a MeOH-induced molecular switch.

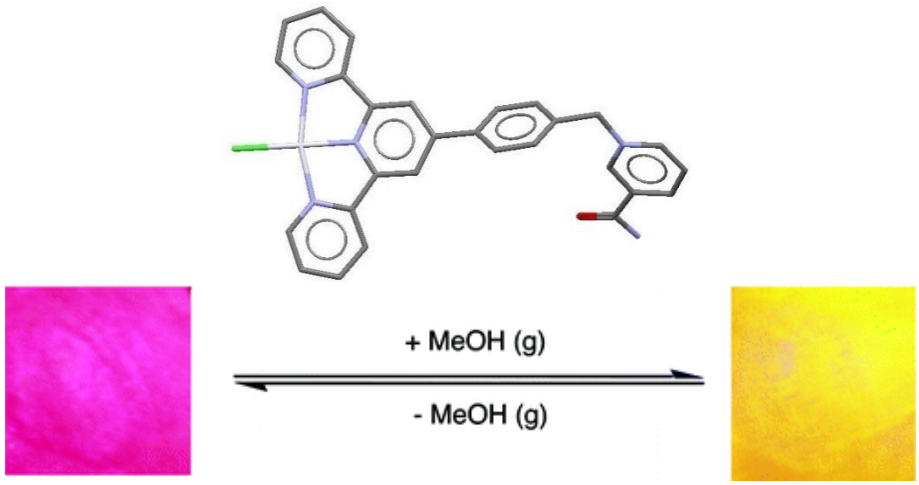


Figure 1.14: The crystal structure of the cationic [Pt(Nttpy)-Cl]$(PF_6)_2$ and its Luminescence as observed by eye in the presence and absence of methanol vapours [135].

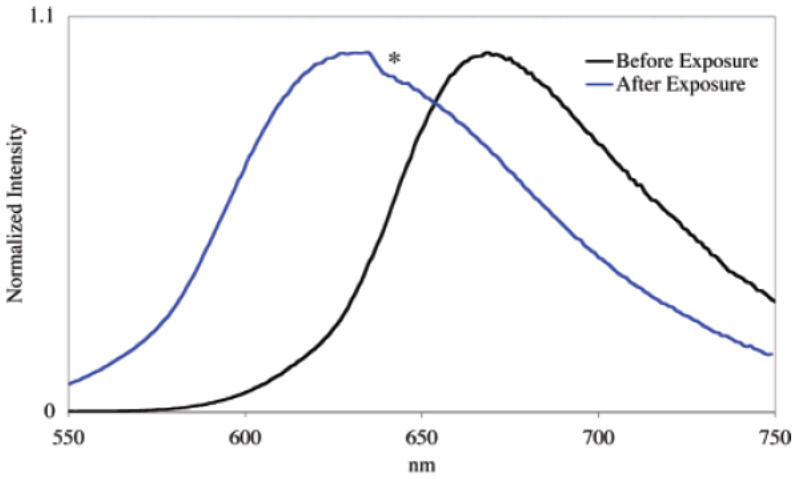


Figure 1.15: Normalized room-temperature solid-state emission spectrum of [Pt(Nttpy)-Cl]$(PF_6)_2$ before and after exposure to methanol vapours. * Denotes instrumental artefact [135].

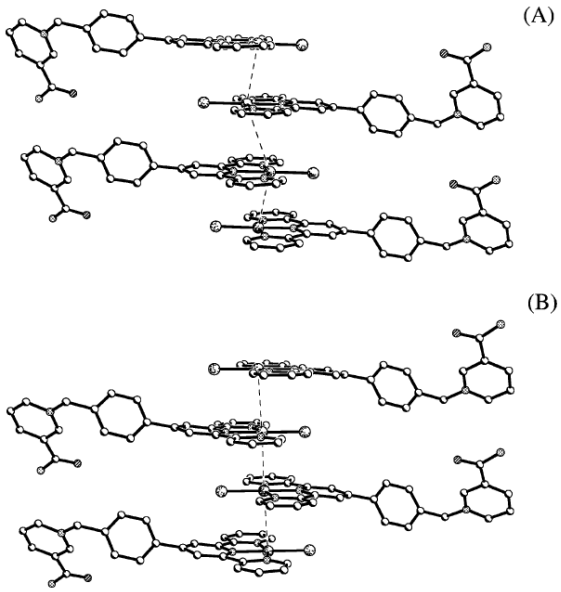


Figure 1.16: The packing arrangements of orange form (A) showing a zigzag stacking and red form (B) showing nearly linear packing [135].

The triflate salt of the complex [Pt(terpy)(C≡C-benzo-15-crown-5)]OTf indicates luminescence enhancement upon binding of Mg^{2+} and Ca^{2+} ions to its crown cavity. Therefore, this complex can be used as luminescent sensors for Mg^{2+} and Ca^{2+} ions [138].

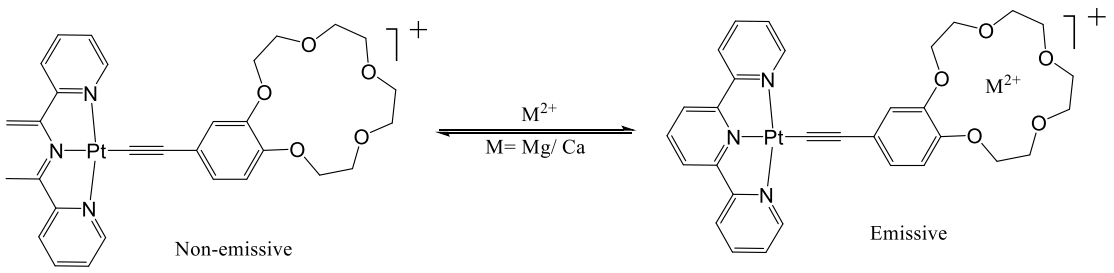


Figure 1.17: Platinum(II) alkynyl terpyridyl complexes with benzo-15-crown-5 as a luminescent sensor for Mg^{2+} and Ca^{2+} ions [138].

Many platinum(II) and palladium(II) complexes with promising activity against tumour cell lines have been prepared [162-166]. It is known that Pd complexes have a considerable anti-tumour activity to cancer cells with lower side effects compared to cisplatin [167,168]. Pd complexes indicate higher solubility compared to Pt complexes that makes Pd complexes more attractive for biological studies. Ulukaya and coworkers synthesised Pd(terpy) complex [Pd(sac)(terpy)](sac).$4H_2O$] (sac = saccharinate) which indicates a strong anti-cancer activity against breast cancer cells (Figure 1.14) [168]. It was noticed that the Pd complex indicated anti-growth effect in a time- and dose-dependent manner.

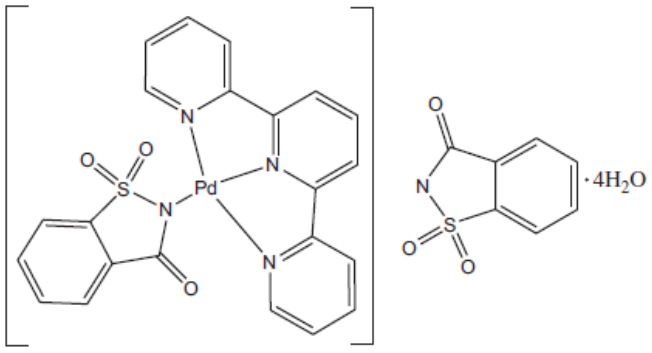


Figure 1.18: The chemical structure of the palladium(II) terpyridine complex [Pd(sac)(terpy)](sac).$4H_2O$.

1.5 Thesis overview

The work reported in this thesis focuses on the synthesis of novel mono and dinuclear palladium(II) 2,2':6',2"-terpyridine complexes with a variety of pyridine derivatives. The crystal structures of these complexes have been mainly determined as triflate salts. However, in some cases, a few crystal structures have been determined as tetrafluoroborate and hexafluorophosphate salts, to illustrate the importance of the anion on the solid-state stacking. It has been found that the presence of substituents at the 4, 4' and 4" positions of the terpyridyl system alters the electronic properties of the terpyridyl ligand. Therefore, (4,4',4"-tri-tert-butyl-2,2':6',2"-terpyridine) has also been studied instead of unsubstituted terpyridine, to study the influence of electron-donating groups on the properties of the crystal structures.

The synthesis of multinuclear ligands combining two or more 2,2':6',2"-terpyridine metal-binding domains extends the area of coordination chemistry from the molecular to the supramolecular level. Therefore, *N,N*–donor ligands are used as a bridge to link two [Pd(terpy)] components. All these ligands were chosen in order to systematically elucidate the role of the length, rigidity, flexibility and the coordination mode of ligands on the crystal structures of Pd complexes.

A novel crystal structure has been determined using *meso*-tetra(4-pyridyl)porphyrins as a ligand. The presence of the four pyridine rings can be exploited to form tetranuclear Pd(terpy) complex.

Tridentate N-donor ligands such as 1,3,5-triazine derivatives have an important role in transition metal complexation and supramolecular interactions. In particular, 2-phenyl-4,6-bis(2-pyridyl)-1,3,5-triazine can be used instead of terpyridine moiety to form Pd complexes. The coplanarity of 2-phenyl-4,6-bis(2-pyridyl)-1,3,5-triazine could increase π-

orbital overlap between the rings. With these particulars in mind, two crystal structures of 2-phenyl-4,6-bis(2-pyridyl)-1,3,5-triazine with palladium (II) have also been studied in this thesis.

1.6 References

1. K. Nicolaou and E. Sorensen, *VCH, New York*, 2003, Vol. 2.
2. K. Nicolaou, D. Vourloumis, N. Winssinger and P. S. Baran, *Angewandte Chemie International Edition*, 2000, **39**, 44-122.
3. E. Corey, *Chemical Society Reviews*, 1988, **17**, 111-133.
4. E. J. Corey, *Angewandte Chemie International Edition*, 1991, **30**, 455-465.
5. L. Stryer, *Biochemistry. WH Freeman, New York*, 1988.
6. D. J. Cram, *Angewandte Chemie International Edition*, 1988, **28**, 1009-1020.
7. C. J. Pedersen, *Angewandte Chemie International Edition*, 1988, **27**, 1021-1027.
8. J. M. Lehn, *Angewandte Chemie International Edition*, 1988, **27**, 89-112.
9. J.-M. Lehn, *Supramolecular Chemistry*, VCH, Weinheim, 1995.
10. D. H. Gracias, J. Tien, T. L. Breen, C. Hsu and G. M. Whitesides, *Science*, 2000, **289**, 1170-1172.
11. Y. Xia, B. Gates, Y. Yin and Y. Lu, *Advanced Materials*, 2000, **12**, 693-713.
12. Y. Huang, X. Duan, Q. Wei and C. M. Lieber, *Science*, 2001, **291**, 630-633.
13. B. Gates and Y. Xia, *Advanced Materials*, 2001, **13**, 1605-1608.
14. D. Braga, *Chemical Communications*, 2002, **3**, 1305-1310.
15. D. Philp and J. F. Stoddart, *Angewandte Chemie International Edition*, 1996, **35**, 1154-1196.
16. G. R. Desiraju, *Angewandte Chemie International Edition*. 2011, **50**, 52-59.
17. L. Isaacs, D. N. Chin, N. Bowden, Y. Xia and G. M. Whitesides, *Perspectives in Supramolecular Chemistry: Supramolecular Materials and Technologies,* 1999, **4**, 1-46.
18. J.-M. Lehn, *Science*, 1993, **260**, 1762-1764.
19. G. V. Oshovsky, D. N. Reinhoudt and W. Verboom, *Angewandte Chemie International Edition*, 2007, **46**, 2366-2393.
20. T. Park, S. C. Zimmerman and S. Nakashima, *Journal of the American Chemical Society*, 2005, **127**, 6520-6521.

21. R. P. Sijbesma, F. H. Beijer, L. Brunsveld, B. J. Folmer, J. K. Hirschberg, R. F. Lange, J. K. Lowe and E. Meijer, *Science*, 1997, **278**, 1601-1604.

22. S. I. Stupp, V. LeBonheur, K. Walker, L.-S. Li, K. E. Huggins, M. Keser and A. Amstutz, *Science*, 1997, **276**, 384-389.

23. J. Ruokolainen, R. Mäkinen, M. Torkkeli, T. Mäkelä, R. Serimaa, G. ten Brinke and O. Ikkala, *Science*, 1998, **280**, 557-560.

24. T. Kato, N. Mizoshita and K. Kishimoto, *Angewandte Chemie International Edition*, 2006, **45**, 38-68.

25. E. Krieg and B. Rybtchinski, *Chemistry-A European Journal*, 2011, **17**, 9016-9026.

26. H. A. Klok and S. Lecommandoux, *Advanced Materials*, 2001, **13**, 1217-1229.

27. C. F. Faul and M. Antonietti, *Advanced Materials*, 2003, **15**, 673-683.

28. B. Rybtchinski, *ACS nano*, 2011, **5**, 6791-6818.

29. D. Braga, *Chemical Communications*, 2003, 2751-2754.

30. J. W. Steed, J. L. Atwood and P. A. Gale, *Definition and Emergence of Supramolecular Chemistry*, Wiley Online Library, 2012.

31. J. W. Steed, D. R. Turner and K. Wallace, *Core Concepts in Supramolecular Chemistry and Nanochemistry*, John Wiley & Sons, 2007.

32. G. M. Schmidt and D. Ginsburg, *Solid State Photochemistry*, Verlag Chemie, 1976.

33. L. Addadi and M. Lahav, *Journal of the American Chemical Society*, 1978, **100**, 2838-2844.

34. J. Thomas, *Nature*, 1981, **289**, 633-634.

35. S. B. Copp, S. Subramanian and M. J. Zaworotko, *Journal of the American Chemical Society*, 1992, **114**, 8719-8720.

36. C. B. Aakeröy and K. R. Seddon, *Chemical Society Reviews*, 1993, **22**, 397-407.

37. G. R. Desiraju, *Angewandte Chemie International Edition*, 1995, **34**, 2311-2327.

38. L. R. Nassimbeni, *Accounts of Chemical Research*, 2003, **36**, 631-637.

39 G. R. Desiraju, M. Johnson, W. Sander, *Journal of Physical Chemistry*, 2013, **14**, 1-4.

40. Ö. Almarsson and M. J. Zaworotko, *Chemical Communications*, 2004, 1889-1896.

41. M. W. Hosseini, *Accounts of Chemical Research*, 2005, **38**, 313-323.

42. G. R. Desiraju, J. J. Vittal and A. Ramanan, *Crystal Engineering: a Textbook*, WorldScientific, 2011.

43. A. D. Bond, *Crystal Engineering Community*, 2012, **14**, 2363-2366.

44. A. I. Cooper, *Angewandte Chemie International Edition*, 2012, **51**, 7892-7894.

45. G. R. Desiraju, *Journal of the American Chemical Society*, 2013, **135**, 9952-9967.

46. R. Pepinsky, *Physical Review*, 1955, **100**, 971-795.

47. G. Schmidt, *Pure and Applied Chemistry*, 1971, **27**, 647-678.

48. G. R. Desiraju and G. W. Parshall, *Materials Science Monographs*, 1989, **54**, 145-150.

49. F. Blau, *Berg. Huettenmaenn. Monatsh*, 1888, **21**, 1077-1082.

50. U. S. Schubert and C. Eschbaumer, *Angewandte Chemie International Edition*, 2002, **41**, 2892-2926.

51. U. S. Schubert and C. Eschbaumer, *Angewandte Chemie*, 2002, **114**, 3016-3050.

52. G. R. Newkome, A. K. Patri, E. Holder and U. S. Schubert, *European Journal of Organic Chemistry*, 2004, **204**, 235-254.

53. N. C. Fletcher, *Journal of the Chemical Society, Perkin Transactions 1*, 2002, 1831-1842.

54. C. Kaes, A. Katz and M. W. Hosseini, *Chemical Reviews*, 2000, **100**, 3553-3590.

55. G. T. Morgan and F. H. Burstall, *Journal of the Chemical Society (Resumed)*, 1932, 20-30.

56. G. T. Morgan and F. H. Burstall, *Journal of the Chemical Society (Resumed)*, 1934, 1498-1500.

57. S. Hayami, Y. Komatsu, T. Shimizu, H. Kamihata and Y. H. Lee, *Coordination Chemistry Reviews*, 2011, **255**, 1981-1990.

58. A. Arrigo, A. Santoro, F. Puntoriero, P. P. Lainé and S. Campagna, *Coordination Chemistry Reviews*, 2015, **304**, 109-116.

59. J. P. Sauvage, J. P. Collin, J. C. Chambron, S. Guillerez, C. Coudret, V. Balzani, F. Barigelletti, L. De Cola and L. Flamigni, *Chemical Reviews*, 1994, **94**, 993-1019.

60. L. Flamigni, J.-P. Collin and J.-P. Sauvage, *Accounts of Chemical Research*, 2008, **41**, 857-871.

61. E. Baranoff, J. P. Collin, L. Flamigni and J.-P. Sauvage, *Chemical Society Reviews*, 2004, **33**, 147-155.

62. I. Eryazici, C. N. Moorefield and G. R. Newkome, *Chemical Reviews*, 2008, **108**, 1834-1895.

63. H. Hofmeier and U. S. Schubert, *Chemical Society Reviews*, 2004, **33**, 373-399.

64. E. C. Constable, *Chemical Society Reviews*, 2007, **36**, 246-253.

65. Y. Gao, D. Rajwar and A. C. Grimsdale, *Macromolecular Rapid Communications*, 2014, **35**, 1727-1740.

66. A. Wild, A. Winter, F. Schlütter and U. S. Schubert, *Chemical Society Reviews*, 2011, **40**, 1459-1511.

67. G. Chelucci and R. P. Thummel, *Chemical Reviews*, 2002, **102**, 3129-3170.

68. A. Winter, M. D. Hager, G. R. Newkome and U. S. Schubert, *Advanced Materials*, 2011, **48**, 5728-48.

69. P. Ceroni, A. Credi, V. Balzani, S. Campagna, G. S. Hanan, C. R. Arana and J. M. Lehn, *European Journal of Inorganic Chemistry*, 1999, 1409-1414.

70. L. E. Helberg, T. B. Gunnoe, B. C. Brooks, M. Sabat and W. D. Harman, *Organometallics*, 1999, **18**, 573-581.

71. G. U. Priimov, P. Moore, P. K. Maritim, P. K. Butalanyi and N. W. Alcock, *Journal of the Chemical Society, Dalton Transactions*, 2000, 445-449.

72. F. P. Pruchnik, F. Robert, Y. Jeannin and S. Jeannin, *Inorganic Chemistry*, 1996, **14**, 4261-4263.

73 E. Rotondo, G. Giordano and D. Minniti, *Journal of the Chemical Society, Dalton Transactions*, 1996, **44**, 253-254.

74. A. Doppiu, G. Minghetti, M. A. Cinellu, S. Stoccoro, A. Zucca and M. Manassero, *Organometallics*, 2001, **20**, 1148-1152.

75. A. Gelling, K. G. Orrell, A. G. Osborne and V. Šik, *Journal of the Chemical Society, Dalton Transactions*, 1998, **35**, 937-946.

76. A. Gelling, M. D. Olsen, K. G. Orrell, A. G. Osborne and V. Šik, *Journal of the Chemical Society, Dalton Transactions*, 1998, 3479-3488.

77. C. Bessel, R. See and D. Jameson, *Journal of the Chemical Society, Dalton Transactions*, 1992, **2801**, 2543-2547.

78. K. F. Bowes, I. P. Clark, J. M. Cole, M. Gourlay, A. M. Griffin, M. F. Mahon, L. Ooi, A. W. Parker, P. R. Raithby and H. A. Sparkes, *Crystal Engineering Communication*, 2005, **7**, 269-275.

79. E. C. Constable, J. Lewis, M. C. Liptrot and P. R. Raithby, *Inorganica Chimica Acta*, 1990, **178**, 47-54.

80. G. D. Storrier, S. B. Colbran and D. C. Craig, *Journal of the Chemical Society, Dalton Transactions*, 1997, **14**, 3011-3028.

81. E. Constable, A. C. Thompson, D. Tocher and M. Daniels, *New Journal of Chemistry*, 1992, **16**, 855-867.

82. F. H. Case and T. J. Kasper, *Journal of the American Chemical Society*, 1956, **78**, 5842-5844.

83. M. G. Drew, M. J. Hudson, P. B. Iveson, M. L. Russell, J.-O. Liljenzin, M. Sklberg, L. Spjuth and C. Madic, *Journal of the Chemical Society, Dalton Transactions*, 1998, 2973-2980.

84. E. W. Abel, K. G. Orrell, A. G. Osborne, H. M. Pain, V. Šik, M. B. Hursthouse and K. A. Malik, *Journal of the Chemical Society, Dalton Transactions*, 1994, 3441-3449.

85. E. Abel, V. Dimitrov, N. Long, K. Orrell, A. Osborne and H. Pain, *Journal of the Chemical Society, Dalton Transactions*, 1993, **597**, 365-369.

86. E. Abel, V. Dimitrov and N. Lon, *Journal of the Chemical Society, Dalton Transactions*, 1993, **291**, 5435-5438.

87. Ž. D. Bugarčić, B. Petrović and E. Zangrando, *Inorganica Chimica Acta*, 2004, **357**, 2650-2656.

88. F. Kroehnke, *Synthesis*, 1976, **1976**, 1-24.

89. K. T. Potts, D. A. Usifer, A. Guadalupe and H. D. Abruna, *Journal of the American Chemical Society*, 1987, **109**, 3961-3967.

90. A. Winter, A. M. van den Berg, R. Hoogenboom, G. Kickelbick and U. S. Schubert, *Synthesis*, 2006, **2006**, 2873-2878.

91. C. B. Smith, C. L. Raston and A. N. Sobolev, *Green Chemistry*, 2005, **7**, 650-654.

92. S. V. Jadhav, P. G. Ingole and H. C. Bajaj, *Synthetic Communications*, 2010, **40**, 1142-1148.

93. G. W. Cave and C. L. Raston, *Journal of the Chemical Society, Perkin Transactions 1*, 2001, 3258-3264.

94. G. Cave and C. Raston, *Chemical Communications*, 2001, 2159-2169.

95. G. W. Cave and C. L. Raston, *Chemical Communications*, 2000, 2199-2200.

96. M. Adib, H. Tahermansouri, S. A. Koloogani, B. Mohammdi and H. R. Bijanzadeh, *Tetrahedron*, 2006, **47**, 5957-5960.

97. S. Tu, R. Jia, B. Jiang, J. Zhang, Y. Zhang, C. Yao and S. Ji, *Tetrahedron*, 2007, **63**, 381-388.

98. S. Tu, T. Li, F. Shi, F. Fang, S. Zhu, X. Wei and Z. Zong, *Chemistry Letters*, 2005, **34**, 732-733.

99. S. Tu, T. Li, F. Shi, Q. Wang, J. Zhang, J. Xu, X. Zhu, X. Zhang, S. Zhu and D. Shi, *Synthesis*, 2005, **2005**, 3045-3050.

100. J. Wang and G. S. Hanan, *Synlett*, 2005, **2005**, 1251-1254.

101. N. Miyaura and A. Suzuki, *Chemical Reviews*, 1995, **95**, 2457-2483.

102. E. Negishi, *by H. Nozaki, Pergamon Press, Oxford*, 1983, 269-280.

103. J. K. Stille, *Angewandte Chemie International Edition*, 1986, **25**, 508-524.

104. D. J. Cárdenas and J. P. Sauvage, *Synthesis Letter*, 1996, **1996**, 916-918.

105. R.-A. Fallahpour, *Synthesis*, 2000, **2000**, 1665-1667.

106. G. Ulrich, S. Bedel, C. Picard and P. Tisnès, *Tetrahedron Letters*, 2001, **42**, 6113-6115.

107. M. Heller and U. S. Schubert, *Synthesis Letter*, 2002, **2002**, 0751-0754.

108. G. R. Newkome, E. He, L. A. Godínez and G. R. Baker, *Chemical Communications*, 1999, **44**, 27-28.

109. P. R. Andres, R. Lunkwitz, G. R. Pabst, K. Böhn, D. Wouters, S. Schmatloch and U. S. Schubert, *European Journal of Organic Chemistry*, 2003, **2003**, 3769-3776.

110. M. L. Muro, C. A. Daws and F. N. Castellano, *Chemical Communications*, 2008, 6134-6136.

111. U. S. Schubert, C. Eschbaumer, O. Hien and P. R. Andres, *Tetrahedron Letters*, 2001, **42**, 4705-4707.

112. S. Burazerovic, J. Gradinaru, J. Pierron and T. R. Ward, *Angewandte Chemie*, 2007, 5510-5514.

113. Z. Zhang, S. Mikkola and H. Lonnberg, *Tetrahedron*, 2007, **63**, 11716-11723.

114. E. J. Cho, S. Jung, K. Lee, H. J. Lee, K. C. Nam and H.-J. Bae, *Chemical Communications*, 2010, **46**, 6557-6559.

115. G. R. Newkome, R. Güther, C. N. Moorefield, F. Cardullo, L. Echegoyen, E. Pérez-Cordero and H. Luftmann, *Angewandte Chemie*, 1995, **107**, 2159-2162.

116. G. R. Newkome and E. He, *Journal of Materials Chemistry*, 1997, **7**, 1237-1244.

117. M. Göritz and R. Krämer, *Journal of the American Chemical Society*, 2005, **127**, 18016-18017.

118. E. C. Constable, P. Harverson, D. R. Smith and L. A. Whall, *Tetrahedron*, 1994, **50**, 7799-7806.

119. E. C. Constable, P. Harverson, D. R. Smith and L. A. Whall, *Polyhedron*, 1997, **16**, 3615-3623.

120. H. Feng, X.-P. Zhou, T. Wu, D. Li, Y.-G. Yin and S. W. Ng, *Inorganica Chimica Acta*, 2006, **359**, 4027-4035.

121. E. C. Constable and A. M. C. Thompson, *Journal of the Chemical Society, Dalton Transactions*, 1994, 1409-1418.

122. F. Ronald and M. RowenáChurchill, *Journal of the Chemical Society, Dalton Transactions*, 1992, 3223-3228.

123. E. Constable and A. Edwards, *Journal of the Chemical Society, Dalton Transactions*, 1994, **645**.

124. G. Albano, V. Balzani, E. C. Constable, M. Maestri and D. R. Smith, *Inorganica Chimica Acta*, 1998, **277**, 225-231.

125. E. C. Constable, M. Neuburger, D. R. Smith and M. Zehnder, *Inorganica Chimica Acta*, 1998, **275**, 359-365.

126. E. C. Constable, B. Kariuki and A. Mahmood, *Polyhedron*, 2003, **22**, 687-698.

127. D. Armspach, E. C. Constable, F. Diederich, C. E. Housecroft and J. F. Nierengarten, *Chemistry-A European Journal*, 1998, **4**, 723-733.

128. E. Constable, *Chemical Communications*, 1997, 1073-1080.

129. S. Pyo, E. Pérez-Cordero, S. G. Bott and L. Echegoyen, *Inorganic Cchemistry*, 1999, **38**, 3337-3343.

130. M. Maestri, N. Armaroli, V. Balzani, E. C. Constable and A. M. C. Thompson, *Inorganic Chemistry*, 1995, **34**, 2759-2767.

131. G. S. Hanan, C. R. Arana, J. M. Lehn and D. Fenske, *Angewandte Chemie International Edition*, 1995, **34**, 1122-1124.

132. D. R. McMillin and J. J. Moore, *Coordination Chemistry Reviews*, 2002, **229**, 113-121.

133. V. W.-W. Yam, R. P.-L. Tang, K. M.-C. Wong and K.-K. Cheung, *Organometallics*, 2001, **20**, 4476-4482.

134. Y. Kunugi, K. R. Mann, L. L. Miller and C. L. Exstrom, *Journal of the American Chemical Society*, 1998, **120**, 589-590.

135. T. J. Wadas, Q.-M. Wang, Y.-j. Kim, C. Flaschenreim, T. N. Blanton and R. Eisenberg, *Journal of the American Chemical Society*, 2004, **126**, 16841-16849.

136. C. L. Exstrom, J. R. J. Sowa, C. A. Daws, D. Janzen, K. R. Mann, G. A. Moore and F. F. Stewart, *Chemistry of Materials*, 1995, **7**, 15-17.

137. C. A. Daws, C. L. Exstrom, J. R. Sowa and K. R. Mann, *Chemistry of Materials*, 1997, **9**, 363-368.

138. W.-S. Tang, X.-X. Lu, K. M.-C. Wong and V. W.-W. Yam, *Journal of Materials Chemistry*, 2005, **15**, 2714-2720.

139. W. D. McFadyen, L. Wakelin, I. Roos and B. Hillcoat, *Biochemical Journal*, 1987, **242**, 177-183.

140. Ž. D. Bugarčić, F. W. Heinemann and R. van Eldik, *Dalton Transactions*, 2004, 279-286.

141. D.-L. Ma, T. Y.-T. Shum, F. Zhang, C.-M. Che and M. Yang, *Chemical Communications*, 2005, 4675-4677.

142. G. Lowe, A. S. Droz, T. Vilaivan, G. W. Weaver, L. Tweedale, J. M. Pratt, P. Rock, V. Yardley and S. L. Croft, *Journal of Medicinal Chemistry*, 1999, **42**, 999-1006.

143. K. Becker, C. Herold-Mende, J. J. Park, G. Lowe and R. H. Schirmer, *Journal of Medicinal Chemistry*, 2001, **44**, 2784-2792.

144. X. Liu, E. J. McInnes, C. A. Kilner, M. Thornton-Pett and M. A. Halcrow, *Polyhedron*, 2001, **20**, 2889-2900.

145. R. Karkali and D. Bugari, *Monatshefte für Chemie/Chemical Monthly*, 2000, **131**, 819-824.

146. E. J. MacLean, R. I. Robinson, S. J. Teat, C. Wilson and S. Woodward, *Journal of the Chemical Society, Dalton Transactions*, 2002, 3518-3524.

147. Ž. Bugarčić, *Journal of the Chemical Society, Dalton Transactions*, 2002, **6**, 951.

148. P. Castan, F. Dahan, S. Wimmer and F. L. Wimmer, *Journal of the Chemical Society, Dalton Transactions*, 1990, 2679-2683.

149. G. Annibale, G. Marangoni, B. Pitteri, F. Visentin and T. Bobbo, *Transition Metal Chemistry*, 2000, **25**, 485-489.

150. X. Liu, S. L. Renard, C. A. Kilner and M. A. Halcrow, *Inorganic Chemistry Communications*, 2003, **6**, 598-603.

151. S. Coşar, M. B. Janik, M. Flock, E. Freisinger, E. Farkas and B. Lippert, *Journal of the Chemical Society, Dalton Transactions*, 1999, 2329-2336.

152. G. Annibale, M. Brandolisio and B. Pitteri, *Polyhedron*, 1995, **14**, 451-453.

153. R. Cini, A. Donati and R. Giannettoni, *Inorganica Chimica Acta*, 2001, **315**, 73-80.

154. S. K. Thomson and G. B. Young, *Polyhedron*, 1988, **7**, 1953-1964.

155. K. Strothkamp and S. Lippard, *Proceedings of the National Academy of Sciences*, 1976, **73**, 2536-2540.

156. G. S. Hill, M. J. Irwin, C. J. Levy, L. M. Rendina, R. J. Puddephatt, R. A. Andersen and L. Mclean, *Inorganic Syntheses, Volume 32*, 1998, 149-153.

157. G. Intille, C. Pfluger and W. Baker, *Journal of Crystal and Molecular Structure*, 1973, **3**, 47-54.

158. R. Mureinik and M. Bidani, *Inorganica Chimica Acta*, 1978, **29**, 37-41.

159. M. Cusumano, G. Guglielmo and V. Ricevuto, *Inorganica Chimica Acta*, 1978, **27**, 197-199.

160. D. Jaganyi, A. Hofmann and R. van Eldik, *Angewandte Chemie International Edition*, 2001, **40**, 1680-1683.

161. A. Hofmann, D. Jaganyi, O. Q. Munro, G. Liehr and R. van Eldik, *Inorganic Chemistry*, 2003, **42**, 1688-1700.

162. A. S. Abu-Surrah, T. A. Al-Allaf, L. J. Rashan, M. Klinga and M. Leskelä, *European Journal of Medicinal Chemistry*, 2002, **37**, 919-922.

163. A. S. Abu-Surrah, K. A. A. Safieh, I. M. Ahmad, M. Y. Abdalla, M. T. Ayoub, A. K. Qaroush and A. M. Abu-Mahtheieh, *European Journal of Medicinal Chemistry*, 2010, **45**, 471-475.

164. A. Divsalar, A. A. Saboury, H. Mansoori-Torshizi and F. Ahmad, *The Journal of Physical Chemistry B*, 2010, **114**, 3639-3647.

165. N. A. Al-Masoudi, B. H. Abdullah, A. H. Essa, R. Loddo and P. LaColla, *Archiv der Pharmazie*, 2010, **343**, 222-227.

166. G. Tamasi, M. Casolaro, A. Magnani, A. Sega, L. Chiasserini, L. Messori, C. Gabbiani, S. M. Valiahdi, M. A. Jakupec and B. K. Keppler, *Journal of Inorganic Biochemistry*, 2010, **104**, 799-814.

167. E. Gao, C. Liu, M. Zhu, H. Lin, Q. Wu and L. Liu, *Anti-Cancer Agents in Medicinal Chemistry (Formerly Current Medicinal Chemistry-Anti-Cancer Agents)*, 2009, **9**, 356-368.

168. E. Ulukaya, F. Ari, K. Dimas, E. I. Ikitimur, E. Guney and V. T. Yilmaz, *European Journal of Medicinal Chemistry*, 2011, **46**, 4957-4963.

Chapter 2

Mono Palladium (2,2':6',2''-Terpyridine) Complexes with *Para*-Substituted Pyridine Derivatives

2.1 Introduction

Supramolecular frameworks offer an attractive direction of research for possible applications in gas or chemical absorption, selective separation and catalysis [1-14]. The metal coordination sphere and orientation of the binding sites in a ligand have important influence on the metal centre and the intermolecular interactions of the ligand can control the formation of the target supramolecular assemblies. Therefore, the design of appropriate ligands as building blocks plays a crucial role for supramolecular assemblies. The tridentate ligands such as diethylenetriamine (dien), bis(2-pyridylmethyl)amine (bpma) and 2,2':6',2"-terpyridine can coordinate to Pd(II) and Pt(II) and form stable square planar complexes (Figure 2.1) [15-24].

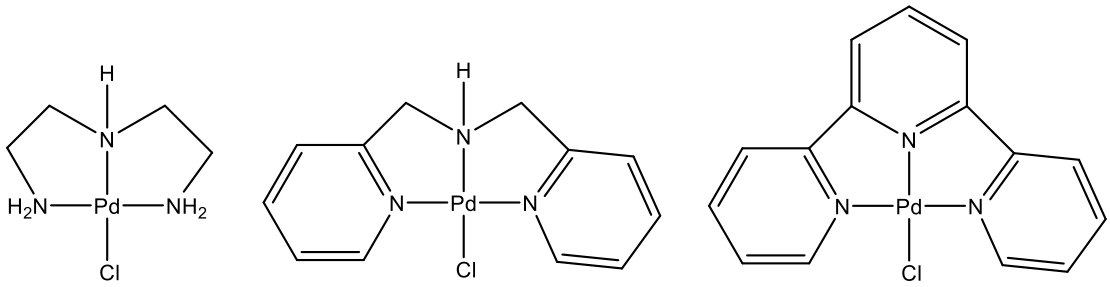


Figure 2.1: Complexes of tridentate ligands diethylenetriamine (dien), bis(2-pyridylmethyl)amine (bpma) and 2,2':6',2"-terpyridine with Pd.

2,2':6',2"-Terpyridine (terpy) has a variety of applications in the synthesis of supramolecular frameworks and functional materials [25-27]. In 1932, Morgan and Burstall isolated 2,2':6',2"-terpyridine from the mixture of oligopyridines obtained by the oxidative coupling of pyridine using anhydrous ferric chloride as a catalyst [28]. Later, it was found that the addition of iron(II) ions to a solution of terpyridine compounds produced a purple colour, the first indication for the formation of a metal terpyridine complex [29].

The rapid development of the synthetic procedures of 2,2':6',2"-terpyridine and its substituted analogues has led to the synthesis of these compounds in good yield in gram or multigram scales [30].

Terpyridine was selected as a building block in this work, for the following reasons: it can make stable complexes with transition metals. In addition to the extreme stability of its metal complexes, its large aromatic area has the ability to produce π· · ·π interactions, potentially leading to stabilisation of solid-state supramolecular assemblies. Triflate ions ($CF_3SO_3^-$) were chosen as anions for the majority of complexes in this work as they are often successfully used for crystal formation, possibly due to their ability to act as hydrogen-bond acceptors.

2.1.1 Crystal structures of Pd(terpy) complexes

A range of Pd(terpy) complexes were prepared and their crystal structures analysed in order to investigate the factors that affect solid-state packing and supramolecular assembly. The interaction between $[Pd(terpy)L]^{n+}$ (L = ligand) cations in the crystal packing structure is described by three main parameters: the dihedral angle, torsion angle and the distance between cation planes. Pd cations usually pack in a face-to-face orientation and the dihedral angle between the cation planes determine the deviation from co-planarity. In addition, cation stacks most often have a torsion angle close to 0°, giving a "head-to-head" relative orientation. The distance between cation planes affects the Pd atom separations. The stacking chains can adopt the same Pd· · ·Pd separation repeating or can have alternating short and long Pd· · ·Pd separations. The Pd· · ·Pd interaction generally as occurring when Pd· · ·Pd separations are less than 3.5 Å [31]. In

addition to Pd· · ·Pd interaction, π· · ·π stacking can be the dominant interaction when the π orbitals of adjacent terpyridines overlap. In general, the distance between the terpyridine moieties in the neighbouring coplanar complexes is less than 3.8 Å and is considered indicative of direct π· · ·π interaction [32]. Four factors have an important influence on the previous parameters: any substituents on terpyridine, the nature of the X ligand, the nature of anion, and the solvents used to grow crystals. The first factor will be discussed in next chapter.

The influence of the anion is obvious as demonstrated by the differences between $[Pt(terpy)(CH_2NO_2)]BPh_4$ and $[Pt(terpy)(CH_2NO_2)]BF_4$. The former is a red powder and the complex cations stack as dimers in head to tail orientation [33]. The latter complex has a yellow colour and the complex cations stack as offset co-parallel dimers [34].

The nature of the ligand in $[Pd(terpy)(X)]^{n+}$ has an interesting influence on the stacking between cations. When the ligand X is pyridine-2-thiol, the cations stack in a head-to-tail orientation. However, the cations exist as discrete molecules in the crystal lattice when the ligand X is pyrimidine-2-thiol [35].

Hydrogen bonds with anions and solvent molecules can stabilize non-stacked crystal structures. The cations of $[Pd(terpy)(Hmcyt)][NO_3]_2{\cdot}5H_2O$ (Hmcyt = 1-methyl cytosine) stack in a head-to-head orientation, but they have a separation of over 3.8 Å. Each row of cations is interconnected by hydrogen bonding interactions between nitrate, water and the Hmcyt ligand [36].

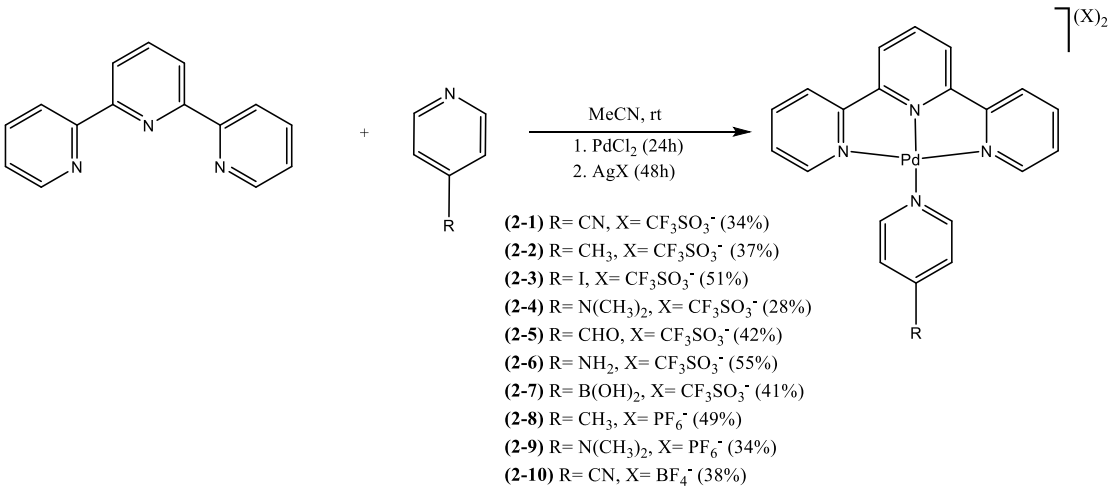
2.2 Results and Discussion

2.2.1 Synthesis of a series of mononuclear palladium (2,2':6',2''-terpyridine) triflate complexes

Considerable attention has been paid toward the synthesis and properties of the $[Pd(terpy)X]^{n+}$ systems. For comparison of the properties of mononuclear palladium (2,2':6',2"-terpyridine) complexes, all complexes were synthesised following the same synthetic procedure. All reactions were conducted in dry acetonitrile. In a typical experiment, commercially available 2,2':6',2"-terpyridine and palladium chloride were dissolved in acetonitrile and the reaction mixture was stirred at room temperature. After stirring for 24 hours, silver triflate (silver hexafluorophosphate for (**2-8**) and (**2-9**), and silver tetrafluoroborate for (**2-10**)) was added. In the absence of light, the reaction mixture was stirred for 48 hours. After 48 hours, the white precipitate (AgCl) was filtered. The target pyridine derivative was added to the reaction solution and stirred for 3 hours. The resulting solution was concentrated *via* rotary evaporation to remove excess acetonitrile solvent. The resulting solid was washed with diethyl ether, before being dried in *vacuo* to afford the title compound in acceptable yield.

Seven pyridine derivatives with different substituents at the *para* position have been used.

To assess the influence of the anion on the crystal packing structure, tetrafluoroborate and hexafluorophosphate were used instead of triflate. Following the previous synthetic procedure, complexes (**2-8**), (**2-9**), and (**2-10**) were synthesised. The conventional numbering system for terpyridine is shown in Figure 2.2.



Scheme 2.1: Synthesis of a series of mononuclear palladium (2,2':6',2''-terpyridine) complexes.

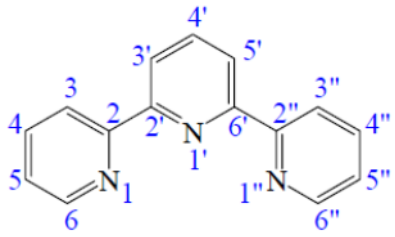


Figure 2.2: Terpyridine conventional numbering system.

2.2.2 X-ray crystallography

Single crystals suitable for X-ray diffraction were obtained for all of the complexes reported herein. Single crystals were grown by dissolution of the product in the minimum amount of acetonitrile and diffusion of diethyl ether vapour into this solution.

*2.2.2.1 Single crystal X-ray structure of 2,2':6',2''-terpyridine (4-cyanopyridine) palladium triflate [Pd(terpy)(4-cyanopyridine)](CF_3SO_3)$_2$ (**2-1**).*

Crystals of [Pd(terpy)(4-cyanopyridine)](CF_3SO_3)$_2$ were found to be colourless plates. The complex crystallises in the triclinic space group *P-1*. Terpyridine is coordinated to palladium as a tridentate ligand and the fourth position is occupied by 4-cyanopyridine. The coordination geometry of the palladium ion is distorted slightly from that found in the perfect square-planar Pd(II) complexes. As shown in Figure 2.3, space above and below the Pd cation is occupied by two triflate anions and one molecule of acetonitrile. Table 2.1 lists important bond lengths and angles for this complex. The angles between the adjacent N atoms in the plane deviate slightly from the theoretical value of 90° (N2A–Pd1A–N1A = 82.1(8)°, and N3A–Pd1A–N2A = 81.0(8)°) and N3A-Pd1A-N1A angle (163.1(8)°) is smaller than the theoretical value of 180°. The Pd–N2 distance to the central nitrogen atom of the terpyridine is shorter than those to the other two nitrogen atoms. A similar distorted square-planar geometry, which is a result of the geometric constraints imposed by coordination of the tridentate terpyridine molecule, also occurs in the related terpyridine complexes of palladium(II) and platinum(II), [Pd(terpy)(py)](ClO_4)$_2$ and [Pt(terpy)(pyridine-4-carboxylic acid)](NO_3) [37, 38]. The complex is slightly distorted compared to an idealized square planar geometry. This is observed in two parameters: the dihedral angle is defined as the angle between the normals to the mean terpyridine plane and X ligand plane, 90° in the ideal case. The tilt angle, is defined as the N-Pd-N angle using the N atom of the central pyridine ring and N atom of X ligand, 180° in the ideal case. This complex shows only slight geometric distortion in terms of both the dihedral angle 84.04(7)° and the tilt angle 179.7(9)°. The dihedral angle indicates that the terpyridine ring and 4-cyanopyridine are almost perpendicular to each other. This geometrical feature is comparable to those observed in

the related species containing methyl cytosine (84°) [36]. The terpyridine is almost coplanar with a maximum displacement of +0.095 and -0.097 Å exhibited by C11A and C4A, respectively, from the mean plane.

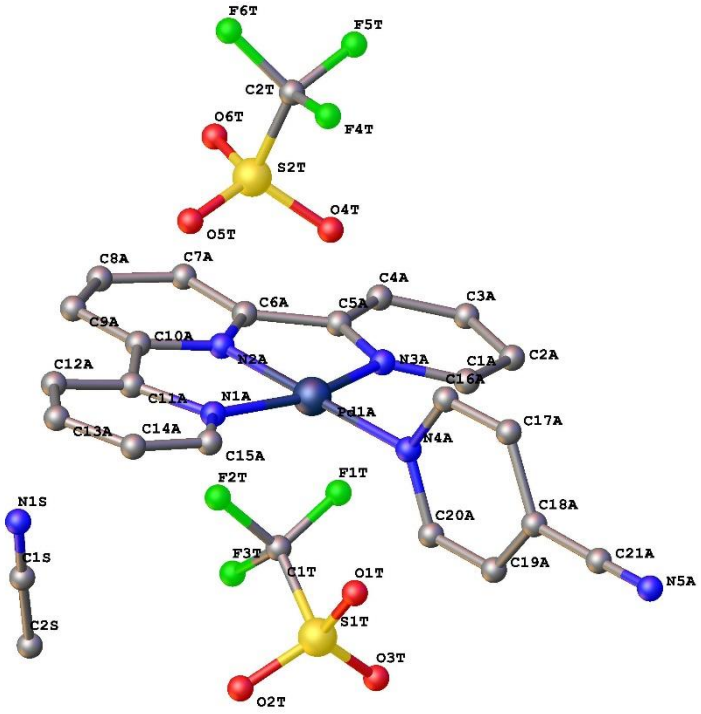
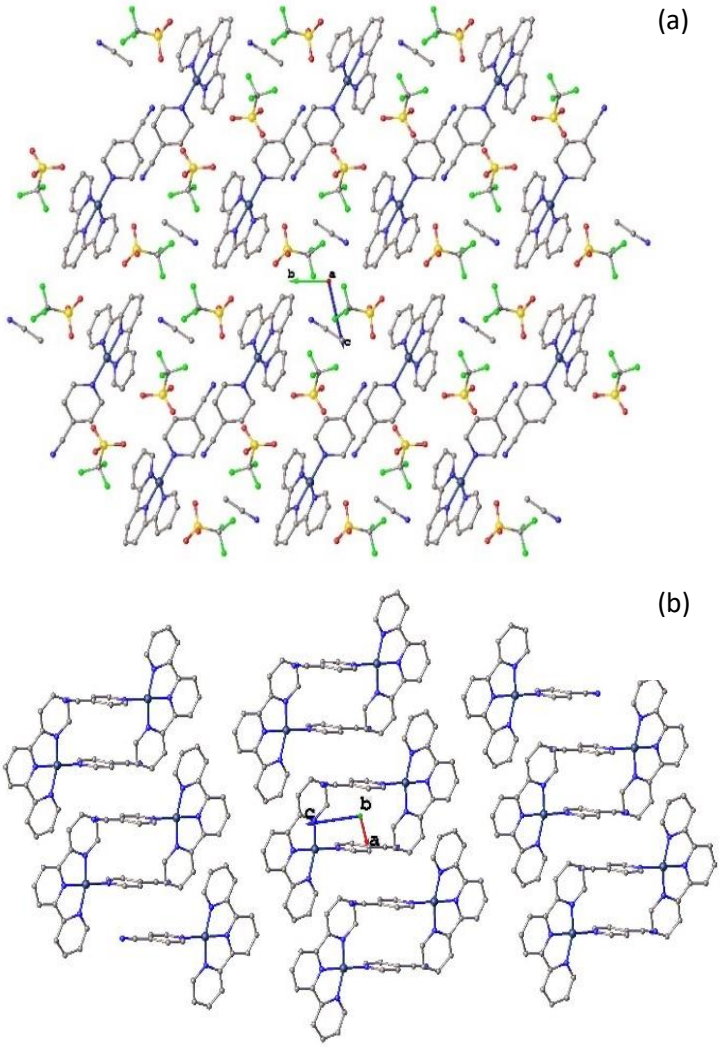


Figure 2.3: X-ray crystal structure of [Pd(terpy)(4-cyanopyridine)]$(CF_3SO_3)_2$ with crystallographically independent atom numbering scheme. Hydrogen atoms have been omitted for clarity. Atom colours: C: grey, O: red, N: blue, Pd: navy F: green and S: yellow.

Table 2.1: Selected bond lengths (Å) and angles (°) for [Pd(terpy)(4-cyanopyridine)]$(CF_3SO_3)_2$.

Pd1A-N1A	1.961(18)	N2A-Pd1A-N1A	82.1(8)
Pd1A-N2A	1.929(19)	N2A-Pd1A-N4A	179.7(9)
Pd1A-N3A	1.952(17)	N3A-Pd1A-N1A	163.1(8)
Pd1A-N4A	2.050(2)	N3A-Pd1A-N2A	81.0(8)

Molecules of (**2-1**) pack in channels parallel to the *a*-axis. The channels of cations are separated from each other by channels of triflate anions. Analysis of packing in the crystal structure showed that stacking interactions form chains with repeating the same overlap (Figure 2.4, a). In this case, one part of the Pd cation is partially overlapped with one neighbour, while the other part overlaps with the other neighbouring cation. The crystal packing evidences triflate anions located above and below the metal (Figure 2.4, b).



2.4: The packing diagram of [Pd(terpy)(4-cyanopyridine)]$(CF_3SO_3)_2$. (a) View down the *a*-crystal axis. (b) View down the *b*-crystal axis. Hydrogen atoms are omitted for clarity.

Each molecule packs with its neighbour *via* intermolecular face-to-face π· · ·π stacking interactions with centroid-centroid separations of 3.676 Å and the slip angle is 5.153° (Figure 2.5).

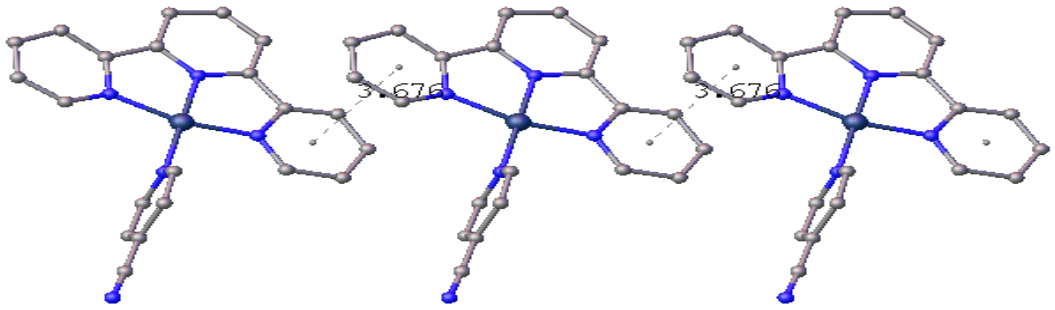


Figure 2.5: Representation of the π· · ·π interactions in [Pd(terpy)(4-cyanopyridine)](CF_3SO_3)$_2$. Dashed lines indicate the presence of π· · ·π interactions.

There is a net of hydrogen bonds, as shown in Figure 2.6. The triflate anion acts as a hydrogen bond acceptor and forms hydrogen bonds with acetonitrile molecule, 4-cyanopyridine, and terpyridine. The C–H…O distances lie in the range 2.206 – 2.995 Å. The C–H....N distances lie in the range 2.393 – 2.847 Å and the C–H…F distances lie in the range 2.485 – 2.897 Å. The cyano groups act as hydrogen bond acceptors *via* two sets of C–H…N hydrogen bonds. The C15A–H15A....N5A and C2S–H2Sc....N5A distances are 2.676 and 2.771 Å, respectively.

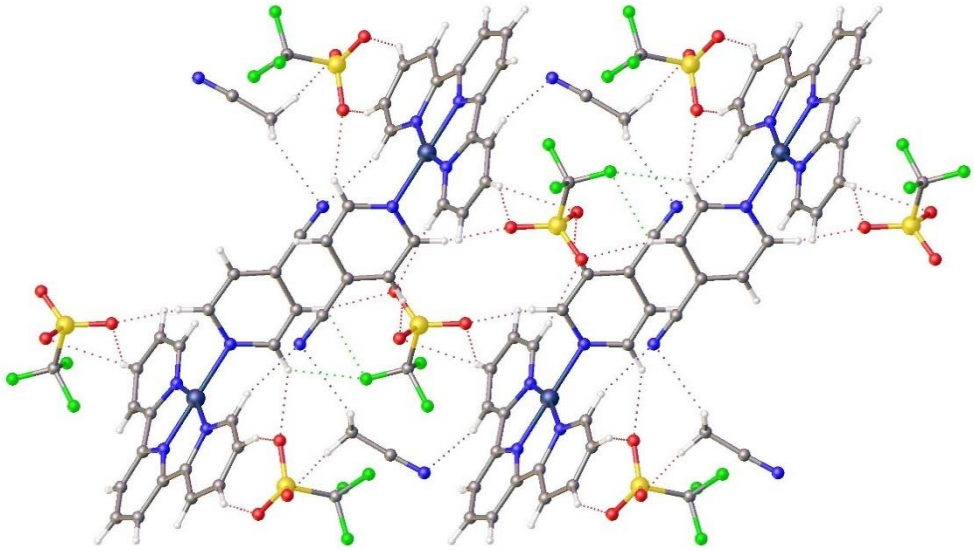


Figure 2.6: A net of hydrogen bonds links Pd(terpy) cations, triflate anions and acetonitrile molecules for [Pd(terpy)(4-cyanopyridine)]$(CF_3SO_3)_2$.

*2.2.2.2 Single crystal X-ray structure of 2,2':6',2''-terpyridine (4-methylpyridine) palladium triflate [Pd(terpy)(4-methylpyridine)]$(CF_3SO_3)_2$ (**2-2**).*

Crystals of [Pd(terpy)(4-methylpyridine)]$(CF_3SO_3)_2$ were found to be colourless plates. The complex crystallises in the triclinic space group *P-1*. The terpyridine moiety is coordinated to the Pd atom in a tridentate fashion, and distorts the square planar geometry of the Pd atom. As shown in Figure 2.7, space above and below the Pd cation is occupied by two triflate anions. Selected bond lengths and angles are summarized in Table 2.2. The central Pd–N bond is noticeably shorter than the other three Pd–N bonds. The Pd–N bond lengths are comparable to those found in other Pd(terpy) complexes in this chapter. The dihedral angle between the square planar coordination sphere of the Pd cation and the 4-methylpyridine ring amounts to 70.01(4)°. The tilt angle is 177.7(2)°. The terpyridine unit is almost coplanar with a maximum displacement of +0.045 and +0.035 Å exhibited by C14 and C8, respectively, from the mean plane. The geometric distortion from square planar in (**2-2**) is higher than that found in (**2-1**), as

seen in the values for the dihedral and tilt angles. In addition, mean planar deviations for the atoms of terpy unit in (**2-2**) are smaller than those in (**2-1**). As a result, the terpyridine unit in (**2-2**) shows less deviation from planarity than (**2-1**).

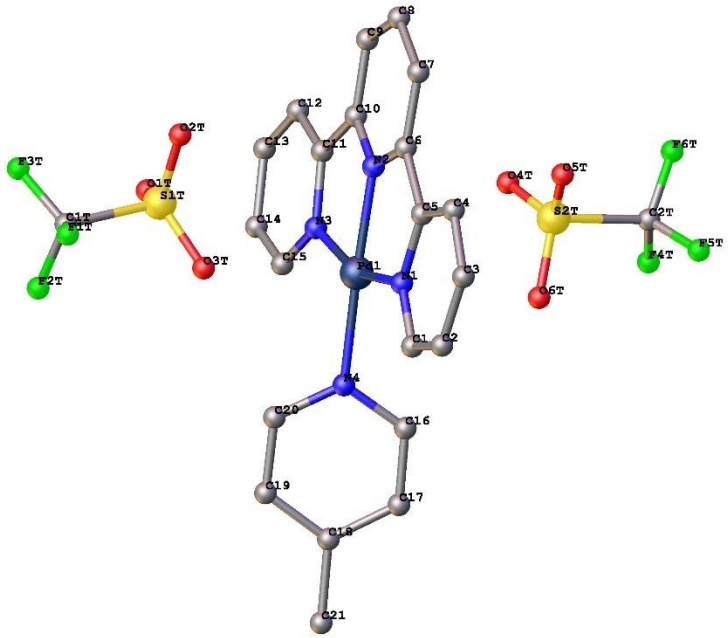


Figure 2.7: X-ray crystal structure of [Pd(terpy)(4-methylpyridine)]$(CF_3SO_3)_2$ with crystallographically independent atom numbering scheme. Hydrogen atoms have been omitted for clarity. Atom colours: C: grey, O: red, N: blue, Pd: navy F: green and S: yellow.

Table 2.2: Selected bond lengths (Å) and angles (°) for [Pd(terpy)(4-methylpyridine)]$(CF_3SO_3)_2$.

Pd1-N1	2.037(6)	N2-Pd1-N1	80.9(2)
Pd1-N2	1.937(6)	N2-Pd1-N4	177.7(2)
Pd1-N3	2.034(6)	N3-Pd1-N1	162.0(3)
Pd1-N4	2.031(6)	N3-Pd1-N2	81.1(2)

In the solid state, the molecules of (**2-2**) are packed as shown in Figure. 2.8, similar to that in complex [Pd(terpy)(pyridine)]$(ClO_4)_2$ [37]. The crystal packing shows triflate anions located above and below the Pd cation. Layers of molecules assemble on top of one another with the dominant interaction being π· · ·π stacking between the terminal pyridine ring of one terpyridine unit and another pyridine ring of a terpyridine unit in the next layer. The centroid-centroid separation is 3.958 Å and the slip angle is 2.677°.

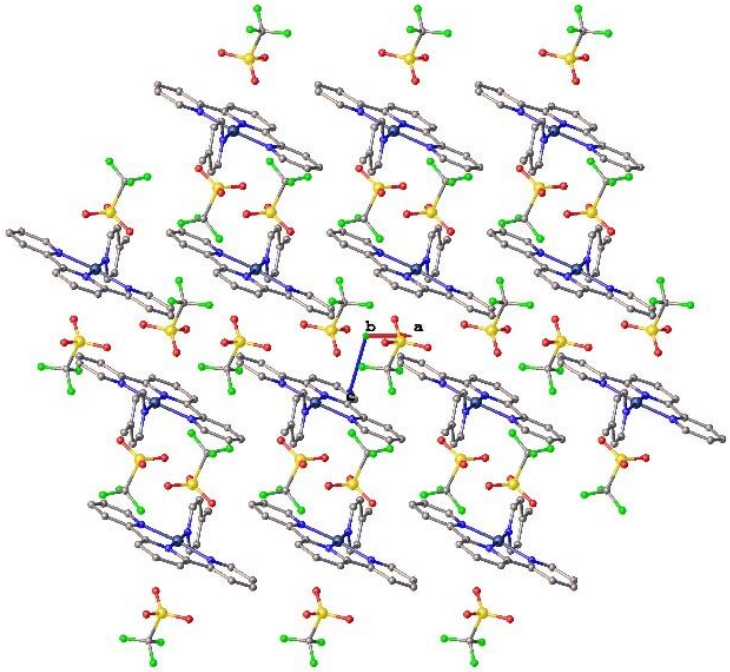


Figure 2.8: The packing diagram for [Pd(terpy)(4-methylpyridine)]$(CF_3SO_3)_2$ along the *b*-crystal axis. Hydrogen atoms are omitted for clarity.

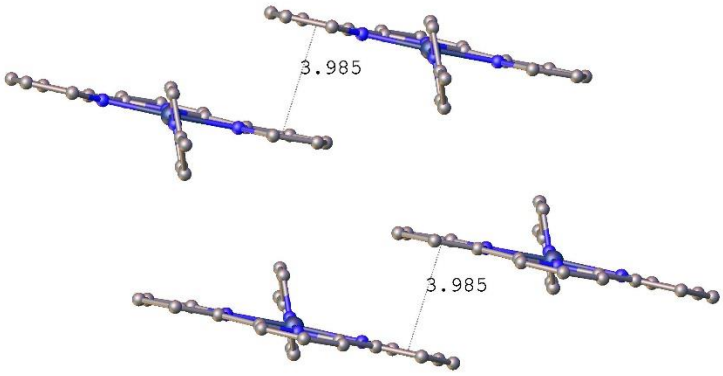


Figure 2.9: Representation of the π· · ·π interactions in [Pd(terpy)(4-methylpyridine)](CF$_3$SO$_3$)$_2$. Dashed lines indicate the presence of π· · ·π interactions.

The oxygen and fluorine atoms of the triflate anion act as hydrogen bond acceptors generating hydrogen bonds with hydrogen atoms of terpyridine and 4-methylpyridine, as shown in Figure 2.5. The C–H…O distances lie in the range 2.423 – 2.916 Å and the C–H…F distances lie in the range 2.398 – 2.977 Å.

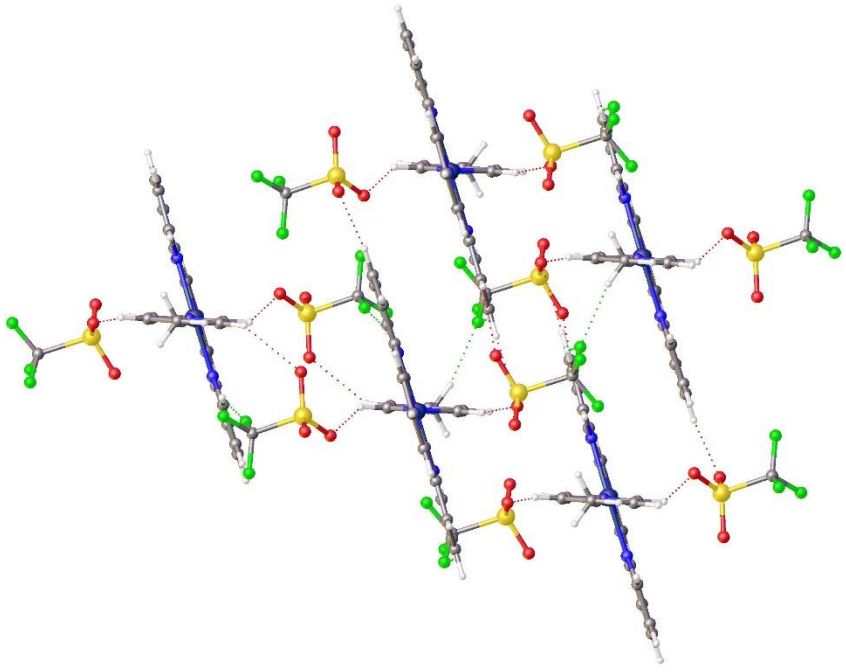


Figure 2.10: A net of hydrogen bonds link Pd(terpy) cations and triflate anions for [Pd(terpy)(4-methylpyridine)](CF$_3$SO$_3$)$_2$.

*2.2.2.3 Single crystal X-ray structure of 2,2':6',2''-terpyridine (4-iodopyridine) palladium triflate [Pd(terpy)(4-iodopyridine)](CF_3SO_3)$_2$ (**2-3**).*

This complex crystallises in the triclinic space group *P-1*. There are two independent molecules in the asymmetric unit and each molecule adopts a distorted square planar geometry. Figure 2.11 shows the coordination geometry and atom labelling scheme for complex (**2-3**). Four triflate anions are presented in the asymmetric unit. Rotational disorder is exhibited by one of the triflate anions. Table 2.3 lists important bond lengths and angles for two independent molecules in this complex. The two molecules are referred to as molecule **A** (containing Pd1A) and molecule **B** (containing Pd1B). The angles N2–Pd1–N1 and N3-Pd-N2 (average = 80.82(11)°) are less than the ideal value of 90°. The angles N3A–Pd1A–N1A = 161.57(11)° and N3B–Pd1B–N1B = 161.64(11)° deviate from the ideal bond angle of 180°. The Pd–N1, Pd–N3 and Pd–N4 distances are in the range 2.031(3)-2.049(3) Å. These bond lengths are slightly longer than other previously reported Pd–N distances (complexes (**1-2**) and (**2-2**)). The central Pd–N2 bond (1.933(3) Å) is noticeably shorter than the other three Pd–N bonds in molecules (**A**) and (**B**). The 4-iodopyridine ligands (molecules **A** and **B**) are significantly bent with respect to Pd(terpy) planes forming dihedral angles of 57.63(8)° and 54.15(8)°, respectively. These geometrical features are similar to those observed in the related species (complexes (**2-1**) and (**2-2**)). However, the latter complexes have an arrangement of the monodentate pyridyl donor almost normal to the tridentate ligands (84.04(7)° and 70.01(4)°, respectively). The tilt angles for molecules (**A**) and (**B**) are 179.43(11)° and 178.90(11)°, respectively. The terpyridine unit of molecule (**A**) is more coplanar than that of molecule (**B**) with a maximum displacement of +0.050 (B +0.092) and -0.057 (B -0.095) Å exhibited by C4A(N1B) and C1A(C3B), respectively, from the mean plane.

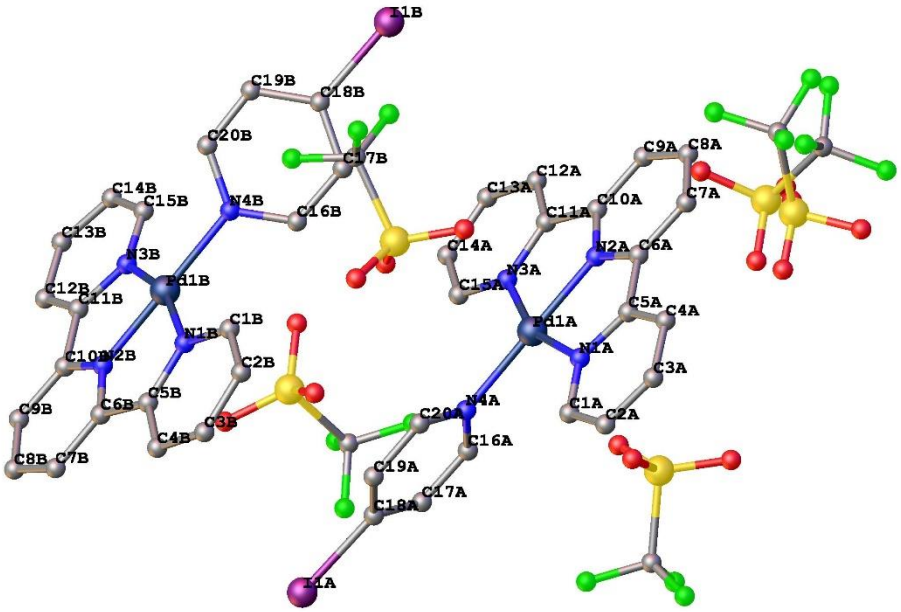


Figure 2.11: X-ray crystal structure of [Pd(terpy)(4-iodopyridine)]$(CF_3SO_3)_2$ with crystallographically independent atom numbering scheme. Hydrogen atoms have been omitted for clarity. The disorder in the triflate anion is shown. Atom colours: C: grey, O: red, N: blue, Pd: navy, I: purple, F: green and S: yellow.

Table 2.3: Selected bond lengths (Å) and angles (°) for [Pd(terpy)(4-iodopyridine)]$(CF_3SO_3)_2$.

Pd1A-N1A	2.041(3)	N2A-Pd1A-N1A	80.66(11)
Pd1A-N2A	1.933(3)	N2A-Pd1A-N4A	179.43(11)
Pd1A-N3A	2.049(3)	N3A-Pd1A-N1A	161.57(11)
Pd1A-N4A	2.031(3)	N3A-Pd1A-N2A	80.92(11)
Pd1B-N1B	2.040(3)	N2B-Pd1B-N1B	81.15(11)
Pd1B-N2B	1.934(3)	N2B-Pd1B-N4B	178.90(11)
Pd1B-N3B	2.036(3)	N3B-Pd1B-N1B	161.64(11)
Pd1B-N4B	2.039(3)	N3B-Pd1B-N2B	80.55(11)

In the solid state, the molecules of (**2-3**) are packed as shown in Figure 2.12, similar to that in complex [Pt(terpy)(MeCN)][$(SbF_6)_2$] [39]. Complex (**2-3**) exhibits a stacking of parallel sheets consisting of cations and anions.

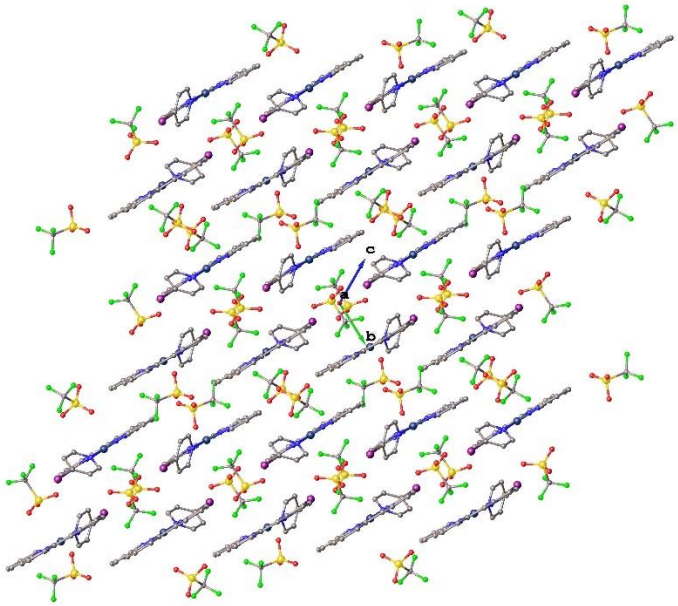


Figure 2.12: The packing diagram for [Pd(terpy)(4-iodopyridine)]$(CF_3SO_3)_2$ along the *a*-crystal axis. Hydrogen atoms are omitted for clarity.

Adjacent complexes are included in a complex web of intermolecular interactions forming an infinite three dimensional network. As shown in Figure 2.13, the molecules of (**2-3**) undergo a series of face-to-face π· · ·π interactions indicated by ring centroid–ring centroid separations of 3.750, 3.902 and 3.923 Å (corresponding slip angles are 3.089°, 2.090° and 2.295°). This arrangement is further stabilised by a series of hydrogen bonds between Pd cations and triflate anions.

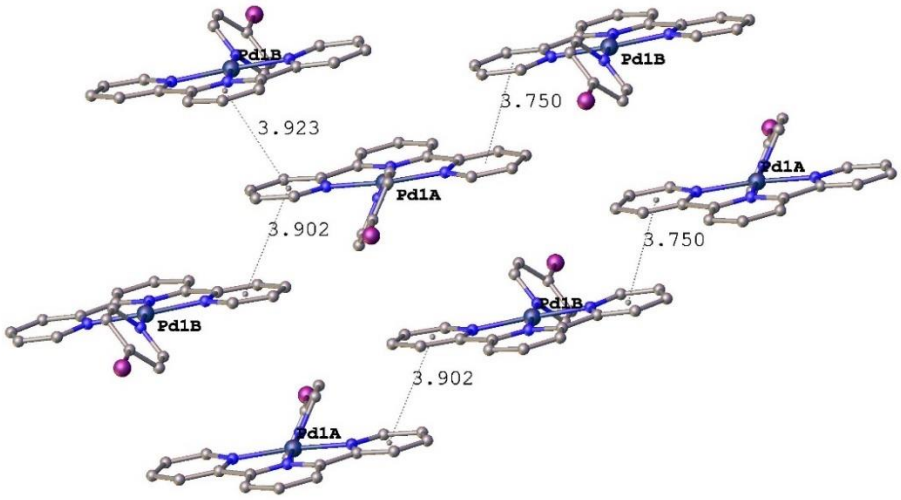


Figure 2.13: Representation of the π· · ·π interactions in [Pd(terpy)(4-iodopyridine)]$(CF_3SO_3)_2$. Dashed lines indicate the presence of π· · ·π interactions.

The oxygen and fluorine atoms of triflate anion act as hydrogen bond acceptors generating hydrogen bonds with hydrogen atoms of terpyridine and 4-iodopyridine, as shown in Figure 2.14. The C–H…O distances lie in the range 2.362 – 2.940 Å and the C–H…F distances lie in the range 2.551 – 2.999 Å.

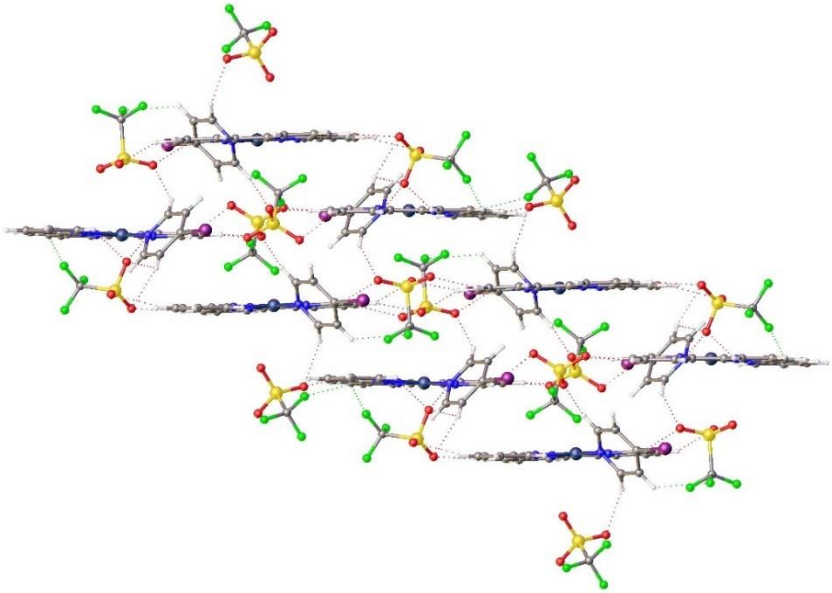


Figure 2.14: A net of hydrogen bonds links Pd(terpy) cations and triflate anions for [Pd(terpy)(4-iodopyridine)]$(CF_3SO_3)_2$.

*2.2.2.4 Single crystal X-ray structure of 2,2':6',2''-terpyridine (4-dimethylaminopyridine) palladium triflate [Pd(terpy)(4-dimethylaminopyridine)]$(CF_3SO_3)_2$ (**2-4**).*

This complex crystallises in the monoclinic space group $P2_1/c$. The asymmetric unit of (**2-4**) contains a pair of crystallographically independent cations and four anions, as shown in Figure 2.10. The two molecules will be referred to as molecule **A** (containing (Pd1A) and molecule **B** (containing Pd1B). The coordination geometry around the palladium(II) ion is considerably distorted from the perfect square-plane. This distortion leads to a narrowing of both N1–Pd–N2 and N2–Pd–N3 angles to 81.15(2), and 81.10(2)° (average of molecule **A** and **B**), respectively, and also a significant shortening of Pd–N2 distances (less than 2 Å ≈ 1.936(5) Å) compared to the other Pd–N distances (more than 2 Å ≈ 2.029(5) Å), as shown in Table 2.4. In general, bond distances for molecule (**A**) are slightly shorter than those for molecule (**B**). Bond distances and angles of this complex compare well with those already reported [Au(terpy)(4-dimethylaminopyridine)]$(CF_3SO_3)_2$ [40].

The angles between the square planar coordination geometry of the Pd(terpy) cation and the plane of 4-dimethylaminopyridine are 77.92(5)° (molecule **A**) and 85.35(5)° (molecule **B**). The dihedral angle for molecule (**B**) indicates that the terpyridine ring and 4-dimethylaminopyridine are almost perpendicular to each other. This geometrical feature is comparable to those observed in the related species containing Au(terpy)(4-dimethylaminopyridine)]$(CF_3SO_3)_2$ (89.15°) [40]. In terms of tilt angles, two molecules have similar values (molecule (**A**) is 178.8(2)° and molecule (**B**) is 178.27(19)°).

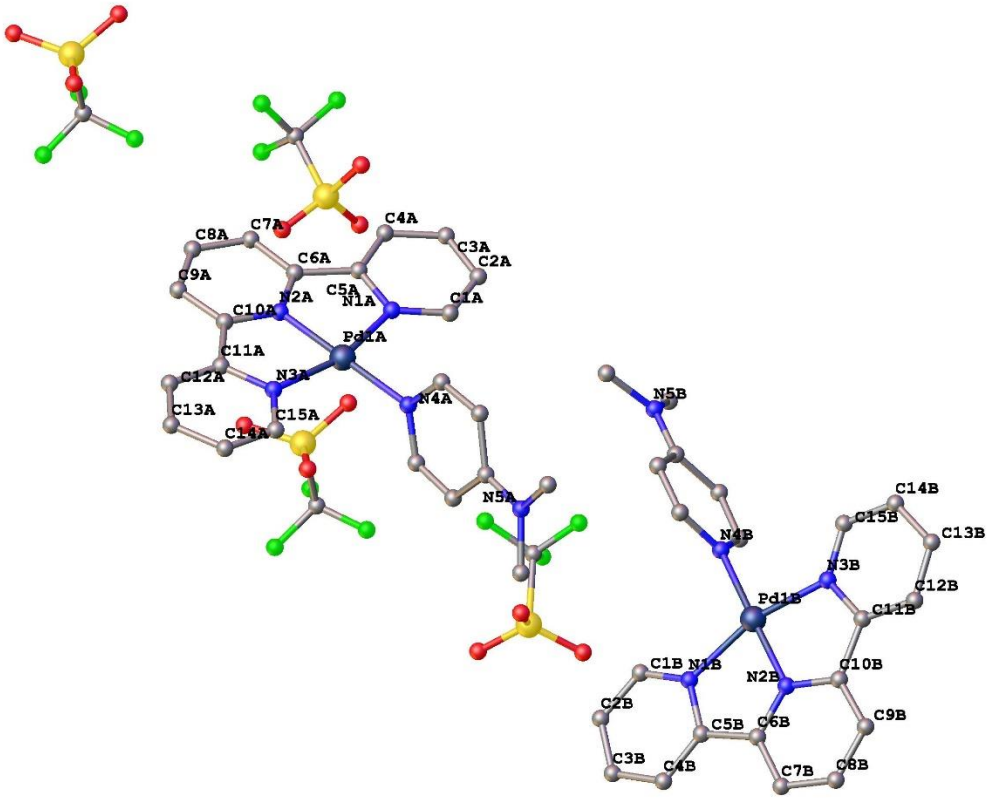


Figure 2.15 X-ray crystal structure of [Pd(terpy)(4-dimethylaminopyridine)]$(CF_3SO_3)_2$ with crystallographically independent atom numbering scheme. Hydrogen atoms have been omitted for clarity. Atom colours: C: grey, O: red, N: blue, Pd: navy F: green and S: yellow.

Table 2.4: Selected bond lengths (Å) and angles (°) for [Pd(terpy)(4-dimethylaminopyridine)]$(CF_3SO_3)_2$.

Pd1A-N1A	2.017(5)	N2A-Pd1A-N1A	81.6(2)
Pd1A-N2A	1.929(5)	N2A-Pd1A-N4A	178.8(2)
Pd1A-N3A	2.032(6)	N3A-Pd1A-N1A	162.6(2)
Pd1A-N4A	2.036(5)	N3A-Pd1A-N2A	81.1(2)
Pd1B-N1B	2.037(5)	N2B-Pd1B-N1B	80.7(2)
Pd1B-N2B	1.943(5)	N2B-Pd1B-N4B	178.27(19)

Pd1B-N3B	2.033(5)	N3B-Pd1B-N1B	161.76(19)
Pd1B-N4B	2.017(5)	N3B-Pd1B-N2B	81.03(19)

The two molecules are arranged in a tilted fashion with respect to each other with a dihedral angle 45.87°, as shown in Figure 2.16. Analysis of packing in the crystal structure showed that cations have staggered orientation, as shown in Figure 2.17 a. The triflate anions fill the space between cations (Figure 2.17 b).

The π· · ·π stacking distance between two terpyridine moieties of neighbouring (**B**) molecules amounts to 3.907Å (corresponding slip angle is 2.793°). In terms of molecule (**A**), the outer pyridyl ring and the other outer pyridyl ring of another molecule have a centroid–centroid distance of 4.307 Å, indicating no significant π· · ·π interaction is present. The different orientation of the triflate anions around the two molecules has an influence on the π· · ·π interaction, as shown in Figure 2.18.

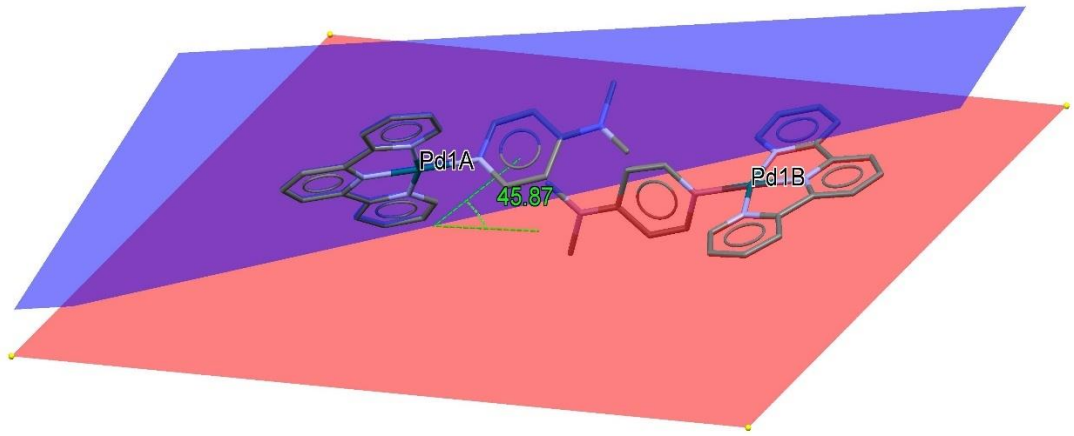


Figure 2.16: The dihedral angle between the planes of molecule A and molecule B in[Pd(terpy)(4-dimethylaminopyridine)] $(CF_3SO_3)_2$.

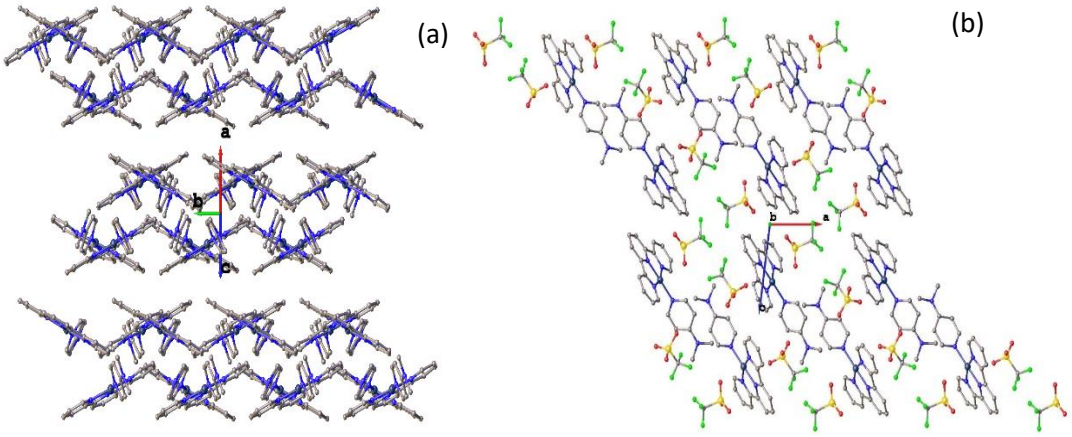


Figure 2.17: The packing diagram for [Pd(terpy)(4-dimethylaminopyridine)]$(CF_3SO_3)_2$. (a) along 101 plane, (b) along the *b*-crystal axis. Hydrogen atoms are omitted for clarity.

The terpyridine unit of molecule (**B**) is more coplanar than that of molecule (**A**) with a maximum displacement of +0.046 (**A** +0.080) and -0.054 (**A** -0.083) Å exhibited by C9B(C4A) and C14B(C1A), respectively, from the mean plane.

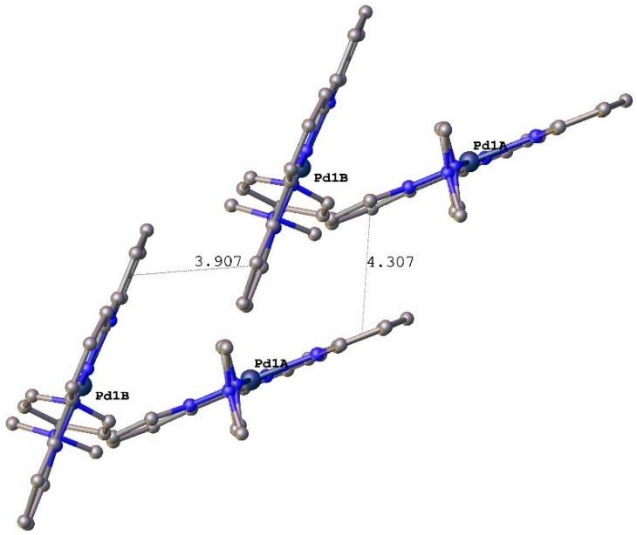


Figure 2.18: Representation of the π· · ·π interactions in [Pd(terpy)(4-dimethylaminopyridine)] $(CF_3SO_3)_2$. Dashed lines indicate the shortest distances between two terminal pyridyl rings in molecule (A) and molecule (B).

There is a net of hydrogen bonds, as shown in Figure 2.19. The triflate anion acts as a hydrogen bond acceptor and forms weak hydrogen bonds with 4-dimethylaminopyridine and terpyridine. The C–H…O distances lie in the range 2.248 – 2.949 Å and the C–H…F distances lie in the range 2.590 – 2.982 Å.

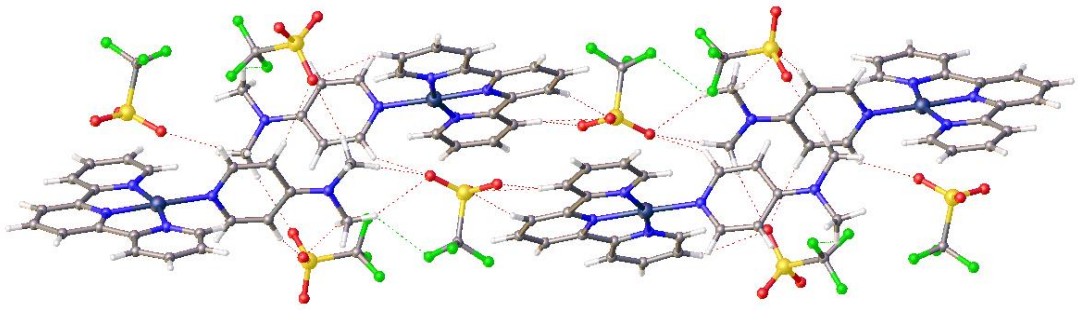


Figure 2.19: A net of hydrogen bonds links Pd(terpy) cations and triflate anions for [Pd(terpy)(4-dimethylaminopyridine)]$(CF_3SO_3)_2$.

*2.2.2.5 Single crystal X-ray structure of 2,2':6',2''-terpyridine (4-pyridinecarboxaldehyde) palladium triflate [Pd(terpy)(4-pyridinecarboxaldehyde)]$(CF_3SO_3)_2$ (**2-5**).*

This complex crystallises in the triclinic space group *P-1* with two chemically identical but crystallographically distinct molecules in the asymmetric unit (Figure 2.20). This complex forms distorted square-planar coordination around Pd cation. As shown in Table 2.5, angles and bond lengths for molecule (**A**) and molecule (**B**) are almost identical within experimental error. As expected, the *cis* N–Pd–N angles, in the range of 81.04(9) – 81.28(9)°, deviate from the ideal value of 90°. The angle N3-Pd-N1 (average = 162.28°) deviates from the ideal value of 180°. In addition, the bond between the central nitrogen and the Pd^{2+} is the shortest (≈ 1.934 Å) with two longer bonds between the terminal nitrogen atoms and the Pd^{2+} (≈ 2.031 Å). Similar values were observed in the crystal structure of the complex [Pt(terpy)(4-CO_2py)](NO_3) [38]. The planar 4-

pyridinecarboxaldehyde ligands coordinate out of the Pd(terpy) planes with dihedral angles of 72.04(6)° and 73.41(6)° corresponding to molecule (**A**) and molecule (**B**), respectively. In terms of tilt angles, molecule (**B**) (175.99(8)°) shows higher deviation than molecule (**A**) (178.74(8)°).

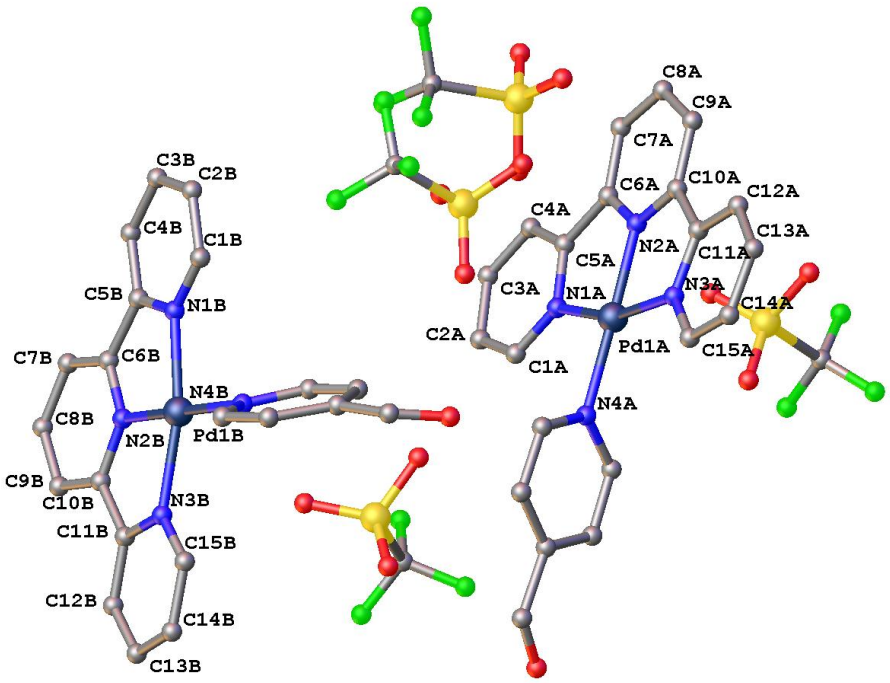


Figure 2.20: X-ray crystal structure of [Pd(terpy)(4-pyridinecarboxaldehyde)]$(CF_3SO_3)_2$ with crystallographically independent atom numbering scheme. Hydrogen atoms have been omitted for clarity. Atom colours: C: grey, O: red, N: blue, Pd: navy F: green and S: yellow.

Table 2.5: Selected bond lengths (Å) and angles (°) for [Pd(terpy)(4-pyridinecarboxaldehyde)]$(CF_3SO_3)_2$.

Pd1A-N1A	2.030(2)	N2A-Pd1A-N1A	81.28(9)
Pd1A-N2A	1.934(2)	N2A-Pd1A-N4A	178.74(8)
Pd1A-N3A	2.033(2)	N3A-Pd1A-N1A	162.34(9)
Pd1A-N4A	2.031(2)	N3A-Pd1A-N2A	81.14(9)

Pd1B-N1B	2.026(2)	N2B-Pd1B-N1B	81.24(9)
Pd1B-N2B	1.933(2)	N2B-Pd1B-N4B	175.99(8)
Pd1B-N3B	2.037(2)	N3B-Pd1B-N1B	162.22(9)
Pd1B-N4B	2.029(2)	N3B-Pd1B-N2B	81.04(9)

The terpyridine unit of molecule (**B**) is more coplanar than that of molecule (**A**) with a maximum displacement of +0.074 (**A** +0.084) and -0.070 (**A** -0.082) Å exhibited by C4B(**A** N2A) and C7B(**A** C13A), respectively, from the mean plane.

Two molecules are nearly parallel with an angle between the planes of molecule (**A**) and molecule (**B**) of 12.58° (Figure 2.21). The close to planar terpyridine units of the cations undergo a series of face-to-face π· · ·π interactions indicated by centroid-centroid separations of 3.627 and 3.763 Å (corresponding slip angles are 175.111° and 0.0°, respectively) (Figure 2.22).

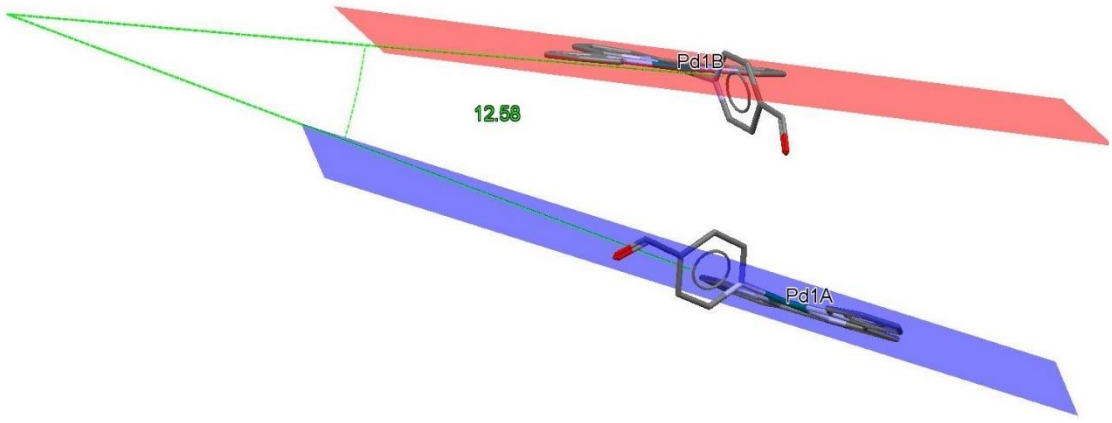


Figure 2.21: The dihedral angle between the planes of molecule (A) and molecule (B) in [Pd(terpy)(4- pyridinecarboxaldehyde)]$(CF_3SO_3)_2$.

Analysis of packing in the crystal structure showed that the cations have a ladder orientation, as shown in Figure 2.23 a. The triflate anions arrange around the cations to form channels along the *b*-axis (Figure 2.23 b).

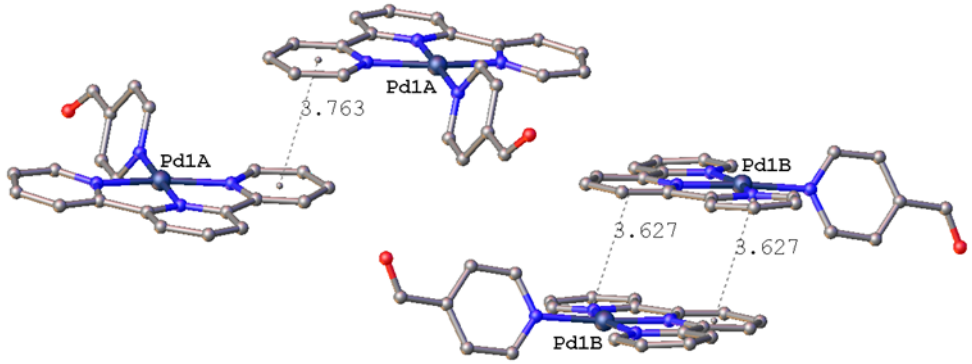


Figure 2.22: Representation of the π· · ·π interactions in [Pd(terpy)(4-pyridinecarboxaldehyde)]$(CF_3SO_3)_2$. Dashed lines indicate the presence of π· · ·π interactions.

This arrangement is further stabilised by a series of hydrogen bonds between aromatic hydrogens, carboxaldehyde unit and triflate anion (Figure 2.24). Carboxaldehyde moieties are involved in intermolecular hydrogen bonds *via* both oxygen and hydrogen atoms and act as hydrogen bond acceptor and donor, respectively. In addition, the triflate anions act as hydrogen bond acceptors and form hydrogen bonds with 4-pyridinecarboxaldehyde and terpyridine moieties. The C–H…O distances lie in the range 2.266 – 2.944 Å and the C–H…F distances lie in the range 2.520 – 2.942 Å.

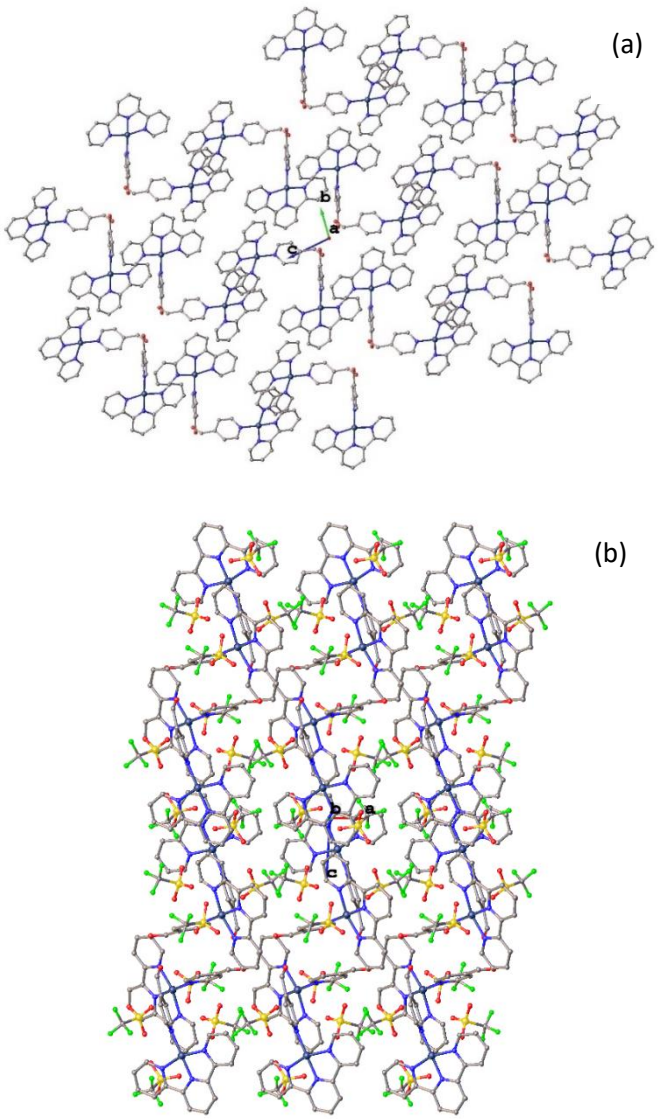


Figure 2.23: The packing diagram for [Pd(terpy)(4-pyridinecarboxaldehyde)]$(CF_3SO_3)_2$. (a) Along the *a*-crystal axis, (b) along the *b*-crystal axis. Hydrogen atoms and anions are omitted for clarity.

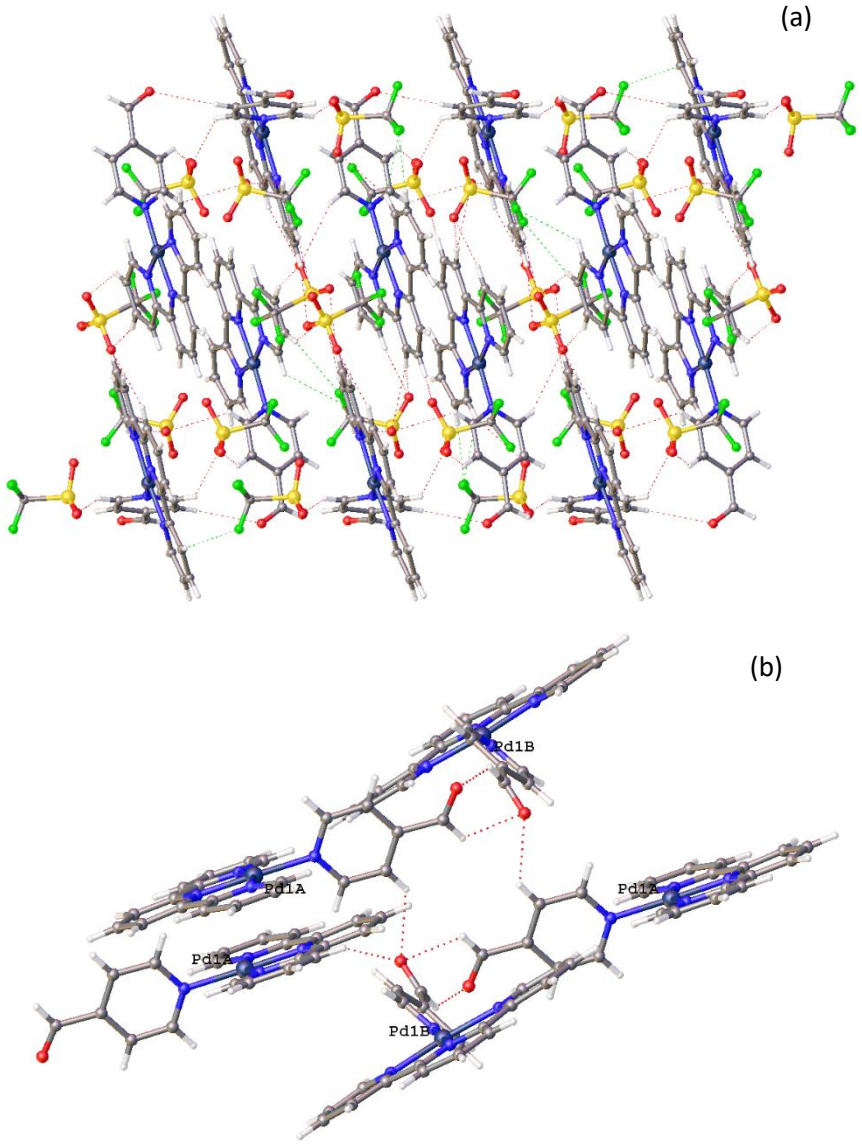


Figure 2.24: (a) A net of hydrogen bonds links Pd(terpy) cations and triflate anions for [Pd(terpy)(4-pyridinecarboxaldehyde)]$(CF_3SO_3)_2$. (b) Hydrogen bonds between 4-pyridinecarboxaldehyde units.

2.2.2.6 Single crystal X-ray structure of 2,2':6',2''-terpyridine (4-aminopyridine) palladium triflate [Pd(terpy)(4-aminopyridine)](CF_3SO_3)$_2$ ***(2-6)***.

Crystals of [Pd(terpy)(4-aminopyridine)](CF_3SO_3)$_2$ were found to be colourless blocks. This complex crystallises in the monoclinic space group *I2/a*. Figure 2.25 exhibits the crystal structure of complex (**2-6**). As before, the angles between the adjacent nitrogen atoms in the plane (≈ 80.90(15)°) and N3-Pd1-N1 angle (161.76(14)°) deviate slightly from the theoretical values of 90° and 180°, respectively. In addition, the bond between central nitrogen and the Pd atom is the shortest, with two longer bonds between the terminal nitrogen atoms and the Pd atom. In terms of the C18-N5 bond between the amine group and the pyridine ring (1.348(6) Å), it is shorter than a normal single bond C-NH_2 (≈ 1.44 Å), which is attributed to the delocalization of the lone pair electrons of the amine nitrogen into the pyridine ring, indicating that the C-NH_2 bond has some double-bond character [41]. These geometrical features are comparable to those observed in the related species [Pt(6-phenyl-2,2'-bipyridine)(4-aminopyridine)] [41].

The 4-aminopyridine ligand is slightly bent with respect to the plane of Pd(terpy) forming a dihedral angle of 76.59(7)°. This complex shows only slight geometric distortion in terms of the tilt angle 178.44(16)°. In terms of planarity, the terpyridine moiety slightly deviates with a maximum displacement of +0.123 and -0.115 Å exhibited by C3 and N1, respectively, from the mean plane.

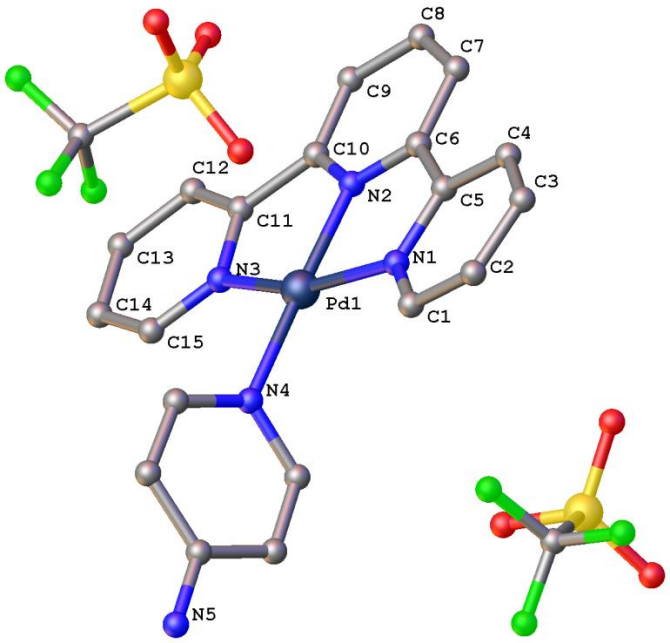


Figure 2.25: X-ray crystal structure of [Pd(terpy)(4-aminopyridine)]$(CF_3SO_3)_2$ with crystallographically independent atom numbering scheme. Hydrogen atoms have been omitted for clarity. Atom colours: C: grey, O: red, N: blue, Pd: navy F: green and S: yellow.

Table 2.6: Selected bond lengths (Å) and angles (°) for [Pd(terpy)(4-aminopyridine)]$(CF_3SO_3)_2$.

Pd1-N1	2.035(4)	N2-Pd1-N1	80.85(15)
Pd1-N2	1.953(3)	N2-Pd1-N4	178.44(16)
Pd1-N3	2.035(4)	N3-Pd1-N1	161.76(14)
Pd1-N4	2.037(3)	N3-Pd1-N2	80.95(15)
C18-N5	1.348(6)		

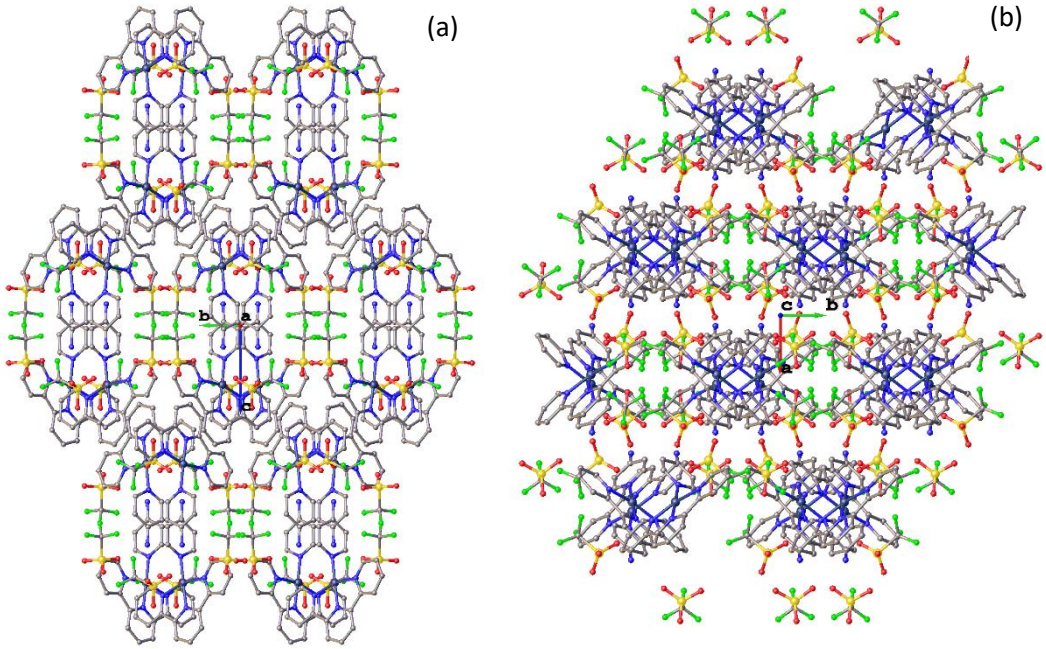


Figure 2.26: The packing diagram for [Pd(terpy)(4-aminopyridine)]$(CF_3SO_3)_2$. (a) Along the *a*-crystal axis. (b) Along the *c*-crystal axis. Hydrogen atoms are omitted for clarity.

Importantly, the positioning of the cations allows the triflate anions to fit well into the space between two adjacent cations (Figure 2.26). The crystal packing of (**2-6**) is different from previous Pd complexes in this Chapter. Molecules of (**2-6**) pack in channels of cations and anions parallel to *c*-axis. Each channel of cations is surrounded by four triflate anion channels and *vice versa*, similar to that found in [Pt(terpy)$(NCCH_3)](CF_3SO_3)_2$ [43]. π· · ·π Stacking is observed between central and central rings of adjacent cations. The distance between two terpyridine moieties of neighbouring molecules amounts to 3.700 Å (corresponding slip angle is 0.0°) (Figure 2.27).

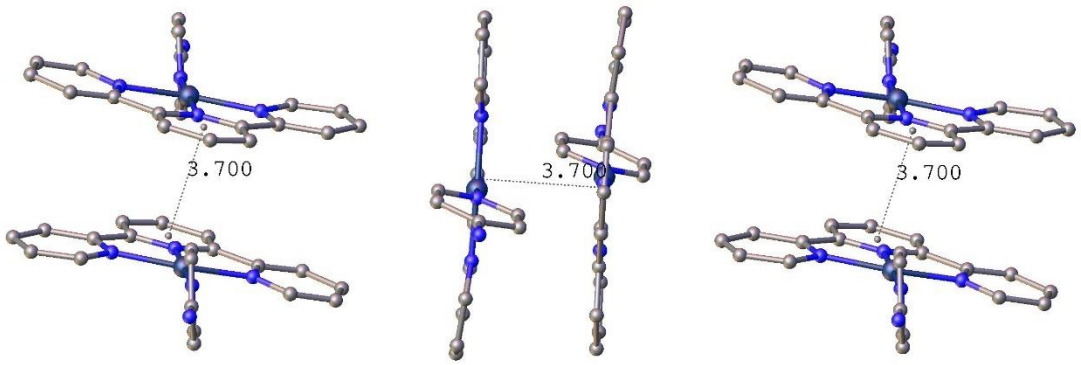


Figure 2.27: Representation of the π· · ·π interactions in [Pd(terpy)(4-aminopyridine)]$(CF_3SO_3)_2$. Dashed lines indicate the presence of π· · ·π interactions.

Within the crystal packing cations and anions are linked by a number of hydrogen bonds where the terpyridine acts as donor and triflate oxygen and fluorine atoms act as acceptors. The C–H…O distances lie in the range 2.303 – 2.867 Å and the C–H…F distances lie in the range 2.573 – 2.972 Å.

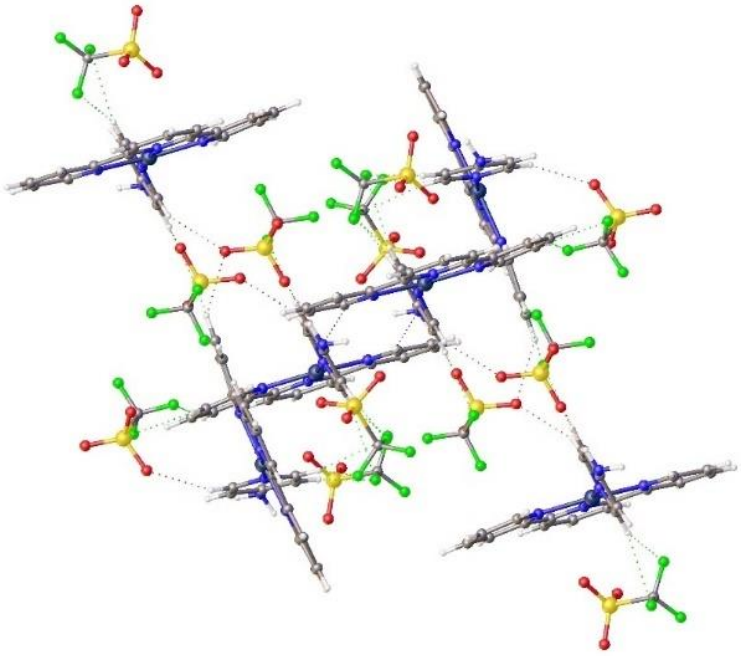


Figure 2.28: A net of hydrogen bonds links Pd(terpy) cations and triflate anions for [Pd(terpy)(4-aminopyridine)]$(CF_3SO_3)_2$.

Interestingly, the amine group of the 4-aminopyridine ligand acts as donor *via* three sets of N–H…O hydrogen bonds and as an acceptor *via* one C–H…N hydrogen bond. The N5–H…O1T, N5–H…O2T and N5–H…O6T distances are 2.714, 2.834 and 2.017 Å, respectively. The C15–H…N5 distance is 2.959 Å.

2.2.2.7 Single crystal X-ray structure of 2,2':6',2''-terpyridine (4-pyridineboronic acid) palladium triflate [Pd(terpy)(4-pyridineboronic acid)](CF_3SO_3)$_2$ ***(2-7).***

Crystals of [Pd(terpy)(4-pyridineboronic acid)](CF_3SO_3)$_2$ were found to be colourless blocks. The complex crystallises in the triclinic space group *P-1*. As shown in Figure 2.29, space above and below the Pd cation is occupied by two triflate anions. The bond lengths and angles are detailed below in Table 2.7. All bond lengths and angles agree well with other structural reports of palladium and platinum terpyridine complexes in this chapter and in the literature [42]. The central Pd–N bond (1.883(14) Å) is noticeably shorter than the other Pd–N bonds and the analogous bond in [Pt(terpy)(4-pyridineboronic acid)](CF_3SO_3)$_2$ (1.930 Å)[42]. The *cis* N–Pd–N angles and N3–Pd–N1 angle deviate from the ideal values by 9° and 18°, respectively. These values are similar to those found in the Pt analogue [42]. The 4-pyridineboronic acid ligand is slightly bent with respect to the plane of terpyridine forming a dihedral angle of 74.26(5)°. In terms of tilt angle, this complex indicates slight deviation with 1° from the ideal value.

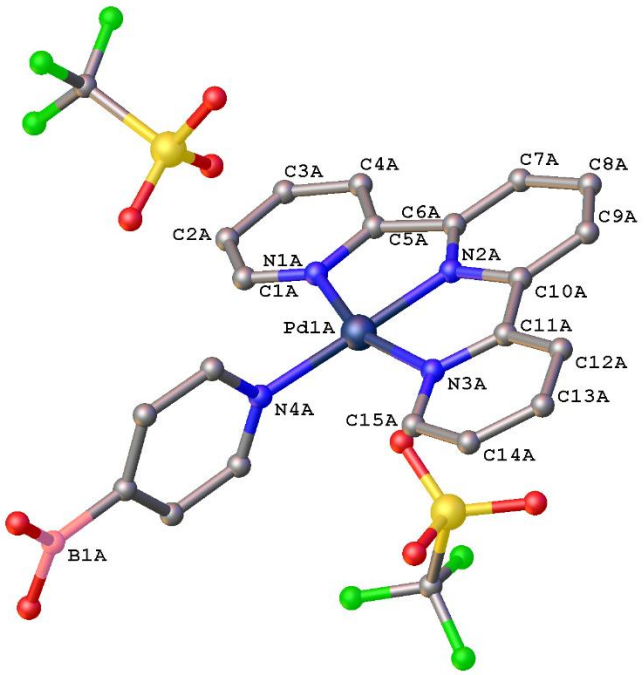


Figure 2.29: X-ray crystal structure of [Pd(terpy)(4- pyridineboronic acid)]$(CF_3SO_3)_2$ with crystallographically independent atom numbering scheme. Hydrogen atoms have been omitted for clarity. Atom colours: B: pink, C: grey, O: red, N: blue, Pd: navy F: green and S: yellow.

Table 2.7: Selected bond lengths (Å) and angles (°) for [Pd(terpy)(4-pyridineboronic acid)]$(CF_3SO_3)_2$.

Pd1A-N1A	2.045(14)	N2A-Pd1A-N1A	80.1(6)
Pd1A-N2A	1.883(14)	N2A-Pd1A-N4A	179.0(7)
Pd1A-N3A	2.046(13)	N3A-Pd1A-N1A	162.0(6)
Pd1A-N4A	1.996(14)	N3A-Pd1A-N2A	81.9(6)

The terpyridine is almost coplanar with a maximum displacement of +0.093 and -0.094 Å exhibited by C15A and C1A, respectively, from the mean plane.

In the solid state, the molecules of (**2-7**) are packed as shown in Figure. 2.30, similar to that in complex [Pt(terpy)(4-pyridineboronic acid)]$(CF_3SO_3)_2$ [42]. Molecules of (**2-7**)

pack in parallel sheets of cations separated by channels of triflate anions. The crystal packing evidences triflate anions located above and below the Pd cation. The outer pyridyl ring and the other outer pyridyl ring of another molecule have a centroid–centroid distance of 4.501 Å, indicating π· · ·π interactions are absent.

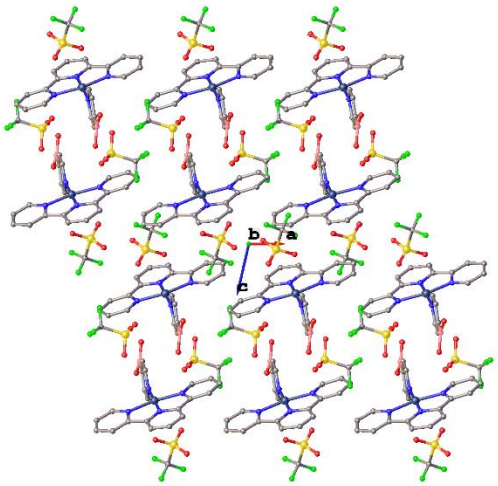


Figure 2.30: The packing diagram of [Pd(terpy)(4- pyridineboronic acid)]$(CF_3SO_3)_2$ along the *b*-crystal axis. Hydrogen atoms are omitted for clarity.

Within the crystal packing cations and anions are linked by a number of hydrogen bonds where the terpyridine ligands act as donors and triflate oxygen and fluorine atoms act as acceptors (Figure 2.31). The C–H…O distances lie in the range 2.269 – 2.944 Å and the C–H…F distances lie in the range 2.216 – 2.954 Å. In addition, the boronic acid group of the 4-pyridineboronic acid ligand acts as a donor *via* three sets of O–H…O hydrogen bonds and as an acceptor *via* one C–H…O hydrogen bond. The O2A–H…O1T, O1A–H…O3T and O2A–H…O3T distances are 1.930, 1.971 and 2.996 Å, respectively. The C13A–H…O1A distance is 2.538 Å.

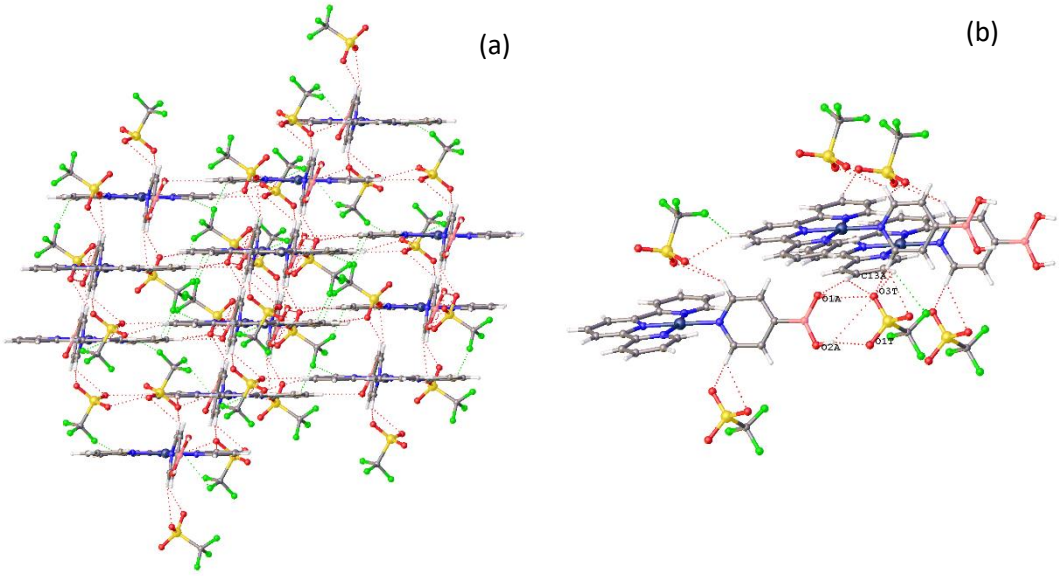


Figure 2.31: (a) A net of hydrogen bonds links Pd(terpy) cations and triflate anions. (b) Hydrogen bonds formed through boronic acid units.

In order to investigate the effect of the triflate anions on the structures, alternative anions were used including hexafluorophosphate (PF_6^-) and tetrafluoroborate (BF_4^-).

2.2.2.8 Single crystal X-ray structure of 2,2':6',2''-terpyridine (4-methylpyridine) palladium hexafluorophosphate [Pd(terpy)(4-methylpyridine)]$(PF_6)_2$ ***(2-8).***

Crystals of [Pd(terpy)(4-methylpyridine)]$(PF_6)_2$ were found to be colourless needles. The complex crystallises in the monoclinic space group $P2_1$. The crystal X-ray structure contains two crystallographically distinct cations having nearly identical structures. Figure 2.32 shows the coordination geometry and atom labelling scheme for complex (**2-8**). Four hexafluorophosphate anions present in the asymmetric unit. Table 2.8 lists important bond lengths and angles for the two independent molecules in this complex. The two molecules will be referred to as molecule **A** (containing Pd1A) and molecule **B** (containing Pd1B). The Pd–N distance to the central nitrogen atom of the terpyridine is

the shortest (average = 1.951(10) Å). The Pd–N distances to the outer pyridine rings from 2.012(18) to 2.070(2) Å are comparable with those in the complexes discussed above. The planar 4-methylpyridine ligand coordinates such that it sits out of the Pd(terpy) plane with a dihedral angle of 68.99(8) and 67.03(8)°, corresponding to molecule (**A**) and molecule (**B**), respectively.

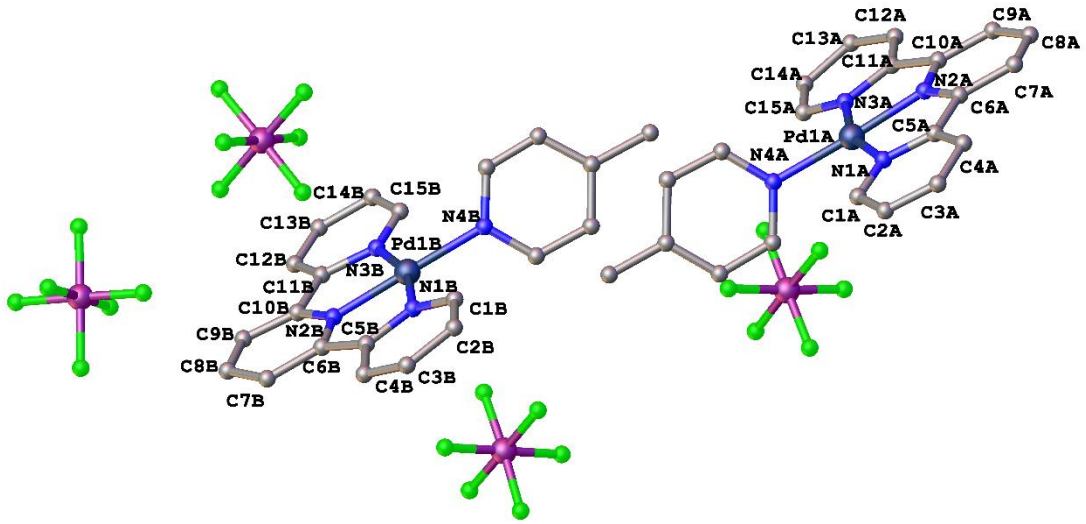


Figure 2.32: X-ray crystal structure of [Pd(terpy)(4-methylpyridine)]$(PF_6)_2$ with crystallographically independent atom numbering scheme. Hydrogen atoms have been omitted for clarity. Atom colours - C: grey, N: blue, Pd: navy F: green, and P: purple.

Table 2.8: Selected bond lengths (Å) and angles (°) for [Pd(terpy)(4-methylpyridine)]$(PF_6)_2$.

Pd1A-N1A	2.070(2)	N2A-Pd1A-N1A	81.00(7)
Pd1A-N2A	1.941(17)	N2A-Pd1A-N4A	177.60(8)
Pd1A-N3A	2.039(16)	N3A-Pd1A-N1A	162.50(7)
Pd1A-N4A	2.040(2)	N3A-Pd1A-N2A	81.50(7)
Pd1B-N1B	2.020(2)	N2B-Pd1B-N1B	80.60(9)

Pd1B-N2B	1.960(2)	N2B-Pd1B-N4B	178.70(9)
Pd1B-N3B	2.032(19)	N3B-Pd1B-N1B	162.10(8)
Pd1B-N4B	2.012(18)	N3B-Pd1B-N2B	81.60(8)

In terms of tilt angles, molecule (**A**) (177.60(8)°) shows higher deviation than molecule (**B**) (178.70(9)°).

The terpyridine unit of molecule (**A**) is more coplanar than that of molecule (**B**) with a maximum displacement of +0.106 (**B** +0.131) and -0.077 (**B** -0.096) Å exhibited by C8A(C8B) and N2A(C14B), respectively, from the mean plane. The two molecules are almost parallel with an angle between the planes of molecule (**A**) and molecule (**B**) of 0.60°.

Analysis of packing in the crystal structure showed that the rows of cations are arranged in a herringbone architecture. Hexafluorophosphate occupied the channels between the cations (Figure 2.33). The close to planar terpyridine units of the cations undergo a series of face-to-face π· · ·π interactions indicated by centroid–centroid separations of 3.683 and 3.738 Å (corresponding slip angles are 2.771 and 3.213°, respectively) (Figure 2.34).

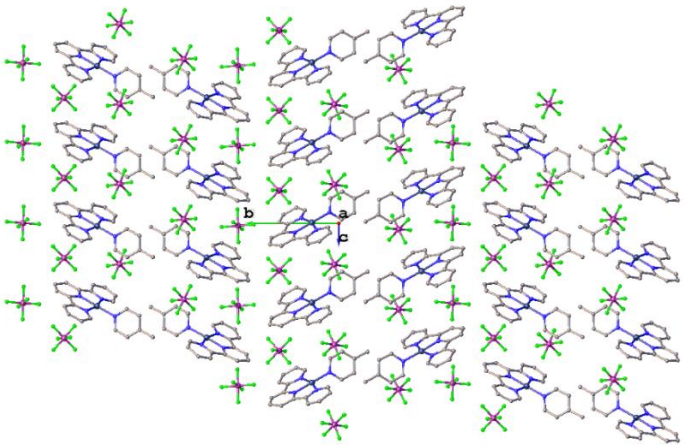


Figure 2.33: The packing diagram for [Pd(terpy)(4-methylpyridine)]$(PF_6)_2$ along the *a*-crystal axis. Hydrogen atoms are omitted for clarity.

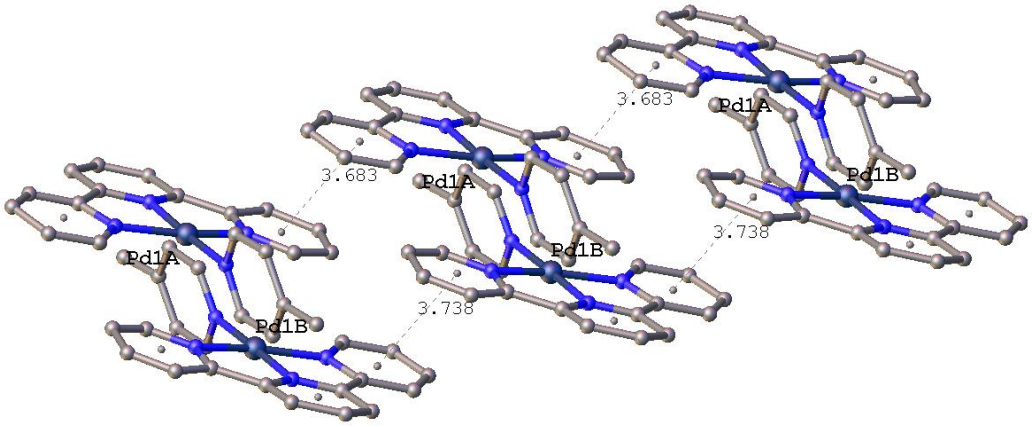


Figure 2.34: Representation of the π· · ·π interactions in [Pd(terpy)(4-methylpyridine)]$(PF_6)_2$. Dashed lines indicate the presence of π· · ·π interactions.

The fluorine atoms of the hexafluorophosphate anion act as hydrogen bond acceptors generating hydrogen bonds with hydrogen atoms of terpyridine and 4-methylpyridine, as shown in Figure 2.35. The C–H…F distances lie in the range 2.162– 2.949 Å.

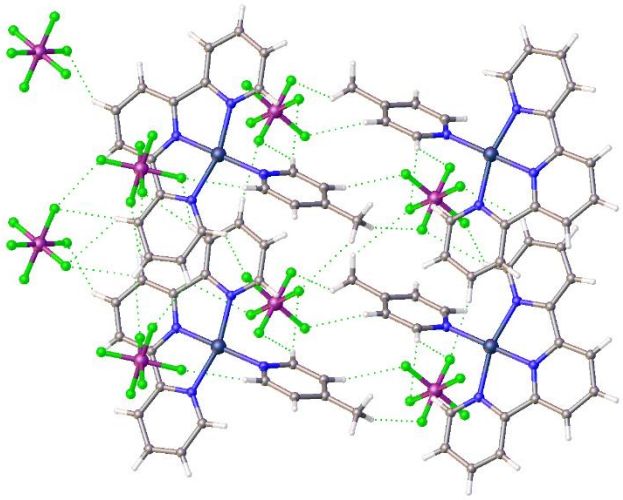


Figure 2.35: A net of hydrogen bonds links Pd(terpy) cations and hexafluorophosphate anions for [Pd(terpy)(4-methylpyridine)]$(PF_6)_2$.

The importance of the anion is illustrated by differences between (**2-2**) and (**2-8**). The former complex has a complete molecule in the asymmetric unit with two triflate anions and the cations pack in layers parallel to the *b*-axis. On the other hand, the (**2-8**) complex contains two crystallographically distinct cations with four hexafluorophosphate anions and its cations arrange in a herringbone architecture.

*2.2.2.9 Single crystal X-ray structure of 2,2':6',2''-terpyridine (4-dimethylaminopyridine) palladium hexafluorophosphate [Pd(terpy)(4-dimethylaminopyridine)]$(PF_6)_2$ (**2-9**).*

Crystals of [Pd(terpy)(4-dimethylaminopyridine)]$(PF_6)_2$ were found to be colourless blocks. The complex crystallises in the orthorhombic space group *Pbca*. As shown in Figure 3.36, space above and below the Pd cation is occupied by two hexafluorophosphate anions and one molecule of acetonitrile. As before, the terpyridine moiety is coordinated to the Pd atom in a tridentate fashion, and distorts the square

planar geometry of the Pd atom. The bond lengths and angles are detailed below in Table 2.9. As before, the Pd–N2 distance remains much shorter the Pd–N1 and Pd–N3 distances. The *cis* N–Pd–N angles deviate from 90° by 8.8° and N3–Pd–N1 angle deviate from 180° by 17.5°. All bond lengths and angles agree well with those for (**2-4**). The 4-dimethylaminopyridine ligand is slightly bent with respect to terpyridine plane forming a dihedral angle of 72.82(3)°. The dihedral angle indicates that 4-dimethylaminopyridine in complex (**2-9**) is twisted more than that in complex (**2-4**). In terms of tilt angle, this complex indicates slight deviation with 0.50° from the ideal value of 180°.

The terpyridine is almost coplanar with a maximum displacement of +0.130 and -0.094 Å exhibited by C3 and N1, respectively, from the mean plane.

Analysis of packing in the crystal structure showed that the rows of cations are arranged in a zigzag architecture. Hexafluorophosphate occupied the channels between the cations (Figure 2.37). The presence of the two anions above and below Pd(terpy) unit hinders the two complex cations from coming into close proximity in the crystalline.

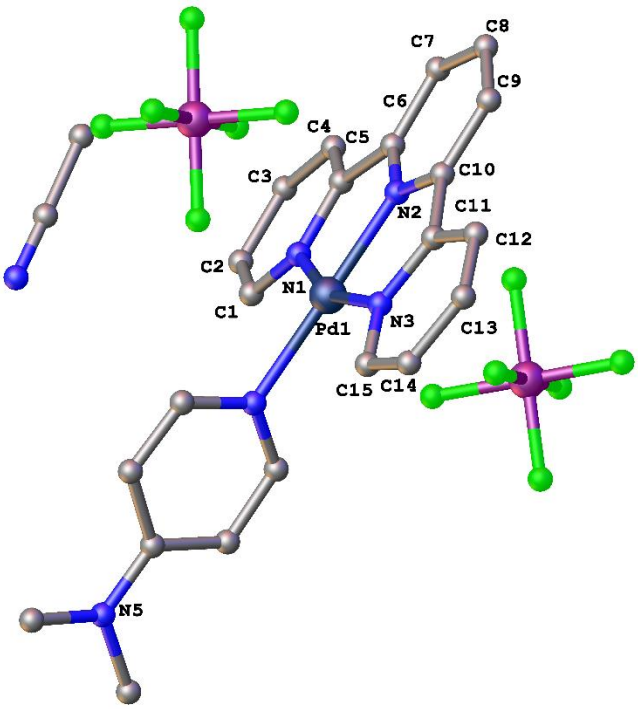


Figure 2.36: X-ray crystal structure of [Pd(terpy)(4-dimethylaminopyridine)]$(PF_6)_2$ with crystallographically independent atom numbering scheme. Hydrogen atoms have been omitted for clarity. Atom colours - C: grey, N: blue, Pd: navy F: green, and P: purple.

Table 2.9: Selected bond lengths (Å) and angles (°) for [Pd(terpy)(4-dimethylaminopyridine)]$(PF_6)_2$.

Pd1-N1	2.043(8)	N2-Pd1-N1	81.10(3)
Pd1-N2	1.958(9)	N2-Pd1-N4	179.50(4)
Pd1-N3	2.038(8)	N3-Pd1-N1	162.50(3)
Pd1-N4	2.063(10)	N3-Pd1-N2	81.40(3)

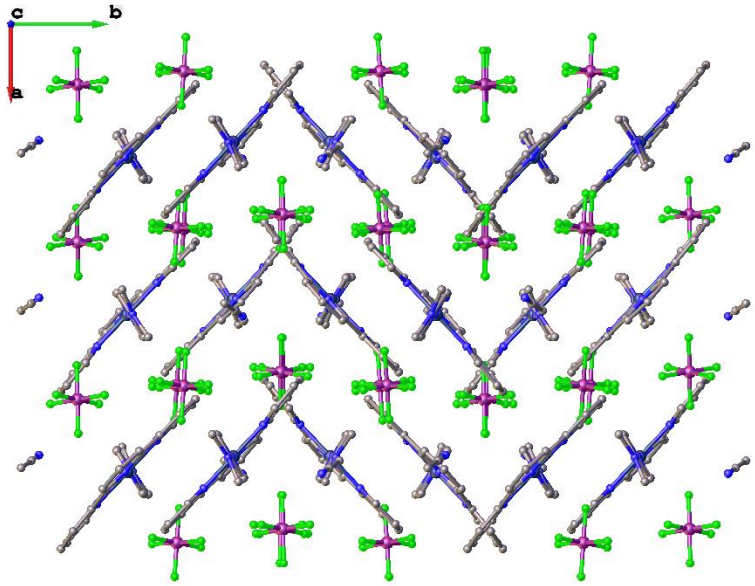


Figure 2.37: The packing diagram for [Pd(terpy)(4-dimethylaminopyridine)]$(PF_6)_2$ along the *c*-crystal axis. Hydrogen atoms are omitted for clarity.

The fluorine atoms of the hexafluorophosphate anion act as hydrogen bond acceptors generating hydrogen bonds with hydrogen atoms of terpyridine, 4-dimethylaminopyridine and acetonitrile molecule, as shown in Figure 2.38. The C–H…F distances lie in the range 2.346 – 2.903 Å.

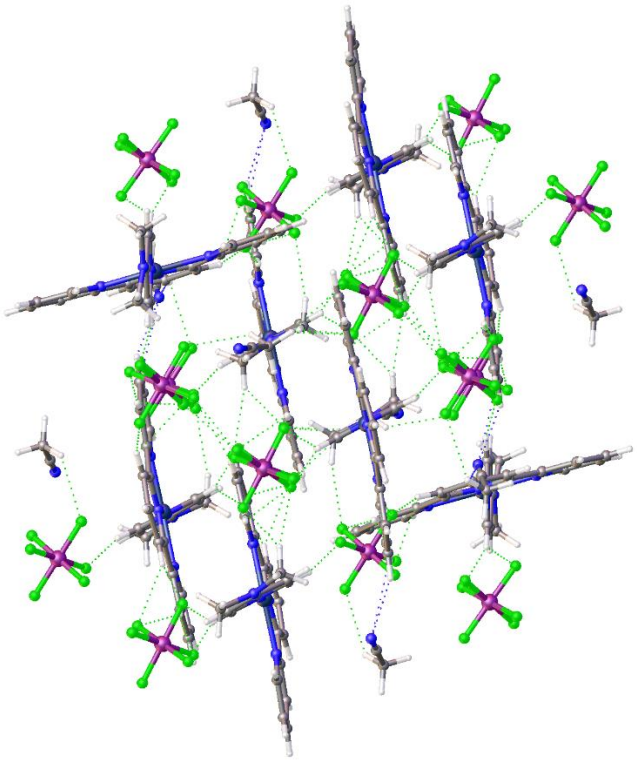


Figure 2.38: A net of hydrogen bonds links Pd(terpy) cations, hexafluorophosphate anions and acetonitrile molecules for [Pd(terpy)(4-dimethylaminopyridine)]$(PF_6)_2$.

2.2.2.10 Single crystal X-ray structure of 2,2':6',2''-terpyridine (4-cyanopyridine) palladium tetrafluoroborate [Pd(terpy)(4-cyanopyridine)]$(BF_4)_2$ ***(2-10).***

Crystals of (**2-10**) were found to be colourless plates. The complex crystallises in the monoclinic space group $P2_1/c$. The X-ray crystal structure contains two crystallographically distinct cations having nearly identical geometry. As shown in Figure 2.39, space around the two cations is occupied by four tetrafluoroborate anions and one molecule of acetonitrile. There is disorder exhibited on one of the BF_4^- anions. The two molecules will be referred to as molecule **A** (containing (Pd1A) and molecule **B** (containing Pd1B). The structure of (**2-10**) confirms the expected tridentate coordination of the terpyridine. Table 2.10 lists important bond lengths and angles for this complex. The bond between Pd ion and the nitrogen of the central rings is 1.927(3) Å in molecule

(**A**) similar to the value seen in complex (**2-1**) and longer than observed in molecule (**B**) 1.938(3) Å. The Pd–N bonds to the terminal rings in molecule (**A**) (average = 2.034 Å) are shorter than those for molecule (**B**) (average = 2.040 Å). The Pd–N bonds to the terminal rings for both molecules are significantly longer than those of complex (**2-1**) (average = 1.979 Å). The averages of the N1–Pd–N3, N1–Pd–N2 and N2–Pd–N3 (162.25, 81.06 and 81.19°, respectively) angles are slightly smaller than those found in complex (**2-1**).

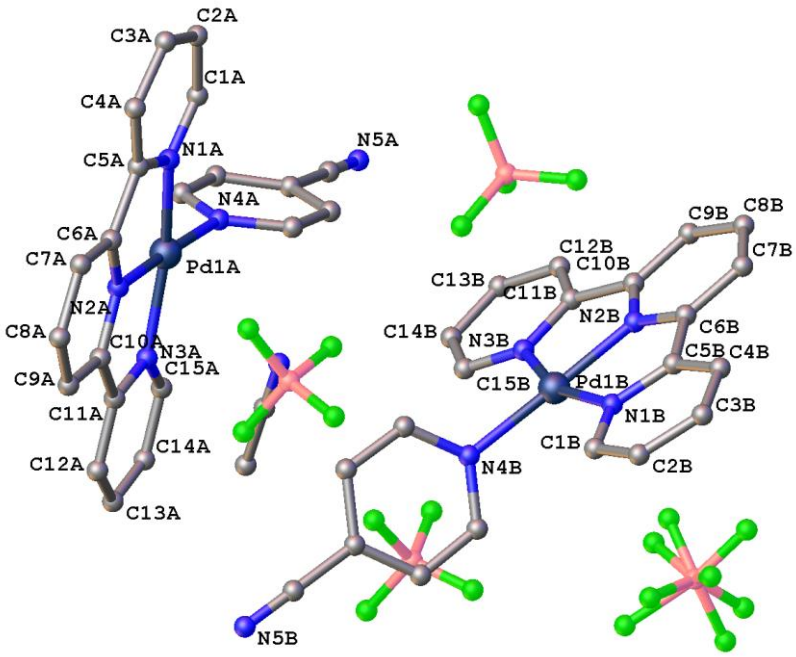


Figure 2.39: X-ray crystal structure of [Pd(terpy)(4-cyanopyridine)]$(BF_4)_2$ with crystallographically independent atom numbering scheme. Hydrogen atoms have been omitted for clarity. Atom colours - C: grey, B: pink, N: blue, Pd: navy, and F: green.

The angle between the square planar coordination geometry of the Pd(terpy) cation and the plane of 4-cyanopyridine in molecule (**A**) is 89.36(7)°. This value is higher than that of molecule (**B**) 73.61(7)° and complex (**2-1**) (84.04(7)°). The dihedral angle for molecule (**A**) indicates that the terpyridine ring and 4-cyanopyridine are almost perpendicular to each other with a negligible deviation. The tilt angles for molecules (**A**) and (**B**) are 177.93(14)°

and 178.04(13)°, respectively. Two molecules show higher deviation in the tilt angle than (**2-1**) (179.7(9)°).

Table 2.10: Selected bond lengths (Å) and angles (°) for [Pd(terpy)(4-cyanopyridine)]$(BF_4)_2$.

Pd1A-N1A	2.026(3)	N2A-Pd1A-N1A	81.34(15)
Pd1A-N2A	1.927(3)	N2A-Pd1A-N4A	177.93(14)
Pd1A-N3A	2.037(4)	N3A-Pd1A-N1A	162.71(15)
Pd1A-N4A	2.040(3)	N3A-Pd1A-N2A	81.36(17)
Pd1B-N1B	2.036(3)	N2B-Pd1B-N1B	80.77(13)
Pd1B-N2B	1.938(3)	N2B-Pd1B-N4B	178.04(13)
Pd1B-N3B	2.040(3)	N3B-Pd1B-N1B	161.78(13)
Pd1B-N4B	2.043(3)	N3B-Pd1B-N2B	81.01(13)

The terpyridine unit of molecule (**B**) is more coplanar than that of molecule (**A**) with a maximum displacement of +0.040 (**A** +0.065) and -0.039 (**A** -0.047) Å exhibited by C4B(C4A) and C1B(C2A), respectively, from the mean plane. Two molecules are more planar than complex (**2-1**). Two molecules are nearly perpendicular to each other with an angle between the planes of molecule (**A**) and molecule (**B**) of 62.56° (Figure 2.40).

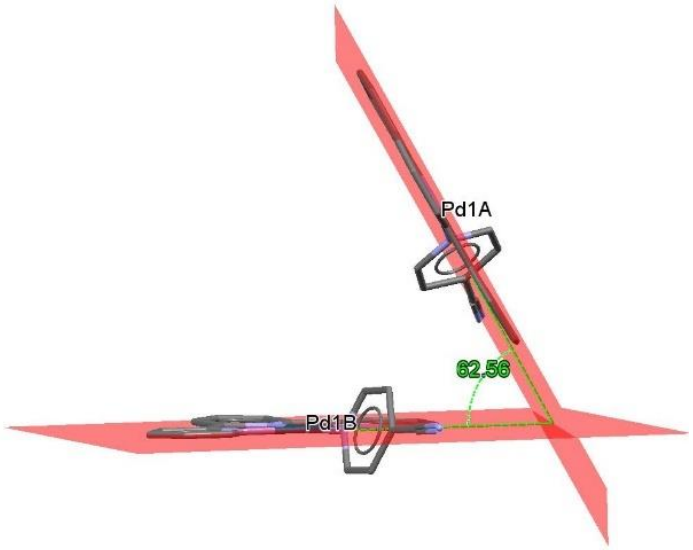


Figure 2.40: The dihedral angle between the planes of molecule (A) and molecule (B) in [Pd(terpy)(4-cyanopyridine)]$(BF_4)_2$.

The cavities formed by cations accommodate tetrafluoroborate anions and acetonitrile molecules. The packing of the molecules reveals that π· · ·π interactions between terpyridine units on adjacent molecules dominate the assembly of the cations. As shown in Figure 2.41, the molecules of (**2-10**) undergo a series of face-to-face π· · ·π interactions indicated by ring centroid–ring centroid separations of 3.504, 3.608 and 3.997 Å (corresponding slip angles are 1.625°, 1.261° and 0.00°). This arrangement is further stabilised by a series of hydrogen bonds between $[Pd(terpy)(4\text{-cyanopyridine})]^{2+}$ and tetrafluoroborate anions. Additional hydrogen bonds between terpyridine and acetonitrile molecules contribute to the overall packing. The C–H…F distances lie in the range 2.145 – 2.978 Å.

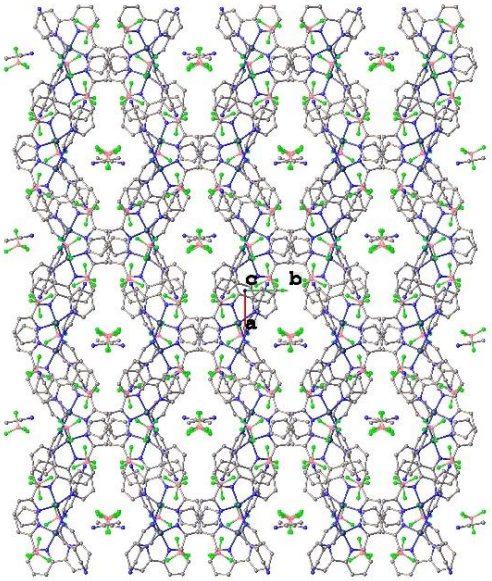


Figure 2.41: The packing diagram of [Pd(terpy)(4-cyanopyridine)]$(BF_4)_2$ along the *a*-crystal axis. Hydrogen atoms are omitted for clarity.

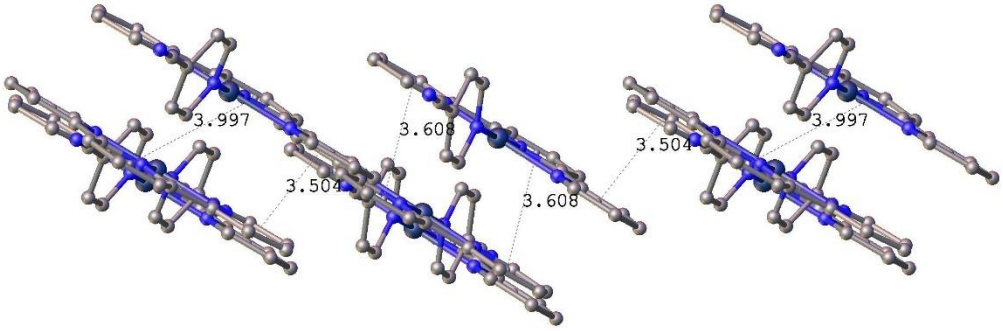


Figure 2.42: Representation of the π· · ·π Stacking interactions between neighbouring molecules in structure[Pd(terpy)(4-cyanopyridine)]$(BF_4)_2$.

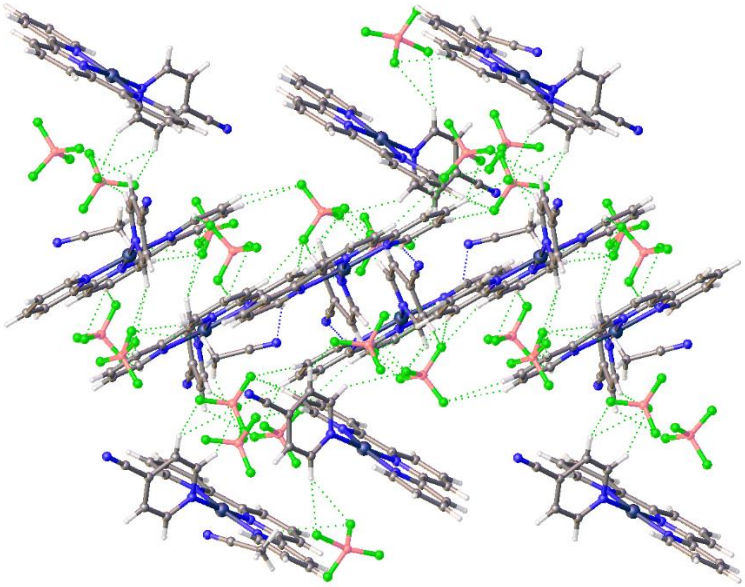


Figure 2.43: A net of hydrogen bonds links Pd(terpy) cations, tetrafluoroborate anions and acetonitrile molecules for [Pd(terpy)(4-cyanopyridine)]$(BF_4)_2$.

2.3 Conclusions

A series of complexes have been synthesised using Pd(II) and terpyridine. A total of 10 complexes were made, using seven pyridine derivatives, and triflate, tetrafluoroborate and hexafluorophosphate anions. It was possible to grow single crystals for all complexes, allowing structure determination by X-ray diffraction. These complexes have shown *cis*–*cis*-configuration upon coordination to terpyridine with the Pd cations adopting distorted square planar geometries. The asymmetric unit of (**2-3**), (**2-4**), (**2-5**), (**2-8**) and (**2-10**) complexes contain a pair of crystallographically independent cations and four anions, leading to more complex structural arrangements.

As expected, these complexes are similar to each other regarding their bond lengths and angles. Terpyridine is coordinated to palladium as a tridentate ligand and the fourth position is occupied by the *para*-substituted pyridine derivative. The coordination geometry of the palladium ion is distorted slightly from that found in perfect square-planar Pd(II) complexes. In terms of the N1–Pd–N3 angle, molecule (**A**) for complex (**2-3**) reveals the highest deviation from the ideal value of 180, by 18.43(11)°, and complex (**2-1**) shows the lowest deviation, by 16.9(8)°. The central Pd–N2 bond is noticeably shorter than the other three Pd–N bonds, less than 2 Å in all complexes. Similar values were observed in the crystal structure of the complex $[Pd(terpy)Cl]^+$ [43]. It can be concluded that the replacement of the chloride atom with any of the 4-pyridine derivatives previously reported in this chapter causes small changes to terpyridine binding angles. This is also proved by the bond lengths of Pd–N with the three nitrogen atoms of terpyridine and the complex $[Pd(terpy)Cl]^+$, which are practically the same.

In complex (**2-3**), the 4-iodopyridine ligand (molecule **B**) is significantly twisted with respect to terpyridine plane adopting a dihedral angle of 54.15(8)°. However, the dihedral

angle for molecule (**A**) in complex (**2-10**) (89.36(7)°) indicates that the terpyridine ring and 4-cyanopyridine are almost perpendicular to each other with a negligible deviation. In terms of planarity, the terpyridine moiety in complex (**2-6**) has the highest deviation with a maximum displacement of +0.123 and -0.115 Å exhibited by C3 and N1, respectively, from the mean plane.

All complexes, except (**2-7**) and (**2-9**), adopt π· · ·π interactions with centroid–centroid separations 3.504 – 3.997 Å. The long centroid–centroid separations in complexes (**2-7**) and (**2-9**) can be attributed to the presence of the two anions above and below Pd(terpy) unit hindering the two complex cations from coming into close proximity in the crystalline state.

As expected, terpyridine moiety acts as a hydrogen donor and the triflate, tetrafluoroborate and hexafluorophosphate anions act as hydrogen acceptors to form intermolecular hydrogen bonds. In addition, the pyridine ligands are involved in intermolecular hydrogen bonds. The data shows that the O…C-H and F…C-H distances are within the range typical for weak hydrogen bond lengths.

Many different experiments and studies have been left for the future due to lack of time. Future work concerns deeper analysis of the crystal structures of the complexes and new proposals to try different pyridine ligands.

2.4 Materials and Methods

All chemicals and solvents were purchased from Alfa-Aesar, Fisher Scientific, VWR International or Sigma-Aldrich and were used as received without any further purification. Reactions sensitive to air and moisture were performed using a standard Schlenk line, with nitrogen as the inert atmosphere. Glassware used was flame dried under vacuum and backfilled with nitrogen. ^{1}H and ^{13}C NMR spectra were recorded using

either a Bruker AV(III)400, AV(III)500, AV400 or DPX400 spectrometer at room temperature. Mass spectrometry was conducted using a Bruker Dalton Ultraflex MALDI-TOF with trans-2-[3-(4-*tert*,-butylphenyl)-2-methyl-2-propenylidene]-malononitrile as the matrix (m/z = 250.3).

Single crystal X-ray diffraction experiments were performed on an Oxford Diffraction SuperNova CCD area detector diffractometer at 120 K using monochromated Cu Kα radiation (λ = 1.54184 Å); on Agilent GV1000 AtlasS2 or TitanS2 CCD area detector diffractometers at 120 K using monochromated CuKα radiation (λ = 1.54184 Å); or at the UK Diamond Light Source I19-1 3-circle diffractometer (λ = 0.6889 Å). Absorption corrections were applied using analytical numerical methods using CrysAlisPro software [44]. The structures were solved by direct methods using either SHELXS or SHELXT and refined with SHELXL using a least squares method [45-47]. In all instances, Olex2 software was used as the solution, refinement and analysis program [48].

2.4.1 Synthesis of 2,2':6',2''-terpyridine (4-cyanopyridine) palladium triflate [Pd(terpy)(4-cyanopyridine)]$(CF_3SO_3)_2$ (2-1).

A mixture of 2,2':6',2''-terpyridine (72.5 mg, 0.311 mmol) and palladium chloride (50 mg, 0.282 mmol) in acetonitrile (20 mL) was stirred at room temperature for 24 h. Silver triflate (290 mg, 1.129 mmol) was added. In the absence of light, the mixture was stirred for 48 h. After 48 h, the white precipitate (AgCl) was filtered. 4-Cyanopyridine (29 mg, 0.279 mmol) was added to the reaction solution and stirred for 3 h. The resulting solution was concentrated *via* rotary evaporation to remove the excess acetonitrile solvent. The resulting beige solid was washed with diethyl ether, before being dried in *vacuo*. Yield (70 mg, 34%). Single crystals suitable for X-ray diffraction were obtained by vapour diffusion of diethyl ether into an acetonitrile solution of [Pd(terpy)(4-cyanopyridine)]$(CF_3SO_3)_2$.

MALDI-TOF MS (RP; m/z): 221.42 $[C_{23}H_{15}F_6N_5O_6PdS_2\text{-}2TOf]^{2+}$. ^1H NMR (400 MHz, CD_3CN) δ ppm: 9.05 (d, *J* = 5.6 Hz, 2H, 2, 6-py), 8.56 (m, 5H, 3, 3`,4`,5`, 3``-terpy), 8.45 (m, 2H, 4, 4``-terpy), 8.01 (d, *J* = 5.6 Hz, 2H, 3, 5-py), 7.79 (m, 2H, 6, 6``-terpy), 7.71 (td, *J* = 6.1, 1.2 Hz, 2H, 5, 5``-terpy).

2.4.2 Synthesis of 2,2':6',2''-terpyridine (4-methylpyridine) palladium triflate $[Pd(terpy)(4\text{-methylpyridine})](CF_3SO_3)_2$ (2-2).

A mixture of 2,2':6',2''-terpyridine (72.5 mg, 0.311 mmol) and palladium chloride (50 mg, 0.282 mmol) in acetonitrile (20 mL) was stirred at room temperature for 24 h. Silver triflate (290 mg, 1.129 mmol) was added. In the absence of light, the mixture was stirred for 48 h. After 48 h, the white precipitate (AgCl) was filtered. 4-Methylpyridine (27 μL, 0.282 mmol) was added to the reaction solution and stirred for 3 h. The resulting solution was concentrated *via* rotary evaporation to remove the excess acetonitrile solvent. The resulting beige solid was washed with diethyl ether, before being dried in *vacuo*. Yield (76 mg, 37%). Single crystals suitable for X-ray diffraction were obtained by vapour diffusion of diethyl ether into an acetonitrile solution of $[Pd(terpy)(4\text{-methylpyridine})](CF_3SO_3)_2$. MALDI-TOF MS (RP; m/z): 221.42 $[C_{23}H_{18}F_6N_4O_6PdS_2\text{-}2TOf]^{2+}$. ^1H NMR (400 MHz, CD_3CN) δ ppm: 8.75 (d, *J* = 6.6 Hz, 2H, 2, 6-py), 8.60 (t, *J* = 8.2 Hz, 1H, 4`-terpy), 8.40 (d, *J* = 8.5 Hz, 2H, 3`, 5`-terpy), 8.17 (m, 4H, 3, 4, 3``, 4``-terpy), 7.75 (d, *J* = 5.6 Hz, 2H, 6, 6``-terpy), 7.55 (d, *J* = 6.3 Hz, 2H, 3, 5-py), 7.42 (m, 2H, 5, 5``-terpy), 2.60 (s, 3H, CH_3).

2.4.3 Synthesis of 2,2':6',2''-terpyridine (4-iodopyridine) palladium triflate [Pd(terpy)(4-iodopyridine)]$(CF_3SO_3)_2$ (2-3).

A mixture of 2,2':6',2''-terpyridine (72.5 mg, 0.311 mmol) and palladium chloride (50 mg, 0.282 mmol) in acetonitrile (20 mL) was stirred at room temperature for 24 h. Silver triflate (290 mg, 1.129 mmol) was added. In the absence of light, the mixture was stirred for 48 h. After 48 h, the white precipitate (AgCl) was filtered. 4-Iodopyridine (58 mg, 0.283 mmol) was added to the reaction solution and stirred for 3 h. The resulting solution was concentrated *via* rotary evaporation to remove the excess acetonitrile solvent. The resulting solid was washed with diethyl ether, before being dried in *vacuo*. Yield (121 mg, 51%). Single crystals suitable for X-ray diffraction were obtained by vapour diffusion of diethyl ether into an acetonitrile solution of [Pd(terpy)(4-iodopyridine)]$(CF_3SO_3)_2$. MALDI-TOF MS (RP; m/z): 271.44 $[C_{22}H_{15}F_6IN_4O_6PdS_2\text{-}2TOf]^{2+}$. ^{1}H NMR (400 MHz, CD_3CN) δ ppm: 8.97 (d, *J* = 5.6 Hz, 2H, 2,6-py), 8.71 (m, 5H, 3, 3`, 4`, 5`, 3``-terpy), 8.63 (d, *J* = 5.6 Hz, 2H, 4, 4`-terpy), 8.40 (d, *J* = 5.6 Hz, 2H, 6, 6``-terpy), 7.87 (m, 2H, 3, 5-py), 7.69(m, 2H, 5, 5``-terpy).

2.4.4 Synthesis of 2,2':6',2''-terpyridine (4-dimethylaminopyridine) palladium triflate [Pd(terpy)(4-dimethylaminopyridine)]$(CF_3SO_3)_2$ (2-4).

A mixture of 2,2':6',2''-terpyridine (72.5 mg, 0.311 mmol) and palladium chloride (50 mg, 0.282 mmol) in acetonitrile (20 mL) was stirred at room temperature for 24 h. Silver triflate (290 mg, 1.129 mmol) was added. In the absence of light, the mixture was stirred for 48 h. After 48 h, the white precipitate (AgCl) was filtered. 4-dimethylaminopyridine (34.4 mg, 0.281 mmol) was added to the reaction solution and stirred for 3 h. The resulting solution was concentrated *via* rotary evaporation to remove the excess acetonitrile solvent. The resulting beige solid was washed with diethyl ether, before being dried in *vacuo*. Yield (60 mg, 28%). Single crystals suitable for X-ray diffraction were

obtained by vapour diffusion of diethyl ether into an acetonitrile solution of [Pd(terpy)(4-dimethylaminopyridine)]$(CF_3SO_3)_2$. MALDI-TOF MS (RP; m/z): 230.43 $[C_{24}H_{21}F_6N_5O_6PdS_2\text{-}2TOf]^{2+}$. ^{1}H NMR (400 MHz, CD_3CN) δ ppm: 8.75 (t, *J* = 8.3 Hz, 1H, 4`-terpy), 8.65 (m, 6H, 3, 4, 3`, 5`, 3``, 4``-terpy), 8.51 (d, *J* = 5.9 Hz, 2H, 2, 6-py), 7.95 (d, *J* = 5.8 Hz, 2H, 6, 6``-terpy ), 7.56 (m, 2H, 5, 5``-terpy), 7.39 (d, *J* = 5.8 Hz, 2H, 3, 5-py), 3.29 (s, 6H, $N(CH_3)_2$). ^{13}C NMR (100 MHz, CD_3CN) δ ppm: 155.74, 152.79, 151.18, 149.47, 148.13, 140.65, 139.40, 126.15, 123.16, 109.10, 39.51.

2.4.5 Synthesis of 2,2':6',2''-terpyridine (4-pyridinecarboxaldehyde) palladium triflate [Pd(terpy)(4-pyridinecarboxaldehyde)]$(CF_3SO_3)_2$ (2-5).

A mixture of 2,2':6',2''-terpyridine (72.5 mg, 0.311 mmol) and palladium chloride (50 mg, 0.282 mmol) in acetonitrile (20 mL) was stirred at room temperature for 24 h. Silver triflate (290 mg, 1.129 mmol) was added. In the absence of light, the mixture was stirred for 48 h. After 48 h, the white precipitate (AgCl) was filtered. 4-Pyridinecarboxaldehyde (26 μL, 0.280 mmol) was added to the reaction solution and stirred for 2 h. The resulting solution was concentrated *via* rotary evaporation to remove the excess acetonitrile solvent. The resulting beige solid was washed with diethyl ether, before being dried in *vacuo*. Yield (87 mg, 42%). Single crystals suitable for X-ray diffraction were obtained by vapour diffusion of diethyl ether into an acetonitrile solution of [Pd(terpy)(4-pyridinecarboxaldehyde)]$(CF_3SO_3)_2$. MALDI-TOF MS (RP; m/z): 223.21 $[C_{23}H_{16}F_6N_4O_7PdS_2\text{-}2TOf]^{2+}$. ^{1}H NMR (400 MHz, CD_3CN) δ ppm: 9.04 (d, *J* = 6.0 Hz, 2H, 2, 6-py), 8.63 (t, *J* = 8.2 Hz, 1H, 4`-terpy), 8.65 (d, *J* = 6.2 Hz, 2H, 3`, 5`-terpy), 8.57 (d, *J* = 6.2 Hz, 2H, 6, 6``-terpy), 8.54 (m, 4H, 3, 3``, 4, 4``-terpy), 7.91 (d, *J* = 6.2 Hz, 2H, 3, 5-py), 7.70 (m, 2H, 5, 5``-terpy).

2.4.6 Synthesis of 2,2':6',2''-terpyridine (4-aminopyridine) palladium triflate [Pd(terpy)(4-aminopyridine)]$(CF_3SO_3)_2$ (2-6).

A mixture of 2,2':6',2''-terpyridine (72.5 mg, 0.311 mmol) and palladium chloride (50 mg, 0.282 mmol) in acetonitrile (20 mL) was stirred at room temperature for 24 h. Silver triflate (290 mg, 1.129 mmol) was added. In the absence of light, the mixture was stirred for 48 h. After 48 h, the white precipitate (AgCl) was filtered. 4-Aminopyridine (27 mg, 0.284 mmol) was added to the reaction solution and stirred for 2 h. The resulting solution was concentrated *via* rotary evaporation to remove the excess acetonitrile solvent. The resulting beige solid was washed with diethyl ether, before being dried in *vacuo*. Yield (133 mg, 55%). Single crystals suitable for X-ray diffraction were obtained by vapour diffusion of diethyl ether into an acetonitrile solution of [Pd(terpy)(4-hydroxypyridine)]$(CF_3SO_3)_2$. MALDI-TOF MS (RP; m/z): 216.22 $[C_{22}H_{17}F_6N_5O_6PdS_2\text{-}2TOf]^{2+}$. ^{1}H NMR (400 MHz, CD_3CN) δ ppm: 8.41 (d, *J*= 5.6 Hz, 2H, 2, 6-py), 8.33 (m, 5H, 3, 3`, 4`, 5`, 3``-terpy), 8.21 (d, *J* = 5.6 Hz, 2H, 4, 4``-terpy), 8.01 (m, 2H, 6, 6``-terpy), 7.52 (d, *J* = 5.6 Hz, 2H, 3, 5-py), 7.34 (m, 2H, 5, 5``-terpy), 5.92 (s, 2H, NH_2).

2.4.7 Synthesis of 2,2':6',2''-terpyridine (4-pyridineboronic acid) palladium triflate [Pd(terpy)(4-pyridineboronic acid)]$(CF_3SO_3)_2$ (2-7).

A mixture of 2,2':6',2''-terpyridine (72.5 mg, 0.311 mmol) and palladium chloride (50 mg, 0.282 mmol) in acetonitrile (20 mL) was stirred at room temperature for 24 h. Silver triflate (290 mg, 1.129 mmol) was added. In the absence of light, the mixture was stirred for 48 h. After 48 h, the white precipitate (AgCl) was filtered. 4-Pyridineboronic acid (35 mg, 0.282 mmol) was added to the reaction solution and stirred for 2 h. The resulting solution was concentrated *via* rotary evaporation to remove the excess acetonitrile solvent. The resulting beige solid was washed with diethyl ether, before being dried in *vacuo*. Yield (88 mg, 41%). Single crystals suitable for X-ray diffraction were obtained by

vapour diffusion of diethyl ether into an acetonitrile solution of [Pd(terpy)(4-pyridineboronic acid)]$(CF_3SO_3)_2$. MALDI-TOF MS (RP; m/z): 231.26 $[C_{22}H_{17}BF_6N_4O_8PdS_2\text{-}2TOf]^{2+}$. ^{1}H NMR (400 MHz, CD_3OD) δ ppm: 9.09 (d, *J* = 5.6 Hz, 2H, 2, 6-py), 8.61 (m, 5H, 3, 3`, 3``, 4`, 5`-terpy), 8.50 (td, *J* = 8.0, 1.6 Hz, 2H, 4, 4``-terpy), 8.07 (d, *J* = 5.6 Hz, 2H, 3, 5-py), 7.84 (dd, *J* = 5.6, 0.8 Hz, 2H, 6, 6``-terpy), 7.79 (td, *J* = 6.2,1.2 Hz, 2H, 5, 5``-terpy). ^{11}B NMR (128 MHz; CD_3OD) δ ppm: 19.32.

2.4.8 Synthesis of 2,2':6',2''-terpyridine (4-methylpyridine) palladium hexafluorophosphate [Pd(terpy)(4-methylpyridine)]$(PF_6)_2$ (2-8).

A mixture of 2,2':6',2''-terpyridine (72.5 mg, 0.311 mmol) and palladium chloride (50 mg, 0.282 mmol) in acetonitrile (20 mL) was stirred at room temperature for 24 h. Silver hexafluorophosphate (285 mg, 1.128 mmol) was added. In the absence of light, the mixture was stirred for 48 h. After 48 h, the white precipitate (AgCl) was filtered. 4-Methylpyridine (27 μL, 0.258 mmol) was added to the reaction solution and stirred for 2 h. The resulting solution was concentrated *via* rotary evaporation to remove the excess acetonitrile solvent. The resulting beige solid was washed with diethyl ether, before being dried in *vacuo*. Yield (91 mg, 49%). Single crystals suitable for X-ray diffraction were obtained by vapour diffusion of diethyl ether into an acetonitrile solution of [Pd(terpy)(4-methylpyridine)]$(PF_6)_2$. MALDI-TOF MS (RP; m/z): 216.24 $[C_{21}H_{18}F_{12}N_4P_2Pd\text{-}2PF_6^-]^{2+}$. ^{1}H NMR (400 MHz, CD_3CN) δ ppm: 8.79 (d, *J* = 6.6 Hz, 2H, 2, 6-py), 8.62 (t, *J* = 8.0 Hz, 1H, 4`-terpy), 8.38 (m, 2H, 3`, 5`-terpy), 8.20 (m, 4H, 3, 3``, 4, 4``-terpy), 7.81 (d, *J* =5.6 Hz, 2H, 6, 6``-terpy), 7.73 (m, 2H, 3, 5-py), 7.40 (m, 2H, 5, 5``-terpy), 2.62 (s, 3H, CH_3).

2.4.9 Synthesis of 2,2':6',2''-terpyridine (4-dimethylaminopyridine) palladium hexafluorophosphate [Pd(terpy)(4-dimethylaminopyridine)]$(PF_6)_2$ (2-9).

A mixture of 2,2':6',2''-terpyridine (72.5 mg, 0.311 mmol) and palladium chloride (50 mg, 0.282 mmol) in acetonitrile (20 mL) was stirred at room temperature for 24 h. Silver hexafluorophosphate (285 mg, 1.128 mmol) was added. In the absence of light, the mixture was stirred for 48 h. After 48 h, the white precipitate (AgCl) was filtered. 4-Dimethylaminopyridine (35 mg, 0.282 mmol) was added to the reaction solution and stirred for 2 h. The resulting solution was concentrated *via* rotary evaporation to remove the excess acetonitrile solvent. The resulting beige solid was washed with diethyl ether, before being dried in *vacuo*. Yield (72 mg, 34%). Single crystals suitable for X-ray diffraction were obtained by vapour diffusion of diethyl ether into an acetonitrile solution of [Pd(terpy)(4-dimethylaminopyridine)]$(PF_6)_2$. MALDI-TOF MS (RP; m/z): 230.61 $[C_{22}H_{21}F_{12}N_5P_2Pd\text{-}2PF_6]^{2+}$. ^{1}H NMR (400 MHz, CD_3CN) δ ppm: 8.77 (t, *J* = 8.2 Hz, 1H, 4`-terpy), 8.61 (d, *J* = 5.9 Hz, 2H, 3` ,5`-terpy), 8.57 (m, 4H, 3, 4, 3``, 4``-terpy), 8.49 (d, *J* = 5.9 Hz, 2H, 2, 6-py), 8.08 (d, *J* = 6.0 Hz, 2H, 6, 6``-terpy), 7.91 (m, 2H, 5, 5``-terpy), 7.07 (d, *J* = 5.9 Hz, 2H, 3, 5-py), 3.29 (s, 6H, $N(CH_3)_2$).

2.4.10 Synthesis of 2,2':6',2''-terpyridine (4-cyanopyridine) palladium tetrafluoroborate [Pd(terpy)(4-cyanopyridine)]$(BF_4)_2$ (2-10).

A mixture of 2,2':6',2''-terpyridine (72.5 mg, 0.311 mmol) and palladium chloride (50 mg, 0.282 mmol) in acetonitrile (20 mL) was stirred at room temperature for 24 h. Silver tetrafluoroborate (220 mg, 1.128 mmol) was added. In the absence of light, the mixture was stirred for 48 h. After 48 h, the white precipitate (AgCl) was filtered. 4-Cyanopyridine (29 mg, 0.279 mmol) was added to the reaction solution and stirred for 2 h. The resulting solution was concentrated *via* rotary evaporation to remove the excess acetonitrile solvent. The resulting beige solid was washed with diethyl ether, before being

dried in *vacuo*. Yield (66 mg, 38%). Single crystals suitable for X-ray diffraction were obtained by vapour diffusion of diethyl ether into an acetonitrile solution of [Pd(terpy)(4-cyanopyridine)]$(BF_4)_2$. MALDI-TOF MS (RP; m/z): 216.22 $[C_{21}H_{15}B_2F_8N_5Pd\text{-}2BF_4^-]^{2+}$. ^{1}H NMR (400 MHz, CD_3CN) δ ppm: 9.03 (d, *J* = 6.0 Hz, 2H, 2, 6-terpy), 8.61 (m, 5H, 3, 3`, 4`, 5`, 3``-terpy), 8.52 (td, *J* = 8.0, 1.6 Hz, 2H, 4, 4``-terpy), 8.10 (d, *J* = 5.6 Hz, 2H, 6, 6``-terpy), 7.75 (m, 2H, 3, 5-py), 7.66 (m, 2H, 5, 5``-terpy).

2.4.11 Crystal data

Crystal data for (**2-1**): $C_{25}H_{16}F_6N_6O_6PdS_2$ (M + MeCN) (*M* =780.96 g/mol): triclinic, space group P-1 (no. 2), *a* = 7.8043(9) Å, *b* = 11.0849(15) Å, *c* = 17.8774(17) Å, *a* = 104.398(10)°, *β* = 98.074(9)°, *γ* = 91.298(11)°, *V* = 1480.5(3) Å^3, *Z* = 2, *T* = 120(2) K, μ(CuKα) = 7.193 mm^{-1}, *Dcalc* = 1.752 g/cm^3, 8450 reflections measured (8.25° ≤ 2θ ≤ 133.19°), 5107 unique (R_{int} = 0.1851, R_{sigma} = 0.1421) which were used in all calculations. The final R_1 was 0.0835 (I > 2σ(I)) and wR_2 was 0.3226 with GOF = 1.039.

Crystal data for (**2-2**): $C_{23}H_{18}F_6N_4O_6PdS_2$ (*M* =730.93 g/mol): triclinic, space group P-1 (no. 2), *a* = 8.1815(7) Å, *b* = 11.6306(9) Å, *c* = 14.7364(10) Å, *a* = 102.082(6)°, *β* = 105.203(7)°, *γ* = 92.310(6)°, *V* = 1316.46(18) Å^3, *Z* = 2, *T* = 120(2) K, μ(CuKα) = 8.010 mm^{-1}, *Dcalc* = 1.844 g/cm^3, 9754 reflections measured (7.814° ≤ 2θ ≤ 133.172°), 4644 unique (R_{int} = 0.0850, R_{sigma} = 0.1021) which were used in all calculations. The final R_1 was 0.0781 (I > 2σ(I)) and wR_2 was 0.2056 with GOF = 1.064.

Crystal data for (**2-3**): $C_{22}H_{15}F_6IN_4O_6PdS_2$ (*M* =842.80 g/mol): triclinic, space group P-1 (no. 2), *a* = 13.4088(3) Å, *b* = 14.7430(3) Å, *c* = 15.5991(3) Å, *a* = 116.899(2)°, *β* = 97.0774(19)°, *γ* = 97.0743(18)°, *V* = 2672.78(11) Å^3, *Z* = 4, *T* = 120(2) K, μ(CuKα) = 16.961 mm^{-1}, *Dcalc* = 2.094 g/cm^3, 35711 reflections measured (6.488° ≤ 2θ ≤ 133.192°),

9429 unique (R_{int} = 0.0473, R_{sigma} = 0.0317) which were used in all calculations. The final R_1 was 0.0310 (I > 2σ(I)) and wR_2 was 0.0852 with GOF = 1.045.

Crystal data for (**2-4**): $C_{24}H_{21}F_6N_5O_6PdS_2$ (M =759.98 g/mol): monoclinic, space group $P2_1/c$ (no. 14), a = 22.0062(4) Å, b = 8.80708(15) Å, c = 30.8206(5) Å, β = 98.8747(16)°, V = 5901.84(18) Å^3, Z = 8, T = 120(2) K, μ(CuKα) = 7.183 mm^{-1}, $Dcalc$ = 1.711 g/cm^3, 36138 reflections measured (7.584° ≤ 2θ ≤ 133.196°), 10429 unique (R_{int} = 0.0674, R_{sigma} = 0.0540) which were used in all calculations. The final R_1 was 0.0651 (I > 2σ(I)) and wR_2 was 0.1949 with GOF = 1.029.

Crystal data for (**2-5**): $C_{23}H_{16}F_6N_4O_7PdS_2$ (M =744.92 g/mol): triclinic, space group P-1 (no. 2), a = 10.1986(2) Å, b = 13.6264(3) Å, c = 20.4557(4) Å, a = 98.9626(17)°, β = 90.1796(16)°, γ = 110.0195(19)°, V = 2633.48(10) Å^3, Z = 4, T = ? K, μ(CuKα) = 8.054 mm^{-1}, $Dcalc$ = 1.879 g/cm^3, 36130 reflections measured (8.768° ≤ 2θ ≤ 149.204°), 10580 unique (R_{int} = 0.0240, R_{sigma} = 0.0216) which were used in all calculations. The final R_1 was 0.0287 (I > 2σ(I)) and wR_2 was 0.0743 with GOF = 1.049.

Crystal data for (**2-6**): $C_{22}H_{17}F_6N_5O_6PdS_2$ (M =731.92 g/mol): monoclinic, space group I2/a (no. 15), a = 16.9607(11) Å, b = 10.9643(7) Å, c = 29.3236(14) Å, β = 102.503(6)°, V = 5323.7(5) Å^3, Z = 8, T = 120(2) K, μ(CuKα) = 7.935 mm^{-1}, $Dcalc$ = 1.826 g/cm^3, 12032 reflections measured (8.636° ≤ 2θ ≤ 149.002°), 5289 unique (R_{int} = 0.0529, R_{sigma} = 0.0655) which were used in all calculations. The final R_1 was 0.0435 (I > 2σ(I)) and wR_2 was 0.1124 with GOF = 1.047.

Crystal data for (**2-7**): $C_{22}H_{17}BF_6N_4O_8PdS_2$ (M =760.72 g/mol): triclinic, space group P-1 (no. 2), a = 9.414(3) Å, b = 10.055(3) Å, c = 15.067(5) Å, a = 98.47(3)°, β = 100.71(3)°, γ = 102.28(3)°, V = 1343.1(8) Å^3, Z = 2, T = 120(2) K, μ(CuKα) = 7.934 mm^{-1}, $Dcalc$ = 1.881 g/cm^3, 15849 reflections measured (6.086° ≤ 2θ≤ 133.194°), 4725 unique (R_{int} =

0.2785, R_{sigma} = 0.2953) which were used in all calculations. The final R_1 was 0.1085 (I > 2σ(I)) and wR_2 was 0.3194 with GOF = 0.887.

Crystal data for (**2-8**): $C_{21}H_{18}F_{12}N_4P_2Pd$ (M =722.73 g/mol): monoclinic, space group $P2_1$ (no. 4), a = 7.9903(4) Å, b = 41.1842(12) Å, c = 8.2614(6) Å, β = 111.488(7)°, V = 2529.7(3) Å^3, Z = 4, T = 120.03(10) K, μ(CuKα) = 8.148 mm^{-1}, $Dcalc$ = 1.898 g/cm^3, 15540 reflections measured (8.588° ≤ 2θ ≤ 149.016°), 8683 unique (R_{int} = 0.0513, R_{sigma} = 0.0487) which were used in all calculations. The final R_1 was 0.1118 (I > 2σ(I)) and wR_2 was 0.3595 with GOF = 1.039.

Crystal data for (**2-9**): $C_{24}H_{24}F_{12}N_6P_2Pd$ (M + MeCN) (M =792.49 g/mol): orthorhombic, space group Pbca (no. 61), a = 14.5330(4) Å, b = 18.8067(6) Å, c = 21.4177(6) Å, V = 5853.8(3) Å^3, Z = 3, T = 120.03(10) K, μ(CuKα) = 2.025 mm^{-1}, $Dcalc$ = 0.407 g/cm^3, 14849 reflections measured (8.256° ≤ 2θ ≤ 147.732°), 5808 unique (R_{int} = 0.1260, R_{sigma} = 0.0901) which were used in all calculations. The final R_1 was 0.1873 (I > 2σ(I)) and wR_2 was 0.3970 with GOF = 1.053.

Crystal data for (**2-10**): $C_{23}H_{18}B_2F_8N_6Pd_2$ (M =658.07 g/mol): monoclinic, space group $P2_1/c$ (no. 14), a = 18.2808(5) Å, b = 17.6290(4) Å, c = 15.6788(4) Å, β = 105.606(3)°, V = 4866.6(2) Å^3, Z = 4, T = 120(2) K, μ(CuKα) = 6.938 mm^{-1}, $Dcalc$ = 1.741 g/cm^3, 24418 reflections measured (7.096° ≤ 2θ ≤ 148.258°), 9562 unique (R_{int} = 0.0490, R_{sigma} = 0.0398) which were used in all calculations. The final R_1 was 0.0571 (I > 2σ(I)) and wR_2 was 0.1798 with GOF = 1.045.

2.5 References

1. H. Li, M. Eddaoudi, T. L. Groy and O. Yaghi, *Journal of the American Chemical Society*, 1998, **120**, 8571-8572.

2. S. i. Noro, S. Kitagawa, M. Kondo and K. Seki, *Angewandte Chemie International Edition*, 2000, **39**, 2081-2084.

3. D. Bradshaw, T. J. Prior, E. J. Cussen, J. B. Claridge and M. J. Rosseinsky, *Journal of the American Chemical Society*, 2004, **126**, 6106-6114.

4. A. Stein, S. W. Keller and T. E. Mallouk, *Science*, 1993, **259**, 1558-1565.

5. M. Fujita, Y. J. Kwon, S. Washizu and K. Ogura, *Journal of the American Chemical Society*, 1994, **116**, 1151-1152.

6. S. R. Batten and R. Robson, *Angewandte Chemie International Edition*, 1998, **37**, 1460-1494.

7. O. Ohmori, M. Kawano and M. Fujita, *Angewandte Chemie*, 2005, **117**, 1998-2000.

8. O. Yaghi and G. Li, *Angewandte Chemie International Edition*, 1995, **34**, 207-209.

9. O. Yaghi and H. Li, *Journal of the American Chemical Society*, 1996, **118**, 295-296.

10. O. M. Yaghi, H. Li, C. Davis, D. Richardson and T. L. Groy, *Accounts of Chemical Research*, 1998, **31**, 474-484.

11. J. S. Seo, D. Whang, H. Lee and S. Im Jun, *Nature*, 2000, **404**, 982.

12. O. R. Evans, H. L. Ngo and W. Lin, *Journal of the American Chemical Society*, 2001, **123**, 10395-10396.

13. R. Q. Zou, H. Sakurai and Q. Xu, *Angewandte Chemie*, 2006, **118**, 2604-2608.

14. D. Jaganyi, A. Hofmann and R. van Eldik, *Angewandte Chemie International Edition*, 2001, **40**, 1680-1683.

15. A. Hofmann, D. Jaganyi, O. Q. Munro, G. Liehr and R. van Eldik, *Inorganic Chemistry*, 2003, **42**, 1688-1700.

16. B. Pitteri, G. Marangoni, L. Cattalini and T. Bobbo, *Journal of the Chemical Society, Dalton Transactions*, 1995, 3853-3859.

17. Ž. D. Bugarčić, G. Liehr and R. van Eldik, *Journal of the Chemical Society, Dalton Transactions*, 2002, 951-956.

18. S. D. Cummings, *Coordination Chemistry Reviews*, 2009, **253**, 449-478.

19. I. Eryazici, C. N. Moorefield and G. R. Newkome, *Chemistry Review*, 2008, **108**, 1834-1895.

20. K. M.-C. Wong and V. W.-W. Yam, *Coordination Chemistry Reviews*, 2007, **251**, 2477-2488.

21. F. N. Castellano, I. E. Pomestchenko, E. Shikhova, F. Hua, M. L. Muro and N. Rajapakse, *Coordination Chemistry Reviews*, 2006, **250**, 1819-1828.

22. V. W.-W. Yam, *Journal of Organometallic Chemistry*, 2004, **689**, 1393-1401.

23. D. R. McMillin and J. J. Moore, *Coordination Chemistry Reviews*, 2002, **229**, 113-121.

24. D. K. C. Tears and D. R. McMillin, *Coordination Chemistry Reviews*, 2001, **211**, 195-205.

25. E. C. Constable, C. E. Housecroft, M. Neuburger, S. Schaffner and E. J. Shardlow, *Crystal Engineering Community*, 2005, **7**, 599-602.

26. A. M. C. Thompson, *Coordination Chemistry Reviews*, 1997, **160**, 1-52.

27. U. Ziener, E. Breuning, J. M. Lehn, E. Wegelius, K. Rissanen, G. Baum, D. Fenske and G. Vaughan, *Chemistry-A European Journal*, 2000, **6**, 4132-4139.

28. G. T. Morgan and F. H. Burstall, *Journal of the Chemical Society,* 1932, 20-30.

29. G. T. Morgan and F. H. Burstall, *Journal of the Chemical Society*, 1934, 1498-1500.

30. U. S. Schubert, H. Hofmeier and G. R. Newkome, *Modern Terpyridine Chemistry*, John Wiley & Sons, 2006.

31. A. J. Goshe, I. M. Steele and B. Bosnich, *Journal of the American Chemical Society*, 2003, **125**, 444-451.

32. J. A. Bailey, V. J. Catalano and H. B. Gray, *Acta Crystallographica Section C: Crystal Structure Communications*, 1993, **49**, 1598-1602.

33. M. Akiba and Y. Sasaki, *Inorganic Chemistry Communications*, 1998, **1**, 61-63.

34. X. Liu, S. L. Renard, C. A. Kilner and M. A. Halcrow, *Inorganic Chemistry Communications*, 2003, **6**, 598-603.

35. V. Miskowski, V. Houlding, C. Che and Y. Wang, *Journal of the Chemical Society, Dalton Transactions*, 1999, **1017**.

36. S. Coşar, M. B. Janik, M. Flock, E. Freisinger, E. Farkas and B. Lippert, *Journal of the Chemical Society, Dalton Transactions*, 1999, 2329-2336.

37. Ž. D. Bugarčić, B. Petrović and E. Zangrando, *Inorganica Chimica Acta*, 2004, **357**, 2650-2656.

38. R. Kaskafetou, M. J. Manos and A. Garoufis, *Inorganic Chemistry Communications*, 2013, **35**, 176-180.

39. R. Büchner, J. S. Field, R. J. Haines, C. T. Cunningham and D. R. McMillin, *Inorganic Chemistry*, 1997, **36**, 3952-3956.

40. R. Corbo, T. P. Pell, B. D. Stringer, C. F. Hogan, D. J. Wilson, P. J. Barnard and J. L. Dutton, *Journal of the American Chemical Society*, 2014, **136**, 12415-12421.

41. J. H. Yip, A. Suwarno and J. J. Vittal, *Inorganic Chemistry*, 2000, **39**, 3537-3543.

42. S. S. Hosseini, M. Bhadbhade, R. J. Clarke, P. J. Rutledge and L. M. Rendina, *Dalton Transactions*, 2011, **40**, 506-513.

43. E. Guney, V. T. Yilmaz, A. Sengul and O. Buyukgungor, *Inorganica Chimica Acta*, 2010, **363**, 438-448.

44. CrysAlisPro, *Agilent Technologies UK Ltd., Oxford, UK*, 2013.

45. G. M. Sheldrick, *Acta Crystallographica Section A: Foundations of Crystallography*, 2008, **64**, 112-122.

46. G. M. Sheldrick, *Acta Crystallographica Section A: Foundations and Advances*, 2015, **71**, 3-8.

47. G. M. Sheldrick, *Acta Crystallographica Section C: Structural Chemistry*, 2015, **71**, 3-8.

48. O. V. Dolomanov, L. J. Bourhis, R. J. Gildea, J. A. Howard and H. Puschmann, *Journal of Applied Crystallography*, 2009, **42**, 339-341.

Chapter 3

Mono Palladium (4,4',4''-Tri-*tert*-butyl-2,2':6',2''-terpyridine) Complexes with *Para*-Substituted Pyridine Derivatives

3.1 Introduction

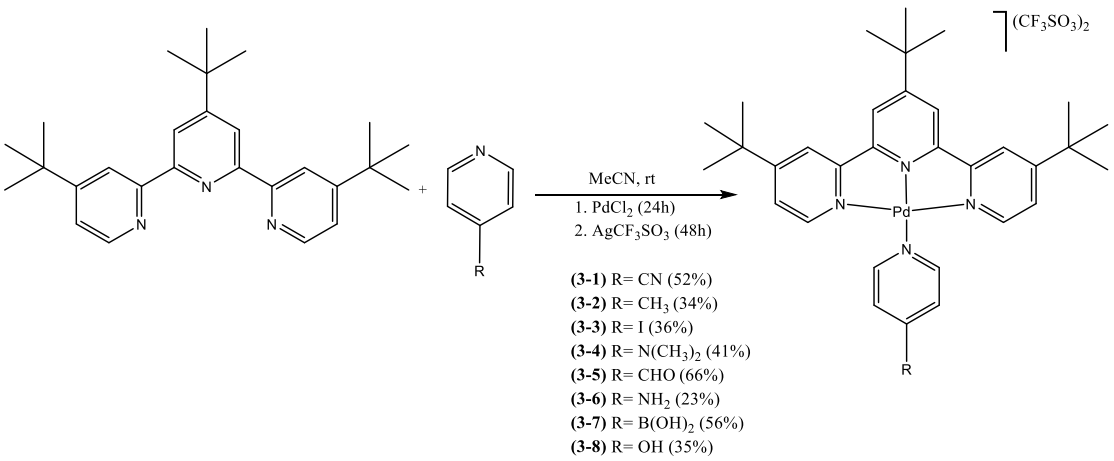
A wide range of functionalized terpy moieties possess a single substituent at the 4' position, or three substituents at the 4,4' and 4" positions. In order to extend the experimental observations and the range of applicability of the proposed interpretation, another system involving the tridentate aromatic nitrogen donor 4,4',4"-tri-*tert*-butyl-2,2':6',2"-terpyridine (*t*Bu$_3$-terpy) has been examined. Substituents on the terpy moiety can alter its properties, the main characteristic of the metal complexes bearing *t*Bu$_3$-terpy is their high solubility, which results from the existence of the hydrophobic *t*Bu groups [1]. Moreover, the bulky nature of the *t*Bu substituents helps to minimize intermolecular interactions between molecules [2]. Thus, in order to compare and contrast the influence of butyl substituents on the crystal structures of this series, an analogous *t*Bu$_3$-terpyridine was used.

3.2 Results and Discussion

3.2.1 Synthesis of a series of mononuclear palladium (4,4',4''-tri-*tert*-butyl-2,2':6',2''-terpyridine) triflate complexes

All complexes were synthesised following the same synthetic procedure. All reactions were conducted in dry acetonitrile. In a typical experiment, commercially available *t*Bu$_3$-terpy and palladium chloride were dissolved in acetonitrile and the reaction mixture was stirred at room temperature. After stirring for 24 hours, silver triflate was added. In the absence of light, the reaction mixture was stirred for 48 hours. After 48 hours, the white precipitate (AgCl) was filtered. A pyridine derivative was added to the reaction solution and stirred for 3 hours. The resulting solution was concentrated *via* rotary evaporation to remove the excess acetonitrile solvent. The resulting solid was washed with diethyl ether,

before being dried in *vacuo* to afford the title compound in acceptable yield (Scheme3.1). Eight pyridine derivatives with different substitutions at the *para*-position were studied.



Scheme 3.1: Synthesis of a series of mononuclear palladium (4,4',4''-tri-*tert*-butyl-2,2':6',2''-terpyridine) complexes.

3.2.2. X-ray crystallography

Single crystals suitable for X-ray diffraction were obtained for all of the complexes reported herein. Single crystals were grown by dissolution of the product in the minimum amount of acetonitrile and diffusion of diethyl ether vapour into this solution.

*3.2.2.1 Single crystal X-ray structure of 4,4',4''-tri-tert-butyl-2,2':6',2''-terpyridine (4-cyanopyridine) palladium triflate [Pd(tBu3-terpy)(4-cyanopyridine)](CF3SO3)2 (**3-1**).*

Crystals of [Pd(*t*Bu$_3$-terpy)(4-cyanopyridine)](CF$_3$SO$_3$)$_2$ were found to be colourless plates. The complex crystallises in the monoclinic space group $P2_1/c$. As shown in Figure 3.1, space above and below the Pd cation is occupied by two triflate anions. Unlike complex (**2-1**), there are no free solvent molecules contained in the unit cell. *t*Bu$_3$-terpyridine is coordinated to palladium as a tridentate ligand and the fourth position is occupied by 4-cyanopyridine. The coordination geometry of the palladium ion is

distorted slightly from that found in perfect square-planar Pd(II) complexes. Table 3.1 lists important bond lengths and angles for this complex. The angles between the adjacent nitrogen atoms in the plane deviate slightly from the theoretical value of 90° (N2A–Pd1A–N1A and N3A–Pd1A–N2A = 80.7(2)°) and N3A-Pd1A-N1A angle (161.5(3)°) is smaller than the theoretical value of 180°. These angles are much smaller than those found in complex (**2-1**), but in excellent agreement with those of a related [Pt(*t*Bu$_3$-terpy)Cl]ClO$_4$ complex reported previously [3]. The Pd–N distance to the central nitrogen atom of the *t*Bu$_3$-terpy is shorter than those to the other two nitrogen atoms, but in excellent agreement with that of complex (**2-1**). There is a significant elongation of the Pd1A–N1A and Pd1A–N3A bonds from 1.961(18) and 1.925(17) Å in (**2-1**) to 2.034(7) and 2.012(6) Å in (**3-1**). A similar distorted square-planar geometry, which is a result of the geometric constraints imposed by coordination of the tridentate *t*Bu$_3$-terpyridine molecule, also occurs in the related palladium(II) terpyridine complexes in Chapter 2. This complex shows higher distortion from an idealized square planar arrangement than that in complex (**2-1**). This is observed in two parameters: the dihedral angle and the tilt angle. The 4-cyanopyridine is twisted with respect to terpyridine plane forming a dihedral angle of 65.71(6)°. The dihedral angle indicates that 4-cyanopyridine in complex (**3-1**) is twisted more than that in complex (**2-1**) (84.04(7)°). The tilt angle of complex (**3-1**) is 179.5(8)°, similar to that found in complex (**2-1**) (179.70(9)°). Cations of (**3-1**) are less planar than those of (**2-1**), with a maximum displacement of +0.095 and -0.140 Å exhibited by C14A and C1A, respectively, from the mean plane.

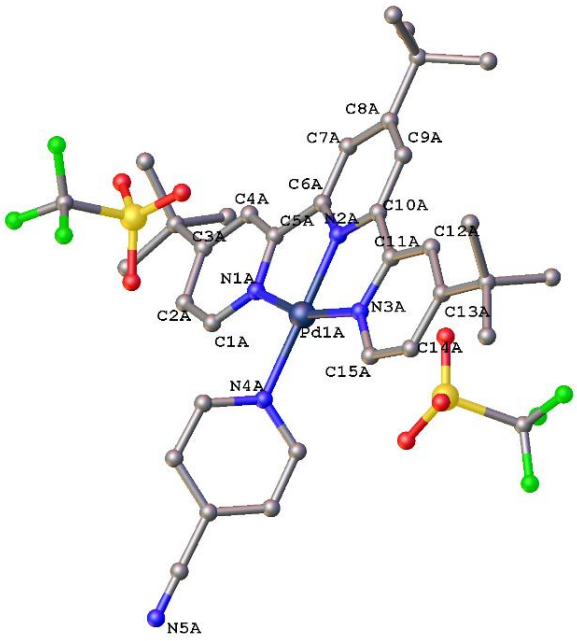


Figure 3.1: X-ray crystal structure of [Pd(*t*Bu$_3$-terpy)(4-cyanopyridine)](CF$_3$SO$_3$)$_2$ with crystallographically independent atom numbering scheme. Hydrogen atoms have been omitted for clarity. Atom colours - C: grey, O: red, N: blue, Pd: navy F: green and S: yellow.

Table 3.1: Selected bond lengths (Å) and angles (°) for [Pd(*t*Bu$_3$-terpy)(4-cyanopyridine)](CF$_3$SO$_3$)$_2$

Pd1A-N1A	2.034(7)	N2A-Pd1A-N1A	80.7(2)
Pd1A-N2A	1.929(7)	N2A-Pd1A-N4A	179.5(2)
Pd1A-N3A	2.012(6)	N3A-Pd1A-N1A	161.5(3)
Pd1A-N4A	2.045(7)	N3A-Pd1A-N2A	80.7(2)

Molecules of (**3-1**) pack in head to tail conformation from the view along the *a*-axis. This conformation minimizes the mutual repulsion between the sterically bulky *t*Bu$_3$-terpyridine moieties. Cations and anions of complex (**3-1**) form parallel sheets along the *b*-axis, where each cation is paired with two triflate anions (Figure 3.2). It is conceivable

that the presence of the bulky *t*Bu$_3$ groups on the terpyridine moiety would hinder the formation of such interactions.

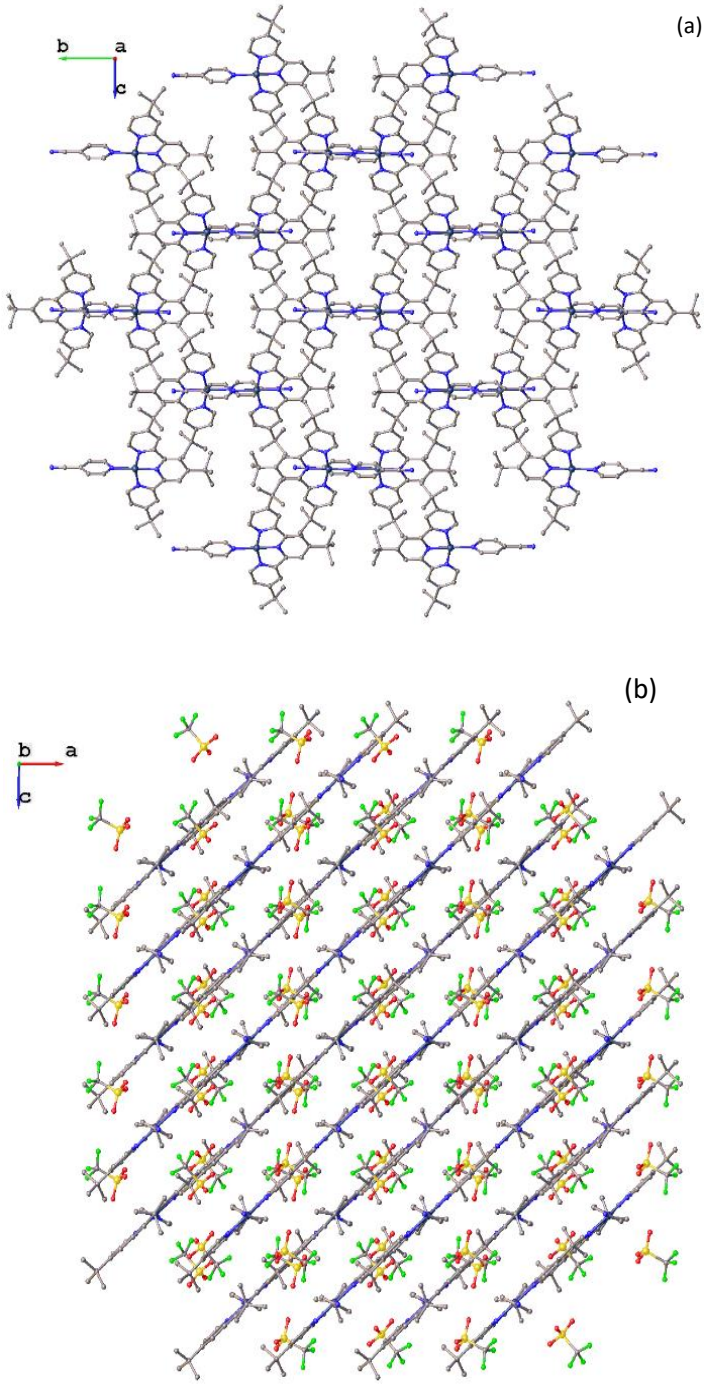


Figure 3.2: (a) The packing diagram of [Pd(*t*Bu$_3$-terpy)(4-cyanopyridine)](CF$_3$SO$_3$)$_2$ along the *a*-crystal axis. (b) View down the *b*-crystal axis. Hydrogen atoms are omitted for clarity.

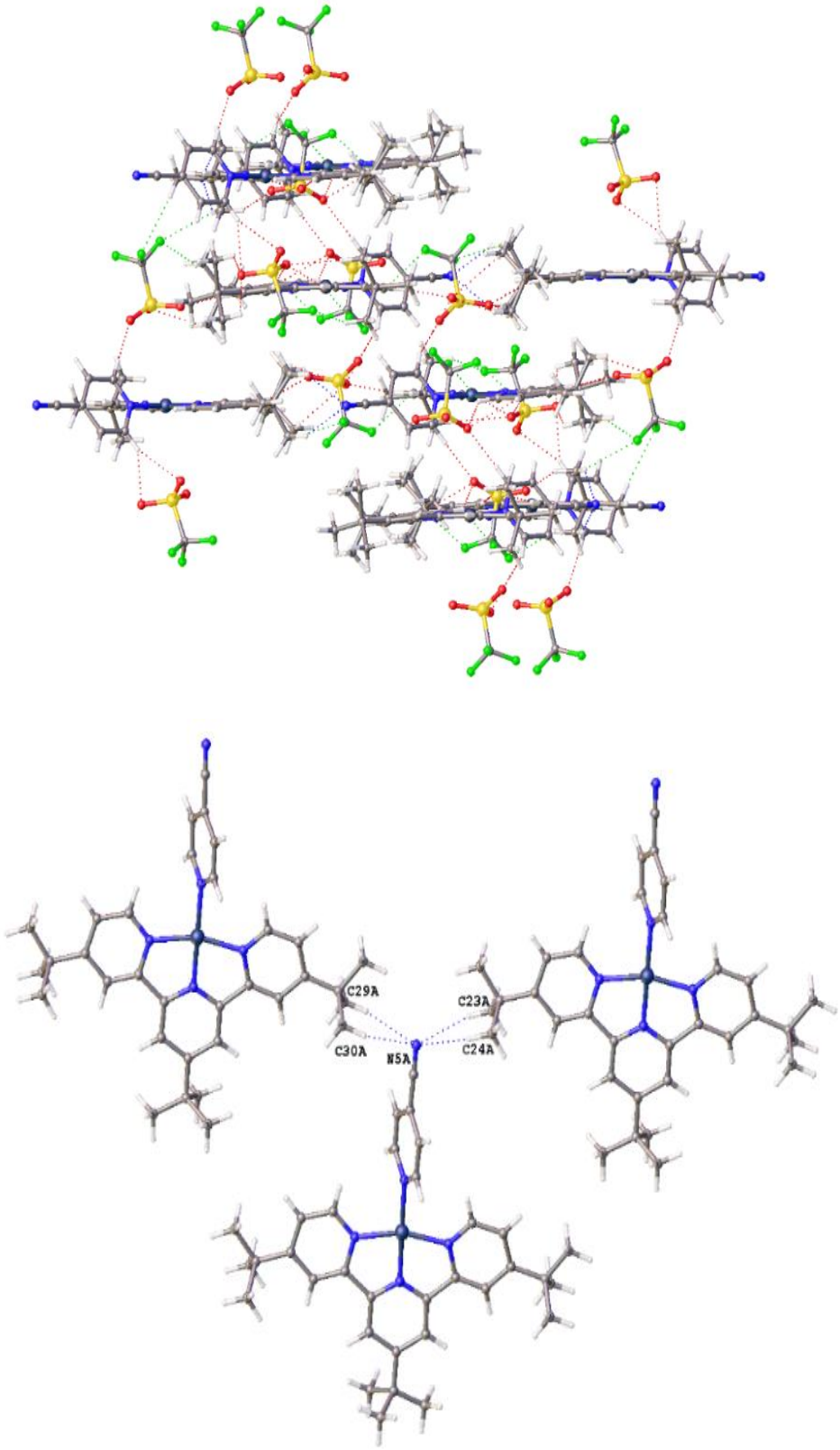


Figure 3.4: (a) A net of hydrogen bonds links Pd(*t*Bu$_3$-terpy) cations and triflate anions for [Pd(*t*Bu$_3$-terpy)(4-cyanopyridine)](CF$_3$SO$_3$)$_2$. (b) Hydrogen bonds formed by 4-cyanopyridine units.

There is a net of hydrogen bonds, as shown in Figure 3.3. The triflate anion acts as a hydrogen bond acceptor and form hydrogen bonds with 4-cyanopyridine and *t*Bu$_3$-terpyridine. The C–H…O distances lie in the range 2.137– 2.997 Å and the C–H…F distances lie in the range 2.461 – 2.959 Å. The cyano groups act as hydrogen bond acceptors via four sets of C–H…N hydrogen bonds. The C23A–H23B....N5A, C24A–H24B....N5A, C29A–H29B....N5A and C30A–H30B....N5A distances are 2.585, 2.830, 2.655 and 2.669 Å, respectively.

*3.2.2.2 Single crystal X-ray structure of 4,4',4''-tri-tert-butyl-2,2':6',2''-terpyridine (4-methylpyridine) palladium triflate [Pd(tBu$_3$-terpy)(4-methylpyridine)](CF$_3$SO$_3$)$_2$ (**3-2**).*

There are four independent molecules in the asymmetric unit and each molecule adopts distorted square planar arrangement. Figure 3.4 shows the coordination geometry and atom labelling scheme for complex (**3-2**). Eight triflate anions are presented in the asymmetric unit. Crystals of [Pd(*t*Bu$_3$-terpy)(4-methylpyridine)](CF$_3$SO$_3$)$_2$ were found to be colourless plates. The complex crystallises in the triclinic space group *P-1*. The Pd cation is coordinated by three N atoms of the tridentate chelating terpyridyl unit and one nitrogen atom from 4-methylpyridine. Selected bond lengths and angles are summarized in Table 3.2. The central Pd–N(terpy) bond is noticeably shorter than the other three Pd–N bonds. The Pd–N bond lengths and angles are comparable to those found in (**2-2**). The dihedral angle between the square planar coordination sphere of the Pd cation and the 4-methylpyridine ring amounts to (average = 61.92(11)°). The dihedral angle indicates that 4-methylpyridine in complex (**3-2**) is bent more than that in complex (**2-2**). The terpyridine unit is twisted with a maximum displacement of +0.116 and -0.167 Å

exhibited by C8A and C15A, respectively, from the mean plane. The terpyridine unit in (**3-2**) shows a greater deviation from planarity than (**2-2**).

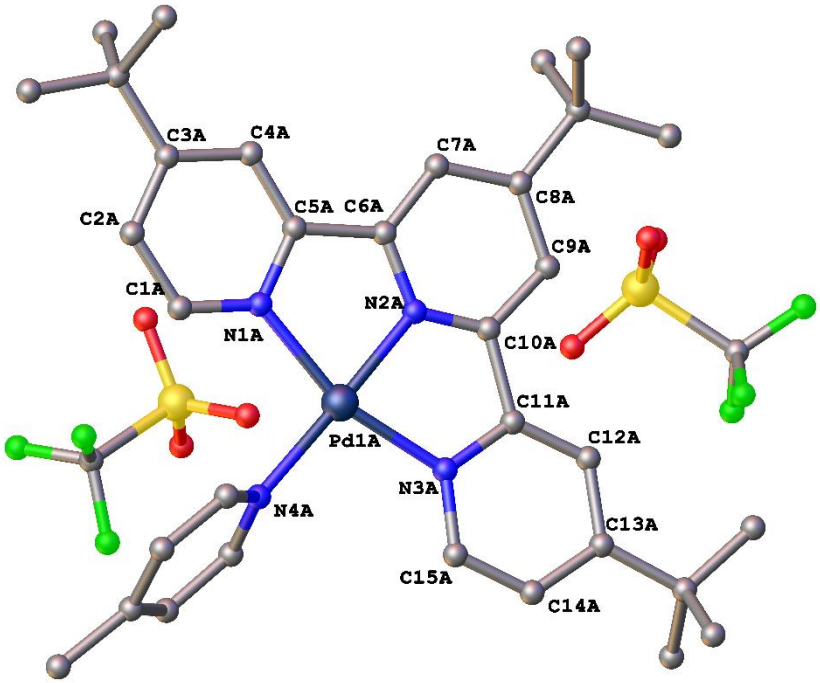


Figure 3.4: X-ray crystal structure of [Pd(*t*Bu$_3$-terpy)(4-methylpyridine)](CF$_3$SO$_3$)$_2$ with crystallographically independent atom numbering scheme. Hydrogen atoms have been omitted for clarity. Atom colours - C: grey, O: red, N: blue, Pd: navy F: green and S: yellow.

Table 3.2: Selected bond lengths (Å) and angles (°) for [Pd(*t*Bu$_3$-terpy)(4-methylpyridine)](CF$_3$SO$_3$)$_2$.*

Pd1-N1	2.039(9)	N2-Pd1-N1	80.90(3)
Pd1-N2	1.943(8)	N2-Pd1-N4	178.0(3)
Pd1-N3	2.033(9)	N3-Pd1-N1	162.0(3)
Pd1-N4	2.041(9)	N3-Pd1-N2	81.60(4)

*The average bond lengths and angles for four complexes.

In the solid state, the molecules of (**3-2**) are packed as shown in Figure. 3.5, similar to that in complex [Pd(*t*Bu$_3$-terpy)(NCCH$_3$)](CF$_3$SO$_3$)$_2$ [4]. The two nearby cations show a head-to-tail conformation to minimize the mutual repulsion between the sterically bulky tri-*tert*-butylterpyridine. Each cation dimer is surrounded by eight triflate anions.

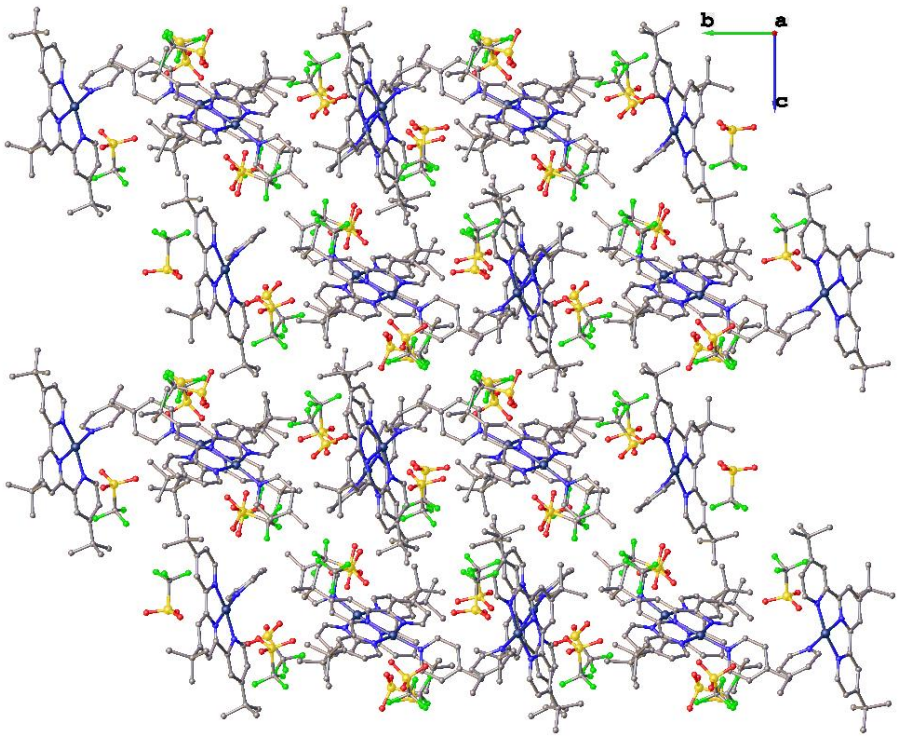


Figure 3.5: The packing diagram for [Pd(*t*Bu$_3$-terpy)(4-methylpyridine)](CF$_3$SO$_3$)$_2$ along the *a*-axis. Hydrogen atoms are omitted for clarity.

The oxygen and fluorine atoms of the triflate anions act as hydrogen bond acceptors generating hydrogen bonds with hydrogen atoms of terpyridine and 4-methylpyridine, as shown in Figure 3.6. The C–H…O distances lie in the range 2.243 – 2.995 Å and the C–H…F distances lie in the range 2.349 – 2.961 Å.

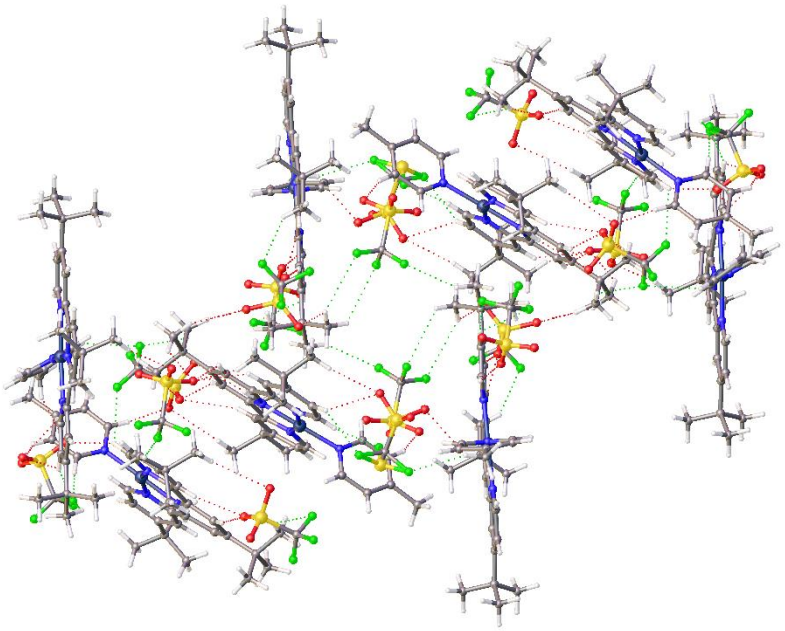


Figure 3.6: A net of hydrogen bonds links Pd(*t*Bu$_3$-terpy) cations and triflate anions for [Pd(tBu$_3$-terpy)(4-methylpyridine)](CF$_3$SO$_3$)$_2$.

*3.2.2.3 Single crystal X-ray structure of 4,4',4''-tri-tert-butyl-2,2':6',2''-terpyridine (4-iodopyridine) palladium triflate [Pd(tBu$_3$-terpy)(4-iodopyridine)](CF$_3$SO$_3$)$_2$ (**3-3**).*

Crystals of [Pd(*t*Bu$_3$-terpy)(4-iodopyridine)](CF$_3$SO$_3$)$_2$ were found to be colourless plates, crystallising in the monoclinic space group *P2$_1$/n*. Figure 3.7 shows the coordination geometry and atom labelling scheme for complex (**3-3**). Space above and below the Pd cation is occupied by two triflate anions and one acetonitrile molecule. Table 3.3 lists important bond lengths and angles for this complex. As before, the *t*Bu$_3$-terpyridine moiety is coordinated to the Pd atom in a tridentate fashion, and distorts the square planar geometry of the Pd atom. The central Pd–N(terpy) bond (1.937(9) Å) is noticeably shorter than the other Pd–N bonds and longer than that found in the unsubstituted complex (**2-3**) (1.934(3) Å). The N-Pd-N angles [N2A–Pd1A–N1A 80.60°(4), N2A–Pd1A–N3A 81.0°(4), N3A–Pd1A–N1A 161.30(4)°] show deviations from the idealized

values of 90° and 180°. These values are similar to those found in the unsubstituted analogue (**2-3**). This complex shows higher distortion from an idealized square plane than that observed in complex (**2-3**). This is observed in two parameters: the dihedral angle and the tilt angle. 4-Iodopyridine ligand is significantly bent with respect to terpyridine plane forming a dihedral angle of 53.95(7)°. This geometrical feature is comparable to those observed in complex (**2-3**). The tilt angle for complex (**3-3**) is 175.20(4)°. This value is smaller than those found in complex (**2-3**), 179.43(11)° and 178.90(11)° for molecule (**A**) and (**B**), respectively. Cations of (**3-3**) are less planar than those of (**2-3**), with a maximum displacement of +0.137 and -0.144 Å exhibited by C7A and C2A, respectively, from the mean plane.

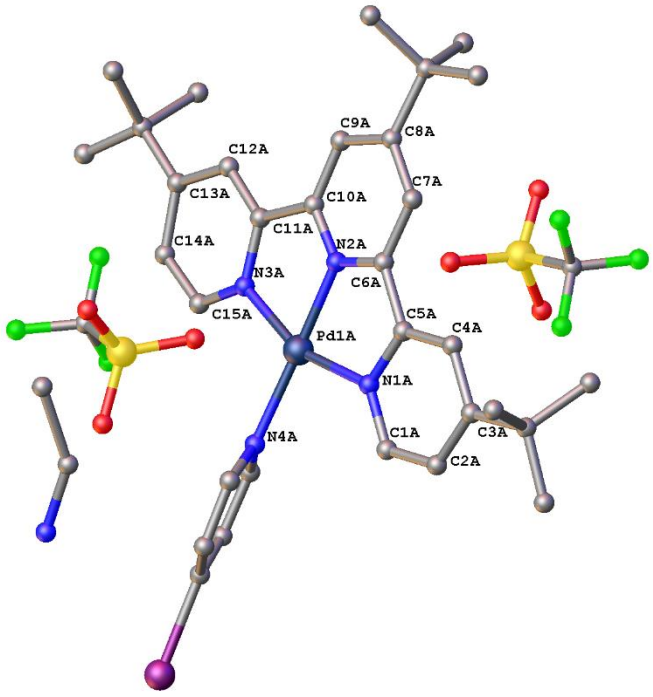


Figure 3.7: X-ray crystal structure of [Pd(*t*Bu$_3$-terpy)(4-iodopyridine)](CF$_3$SO$_3$)$_2$ with crystallographically independent atom numbering scheme. Hydrogen atoms have been omitted for clarity. The disorder in the triflate anion is shown. Atom colours - C: grey, O: red, N: blue, Pd: navy, I: purple, F: green and S: yellow.

Table 3.3: Selected bond lengths (Å) and angles (°) for [Pd(*t*Bu$_3$-terpy)(4-iodopyridine)](CF$_3$SO$_3$)$_2$.

Pd1A-N1A	2.045(10)	N2A-Pd1A-N1A	80.60(4)
Pd1A-N2A	1.937(9)	N2A-Pd1A-N4A	175.20(4)
Pd1A-N3A	2.048(11)	N3A-Pd1A-N1A	161.30(4)
Pd1A-N4A	2.053(9)	N3A-Pd1A-N2A	81.0(4)

In the solid state, the cations of (**3-3**) are packed as head-to-tail dimers in the crystal lattice, as shown in Figure 3.8. This orientation will reduce the mutual repulsion between the sterically bulky *t*Bu$_3$-terpyridine moieties. The triflate anions and acetonitrile molecules fill the space between cations.

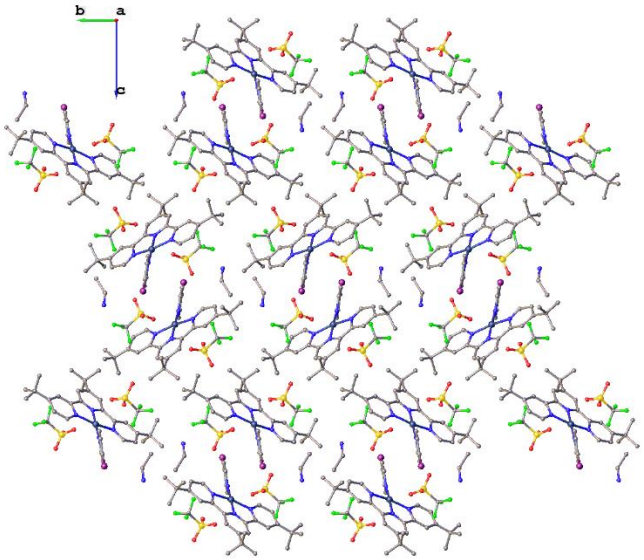


Figure 3.8: The packing diagram for [Pd(*t*Bu$_3$-terpy)(4-iodopyridine)](CF$_3$SO$_3$)$_2$ along the *a*-axis. Hydrogen atoms are omitted for clarity.

The oxygen and fluorine atoms of triflate anion act as hydrogen bond acceptors generating hydrogen bonds with hydrogen atoms of *t*Bu$_3$-terpyridine and 4-iodopyridine

(Figure 3.9). The C–H…O distances lie in the range 2.298 – 2.945 Å and the C–H…F distances lie in the range 2.521 – 2.963 Å.

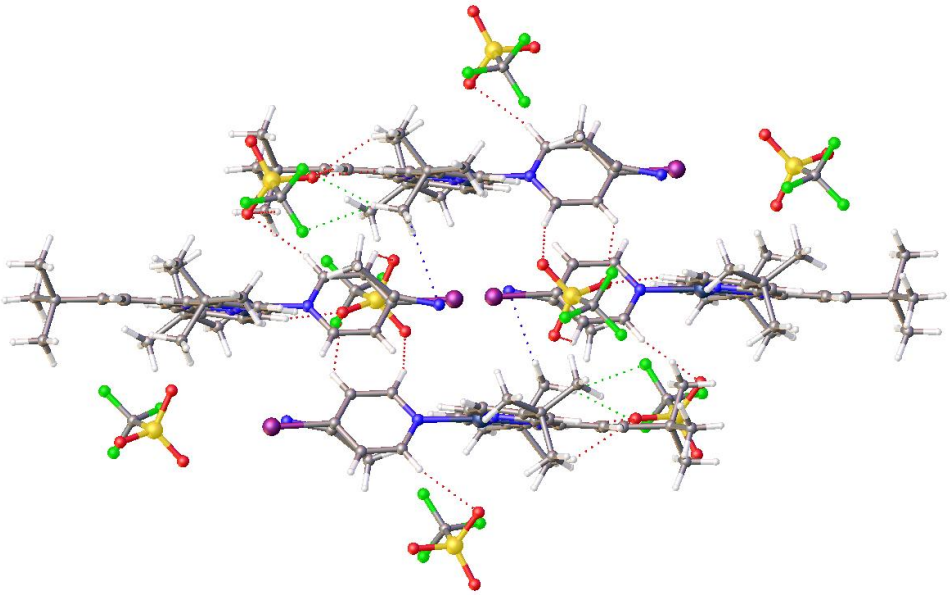


Figure 3.9: A net of hydrogen bonds links Pd(*t*Bu$_3$-terpy) cations, acetonitrile molecules and triflate anions for [Pd(*t*Bu$_3$-terpy)(4-iodopyridine)](CF$_3$SO$_3$)$_2$.

*3.2.2.4 Single crystal X-ray structure of 4,4',4''-tri-tert-butyl-2,2':6',2''-terpyridine (4-dimethylaminopyridine) palladium triflate [Pd(tBu$_3$-terpy)(4-dimethylaminopyridine)](CF$_3$SO$_3$)$_2$ (**3-4**).*

Crystals of [Pd(*t*Bu$_3$-terpy)(4-dimethylaminopyridine)](CF$_3$SO$_3$)$_2$ were found to be colourless plates, crystallising in the monoclinic space group $P2_1/n$. Figure 3.10 shows the coordination geometry and atom labelling scheme for complex (**3-4**). Space above and below the Pd cation is occupied by two triflate anions. Table 3.4 lists important bond lengths and angles for this complex. The coordination geometry around the palladium(II) cation is considerably distorted from the perfect square-plane. This distortion leads to a narrowing of N1–Pd–N2 and N2–Pd–N3 angles to 80.98(6)° and 81.02(6)°, respectively, and also a significant shortening of Pd–N2 distances (1.935(16) Å) compared to the other

Pd–N distances (Pd–N1 = 2.026(16) Å and Pd–N3 = 2.028(16) Å), as shown in Table 3.4. In general, bond distances for complex (**3-4**) are slightly longer than those found in molecule (**A**) in complex (**2-4**) and shorter than those found in molecule (**B**). Bond distances and angles of this complex compare well with those already reported [Au(terpy)(4-dimethylaminopyridine)]$(CF_3SO_3)_3$ [5].

The angle between the square planar coordination geometry of the Pd(*t*Bu_3-terpy) cation and the plane of 4-dimethylaminopyridine is 82.31(7)°. The dihedral angle indicates that the *t*Bu_3-terpyidine ring and 4-dimethylaminopyridine are almost perpendicular to each other, similar to that found in complex (**2-4**) molecule (**B**) (85.35(5)°). This geometrical feature is comparable to those observed in the related species [Au(terpy)(4-dimethylaminopyridine)]$(CF_3SO_3)_3$ (89.15°) and [Pd(terpy)(Hmcyt-N^3)]$[NO_3]_2.5H_2O$ (84°) [5,6]. In terms of tilt angle, complex (**3-4**) 176.46(6)° indicates higher deviation from the theoretical value of 180° than two molecules in complex (**2-4**) (molecule (**A**) is 178.8(2)° and molecule (**B**) is 178.27(19)°).

Cations of (**3-4**) pack in a head-to-tail fashion as shown in Figure 3.11. The stacks of cations orient themselves into channels and the triflate anions fill the space between these channels.

The outer pyridyl ring and the central pyridyl ring of another molecule have a centroid–centroid distance of 4.182 Å, indicating π· · ·π interaction is absent, as shown in Figure 3.12.

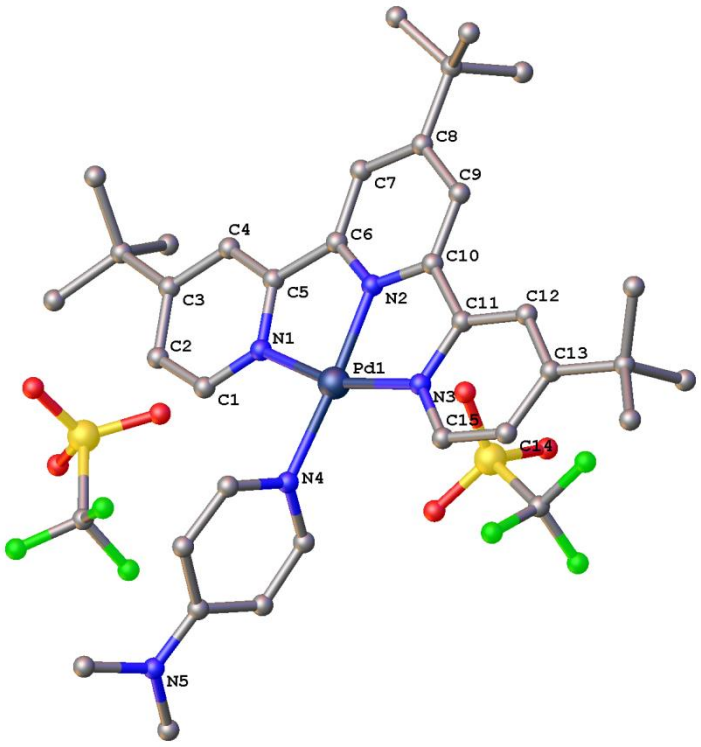


Figure 3.10: X-ray crystal structure of [Pd(*t*Bu$_3$-terpy)(4-dimethylaminopyridine)](CF$_3$SO$_3$)$_2$ with crystallographically independent atom numbering scheme. Hydrogen atoms have been omitted for clarity. Atom colours - C: grey, O: red, N: blue, Pd: navy F: green and S: yellow.

Table 3.4: Selected bond lengths (Å) and angles (°) for [Pd(*t*Bu$_3$-terpy)(4-dimethylaminopyridine)](CF$_3$SO$_3$)$_2$

Pd1-N1	2.026(16)	N2-Pd1-N1	80.98(6)
Pd1-N2	1.935(16)	N2-Pd1-N4	176.46(6)
Pd1-N3	2.028(16)	N3-Pd1-N1	162.00(6)
Pd1-N4	2.026(16)	N3-Pd1-N2	81.02(6)

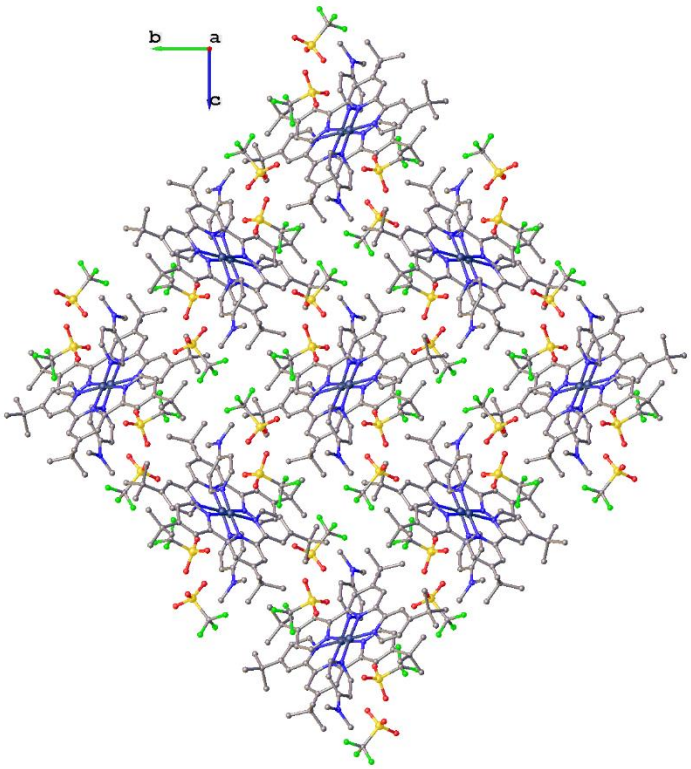


Figure 3.11: The packing diagram for [Pd(*t*Bu$_3$-terpy)(4-dimethylaminopyridine)](CF$_3$SO$_3$)$_2$ along the *a*-axis. Hydrogen atoms are omitted for clarity.

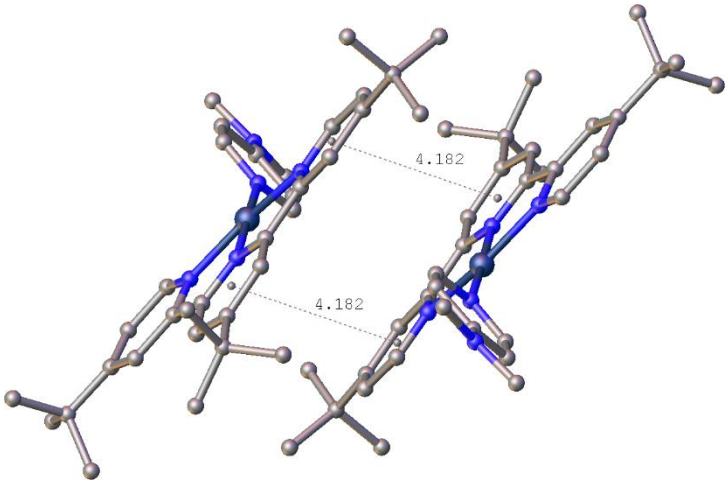


Figure 3.12: Dashed lines indicate the shortest distances between two pyridyl rings in [Pd(*t*Bu$_3$-terpy)(4-dimethylaminopyridine)](CF$_3$SO$_3$)$_2$.

Cations of (**3-4**) are less planar than those of (**2-4**), with a maximum displacement of +0.293 and +0.234 Å exhibited by C15 and N3, respectively, from the mean plane.

There is a net of hydrogen bonds, as shown in Figure 3.13. The triflate anion acts as a hydrogen bond acceptor and forms hydrogen bonds with 4-dimethylaminopyridine and *t*Bu$_3$-terpyridine. The C–H…O distances lie in the range 2.247 – 2.980 Å and the C–H…F distances lie in the range 2.650 – 2.984 Å. Each dimethylamino unit is involved in hydrogen bonds to a triflate anion via three hydrogen bonds. The C33–H33c…O2, C34–H34c…O1 and C33–H33a…F2 distances are 2.672, 2.772 and 2.934 Å, respectively.

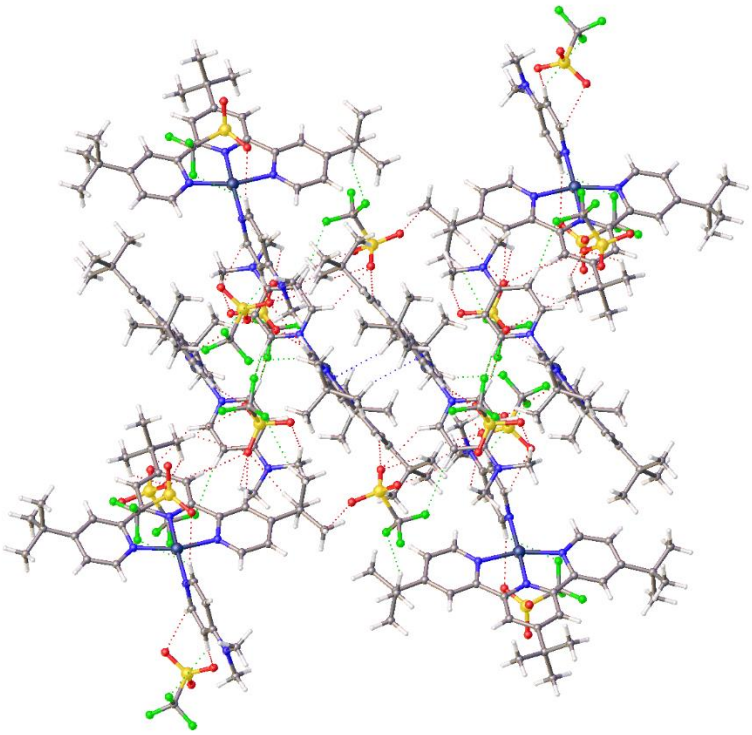


Figure 3.13: A net of hydrogen bonds links Pd(*t*Bu$_3$-terpy) cations and triflate anions for [Pd(*t*Bu$_3$-terpy)(4-dimethylaminopyridine)](CF$_3$SO$_3$)$_2$.

*3.2.2.5 Single crystal X-ray structure of 4,4',4''-tri-tert-butyl-2,2':6',2''-terpyridine (4-pyridinecarboxaldehyde) palladium triflate [Pd(tBu$_3$-terpy)(4-pyridinecarboxaldehyde)](CF$_3$SO$_3$)$_2$ (**3-5**).*

Crystals of [Pd(*t*Bu$_3$-terpy)(4-pyridinecarboxaldehyde)](CF$_3$SO$_3$)$_2$ were found to be colourless plates, crystallising in the monoclinic space group *P2$_1$/n*. As is usually observed, terpyridine acts as a tridentate ligand and an N-bound pyridinecarboxaldehyde ligand completes the distorted square-planar coordination around Pd (Figure 3.14). As expected, the N–Pd–N angles and Pd–N distances are very similar to those in (**2-5**). The central Pd–N bond (1.924(9) Å) is noticeably shorter than the other Pd–N bonds and shorter than that found in the unsubstituted complex (**2-5**) (1.934(3) Å). The N-Pd-N angles [N2–Pd1–N1 81.30°(4), N2–Pd1–N3 80.90°(4) and N3–Pd1–N1 162.30(4)°] show deviations from the idealized values of 90° and 180°. These values are similar to those found the unsubstituted analogue (**2-5**). Similar values were observed in the crystal structure of the complex [Pt(terpy)(4-CO$_2$py)](NO$_3$) [7]. The planar 4-pyridinecarboxaldehyde ligand coordinates out of the Pd(terpy) plane with a dihedral angle of 68.07°(6). The 4-pyridinecarboxaldehyde in complex (**3-5**) is bent more than that in complex (**2-5**).

The terpyridine unit of (**3-5**) is less coplanar than that of molecule (**A**) and (**B**) in complex (**2-5**) with a maximum displacement of -0.148 and -0.129 Å exhibited by C1 and C15, respectively, from the mean plane.

Cations of (**3-5**) pack in a head-to-tail fashion (Figure 3.15). The triflate anions are arranged above and below the cations.

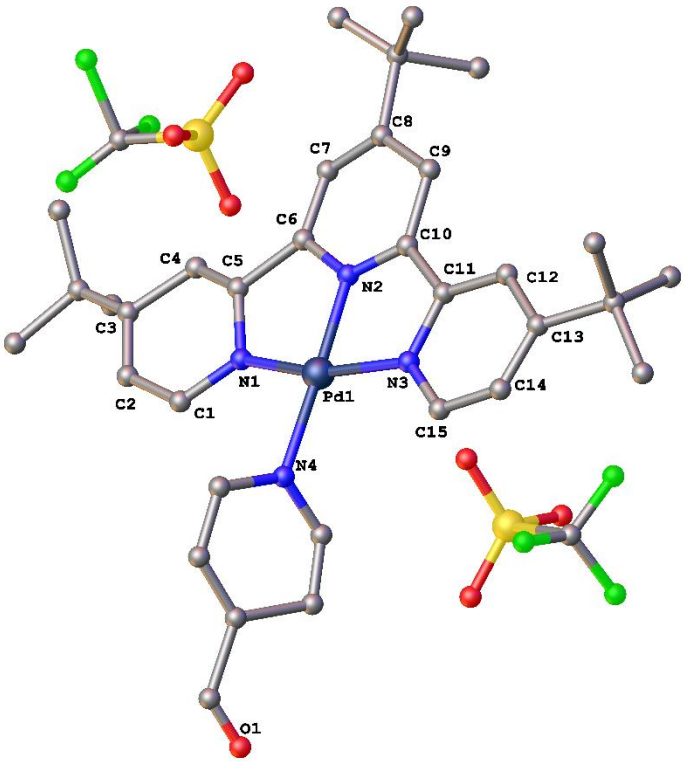


Figure 3.14: X-ray crystal structure of [Pd(*t*Bu$_3$-terpy)(4-pyridinecarboxaldehyde)](CF$_3$SO$_3$)$_2$ with crystallographically independent atom numbering scheme. Hydrogen atoms have been omitted for clarity. Atom colours - C: grey, O: red, N: blue, Pd: navy F: green and S: yellow.

Table 3.5: Selected bond lengths (Å) and angles (°) for [Pd(*t*Bu$_3$-terpy)(4-pyridinecarboxaldehyde)](CF$_3$SO$_3$)$_2$

Pd1-N1	2.005(10)	N2-Pd1-N1	81.30(4)
Pd1-N2	1.924(9)	N2-Pd1-N4	178.20(3)
Pd1-N3	2.030(10)	N3-Pd1-N1	162.30(4)
Pd1-N4	2.052(9)	N3-Pd1-N2	80.90(4)

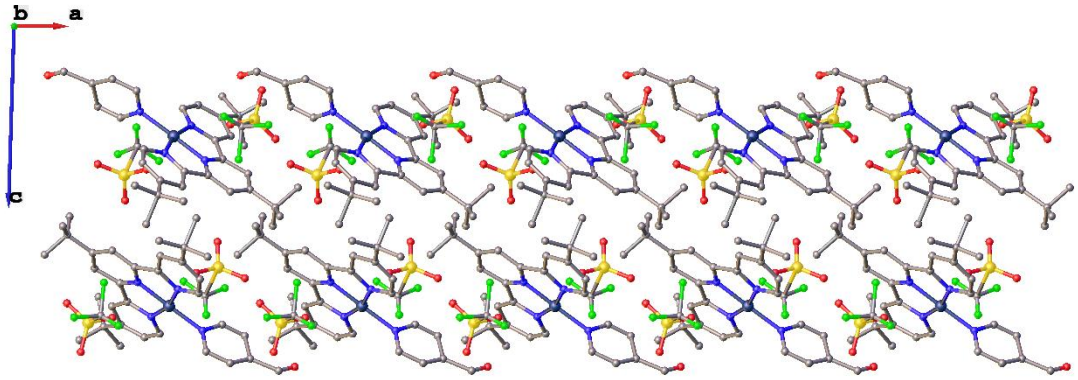


Figure 3.15: The packing diagram for [Pd(*t*Bu$_3$-terpy)(4-pyridinecarboxaldehyde)](CF$_3$SO$_3$)$_2$ along the *b*-axis. Hydrogen atoms and anions are omitted for clarity.

This arrangement is further stabilised by a series of hydrogen bonds between aromatic protons and triflate anions. The C–H…O distances lie in the range 1.957 – 2.981 Å and the C–H…F distances lie in the range 2.425 – 2.868 Å (Figure 3.16).

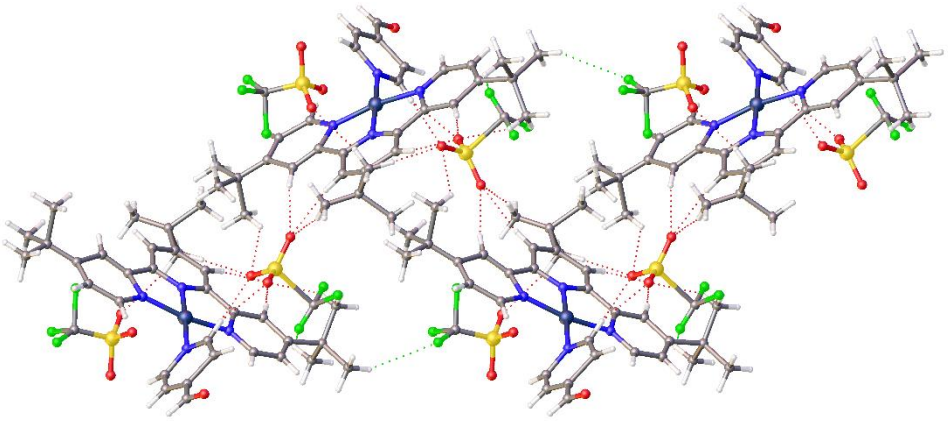


Figure 3.16: A net of hydrogen bonds links Pd(terpy) cations and triflate anions for [Pd(*t*Bu$_3$-terpy)(4-pyridinecarboxaldehyde)](CF$_3$SO$_3$)$_2$.

*3.2.2.6 Single crystal X-ray structure of 2,2':6',2''-terpyridine (4-aminopyridine) palladium triflate [Pd(tBu$_3$-terpy)(4-aminopyridine)](CF$_3$SO$_3$)$_2$ (**3-6**).*

Crystals of [Pd(*t*Bu$_3$-terpy)(4-aminopyridine)](CF$_3$SO$_3$)$_2$ were found to be colourless plates, crystallising in the orthorhombic space group *Pca2$_1$*. As expected, *t*Bu$_3$-terpyridine acts as a tridentate ligand and an N-bound 4-aminopyridine ligand completes the distorted square-planar coordination around Pd. Unlike complex (**2-6**), there are free acetonitrile molecules contained in the unit cell. As before, the angles between the adjacent N atoms in the plane (N2-Pd1-N1=80.89(16)° and N2-Pd1-N3=81.11(16)°) and N3-Pd1-N1 angle (161.92(16)°) deviate slightly from the theoretical values of 90° and 180°. Interestingly, these values are slightly higher than those found in complex (**2-6**). In addition, the bond between the central terpy nitrogen and the Pd atom is the shortest (1.927(4)°), with two longer bonds between the terminal nitrogen atoms and the Pd atom. In general, the Pd–N bonds are slightly shorter than those found in complex (**2-6**), with the Pd–N bonds for (**3-6**) shorter by less than 0.043 Å. In terms of the C18-N5 bond between the amine group and the pyridine ring (1.358(7) Å), it is shorter than a normal single bond C-NH$_2$ (≈ 1.44 Å), which is attributed to the delocalization of the lone pair of the amino nitrogen into the pyridine ring and the C-NH$_2$ bond has some double-bond character [8].

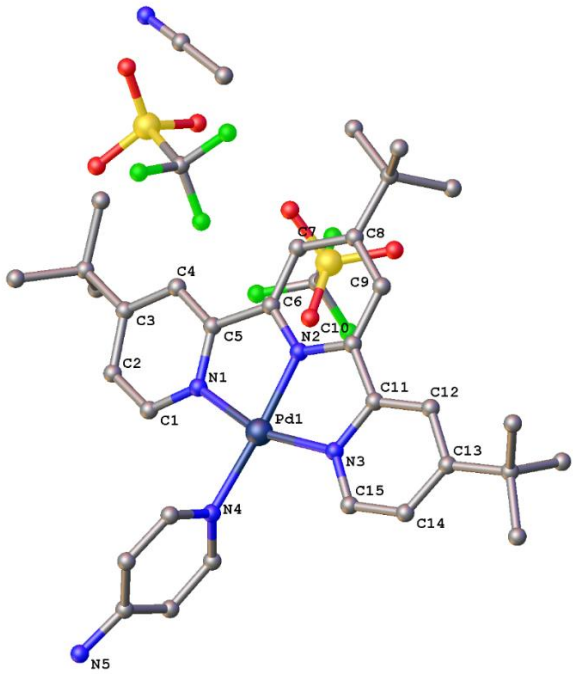


Figure 3.17: X-ray crystal structure of [Pd(*t*Bu$_3$-terpy)(4-aminopyridine)](CF$_3$SO$_3$)$_2$ with crystallographically independent atom numbering scheme. Hydrogen atoms have been omitted for clarity. Atom colours - C: grey, O: red, N: blue, Pd: navy F: green and S: yellow.

Table 3.6: Selected bond lengths (Å) and angles (°) for [Pd(*t*Bu$_3$-terpy)(4-aminopyridine)](CF$_3$SO$_3$)$_2$.

Pd1-N1	2.028(4)	N2-Pd1-N1	80.89(16)
Pd1-N2	1.927(4)	N2-Pd1-N4	174.42(16)
Pd1-N3	2.025(4)	N3-Pd1-N1	161.92(16)
Pd1-N4	2.037(3)	N3-Pd1-N2	81.11(16)
C18-N5	1.358(7)		

These geometrical features are comparable to those observed in the related species [Pt(6-phenyl-2,2'-bipyridine)(4-aminopyridine)] [8].

The 4-aminopyridine ligand is slightly twisted with respect to the terpyridine plane forming a dihedral angle of 88.39(4)°. Interestingly, the 4-aminopyridine in complex (**2-6**), with dihedral angle of 76.59(7)°, is bent more than that in complex (**3-6**). In terms of the tilt angle, this complex, with tilt angle of 174.42(16)°, shows more distortion than complex (**2-6**) (178.44(16)°). In terms of planarity, cations of (**3-6**) are less planar than those of (**2-6**), with a maximum displacement of +0.159 and +0.176 Å exhibited by C15 and N3, respectively, from the mean plane.

Analysis of packing in crystal structure showed that the cavities formed, along the b-axis, by cations and one of the triflate anions accommodate the second triflate anion and the acetonitrile molecule (Figure 3.18).

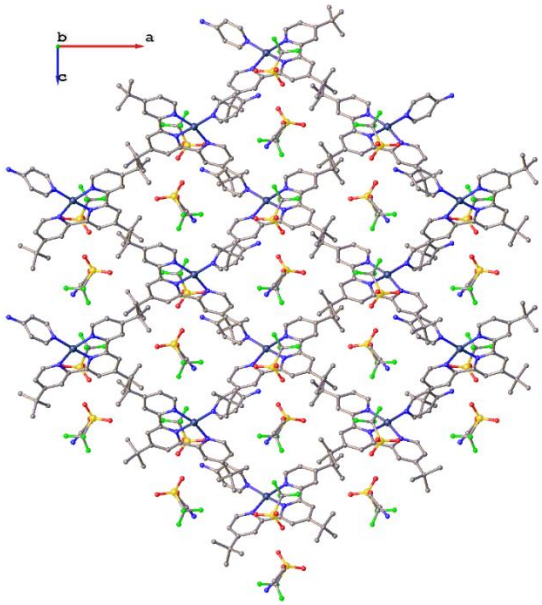


Figure 3.18: The packing diagram for [Pd(*t*Bu$_3$-terpy)(4-aminopyridine)](CF$_3$SO$_3$)$_2$ along the c crystal axis. Hydrogen atoms are omitted for clarity.

Within the crystal packing cations and anions are linked up by a number of hydrogen bonds where the tBu$_3$-terpyridine acts as donor and triflate oxygen and fluorine atoms act as acceptor (Figure 3.19). The C–H…O distances lie in the range 2.299 – 2.968 Å and the

C–H…F distances lie in the range 2.625 – 2.956 Å. Interestingly, the amine group of the 4-aminopyridine ligand acts as a hydrogen donor through two sets of N–H…O hydrogen bonds. The N5–H5a…O1T and N5–H5b…O4T distances are 2.299 and 2.314 Å, respectively.

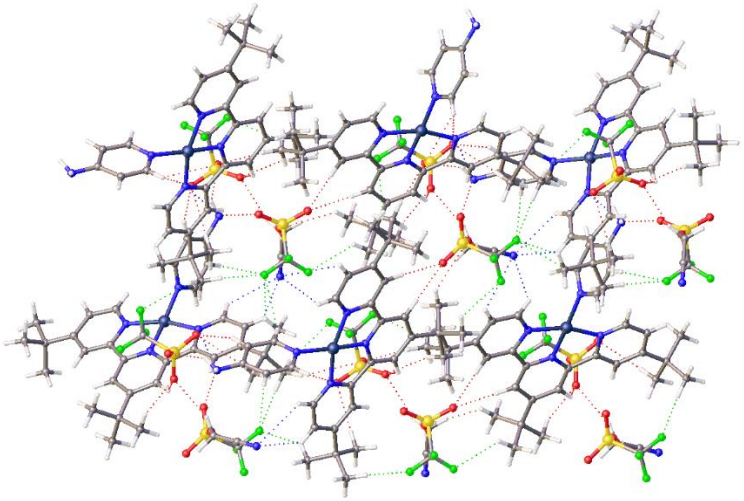


Figure 3.19: A net of hydrogen bonds links Pd(tBu$_3$-terpy) cations and triflate anions for [Pd(tBu$_3$-terpy)(4-aminopyridine)](CF$_3$SO$_3$)$_2$

*3.2.2.7 Single crystal X-ray structure of 2,2':6',2''-terpyridine (4-pyridineboronic acid) palladium triflate [Pd(terpy)(4-pyridineboronic acid)](CF$_3$SO$_3$)$_2$ (**3-7**).*

Crystals of [Pd(*t*Bu$_3$-terpy)(4-pyridineboronic acid)](CF$_3$SO$_3$)$_2$ were found to be colourless plates, crystallising in the monoclinic space group *P2$_1$/n*. As shown in Figure 3.20, space above and below the Pd cation is occupied by two triflate anions. The bond lengths and angles are detailed below in Table 3.7. All bond lengths and angles agree well with other structural reports of palladium terpyridine complexes in the previous Chapter and platinum terpyridine complex in the literature [9]. As before, the *t*Bu$_3$-terpyridine moiety is coordinated to the Pd atom in a tridentate fashion, and distorts the square planar geometry of the Pd atom. The central Pd1A–N2A bond (1.937(16) Å) is noticeably

shorter than the other Pd1A–N1A and Pd1A–N3A bonds and significantly longer than the analogous bond in [Pd(terpy)(4-pyridineboronic acid)]$(CF_3SO_3)_2$ (1.883(14)°). The *cis* N–Pd–N angles and N3A–Pd1A–N1A angle deviate from the ideal values by 9° and 18°, respectively. These values are similar to those found in Pt analogue [9].

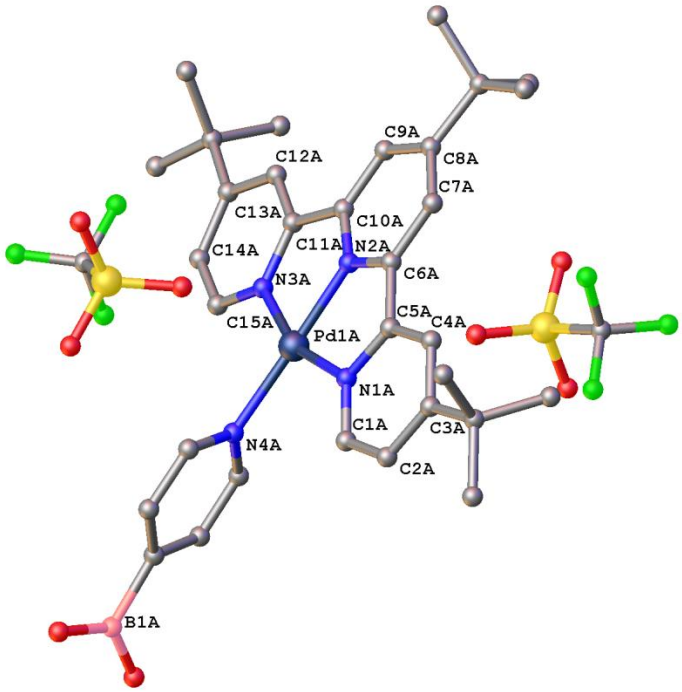


Figure 3.20: X-ray crystal structure of [Pd(*t*Bu$_3$-terpy)(4- pyridineboronic acid)]$(CF_3SO_3)_2$ with crystallographically independent atom numbering scheme. Hydrogen atoms have been omitted for clarity. Atom colours: B: pink, C: grey, O: red, N: blue, Pd: navy F: green and S: yellow.

Table 3.7: Selected bond lengths (Å) and angles (°) for [Pd(*t*Bu$_3$-terpy)(4-pyridine boronic acid)]$(CF_3SO_3)_2$

Pd1A-N1A	2.031(17)	N2A-Pd1A-N1A	80.73(7)
Pd1A-N2A	1.937(16)	N2A-Pd1A-N4A	177.16(6)
Pd1A-N3A	2.026(17)	N3A-Pd1A-N1A	161.56(7)
Pd1A-N4A	2.039(16)	N3A-Pd1A-N2A	80.99(7)

The 4-pyridineboronic acid ligand is slightly twisted with respect to terpyridine plane forming a dihedral angle of 68.66(5)°. The 4-pyridineboronic acid in complex (**3-7**) is twisted more than that in complex (**2-7**). This is due to a significant steric hindrance to an axial approach to Pd from in complex (3-**7**). Cations of (**3-7**) are less planar than those of (**2-7**), with a maximum displacement of +0.144 and -0.141 Å exhibited by C2A and C7A, respectively, from the mean plane.

In the solid state, the molecules of (**3-7**) are packed as shown in Figure. 3.21, similar to that in complex [Pt(terpy)(4-pyridineboronic acid)]$(CF_3SO_3)_2$ [9]. Pairs of complex cations are stacked in head-to-tail orientations. The crystal packing evidences triflate anions located above and below the Pd cation.

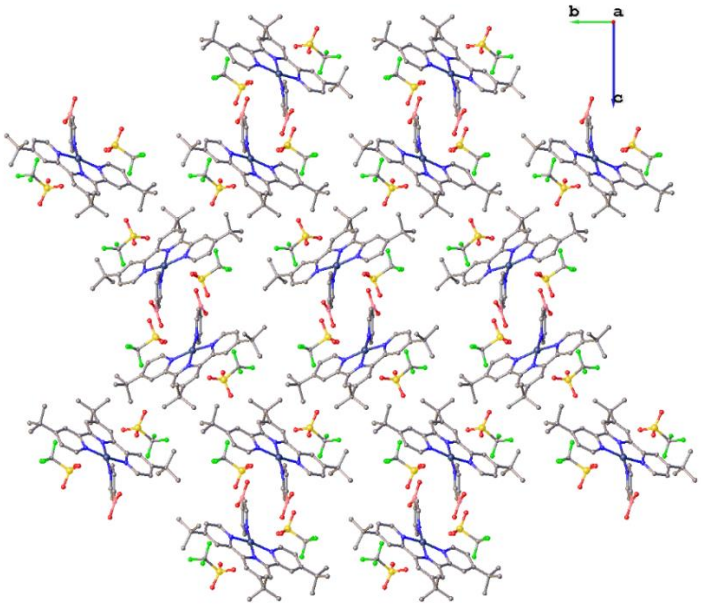


Figure 3.21: The packing diagram of [Pd(*t*Bu$_3$-terpy)(4-pyridineboronic acid)]$(CF_3SO_3)_2$ along the *a*-axis. Hydrogen atoms are omitted for clarity.

Within the crystal packing cations and anions are linked by a number of hydrogen bonds where the terpyridine acts as donor and triflate oxygen and fluorine atoms act as acceptor. The C–H…O distances lie in the range 2.269 – 2.944 Å and the C–H…F

distances lie in the range 2.216 – 2.954 Å. In addition, the boronic acid group of the 4-pyridineboronic acid ligand acts as donor via three sets of O–H…O hydrogen bonds. The O2A–H…O1T, O1A–H…O3T and O2A–H…O3T distances are 1.930, 1.971 and 2.996 Å, respectively (Figure 3.22).

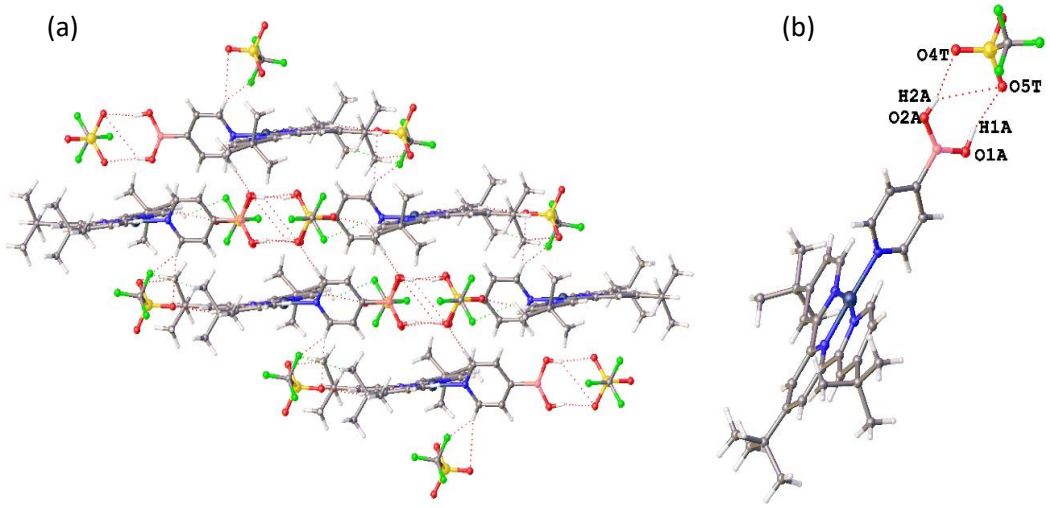


Figure 3.22: (a) A net of hydrogen bonds links Pd(tBu$_3$-terpy) cations and triflate anions for [Pd(*t*Bu$_3$-terpy)(4-pyridineboronic acid)](CF$_3$SO$_3$)$_2$. (b) Hydrogen bonds formed through boronic acid units.

*3.2.2.8 Single crystal X-ray structure of 4,4',4''-tri-tert-butyl-2,2':6',2''-terpyridine (4-hydroxypyridine) palladium triflate [Pd(tBu$_3$-terpy)(4-hydroxypyridine)](CF$_3$SO$_3$)$_2$ (**3-8**).*

Crystals of [Pd(*t*Bu$_3$-terpy)(4-hydroxypyridine)](CF$_3$SO$_3$)$_2$ were found to be colourless blocks, crystallising in the monoclinic space group *P2$_1$/c*. Figure 3.23 shows the coordination geometry and atom labelling scheme for complex (**3-8**). Space above and below the Pd cation is occupied by two triflate anions. Table 3.8 lists important bond lengths and angles for this complex. The coordination geometry around the palladium(II) cation is considerably distorted from the perfect square-plane. This distortion leads to a

narrowing of N1–Pd–N2 and N2–Pd–N3 angles to 80.94(9) and 80.70(10), respectively, and also a significant shortening of Pd–N2 distances (1.933(2) Å) compared to the other Pd–N distances (Pd–N1 = 2.027(2) Å and Pd–N3 = 2.029(2) Å).

The 4-hydroxypyridine is bent with respect to terpyridine plane forming a dihedral angle of 67.71(8)°.

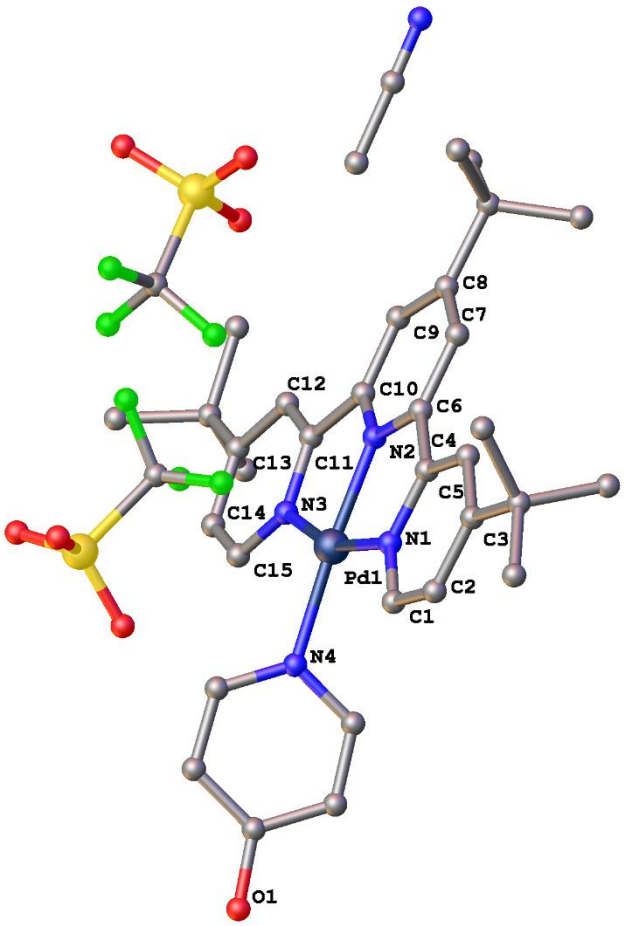


Figure Figure 3.23: X-ray crystal structure of [Pd(*t*Bu$_3$-terpy)(4-hydroxypyridine)](CF$_3$SO$_3$)$_2$ with crystallographically independent atom numbering scheme. Hydrogen atoms have been omitted for clarity. Atom colours - C: grey, O: red, N: blue, Pd: navy F: green and S: yellow.

Table 3.8: Selected bond lengths (Å) and angles (°) for [Pd(*t*Bu$_3$-terpy)(4-hydroxypyridine)](CF$_3$SO$_3$)$_2$

Pd1-N1	2.027(2)	N2-Pd1-N1	80.94(9)
Pd1-N2	1.933(2)	N2-Pd1-N4	175.86(9)
Pd1-N3	2.029(2)	N3-Pd1-N1	161.61(10)
Pd1-N4	2.036(2)	N3-Pd1-N2	80.70(10)

Importantly, analysis of packing in the crystal structure showed that the cavities formed, along the *a*-axis, by cations and one of the triflate anions accommodate the second triflate anion and the acetonitrile molecule, as shown in Figure 3.24.

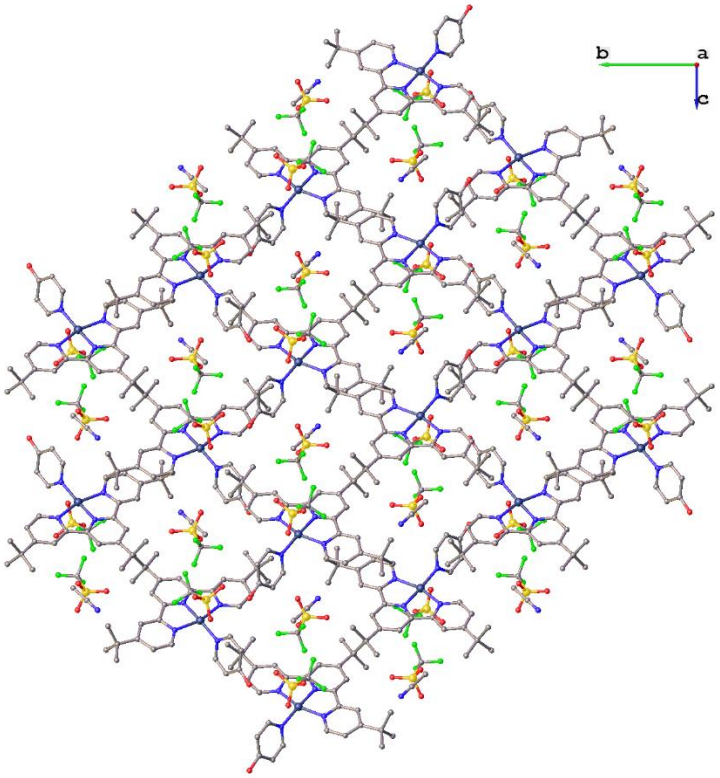


Figure 3.24: The packing diagram for [Pd(*t*Bu$_3$-terpy)(4-hydroxypyridine)](CF$_3$SO$_3$)$_2$. Along the *a*-axis. Hydrogen atoms are omitted for clarity.

In terms of planarity, the *t*Bu$_3$-terpyridine moiety slightly deviates with a maximum displacement of +0.141 and +0.106 Å exhibited by C1 and C2, respectively, from the mean plane.

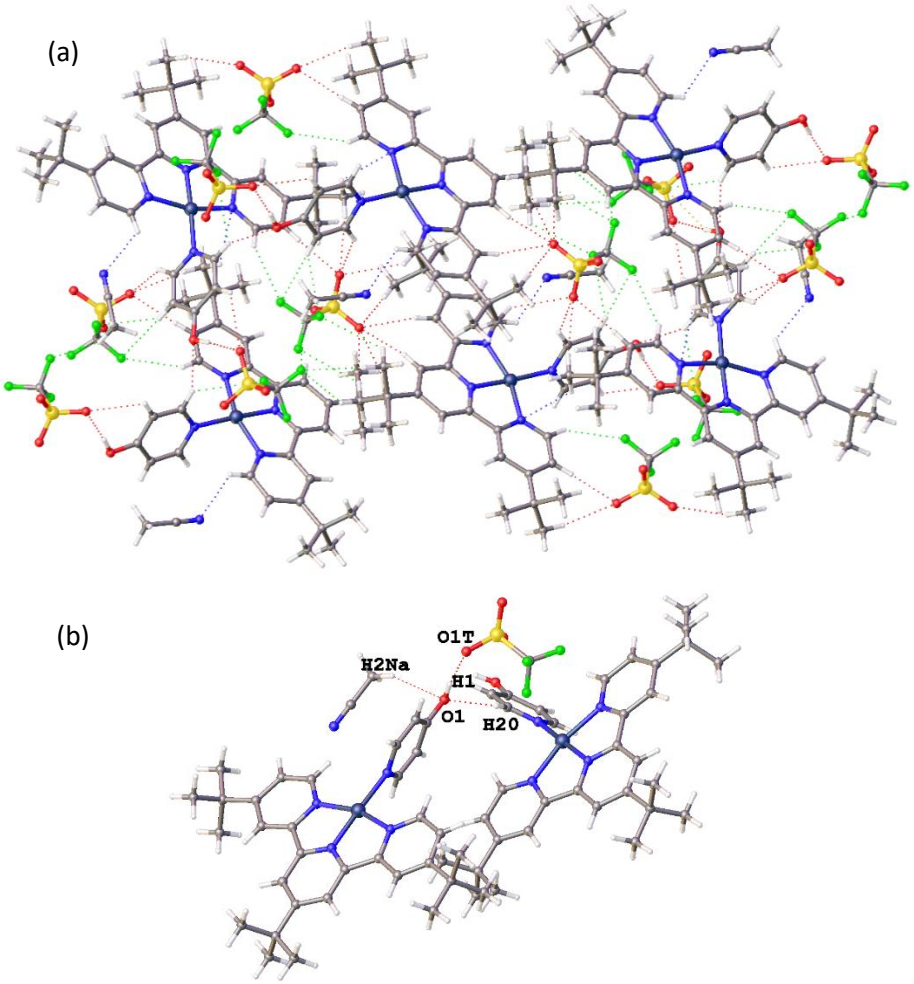


Figure 3.25: (a) A net of hydrogen bonds links Pd(tBu$_3$-terpy) cations and triflate anions for [Pd(tBu$_3$-terpy)(4-hydroxypyridine)](CF$_3$SO$_3$)$_2$. (b) Hydrogen bonds formed through hydroxy units.

There is a net of hydrogen bonds, as shown in Figure 3.25 a. The triflate anion acts as a hydrogen acceptor and forms hydrogen bonds with *t*Bu$_3$-terpyridine, 4-hydroxypyridine and acetonitrile molecule. The C–H…O distances lie in the range 2.327 – 2.934 Å and

the C–H…F distances lie in the range 2.668 – 2.957 Å. Each hydroxy group is involved in hydrogen bonds to a triflate anion, *t*Bu$_3$ moiety and acetonitrile molecule, as shown in Figure 3.25 b. The C20–H20…O1, C2N–H2Na…O1 and O1–H1…O1T distances are 2.486, 2.896 and 1.813 Å, respectively.

3.3 Conclusions

In order to compare and contrast the influence of butyl substituents on the crystal structures of Pd(terpy) complexes, an analogous *t*Bu$_3$-terpyridine was used. A series of Pd(*t*Bu$_3$-terpy) complexes have been synthesised using eight *para*-substituted pyridine derivatives. It was possible to grow crystals suitable for single crystal X-ray diffraction for all complexes. In each complex, the Pd cation adopts a distorted square planar geometry. The bond lengths are comparable among the complexes. The bond angles exhibit the usual deviations from idealized geometry as are seen in the Pd(terpy) complexes. In terms of the N1–Pd–N3 angle, complex (**3-3**) reveals the highest deviation from the ideal value of 180, by 18.70(4)°, and complex (**3-5**) shows the lowest deviation, by 17.70(4)°. In complex (**3-3**), the 4-iodopyridine ligand is significantly twisted with respect to *t*Bu$_3$-terpy plane adopting a dihedral angle of 53.95(7)°. However, the dihedral angle in complex (**3-6**) (88.39(11)°) indicates that the *t*Bu$_3$-terpy ring and 4-aminopyridine are almost perpendicular to each other with a small deviation. In terms of planarity, the *t*Bu$_3$-terpy moiety in complex (**3-4**) has the highest deviation with a maximum displacement of +0.293 and +0.234 Å exhibited by C15 and N3, respectively, from the mean plane. It is conceivable that the presence of the bulky *t*Bu$_3$ groups on the terpyridine moiety would hinder the formation of such interactions. Molecules of Pd(*t*Bu$_3$-terpy) complexes pack in a head to tail conformation minimizing the mutual repulsion between the sterically bulky *t*Bu$_3$-terpyridine moieties.

In general, the bond lengths and angles are largely unaffected by the electron rich *t*Bu$_3$-terpy moiety. It is interesting to note that Pd(*t*Bu$_3$-terpy) complexes are less planar than the corresponding unsubstituted terpyridine analogues. This observed deviation can be attributed to the presence of electron-donating groups in the ancillary positions that lead to the puckering of the terpyridine rings.

In addition, the pyridine ligand in the Pd(*t*Bu$_3$-terpy) complexes is twisted more than that in unsubstituted terpyridine analogues.

3.4 Materials and Methods

All chemicals and solvents were purchased from Alfa-Aesar, Fisher Scientific, VWR International or Sigma-Aldrich and were used as received without any further purification. Reactions sensitive to air and moisture were performed using a standard Schlenk line, with nitrogen as the inert atmosphere. Glassware used was flame dried under vacuum and backfilled with nitrogen. ^{1}H and ^{13}C NMR spectra were recorded using either a Bruker AV(III)400, AV(III)500, AV400 or DPX400 machines at room temperature. Mass spectroscopy was conducted using a Bruker Dalton Ultraflex MALDI-TOF with trans-2-[3-(4-*tert*,-butylphenyl)-2-methyl-2-propenylidene]-malononitrile as the matrix (m/z = 250.3).

Single crystal X-ray diffraction experiments were performed on an Oxford Diffraction SuperNova CCD area detector diffractometer at 120 K using monochromated Cu Kα radiation (λ = 1.54184 Å); on Agilent GV1000 AtlasS2 or TitanS2 CCD area detector diffractometers at 120 K using monochromated CuKα radiation (λ = 1.54184 Å); or at the UK Diamond Light Source I19-1 3-circle diffractometer (λ = 0.6889 Å). Absorption 202 corrections were applied using analytical numerical methods using CrysAlisPro software [10]. The structures were solved by direct methods using either SHELXS or

SHELXT and refined with SHELXL using a least squares method [11-13]. In all instances, Olex2 software was used as the solution, refinement and analysis program [14].

3.4.1 Synthesis of 4,4',4''-tri-*tert*-butyl-2,2':6',2''-terpyridine (4-cyanopyridine) palladium triflate [Pd(*t*Bu$_3$-terpy)(4-cyanopyridine)](CF$_3$SO$_3$)$_2$.

A mixture of *t*Bu$_3$-terpy (113 mg, 0.311 mmol) and palladium chloride (50 mg, 0.282 mmol) in acetonitrile (20 mL) was stirred at room temperature for 24 h. Silver triflate (290 mg, 1.129 mmol) was added. In the absence of light, the mixture was stirred for 48 h. After 48 h, the white precipitate (AgCl) was filtered. 4-Cyanopyridine (29 mg, 0.282 mmol) was added to the reaction solution and stirred for 3 h. The resulting solution was concentrated *via* rotary evaporation to remove the excess acetonitrile solvent. The resulting solid was washed with diethyl ether, before being dried in *vacuo*. Yield (133 mg, 52%). Single crystals suitable for X-ray diffraction were obtained by vapour diffusion of diethyl ether into an acetonitrile solution of [Pd(*t*Bu$_3$-terpy)(4-cyanopyridine)](CF$_3$SO$_3$)$_2$. MALDI-TOF MS (RP; m/z): 305.10 [$C_{35}H_{39}F_6N_5O_6PdS_2$-2OTf]$^{2+}$.^{1}H NMR (400 MHz, CD_3CN) δ ppm: 9.07 (d, *J* = 5.6 Hz, 2H, 2, 6-py), 8.98 (d, *J* = 6.4 Hz, 2H, 6, 6``-*t*Bu$_3$-terpy), 8.52 (s, 2H, 3`, 5`-*t*Bu$_3$-terpy), 8.12 (m, 2H, 3, 3``- *t*Bu$_3$-terpy), 7.83 (m, 4H, 5, 5``-*t*Bu$_3$-terpy, 3, 5-py), 1.53 (s, 9H, *t*Bu$_3$), 1.54 (s, 18H, *t*Bu$_3$).

3.4.2 Synthesis of 4,4',4''-tri-*tert*-butyl-2,2':6',2''-terpyridine (4-methylpyridine) palladium triflate [Pd(*t*Bu$_3$-terpy)(4-methylpyridine)](CF$_3$SO$_3$)$_2$.

A mixture of *t*Bu$_3$-terpy (72.5 mg, 0.311 mmol) and palladium chloride (50 mg, 0.282 mmol) in acetonitrile (20 mL) was stirred at room temperature for 24 h. Silver triflate (290 mg, 1.129 mmol) was added. In the absence of light, the mixture was stirred for 48 h. After 48 h, the white precipitate (AgCl) was filtered. 4-Methylpyridine (27 μL, 0.282 mmol) was added to the reaction solution and stirred for 3 h. The resulting solution was

concentrated *via* rotary evaporation to remove the excess acetonitrile solvent. The resulting solid was washed with diethyl ether, before being dried in *vacuo*. Yield (86 mg, 34%). Single crystals suitable for X-ray diffraction were obtained by vapour diffusion of diethyl ether into an acetonitrile solution of [Pd(*t*Bu$_3$-terpy)(4-methylpyridine)](CF$_3$SO$_3$)$_2$. MALDI-TOF MS (RP; m/z): 300.06 [$C_{35}H_{42}F_6N_4O_6PdS_2$-2OTf]$^{2+}$.^{1}H NMR (400 MHz, CD_3CN) δ ppm: 8.80 (d, *J* = 6.5 Hz, 2H, 2, 6-py), 8.31 (m, 4H, 3, 3`, 5`, 3``-*t*Bu$_3$-terpy), 8.11 (d, *J* = 6.4 Hz, 2H, 6, 6``-3, 3`, 5`, 3``-*t*Bu$_3$-terpy), 7.61 (m, 2H, 3, 5-py), 7.34 (m, 2H, 5, 5``-*t*Bu$_3$-terpy), 2.60 (s, 3H, CH_3), 1.51 (s, 9H, *t*Bu$_3$), 1,44 (s, 18H, *t*Bu$_3$).

3.4.3 Synthesis of 4,4',4''-tri-*tert*-butyl-2,2':6',2''-terpyridine (4-iodopyridine) palladium triflate [Pd(*t*Bu$_3$-terpy)(4-iodopyridine)](CF$_3$SO$_3$)$_2$.

A mixture of *t*Bu$_3$-terpy (72.5 mg, 0.311 mmol) and palladium chloride (50 mg, 0.282 mmol) in acetonitrile (20 mL) was stirred at room temperature for 24 h. Silver triflate (290 mg, 1.129 mmol) was added. In the absence of light, the mixture was stirred for 48 h. After 48 h, the white precipitate (AgCl) was filtered. 4-Iodopyridine (58 mg, 0.283 mmol) was added to the reaction solution and stirred for 3 h. The resulting solution was concentrated *via* rotary evaporation to remove the excess acetonitrile solvent. The resulting solid was washed with diethyl ether, before being dried in *vacuo*. Yield (103 mg, 36%). Single crystals suitable for x-ray diffraction were obtained by vapour diffusion of diethyl ether into an acetonitrile solution of [Pd(*t*Bu$_3$-terpy)(4-iodopyridine)](CF$_3$SO$_3$)$_2$. MALDI-TOF MS (RP; m/z): 356.01 [$C_{34}H_{39}F_6IN_4O_6PdS_2$-2OTf]$^{2+}$. ^{1}H NMR (400 MHz, CD_3CN) δ ppm: 8.88 (d, *J* = 6.2 Hz, 2H, 2, 6-py), 8.56 (m, 4H, 3, 3`, 3```, 5`-*t*Bu$_3$-terpy), 8.41 (d, *J* = 6.2 Hz, 2H, 6, 6``-*t*Bu$_3$-terpy), 7.81 (m, 2H, 5, 5``-*t*Bu$_3$-terpy), 7.63 (m, 2H, 3, 5-py), 1.53 (s, 9H, *t*Bu$_3$), 1.40 (s, 18H, *t*Bu$_3$).

3.4.4 Synthesis of 4,4',4''-tri-*tert*-butyl-2,2':6',2''-terpyridine (4-dimethylaminopyridine) palladium triflate [Pd(*t*Bu$_3$-terpy)(4-dimethylaminopyridine)](CF$_3$SO$_3$)$_2$.

A mixture of *t*Bu$_3$-terpy (72.5 mg, 0.311 mmol) and palladium chloride (50 mg, 0.282 mmol) in acetonitrile (20 mL) was stirred at room temperature for 24 h. Silver triflate (290 mg, 1.129 mmol) was added. In the absence of light, the mixture was stirred for 48 h. After 48 h, the white precipitate (AgCl) was filtered. 4-Dimethylaminopyridine (34.4 mg, 0.281 mmol) was added to the reaction solution and stirred for 3 h. The resulting solution was concentrated *via* rotary evaporation to remove the excess acetonitrile solvent. The resulting solid was washed with diethyl ether, before being dried in *vacuo*. Yield (107 mg, 41%). Single crystals suitable for X-ray diffraction were obtained by vapour diffusion of diethyl ether into an acetonitrile solution of [Pd(*t*Bu$_3$-terpy)(4-dimethylaminopyridine)](CF$_3$SO$_3$)$_2$. MALDI-TOF MS (RP; m/z): 314.30 $[C_{36}H_{45}F_6N_5O_6PdS_2\text{-}2OTf]^{2+}$. ^{1}H NMR (400 MHz, CD_3CN) δ ppm: 8.75 (m, 4H, 3, 3`, 3```, 5`-*t*Bu$_3$-terpy), 8.59 (d, *J* = 6.0 Hz, 2H, 2, 6-py), 8.39 (d, *J* = 6.0 Hz, 2H, 6, 6``-*t*Bu$_3$-terpy), 7.53 (m, 2H, 5, 5``-*t*Bu$_3$-terpy), 7.10 (m, 2H, 3, 5-py), 3.20 (s, 6H, N(CH$_3$)$_2$), 1.50 (s, 9H, *t*Bu$_3$), 1.43 (s, 18H, *t*Bu$_3$).

3.4.5 Synthesis of 4,4',4''-tri-*tert*-butyl-2,2':6',2''-terpyridine (4-pyridinecarboxaldehyde) palladium triflate[Pd(*t*Bu$_3$-terpy)(4-pyridinecarboxaldehyde)](CF$_3$SO$_3$)$_2$.

A mixture of *t*Bu$_3$-terpy (72.5 mg, 0.311 mmol) and palladium chloride (50 mg, 0.282 mmol) in acetonitrile (20 mL) was stirred at room temperature for 24 h. Silver triflate (290 mg, 1.129 mmol) was added. In the absence of light, the mixture was stirred for 48 h. After 48 h, the white precipitate (AgCl) was filtered. 4-Pyridinecarboxaldehyde (26 μL, 0.280 mmol) was added to the reaction solution and stirred for 2 h. The resulting solution

was concentrated *via* rotary evaporation to remove the excess acetonitrile solvent. The resulting solid was washed with diethyl ether, before being dried in *vacuo*. Yield (169 mg, 66%). Single crystals suitable for X-ray diffraction were obtained by vapour diffusion of diethyl ether into an acetonitrile solution of [Pd(*t*Bu_3-terpy)(4-pyridinecarboxaldehyde)](CF_3SO_3)$_2$. MALDI-TOF MS (RP; m/z): 307.13 [$C_{35}H_{40}F_6N_4O_7PdS_2$-2OTf]$^{2+}$. ^{1}H NMR (400 MHz, CD_3CN) δ ppm: 9.01 (d, *J* = 6.2 Hz, 2H, 2, 6-py), 8.63 (m, 4H, 3, 3`, 3```, 5`-*t*Bu_3-terpy), 8.50 (d, *J* = 6.5 Hz, 2H, 6, 6``-*t*$Bu_3$-terpy), 7.90 (d, *J* = 6.5 Hz, 2H, 3, 5-py), 7.73 (m, 2H, 5, 5``-*t*Bu_3-terpy), 1.58 (s, 9H, *t*Bu_3), 1.50 (s, 18H, *t*Bu_3).

3.4.6 Synthesis of 4,4',4''-tri-*tert*-butyl-2,2':6',2''-terpyridine (4-aminopyridine) palladium triflate [Pd(*t*Bu_3-terpy)(4-aminopyridine)](CF_3SO_3)$_2$.

A mixture of *t*Bu_3-terpy (72.5 mg, 0.311 mmol) and palladium chloride (50 mg, 0.282 mmol) in acetonitrile (20 mL) was stirred at room temperature for 24 h. Silver triflate (290 mg, 1.129 mmol) was added. In the absence of light, the mixture was stirred for 48 h. After 48 h, the white precipitate (AgCl) was filtered. 4-Aminopyridine (27 mg, 0.284 mmol) was added to the reaction solution and stirred for 2 h. The resulting solution was concentrated *via* rotary evaporation to remove the excess acetonitrile solvent. The resulting beige solid was washed with diethyl ether, before being dried in *vacuo*. Yield (58 mg, 23%). Single crystals suitable for X-ray diffraction were obtained by vapour diffusion of diethyl ether into an acetonitrile solution of [Pd(*t*Bu_3-terpy)(4-aminopyridine)](CF_3SO_3)$_2$. MALDI-TOF MS (RP; m/z): 300.56 [$C_{34}H_{41}F_6N_5O_6PdS_2$-2OTf]$^{2+}$. ^{1}H NMR (400 MHz, CD_3CN) δ ppm: 8.57 (m, 2H, 2, 6`-py), 8.44 (m, 4H, 3, 3`, 3```, 5`-*t*Bu_3-terpy), 8.13 (d, *J* = 6.5 Hz, 2H, 6, 6``-*t*$Bu_3$-terpy), 7.47 (d, *J* = 6.2 Hz, 2H, 3, 5-py), 7.39 (m, 2H, 5, 5``-*t*Bu_3-terpy), 5.70 (s, 2H, NH_2), 1.51 (s, 9H, *t*Bu_3), 1.47 (s, 18H, *t*Bu_3).

3.4.7 Synthesis of 4,4',4''-tri-*tert*-butyl-2,2':6',2''-terpyridine (4-pyridineboronic acid) palladium triflate[Pd(*t*Bu$_3$-terpy)(4-pyridineboronic acid)](CF$_3$SO$_3$)$_2$.

A mixture of *t*Bu$_3$-terpy (113 mg, 0.311 mmol) and palladium chloride (50 mg, 0.282 mmol) in acetonitrile (20 mL) was stirred at room temperature for 24 h. Silver triflate (290 mg, 1.129 mmol) was added. In the absence of light, the mixture was stirred for 48 h. After 48 h, the white precipitate (AgCl) was filtered. 4-Pyridineboronic acid (35 mg, 0.285 mmol) was added to the reaction solution and stirred for 2 h. The resulting solution was concentrated *via* rotary evaporation to remove the excess acetonitrile solvent. The resulting solid was washed with diethyl ether, before being dried in *vacuo*. Yield (147 mg, 56%). Single crystals suitable for X-ray diffraction were obtained by vapour diffusion of diethyl ether into an acetonitrile solution of [Pd(*t*Bu$_3$-terpy)(4-pyridineboronic acid)](CF$_3$SO$_3$)$_2$. MALDI-TOF MS (RP; m/z): 315.10 $[C_{34}H_{41}BF_6N_4O_8PdS_2\text{-}2OTf]^{2+}$. ^{1}H NMR (400 MHz, DMSO) δ ppm: 9.05 (d, *J* = 5.6 Hz, 2H, 2, 6-py), 8.57 (m, 4H, 3, 3`, 3``, 5`-*t*Bu$_3$-terpy), 8.59 (m, 2H, 3, 5-py), 7.93 (d, *J* = 6.5 Hz, 2H, 6, 6``-*t*Bu$_3$-terpy), 7.75 (m, 2H, 5, 5``-*t*Bu$_3$-terpy), 1.55 (s, 9H, *t*Bu$_3$), 1.49 (s, 18H, *t*Bu$_3$).

3.4.8 Synthesis of 4,4',4''-tri-*tert*-butyl-2,2':6',2''-terpyridine (4-hydroxypyridine) palladium triflate[Pd(*t*Bu$_3$-terpy)(4-hydroxypyridine)](CF$_3$SO$_3$)$_2$.

A mixture of *t*Bu$_3$-terpy (113 mg, 0.311 mmol) and palladium chloride (50 mg, 0.282 mmol) in acetonitrile (20 mL) was stirred at room temperature for 24 h. Silver triflate (290 mg, 1.129 mmol) was added. In the absence of light, the mixture was stirred for 48 h. After 48 h, the white precipitate (AgCl) was filtered. 4-Hydroxypyridine (27 mg, 0.284 mmol) was added to the reaction solution and stirred for 2 h. The resulting solution was concentrated *via* rotary evaporation to remove the excess acetonitrile solvent. The resulting solid was washed with diethyl ether, before being dried in *vacuo*. Yield (89 mg, 35%). Single crystals suitable for X-ray diffraction were obtained by vapour diffusion of

diethyl ether into an acetonitrile solution of [Pd(*t*Bu$_3$-terpy)(4-hydroxypyridine)](CF$_3$SO$_3$)$_2$. MALDI-TOF MS (RP; m/z): 301.00 [$C_{34}H_{40}F_6N_4O_7PdS_2$-2OTf]$^{2+}$. ^{1}H NMR (400 MHz, CD_3CN) δ ppm: 8.80 (m, 2H, 2, 6-py), 8.66 (m, 4H, 3, 3`, 3``, 5-*t*Bu$_3$-terpy), 8.43 (d, *J* =5.6 Hz, 2H, 6, 6``-*t*Bu$_3$-terpy), 7.81 (m, 2H, 5, 5``-*t*Bu$_3$-terpy), 7.41 (d, *J* = 5.5 Hz, 2H, 3, 5-py), 1.53 (s, 8H, *t*Bu$_3$), 1.48 (s, 18H, *t*Bu$_3$).

3.4.9 Crystal data

Crystal data for (**3-1**): $C_{35}H_{39}F_6N_5O_6PdS_2$ (*M* =910.23 g/mol): monoclinic, space group $P2_1/c$ (no. 14), *a* = 14.4171(6) Å, *b* = 21.5580(10) Å, *c* = 12.4794(6) Å, *β* = 90.523(5)°, *V* = 3878.5(3) Å^3, *Z* = 4, *T* = 120(2) K, μ(CuKα) = 5.568 mm^{-1}, *Dcalc* = 1.559 g/cm^3, 17370 reflections measured (6.13° ≤ 2θ ≤ 133.202°), 6118 unique (R_{int} = 0.0829, R_{sigma} = 0.0547) which were used in all calculations. The final R_1 was 0.0894 (I > 2σ(I)) and wR_2 was 0.2505 with GOF = 1.119.

Crystal data for (**3-2**): $C_{35}H_{42}F_6N_4O_6PdS_2$ (*M* =899.24 g/mol): triclinic, space group P-1 (no. 2), *a* = 18.4138(5) Å, *b* = 20.1539(4) Å, *c* = 22.3722(6) Å, *a* = 86.560(2)°, *β* = 75.076(2)°, *γ* = 76.001(2)°, *V* = 7784.2(3) Å^3, *Z* = 7, *T* = 119.97(13) K, μ(CuKα) = 4.840 mm^{-1}, *Dcalc* = 1.343 g/cm^3, 64242 reflections measured (6.088° ≤ 2θ ≤ 149.372°), 30974 unique (R_{int} = 0.0421, R_{sigma} = 0.0496) which were used in all calculations. The final R_1 was 0.1379 (I > 2σ(I)) and wR_2 was 0.3518 with GOF = 1.427.

Crystal data for (**3-3**): $C_{36}H_{42}F_6IN_5O_6PdS_2$ (M + MeCN) (*M* =1052.20 g/mol): monoclinic, space group $P2_1/n$ (no. 14), *a* = 9.6490(6) Å, *b* = 14.1841(11) Å, *c* = 31.311(2) Å, *β* = 91.787(6)°, *V* = 4283.2(5) Å^3, *Z* = 4, *T* = 120(2) K, μ(CuKα) = 10.703 mm^{-1}, *Dcalc* = 1.600 g/cm^3, 26057 reflections measured (8.414° ≤ 2θ ≤ 133.152°), 7576 unique (R_{int} = 0.0945, R_{sigma} = 0.0931) which were used in all calculations. The final R_1 was 0.0989 (I > 2σ(I)) and wR_2 was 0.2290 with GOF =1.085.

Crystal data for (**3-4**): $C_{36}H_{44}F_6N_6O_6PdS_2$ (M =941.29 g/mol): orthorhombic, space group $Pca2_1$ (no. 29), a = 31.0027(7) Å, b = 11.4245(3) Å, c = 11.8498(3) Å, V = 4197.08(18) Å^3, Z = 4, T = 120(2) K, μ(CuKα) = 5.171 mm^{-1}, $Dcalc$ = 1.490 g/cm^3, 27163 reflections measured (8.248° ≤ 2θ ≤ 133.184°), 6651 unique (R_{int} = 0.0490, R_{sigma} = 0.0357) which were used in all calculations. The final R_1 was 0.0318 (I > 2σ(I)) and wR_2 was 0.0949 with GOF = 0.796.

Crystal Data for (**3-5**): $C_{35}H_{40}N_4O_7F_6S_2Pd$ (M =913.23 g/mol): monoclinic, space group $P2_1/n$ (no. 14), a = 9.56820(10) Å, b = 15.0481(3) Å, c = 41.2050(6) Å, β = 91.7300(10)°, V = 5930.13(16) Å^3, Z = 2, T = 119.96(14) K, μ(CuKα) = 1.825 mm^{-1}, $Dcalc$ = 0.511 g/cm^3, 86896 reflections measured (6.254° ≤ 2θ ≤ 148.888°), 11976 unique (R_{int} = 0.0555, R_{sigma} = 0.0262) which were used in all calculations. The final R_1 was 0.0875 (I > 2σ(I)) and wR_2 was 0.2502 with GOF = 1.321.

Crystal data for (**3-6**): $C_{36}H_{44}F_6N_6O_6PdS_2$ (M + MeCN) (M =941.29 g/mol): orthorhombic, space group $Pca2_1$ (no. 29), a = 31.0027(7) Å, b = 11.4245(3) Å, c = 11.8498(3) Å, V = 4197.08(18) Å^3, Z = 4, T = 120(2) K, μ(CuKα) = 5.171 mm^{-1}, $Dcalc$ = 1.490 g/cm^3, 27163 reflections measured (8.248° ≤ 2θ ≤ 133.184°), 6651 unique (R_{int} = 0.0490, R_{sigma} = 0.0357) which were used in all calculations. The final R_1 was 0.0318 (I > 2σ(I)) and wR_2 was 0.0949 with GOF = 0.796.

Crystal data for (**3-7**): $C_{42}H_{54}BF_6N_8O_8PdS_2$ (M =1094.26 g/mol): monoclinic, space group $P2_1/n$ (no. 14), a = 9.70234(8) Å, b = 14.30361(11) Å, c = 31.7854(2) Å, β = 92.8220(6)°, V = 4405.78(6) Å^3, Z = 4, T = 120(2) K, μ(CuKα) = 5.066 mm^{-1}, $Dcalc$ = 1.650 g/cm^3, 48671 reflections measured (6.778° ≤ 2θ ≤ 147.43°), 8816 unique (R_{int} = 0.0378, R_{sigma} = 0.0219) which were used in all calculations. The final R_1 was 0.0296 (I > 2σ(I)) and wR_2 was 0.0746 with GOF = 1.046.

Crystal data for (**3-8**): $C_{36}H_{43}F_6N_5O_7PdS_2$ (M + MeCH) (M =942.27 g/mol): monoclinic, space group $P2_1/c$ (no. 14), a = 11.1484(2) Å, b = 30.7665(5) Å, c = 12.1073(3) Å, β = 97.080(2)°, V = 4121.11(14) Å^3, Z = 4, T = 120(2) K, μ(CuKα) = 5.279 mm^{-1}, $Dcalc$ = 1.519 g/cm^3, 23369 reflections measured (7.9° ≤ 2θ ≤ 147.208°), 8124 unique (R_{int} = 0.0306, R_{sigma} = 0.0313) which were used in all calculations. The final R_1 was 0.0384 (I > 2σ(I)) and wR_2 was 0.1243 with GOF = 0.982.

3.5 References

1. J. A. Bailey, M. G. Hill, R. E. Marsh, V. M. Miskowski, W. P. Schaefer and H. B. Gray, *Inorganic Chemistry*, 1995, **34**, 4591-4599.
2. S. Pyo, E. Pérez-Cordero, S. G. Bott and L. Echegoyen, *Inorganic Chemistry*, 1999, **38**, 3337-3343.
3. D. Reddy and D. Jaganyi, *Dalton Transactions*, 2008, 6724-6731.
4. T. M. Pappenfus, J. R. Burney, K. A. McGee, G. G. Lee, L. R. Jarvis, D. P. Ekerholm, M. Farah, L. I. Smith, L. M. Hinkle and K. R. Mann, *Inorganica Chimica Acta*, 2010, **363**, 3214-3221.
5. R. Corbo, T. P. Pell, B. D. Stringer, C. F. Hogan, D. J. Wilson, P. J. Barnard and J. L. Dutton, *Journal of the American Chemical Society*, 2014, **136**, 12415-12421.
6. S. Coşar, M. B. Janik, M. Flock, E. Freisinger, E. Farkas and B. Lippert, *Journal of the Chemical Society, Dalton Transactions*, 1999, 2329-2336.
7. R. Kaskafetou, M. J. Manos and A. Garoufis, *Inorganic Chemistry Communications*, 2013, **35**, 176-180.
8. J. H. Yip, a. Suwarno and J. J. Vittal, *Inorganic Chemistry*, 2000, **39**, 3537-3543.
9. S. S. Hosseini, M. Bhadbhade, R. J. Clarke, P. J. Rutledge and L. M. Rendina, *Dalton Transactions*, 2011, **40**, 506-513.
10. CrysAlisPro, *Agilent Technologies UK Ltd., Oxford, UK*, 2013.
11. G. M. Sheldrick, *Acta Crystallographica Section A: Foundations of Crystallography*, 2008, **64**, 112-122.
12. G. M. Sheldrick, *Acta Crystallographica Section A: Foundations and Advances*, 2015, **71**, 3-8.

13. G. M. Sheldrick, *Acta Crystallographica Section C: Structural Chemistry*, 2015, **71**, 3-8.

14. O. V. Dolomanov, L. J. Bourhis, R. J. Gildea, J. A. Howard and H. Puschmann, *Journal of Applied Crystallography*, 2009, **42**, 339-341.

Chapter 4

Mono Palladium (2,2':6',2''-Terpyridine) Complexes with *Meta*-Substituted Pyridine Derivatives

4.1. Introduction

In order to extend the experimental observations and the range of applicability of the proposed interpretation, the system involving the tridentate aromatic nitrogen donor 2,2':6',2"-terpyridine and 4,4',4"-tri-*tert*-butyl-2,2':6',2"-terpyridine has been examined with *meta*-substituted pyridine derivatives.

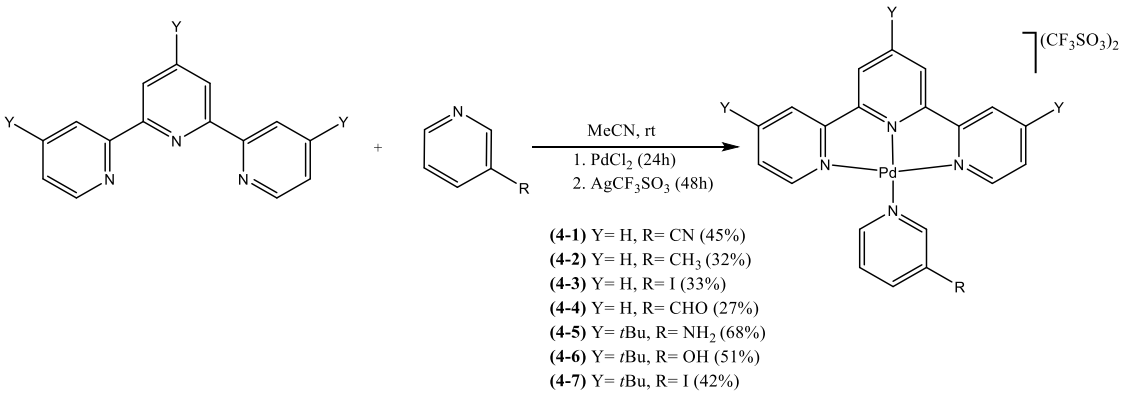
No Pd(Yterpy) (Y = H or *t*Bu$_3$) complex of *meta*-substituted pyridine has been characterized by single crystal X-ray diffraction previously, while there are only few platinum(II) complexes reported in this field [1,2]. In order to compare and contrast the effects of the *meta*-substituted pyridine ligands on the crystal structures, six *meta*-substituted pyridine derivatives were used.

4.2. Results and Discussion

4.2.1. Synthesis of a series of mononuclear Pd(Yterpy) (Y = H or *t*Bu$_3$) triflate complexes with *meta*-substituted pyridine derivatives

All complexes were synthesised following the same synthetic procedure. All reactions were conducted in dry acetonitrile. In a typical experiment, commercially available terpy or *t*Bu$_3$-terpy and palladium chloride were dissolved in acetonitrile and the reaction mixture was stirred at room temperature. After stirring for 24 hours, silver triflate was added. In the absence of light, the reaction mixture was stirred for 48 hours. After 48 hours, the white precipitate (AgCl) was filtered. The target pyridine was added to the reaction solution and stirred for 3 hours. The resulting solution was concentrated via rotary evaporation to remove the excess acetonitrile solvent. The resulting solid was washed with diethyl ether, before being dried in *vacuo* to afford the title compound in

acceptable yield (Scheme 4.1). Seven pyridine derivatives with different substitutions at the 3-position have been used.



Scheme 4.1: Synthesis of a series of mononuclear Pd(Yterpy) (Y = H or *t*Bu$_3$) triflate complexes with *meta*-substituted pyridine derivatives.

4.2.2. X-ray crystallography

Single crystals suitable for X-ray diffraction were obtained for all of the complexes reported herein. Single crystals were grown by dissolution of the product in the minimum amount of acetonitrile and diffusion of diethyl ether vapour into this solution.

*4.2.2.1. Single crystal X-ray structure of 2,2':6',2''-terpyridine(3-cyanopyridine) palladium triflate [Pd(terpy)(3-cyanopyridine)](CF$_3$SO$_3$)$_2$ (**4-1**).*

Crystals of [Pd(terpy)(3-cyanopyridine)](CF$_3$SO$_3$)$_2$ were found to be colourless needles. The complex crystallises in the triclinic space group *P-1*. As shown in Figure 4.1, space above and below the Pd(terpy) cation is occupied by two triflate anions and one acetonitrile molecule, respectively. The structure of the cation of (**4-1**) is similar to the structures of (**2-1**) and (**3-2**). As before, terpyridine is coordinated to palladium as a tridentate ligand and the fourth position is occupied by 3-cyanopyridine. The

coordination geometry of the palladium ion is distorted slightly from that found in the perfect square-planar Pd(II) complexes. Table 4.1 lists important bond lengths and angles for this complex. The angles between the adjacent nitrogen atoms in the plane deviate slightly from the theoretical value of 90° (N2–Pd1–N1 = 80.90(9)° and N3–Pd1–N2 = 80.96(9)°) and N3-Pd1-N1 angle (161.81(10)°) is smaller than the theoretical value of 180°. These angles are much smaller than those found in complex (**2-1**) (average ≈ 81.55(8)°), but in excellent agreement with those of complex (**3-1**) (average ≈ 80.70(2)°) reported previously. The Pd–N distance to the central nitrogen atom of the terpy is shorter than those to the other two nitrogen atoms, but in excellent agreement with those of (**2-1**) and (**3-1**). There is a significant elongation of the Pd1–N1 and Pd1–N3 bonds from 1.961(18) and 1.925(17) Å in (**2-1**) to 2.032(2) and 2.037(2) Å in (**4-1**), similar to complex (**3-1**). A similar distorted square-planar geometry, which is a result of the geometric constraints imposed by coordination of the tridentate terpyridine molecule, also occurs in the related palladium(II) terpyridine complexes in Chapters 2 and 3. This complex shows higher distortion from an idealized square planar geometry than (**2-1**) and (**3-1**). The most notable feature of the structure is the orientation of the 3-cyanopyridine ring with respect to the palladium square plane. The 3-cyanopyridine is bent with respect to terpyridine plane forming a dihedral angle of 59.14(3)°. The dihedral angle indicates that 3-cyanopyridine in complex (**4-1**) is twisted more than 4-cyanopyridine ligands in complexes (**2-1**) and (**3-1**), 84.04(7)° and 65.71(6)°, respectively. The tilt angle of complex (**4-1**) 177.01(8)° is slightly lower than those found in (**2-1**) and (**3-1**), 179.7(9)° and 179.5(2)°, respectively. Cations of (**4-1**) are less planar than those of (**2-1**) and more planar than those of (**3-1**), with a maximum displacement of +0.087 and -0.105 Å exhibited by C9 and C4, respectively, from the mean plane.

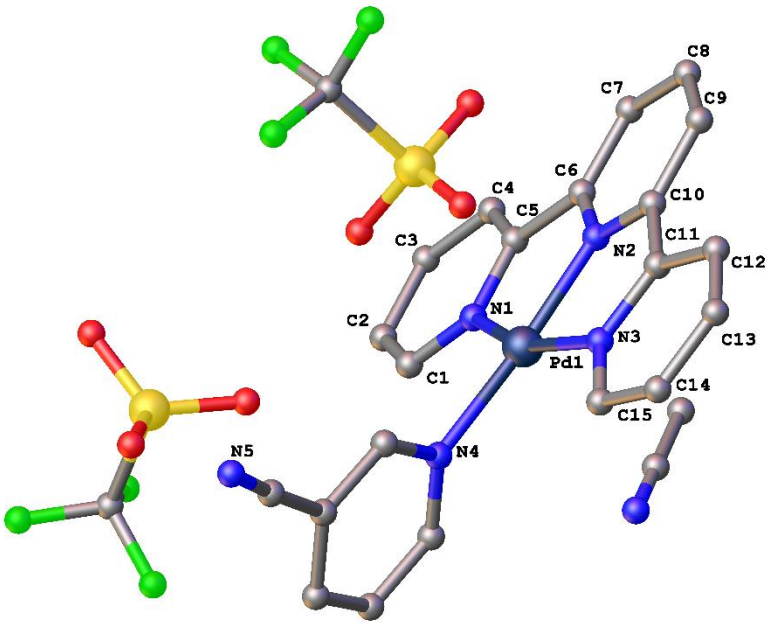


Figure 4.1: X-ray crystal structure of [Pd(terpy)(3-cyanopyridine)]$(CF_3SO_3)_2$ with crystallographically independent atom numbering scheme. Hydrogen atoms have been omitted for clarity. Atom colours - C: grey, O: red, N: blue, Pd: navy F: green and S: yellow.

Table 4.1: Selected bond lengths (Å) and angles (°) for [Pd(terpy)(3-cyanopyridine)]$(CF_3SO_3)_2$

Pd1-N1	2.032(2)	N2-Pd1-N1	80.90(9)
Pd1-N2	1.932(2)	N2-Pd1-N4	177.01(8)
Pd1-N3	2.037(2)	N3-Pd1-N1	161.81(10)
Pd1-N4	2.035(2)	N3-Pd1-N2	80.96(9)

Molecules of (**4-1**) pack in head to head conformation from the view along the *a*-axis. Analysis of packing in the crystal structure showed that cations are arranged in a herringbone architecture (Figure 4.2).

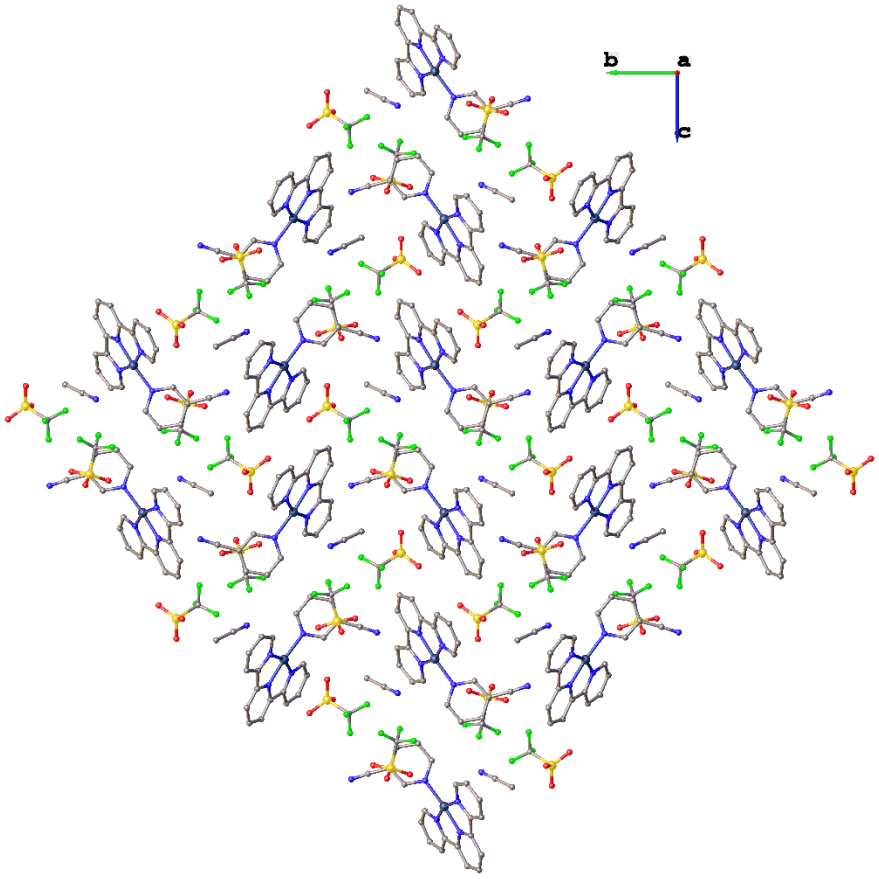


Figure 4.2: The packing diagram for [Pd(terpy)(3-cyanopyridine)]$(CF_3SO_3)_2$ along the *a*-axis. Hydrogen atoms are omitted for clarity.

As shown in Figure 4.3, the molecules of (**4-1**) undergo a series of face-to-face π· · ·π interactions indicated by ring centroid–ring centroid separations of 3.629 Å (corresponding slip angle is 4.890°). This arrangement is further stabilised by a series of hydrogen bonds between Pd cations and triflate anions.

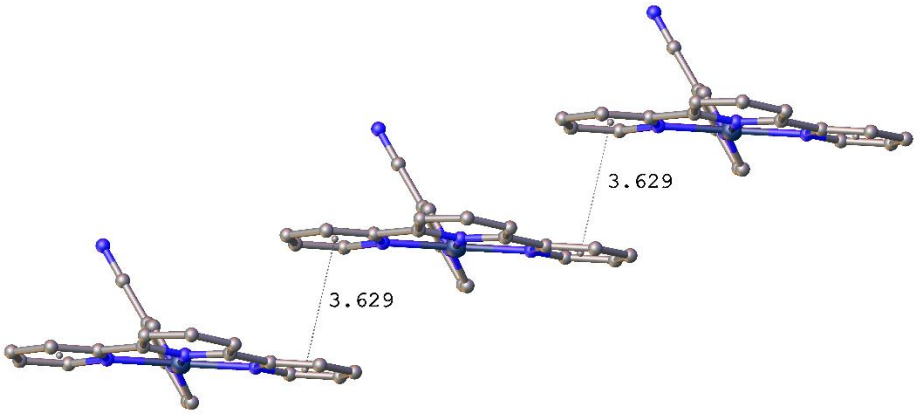


Figure 4.3: Representation of the π· · ·π interactions in [Pd(terpy)(3-cyanopyridine)]$(CF_3SO_3)_2$. Dashed lines indicate the presence of π· · ·π interactions.

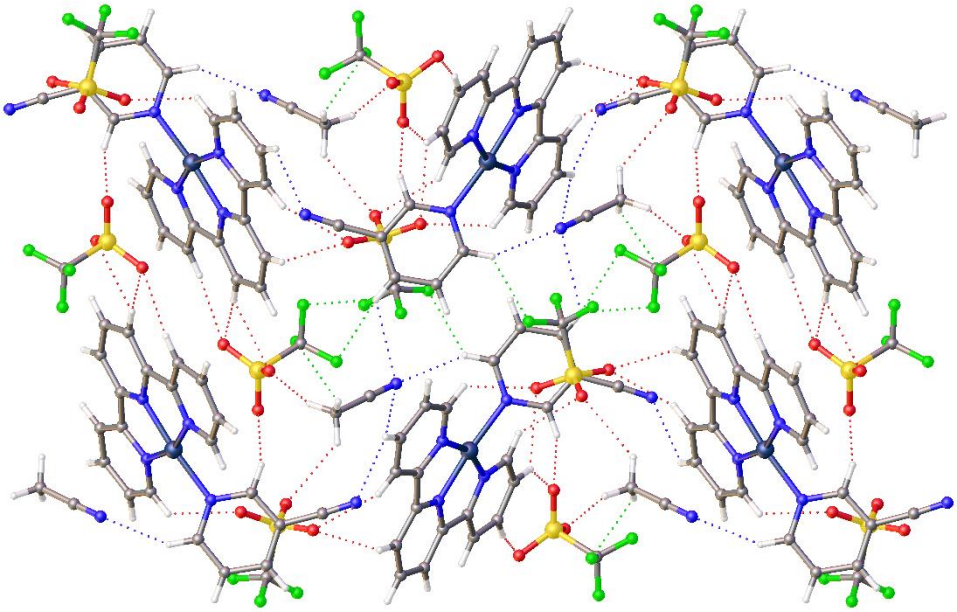


Figure 4.4: A net of hydrogen bonds links Pd(terpy) cations, triflate anions and acetonitrile molecules for [Pd(terpy)(3-cyanopyridine)]$(CF_3SO_3)_2$.

There is a net of hydrogen bonds, as shown in Figure 4.4. The triflate anion acts as a hydrogen bond acceptor and form hydrogen bonds with 3-cyanopyridine, terpyridine and acetonitrile molecule. The C–H…O distances lie in the range 2.315– 2.713 Å and the C–H…F distances lie in the range 2.668 – 2.979 Å. The C–H....N distances lie in the range

2.579 – 2.899 Å. The cyano groups act as hydrogen acceptors *via* C–H…N hydrogen bonds 2.672 Å.

*4.2.2.2. Single crystal X-ray structure of 2,2':6',2''-terpyridine (3-methylpyridine) palladium triflate [Pd(terpy)(3-methylpyridine)](CF_3SO_3)$_2$ (**4-2**).*

Crystals of [Pd(terpy)(3-methylpyridine)](CF_3SO_3)$_2$ were found to be colourless plates. The complex crystallises in the triclinic space group $P2_1/n$. The Pd cation is coordinated by three N atoms of the tridentate chelating terpyridine unit and one N atom from 3-methylpyridine. The Pd cation adopts a distorted square planar geometry. As shown in Figure 4.5, space above and below the Pd cation is occupied by two triflate anions. Selected bond lengths and angles are summarized in Table 4.2. The central Pd–N bond is noticeably shorter than the other three Pd–N bonds. The Pd–N bond lengths are comparable to those found in complexes (**2-2**) and (**3-2**). The dihedral angle between the square planar coordination sphere of the Pd cation and the 3-methylpyridine ring amounts to 64.48(8)°. The dihedral angle indicates that 3-methylpyridine ligand in this complex is bent more than that in (**2-2**) (70.01(4)°). In terms of tilt angle, this complex shows slightly larger distortions in tilt angle (175.90(5)°) when compared to (**2-2**) (177.7(2)°) and (**3-2**) (178.0(3)°). In terms of planarity, cations of (**4-2**) are less planar than those of (**2-2**) and more planar than those of (**3-2**), with a maximum displacement of +0.069 and -0.057 Å exhibited by C1 and C15, respectively, from the mean plane.

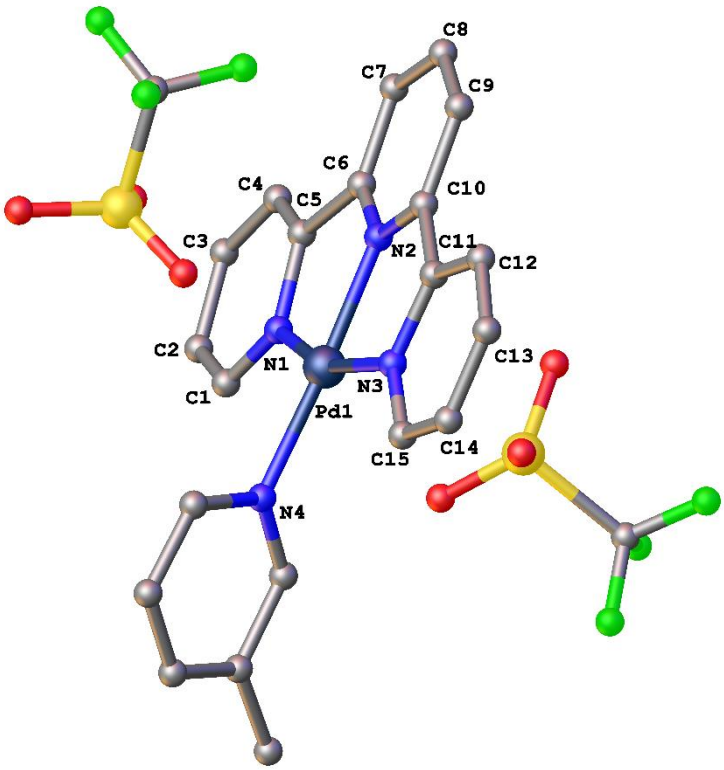


Figure 4.5: X-ray crystal structure of [Pd(terpy)(3-methylpyridine)]$(CF_3SO_3)_2$ with crystallographically independent atom numbering scheme. Hydrogen atoms have been omitted for clarity. Atom colours - C: grey, O: red, N: blue, Pd: navy F: green and S: yellow.

Table 4.2: Selected bond lengths (Å) and angles (°) for [Pd(terpy)(3-methylpyridine)]$(CF_3SO_3)_2$

Pd1-N1	2.053(15)	N2-Pd1-N1	80.30(5)
Pd1-N2	1.940(11)	N2-Pd1-N4	175.90(5)
Pd1-N3	2.033(15)	N3-Pd1-N1	162.20(6)
Pd1-N4	2.010(13)	N3-Pd1-N2	82.00(5)

In the solid state, the molecules of (**4-2**) are packed as shown in Figure. 4.6, similar to that in complexes (**2-2**) and [Pd(terpy)(py)]$(ClO_4)_2$ [3]. The crystal packing evidences

triflate anions located upper and below the Pd cation. Layers of molecules assemble on top of one another with the dominant interaction being π· · ·π stacking between the terminal pyridine ring of one terpy unit and the central pyridine ring of a terpyridine unit in the next layer. The centroid-centroid separation is 3.825 Å and slip angle is 2.171° (Figure 4.7).

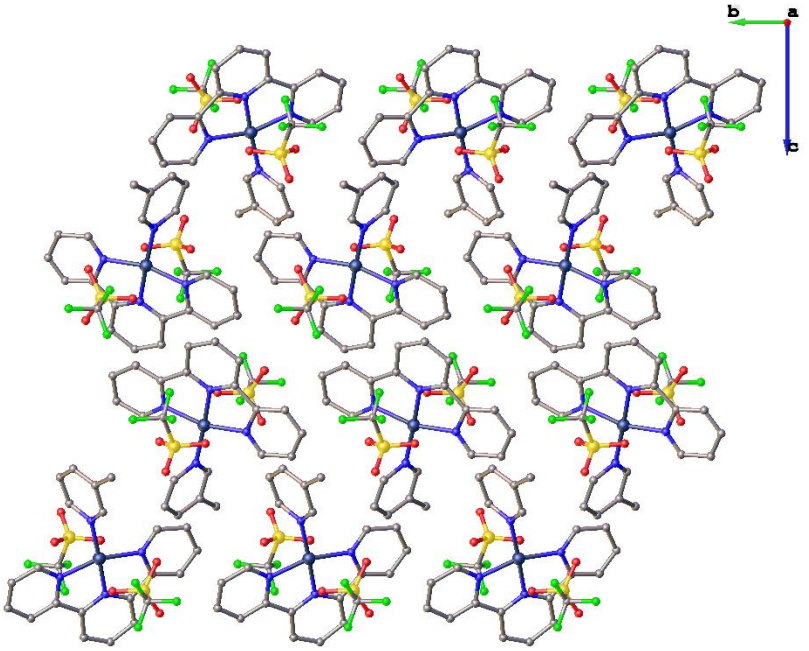


Figure 4.6: The packing diagram for [Pd(terpy)(3-methylpyridine)]$(CF_3SO_3)_2$ along the *a*-axis. Hydrogen atoms are omitted for clarity.

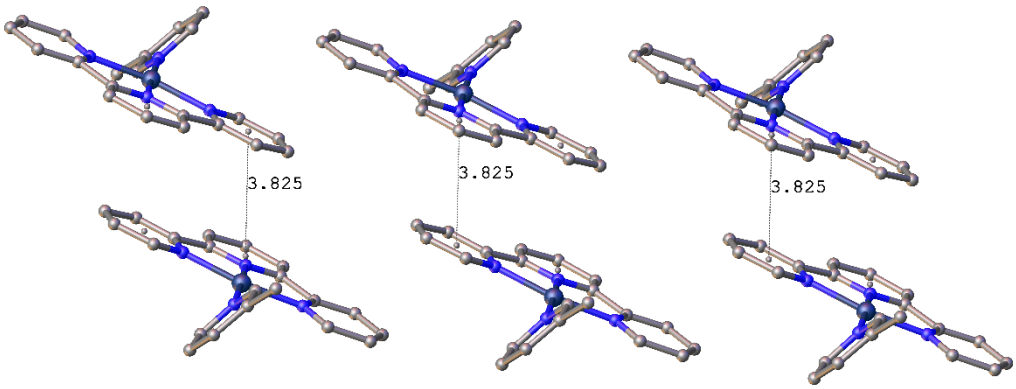


Figure 4.7: Representation of the π· · ·π interactions in [Pd(terpy)(3-methylpyridine)]$(CF_3SO_3)_2$. Dashed lines indicate the presence of π· · ·π interactions.

The oxygen and fluorine atoms of the triflate anion act as hydrogen bond acceptors generating hydrogen bonds with hydrogen atoms of terpyridine and 3-methylpyridine, as shown in Figure 4.8. The C–H…O distances lie in the range 2.123 – 2.913 Å and the C–H…F distances lie in the range 2.707 – 2.958 Å.

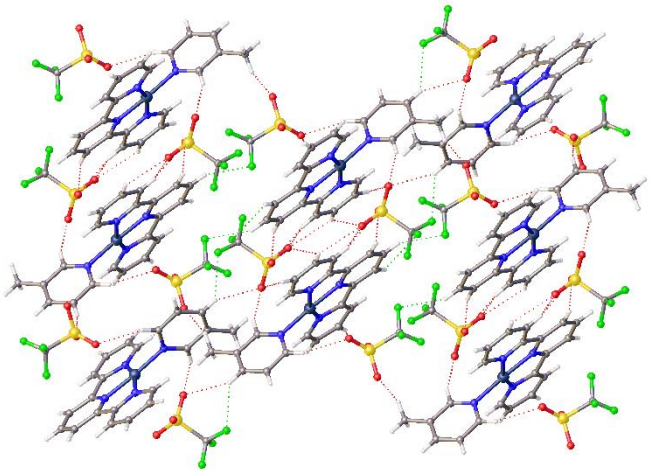


Figure 4.8: A net of hydrogen bonds links Pd(terpy) cations and triflate anions for [Pd(terpy)(3-methylpyridine)]$(CF_3SO_3)_2$.

*4.2.2.3. Single crystal X-ray structure of 2,2':6',2''-terpyridine (3-iodopyridine) palladium triflate [Pd(terpy)(3-iodopyridine)](CF_3SO_3)$_2$ (**4-3**).*

Crystals of [Pd(terpy)(3-iodopyridine)](CF_3SO_3)$_2$ were found to be colourless plates. This complex is monoclinic and crystallises in the space group $P2_1/c$. Figure 4.9 shows the coordination geometry and atom labelling scheme for complex (**4-3**). Space above and below the Pd cation is occupied by two triflate anions. Table 4.3 lists important bond lengths and angles for this complex. As before, the coordination sphere for (**4-3**) is also distorted square planar. The central Pd–N bond (1.934(3) Å) is noticeable shorter than the outer Pd–N bonds. This value is similar to those found in (**2-3**) (1.933(3) Å for (**A**) and 1.934(3) Å for (**B**)) and slightly shorter than that in (**3-3**) (1.937(9) Å). The N-Pd-N angles [N2–Pd1–N1 81.25°(13), N2–Pd1–N3 81.01°(13), N3–Pd1–N1 162.30(13)°] show deviations from the idealized values of 90° and 180°. These values are slightly higher than those found in (**2-3**) and (**3-3**). This complex shows only slight geometric distortion in terms of the dihedral angle 89.58(7)°. The dihedral angle indicates that the terpyridine ring and 3-iodopyridine are almost perpendicular to each other with a negligible deviation. However, at the cases of complexes (**2-3**) and (**3-3**) this dihedral angle deviates significantly from verticality. The tilt angle for complex (**4-3**) is 175.93(13)°. This value is similar to that found in (**3-3**) 175.20(4)°. However, it is smaller than those found in (**2-3**), 179.43(11)° and 178.90(11)° for molecule (**A**) and (**B**), respectively.

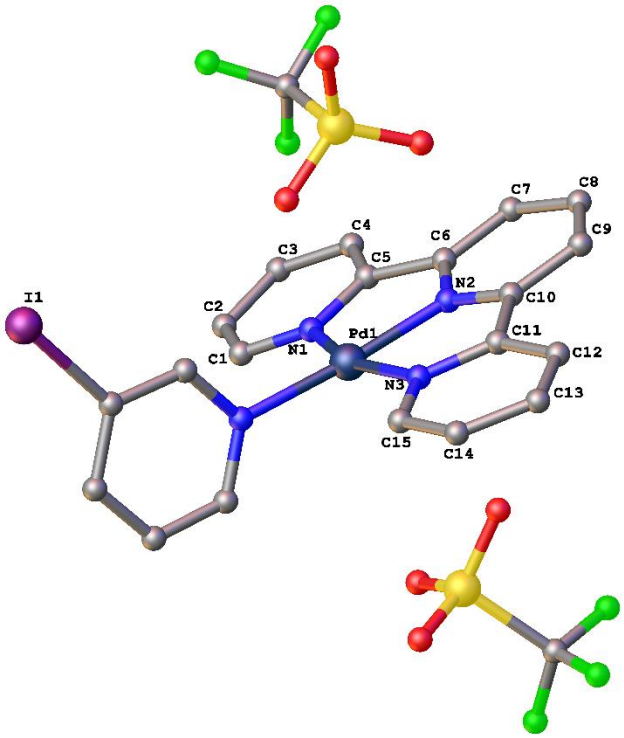


Figure 4.9: X-ray crystal structure of [Pd(terpy)(3-iodopyridine)]$(CF_3SO_3)_2$ with crystallographically independent atom numbering scheme. Hydrogen atoms have been omitted for clarity. The disorder in the triflate anion is shown. Atom colours - C: grey, O: red, N: blue, Pd: navy, I: purple, F: green and S: yellow.

Table 4.3: Selected bond lengths (Å) and angles (°) for [Pd(terpy)(3-iodopyridine)]$(CF_3SO_3)_2$.

Pd1-N1	2.041(3)	N2-Pd1-N1	81.25(13)
Pd1-N2	1.934(3)	N2-Pd1-N4	175.93(13)
Pd1-N3	2.034(3)	N3-Pd1-N1	162.19(13)
Pd1-N4	2.033(3)	N3-Pd1-N2	81.01(13)

Interestingly, cations of (**4-3**) are less planar than those of (**2-3**) and (**3-3**), with a maximum displacement of +0.183 and -0.173 Å exhibited by C12 and C15, respectively, from the mean plane.

In the solid state, the cations of (**4-3**) pack as head-to-head dimers in the crystal lattice, as shown in Figure 4.10. The crystal packing evidences triflate anions located above and below the Pd cation. The outer pyridyl ring and the central pyridyl ring of another molecule have a centroid–centroid distance of 4.452 Å, indicating π· · ·π interactions are absent.

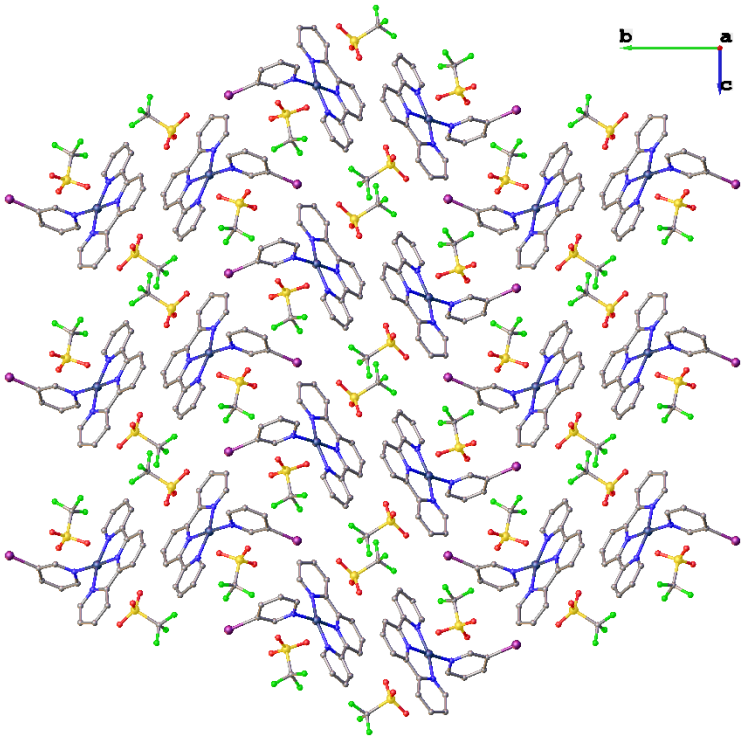


Figure 4.10: The packing diagram for [Pd(terpy)(3-iodopyridine)]$(CF_3SO_3)_2$ along the *a*-axis. Hydrogen atoms are omitted for clarity.

The oxygen and fluorine atoms of the triflate anion act as hydrogen bond acceptors generating hydrogen bonds with hydrogen atoms of terpyridine and 3-iodopyridine, as shown in Figure 4.11. The C–H…O distances lie in the range 2.241 – 2.992 Å and the C–H…F distances lie in the range 2.491 – 2.930 Å.

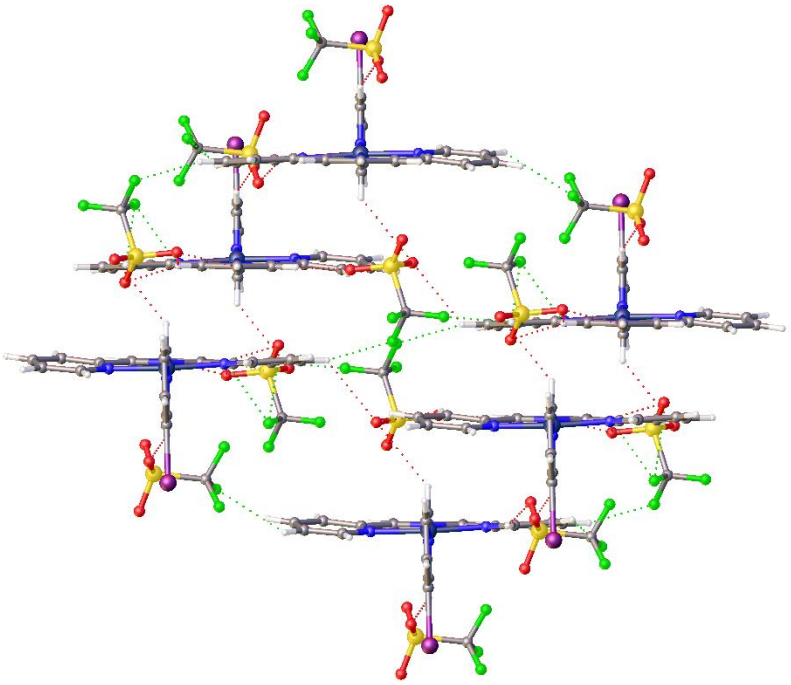


Figure 4.11: A net of hydrogen bonds links Pd(terpy) cations and triflate anions for [Pd(terpy)(3-iodopyridine)]$(CF_3SO_3)_2$.

*4.2.2.4. Single crystal X-ray structure of 2,2':6',2''-terpyridine (3-pyridinecarboxaldehyde) palladium triflate [Pd(terpy)(3-pyridinecarboxaldehyde)]$(CF_3SO_3)_2$ (**4-4**).*

Crystals of [Pd(terpy)(3-pyridinecarboxaldehyde)]$(CF_3SO_3)_2$ were found to be colourless plates. This complex crystallises in the triclinic space group *P-1*. Figure 4.12 shows the coordination geometry and atom labelling scheme for complex (**4-4**). Space above and below the Pd cation is occupied by two triflate anions and one acetonitrile molecule. Table 4.4 lists important bond lengths and angles for this complex. As before, the coordination geometry around the palladium(II) ion is considerably distorted from the perfect square-plane. This distortion leads to a narrowing of N1–Pd–N2 and N2–Pd–N3 angles to 80.90(9)° and 80.96(9)°, respectively, and also a significant shortening of Pd–N2 distances (1.933(3) Å) compared to the other Pd–N distances (Pd–N1 = 2.032(3) Å and

Pd–N3 = 2.037(3) Å). In general, bond distances and angles of this complex compare well with those already reported in this work (complexes (**2-5**) and (**3-5**) and in literature [Pt(terpy)(4-CO_2py)](NO_3) [2]. In terms of tilt angle, complex (**4-4**) 177.01(8)° indicates higher deviation from the theoretical value of 180° than molecule (**A**) in complex (**2-5**) (178.74(8)° and complex (**3-5**) (178.20(3)°).The angle between the square planar coordination geometry of the Pd(terpy) cation and the plane of 3-pyridinecarboxaldehyde is 86.36(6)°, which is close to the value observed for carboxy substituted pyridines [2-4]. The dihedral angle for (**4-4**) is substantially larger than for the other complexes (**2-5**) and (**3-5**) with 4-pyridinecarboxaldehyde ligand.

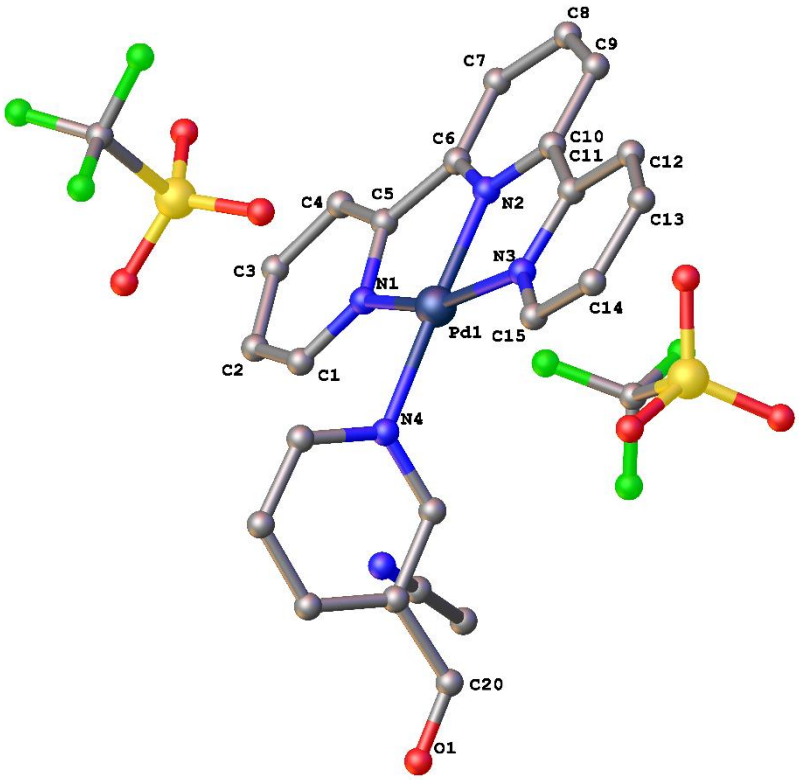


Figure 4.12: X-ray crystal structure of [Pd(terpy)(3-pyridinecarboxaldehyde))](CF_3SO_3)$_2$ with crystallographically independent atom numbering scheme. Hydrogen atoms have been omitted for clarity. Atom colours - C: grey, O: red, N: blue, Pd: navy F: green and S: yellow.

Table 4.4: Selected bond lengths (Å) and angles (°) for [Pd(terpy)(3-pyridinecarboxaldehyde))]$(CF_3SO_3)_2$

Pd1-N1	2.032(3)	N2-Pd1-N1	80.90(9)
Pd1-N2	1.934(3)	N2-Pd1-N4	177.01(8)
Pd1-N3	2.037(3)	N3-Pd1-N1	161.81(10)
Pd1-N4	2.035(3)	N3-Pd1-N2	80.96(9)

Cations of (**4-4**) are less planar than those of (**2-5**) and (**3-5**), with a maximum displacement of +0.085 and -0.116 Å exhibited by C1 and C4, respectively, from the mean plane.

Cations of (**4-4**) pack as head-to-head dimers, as shown in Figure 4.13. The triflate anions and acetonitrile molecules orient themselves into channels and fill the space between dimers. The cations of (**4-4**) undergo a series of face-to-face π· · ·π interactions indicated by ring centroid–ring centroid separations of 3.581 and 3.874 Å (corresponding slip angles are 5.075 and 0.00°), as shown in Figure 4.14.

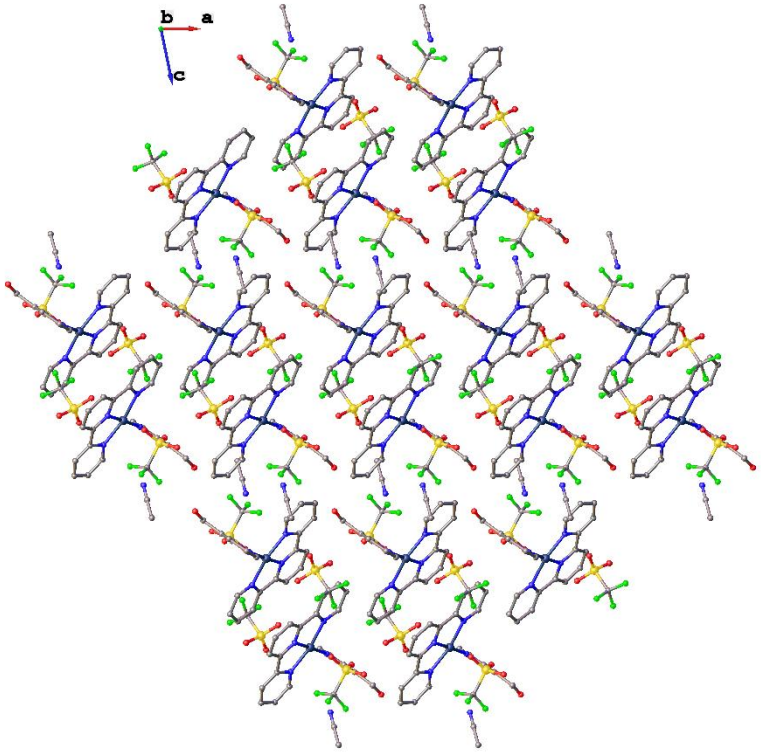


Figure 4.13: The packing diagram for [Pd(terpy)(3-pyridinecarboxaldehyde)]$(CF_3SO_3)_2$ along the *a*-axis. Hydrogen atoms are omitted for clarity.

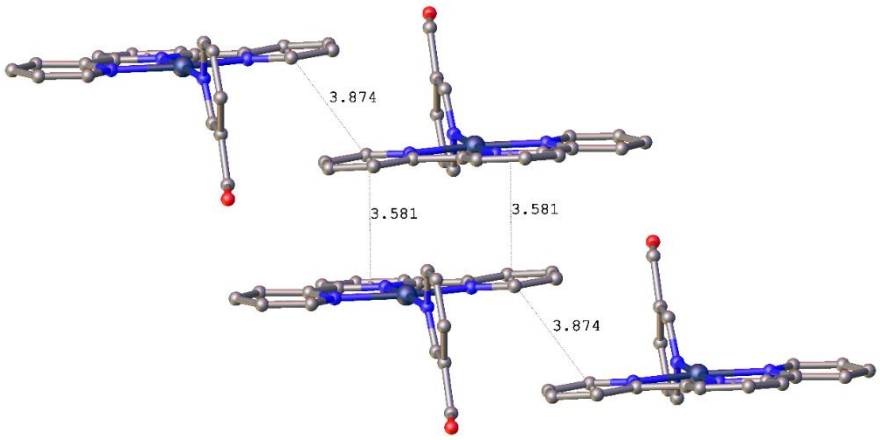


Figure 4.14: Representation of the π· · ·π interactions in [Pd(terpy)(3-pyridinecarboxaldehyde)]$(CF_3SO_3)_2$. Dashed lines indicate the presence of π· · ·π interactions.

This arrangement is further stabilised by a series of hydrogen bonds between aromatic protons, carboxaldehyde unit, acetonitrile molecule and triflate anion (Figure 4.15). Carboxaldehyde moieties are involved in intermolecular hydrogen bonds through oxygen atoms and act as hydrogen bond acceptors. The C2–H2…O1 and C3–H3…O1 distances are 2.707 and 2.671, respectively. In addition, the triflate anions act as hydrogen bond acceptors and form hydrogen bonds with 4-pyridinecarboxaldehyde, acetonitrile molecule and terpyridine moiety. The C–H…O distances lie in the range 2.329 – 2.959 Å and the C–H…F distances lie in the range 2.532 – 2.905 Å. The C–H…N distance is 2.641 Å.

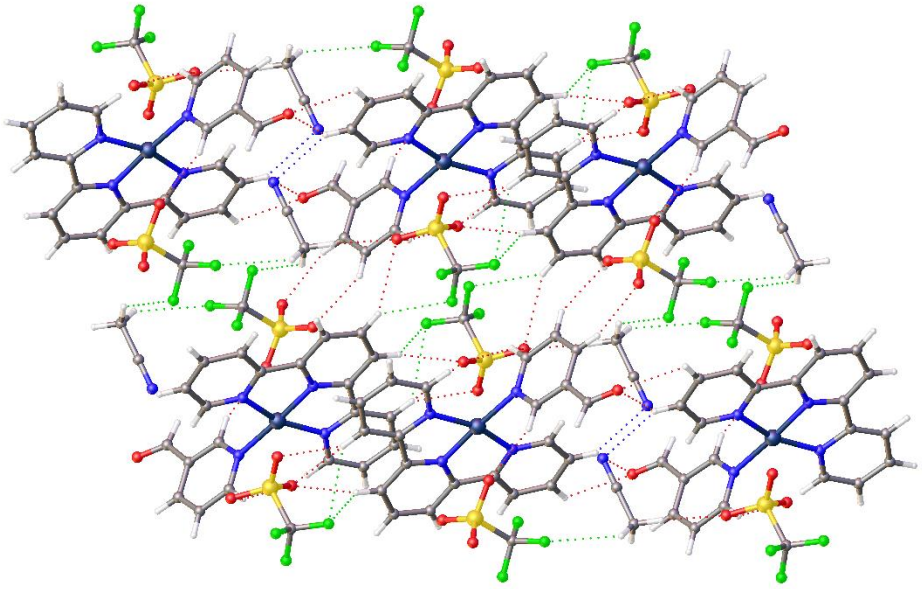


Figure 4.15: A net of hydrogen bonds links Pd(terpy) cations and triflate anions for [Pd(terpy)(3- pyridinecarboxaldehyde)]$(CF_3SO_3)_2$.

*4.2.2.5. Single crystal X-ray structure of 4,4',4''-tri-tert-butyl-2,2':6',2''-terpyridine (3-aminopyridine) palladium triflate [Pd(tBu$_3$-terpy)(3-aminopyridine)](CF$_3$SO$_3$)$_2$ (**4-5**).*

Crystals of [Pd(*t*Bu$_3$-terpy)(3-aminoopyridine)](CF$_3$SO$_3$)$_2$ were found to be colourless plates. The complex crystallises in the monoclinic space group *P2$_1$/c*. Complex (**4-5**) consists of one Pd(*t*Bu$_3$-terpy) cation, two triflate anions and one acetonitrile molecule (Figure 4.16). As is usually observed, *t*Bu$_3$-terpyridine acts as a tridentate ligand and an N-bound 3-aminopyridine ligand completes the distorted square-planar coordination around Pd. There is disorder exhibited on the 3-amino substituent, resulting from the free rotation of this ligand, which was modelled with a simple two-site disorder model. The occupancies of each component were allowed refine freely and show a 3:1 ratio with N5 as the major component. Table 4.5 lists important bond lengths and angles for this complex. In general, the Pd–N bonds are similar than those found in (**3-6**). However, these bonds are slightly shorter than those found in complex (**2-6**), with the Pd–N bonds for (**4-5**) shorter by less than 0.042 Å. In terms of angles, the bond angles show the usual deviations from idealized geometry as are seen in (**2-6**) and (**3-6**). The 3-aminopyridine is significantly bent with respect to *t*Bu$_3$-terpyridine plane forming a dihedral angle of 69.42(9)°. The dihedral angle indicates that 3-aminopyridine ligand in complex (**4-5**) is bent more than those in (**2-6**) and (**3-6**). In terms of tilt angle, complex (**3-6**) shows slightly larger distortions in tilt angle (174.42(16)°) when compared to (**2-6**) (178.44(16)°) and (**4-5**) (177.94(10)°).

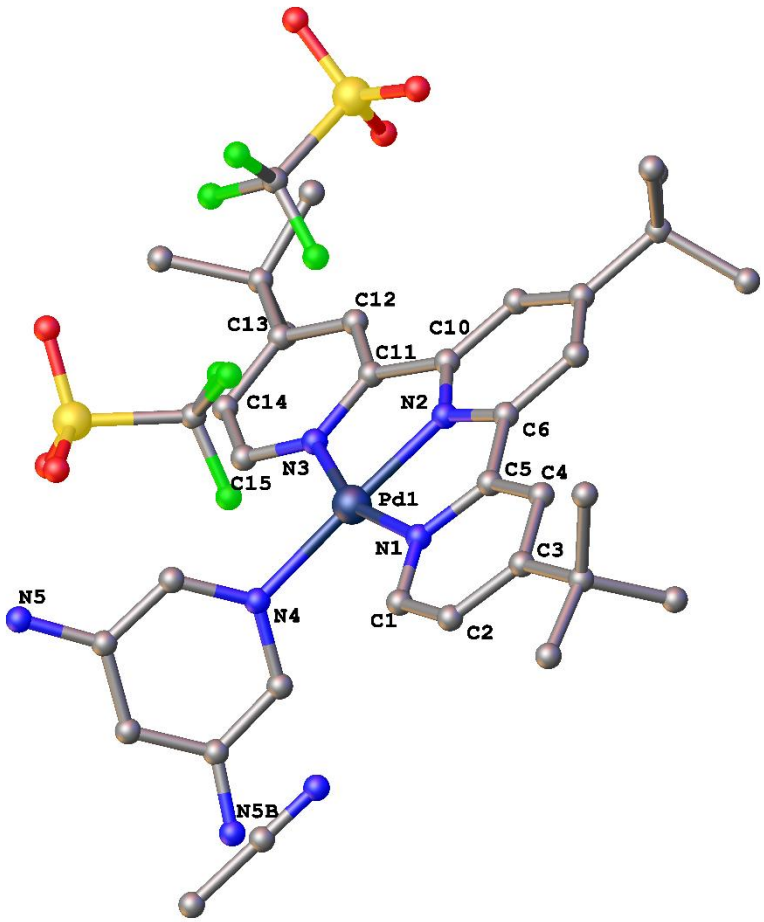


Figure 4.16: X-ray crystal structure of [Pd(*t*Bu$_3$-terpy)(3-aminopyridine)](CF$_3$SO$_3$)$_2$ with crystallographically independent atom numbering scheme. Hydrogen atoms have been omitted for clarity. Atom colours - C: grey, O: red, N: blue, Pd: navy F: green and S: yellow.

Table 4.5: Selected bond lengths (Å) and angles (°) for [Pd(*t*Bu$_3$-terpy)(3-aminopyridine)](CF$_3$SO$_3$)$_2$

Pd1-N1	2.021(2)	N2-Pd1-N1	80.76(9)
Pd1-N2	1.934(2)	N2-Pd1-N4	177.94(10)
Pd1-N3	2.026(2)	N3-Pd1-N1	161.73(10)
Pd1-N4	2.031(2)	N3-Pd1-N2	80.99(10)

In terms of planarity, cations of (**4-5**) are more planar than those of (**2-6**) and (**3-6**), with a maximum displacement of +0.094 and -0.083 Å exhibited by C4 and C9, respectively, from the mean plane. There is no obvious reason for this result.

Analysis of packing in the crystal structure showed that the cavities formed, along the *a*-axis, by cations and one of the triflate anions accommodate the second triflate anion and the acetonitrile molecule, as shown in Figure 4.17. Cations of complex (**4-5**) pack in a similar fashion to those of (**3-6**).

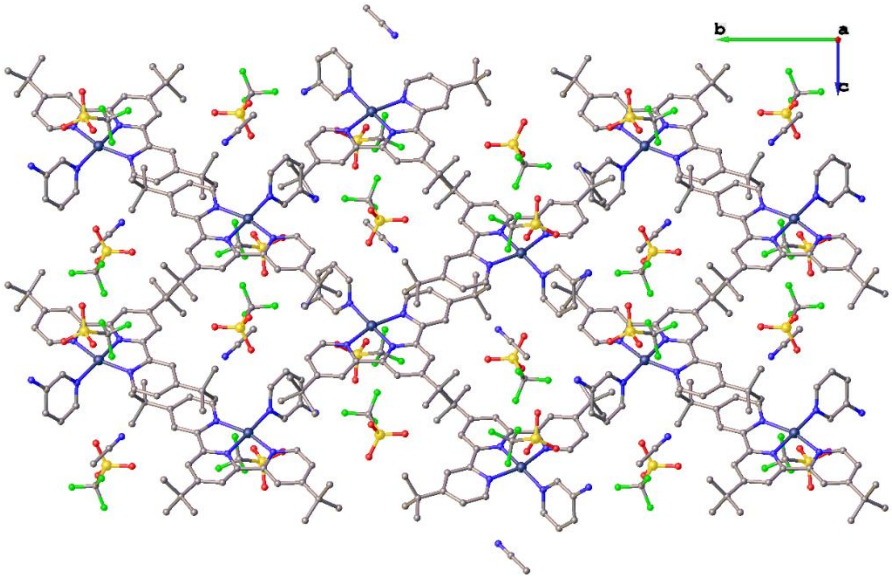


Figure 4.17: The packing diagram for [Pd(*t*Bu$_3$-terpy)(3-aminopyridine)](CF$_3$SO$_3$)$_2$ along the *a*-axis. Hydrogen atoms and anions are omitted for clarity.

Within the crystal packing cations, anions and solvent molecules are linked by a number of hydrogen bonds where triflate oxygen and fluorine atoms act as acceptor, as shown in Figure 4.18. The C–H…O distances lie in the range 2.314 – 2.993 Å and the C–H…F distances lie in the range 2.392 – 2.825 Å. In addition, every acetonitrile molecule acts as both a hydrogen donor and acceptor through two sets of C–H…O and two sets of C–H…N hydrogen bonds, respectively. The C2A–H2Ab…O4T and C2A–H2Ac…O2T

distances are 2.911 and 2.347 Å, respectively. The C1–H1…N1A and C19–H19c…N1A distances are 2.524 and 2.960 Å, respectively. Interestingly, the amino group of the 3-aminopyridine ligand acts as a hydrogen bond donor through two sets of N–H…O hydrogen bonds. The N5–H5a…O2T and N5–H5b…O1T distances are 2.314 and 2.393 Å, respectively.

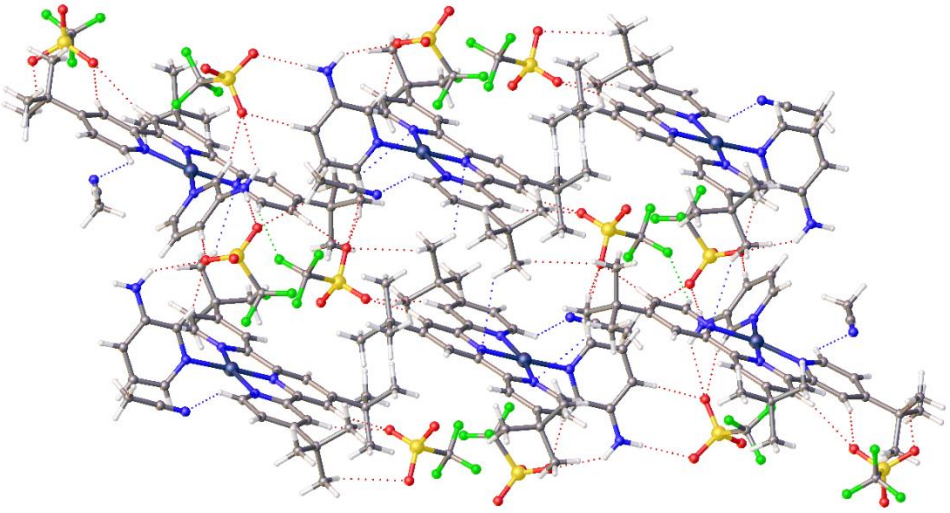


Figure 4.18: A net of hydrogen bonds links Pd(*t*Bu$_3$-terpy) cations, triflate anions and acetonitrile molecules for[Pd(*t*Bu$_3$-terpy)(3-aminopyridine)](CF$_3$SO$_3$)$_2$.

*4.2.2.6. Single crystal X-ray structure of 4,4',4''-tri-tert-butyl-2,2':6',2''-terpyridine (3-hydroxypyridine) palladium triflate [Pd(tBu$_3$-terpy)(3-hydroxypyridine)](CF$_3$SO$_3$)$_2$ (**4-6**).*

Crystals of [Pd(*t*Bu$_3$-terpy)(3-hydroxypyridine)](CF$_3$SO$_3$)$_2$ were found to be colourless plates, crystallising in the monoclinic space group *P2$_1$/c*. As anticipated, *t*Bu$_3$-terpyridine acts as a tridentate ligand and an N-bound 3-hydroxypyridine ligand completes the distorted square-planar coordination around Pd (Figure 4.19). Disorder is observed for the acetonitrile molecule contained in the unit cell. Similarly to complex (**4-5**), disorder is also exhibited by the 3-hydroxy substituent. This substituent shows a simple two-site

disorder which was easily modelled, by allowing the occupancies to refine as a free parameter and show a 3:1 ratio with O1 as the major component. Table 4.6 lists important bond lengths and angles for this complex. In general, the Pd–N bonds are slightly shorter than those found in complex (**3-8**), with the Pd–N bonds for (**4-6**) shorter by less than 0.043 Å. As before, the angles between the adjacent N atoms in the plane (N2-Pd1-N1=79.89(16)° and N2-Pd1-N3=81.69(17)°) and N3-Pd1-N1(161.57(17)°) angle show the usual deviations from idealized geometry as are seen in (**3-8**).

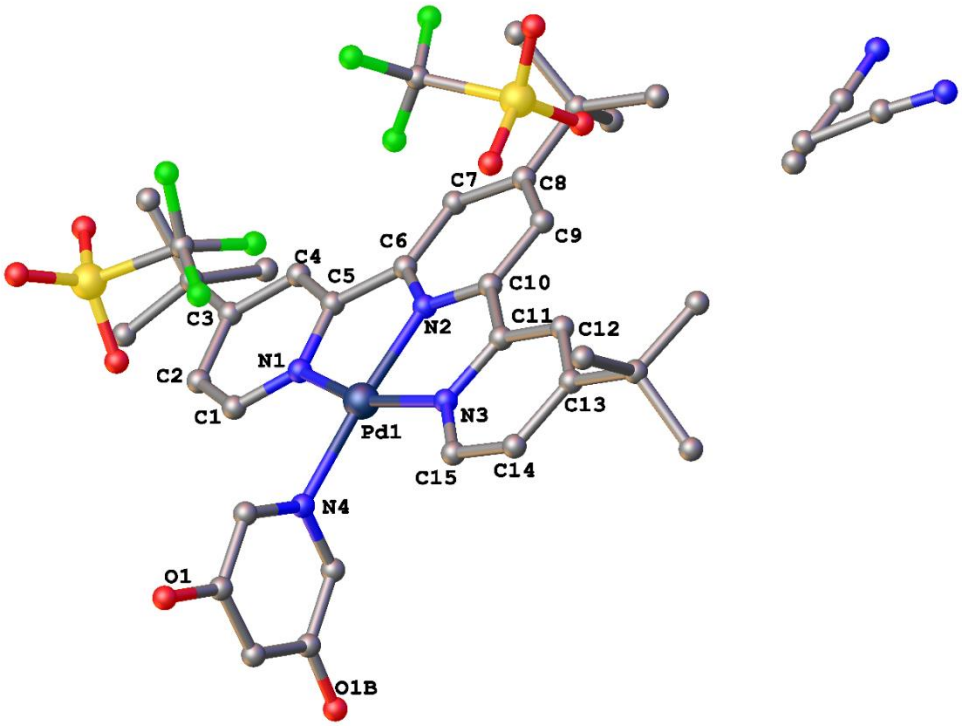


Figure 4.19: X-ray crystal structure of [Pd(*t*Bu$_3$-terpy)(3-hydroxypyridine)](CF$_3$SO$_3$)$_2$ with crystallographically independent atom numbering scheme. Hydrogen atoms have been omitted for clarity. Atom colours - C: grey, O: red, N: blue, Pd: navy F: green and S: yellow.

Table 4.6: Selected bond lengths (Å) and angles (°) for [Pd(*t*Bu$_3$-terpy)(3-hydroxypyridine)](CF$_3$SO$_3$)$_2$.

Pd1-N1	2.010(4)	N2-Pd1-N1	79.89(16)
Pd1-N2	1.926(4)	N2-Pd1-N4	175.64(18)
Pd1-N3	2.010(4)	N3-Pd1-N1	161.57(17)
Pd1-N4	2.024(4)	N3-Pd1-N2	81.69(17)

The angle between the square planar coordination geometry of the Pd(*t*Bu$_3$-terpy) cation and the plane of 3-hydroxypyridine is 84.84(9)°, which is larger than that for complex (**3-8**) (67.71(8)°). The deviation in tilt angle (175.64(18)°) is similar to that observed in (**3-8**) (175.86(9)°).

In terms of planarity, cations of (**4-6**) are more planar than those of (**3-8**), with a maximum displacement of +0.131 and +0.130 Å exhibited by C14 and C15, respectively, from the mean plane. Analysis of packing in the crystal structure showed that cations of (**4-6**) pack in a similar fashion to those of (**3-8**), as shown in Figure 4.20.

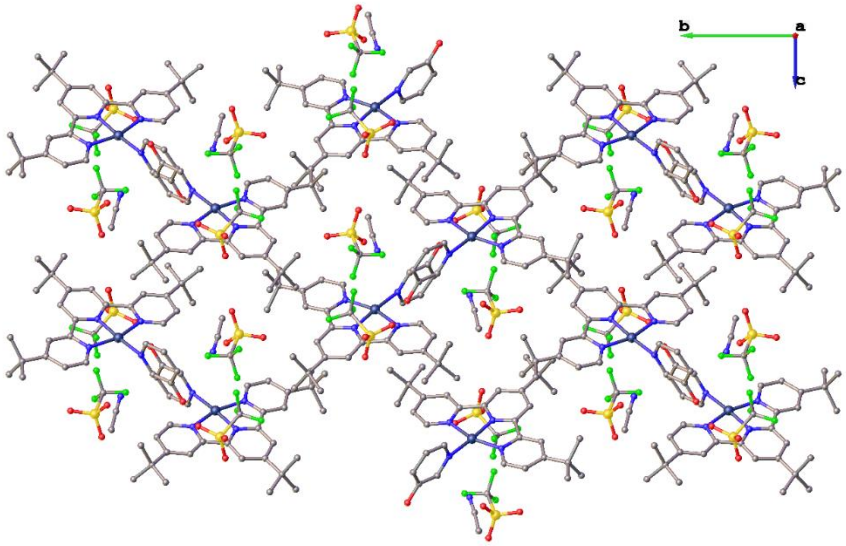


Figure 4.20: The packing diagram for [Pd(*t*Bu$_3$-terpy)(3-hydroxypyridine)](CF$_3$SO$_3$)$_2$ along the c crystal axis. Hydrogen atoms are omitted for clarity.

Within the crystal packing cations, anions and solvent molecules are linked by a number of hydrogen bonds where the *t*Bu$_3$-terpyridine acts as a donor and triflate oxygen and fluorine atoms act as acceptors, as shown in Figure 4.21. The C–H…O distances lie in the range 2.314 – 2.986 Å and the C–H…F distances lie in the range 2.441 – 2.970 Å. Each hydroxy group is involved in hydrogen bonds to a triflate anion. The O1–H1a…O3T distance is 1.904 Å.

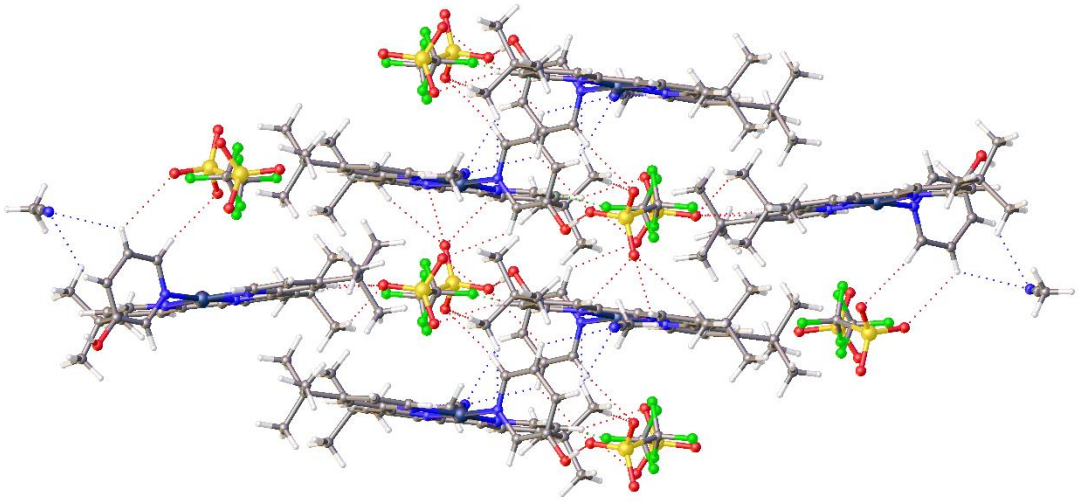


Figure 4.21: A net of hydrogen bonds links Pd(*t*Bu$_3$-terpy) cations and triflate anions for [Pd(*t*Bu$_3$-terpy)(3-hydroxypyridine)](CF$_3$SO$_3$)$_2$.

*4.2.2.7. Single crystal X-ray structure of 4,4',4''-tri-tert-butyl-2,2':6',2''-terpyridine (3-iodopyridine) palladium triflate and Palladium(tetrakis(3-iodoopyridine)$_4$) triflate [Pd(tBu$_3$-terpy)(3-iodopyridine)].[Pd(3-iodopyridine)$_4$](CF$_3$SO$_3$)$_4$ (**4-7**).*

The single crystal structure of (**4-7**) indicates the formation a three component discrete assembly consisting of one [Pd(*t*Bu$_3$-terpy)(3-iodopyridine)]$^{2+}$ and two [Pd(3-iodoopyridine)$_4$]$^{2+}$ molecules with four triflate anions and one acetonitrile molecule. Co-crystallization of two or more molecular components allows them to be incorporated in the same crystal reliably while keeping their own chemical properties. Crystals of (**4-7**) were found to be colourless plates. This complex crystallises in the monoclinic space group *P-1*. The coordination geometry and atom labelling scheme for this complex is shown in Figure 4.22. Interestingly, there are two crystallographically independent [Pd(3-iodoopyridine)$_4$]$^{2+}$ molecules which contain symmetry inversion centres at their Pd atom positions. Both molecules have coordination cores that are comprised of palladium and four nitrogen atoms from the 3-iodopyridine ligands. The PdN4 group is crystallographically required to be planar. The planes of the pyridine rings are

approximately perpendicular to the PdN4 plane. The average Pd–N distance is 2.026 Å in close agreement with 2.027 Å in $Pd(F_6acac)_2(4\text{-}ClC_5H_4N)_4$, 2.024 Å in $[Pd(C_6H_7N)_4]C1_2.2H_2O$ and 2.038 Å in $[(bpy)_2Pd(H_2O)_2](NO_3)_2$ [5-7]. In terms of $[Pd(t\text{Bu}_3\text{-terpy})(3\text{-iodopyridine})]^{2+}$ complex, the coordination geometry around the palladium(II) cation is considerably distorted from the perfect square-plane. Table 4.7 lists important bond lengths and angles for this complex. This distortion leads to a narrowing of N1–Pd–N2 and N2–Pd–N3 angles to 80.90(6) and 81.40(5)°, respectively, and also a significant shortening of Pd–N2 distances (1.987(13) Å) compared to the other Pd–N distances (Pd–N1 = 1.994(13) Å and Pd–N3 = 2.022(13) Å). The 3-iodopyridine is bent with respect to the coordination N4 donors forming a dihedral angle of 65.11(8)°. The dihedral angle decreases for this cation when 4',4",4"'-H atoms in (**4-3**) (the dihedral angle of $Pd(terpy)(3\text{-iodopyridine})](CF_3SO_3)_2$ is 89.58(7)°) are replaced with larger *t*Bu groups. In terms of tilt angle, complex (**4-7**) 178.3(5)° indicates smaller deviation from the theoretical value of 180° than in complexes (**4-3**) 175.93(13)° and (**3-3**) 175.20(4)°, but in excellent agreement with those of complex (**2-3**) reported previously 179.43(11) and 178.90(11)°.

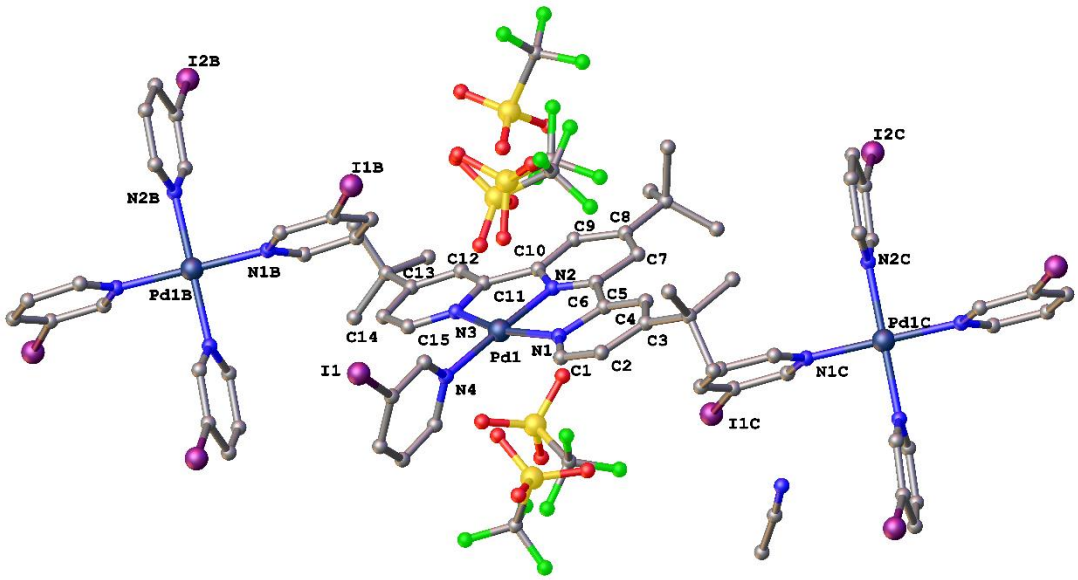


Figure 4.22: X-ray crystal structure of [Pd(*t*Bu$_3$-terpy)(3-iodopyridine)].[Pd(3-iodopyridine)$_4$](CF$_3$SO$_3$)$_4$ with crystallographically independent atom numbering scheme. Hydrogen atoms have been omitted for clarity. Atom colours - C: grey, O: red, N: blue, Pd: navy F: green, I: purple and S: yellow.

Table 4.7: Selected bond lengths (Å) and angles (°) for [Pd(*t*Bu$_3$-terpy)(3-iodopyridine)].[Pd(3-iodopyridine)$_4$](CF$_3$SO$_3$)$_4$.

Pd1-N1	1.994 (14)	N2-Pd1-N1	80.90(6)
Pd1-N2	1.987(13)	N2-Pd1-N4	178.3(5)
Pd1-N3	2.022(13)	N3-Pd1-N1	162.30(5)
Pd1-N4	2.054(11)	N3-Pd1-N2	81.40(5)

[Pd(*t*Bu$_3$-terpy)(3-iodopyridine)]$^{2+}$ cations pack in head to tail conformation from the view along the *c*-axis, as shown in Figure 4.23. These cations orient themselves into sheets separated by channels containing the [Pd(3-iodoopyridine)$_4$]$^{2+}$, triflate anions and the acetonitrile molecule.

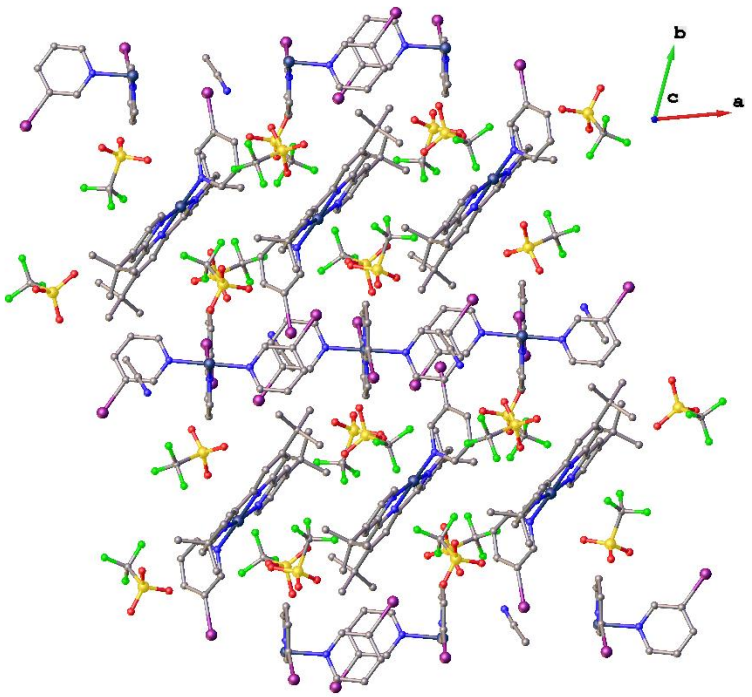


Figure 4.23: The packing diagram for [Pd(*t*Bu$_3$-terpy)(3-iodopyridine)].[Pd(3-iodopyridine)$_4$](CF$_3$SO$_3$)$_4$ along the *c*-axis. Hydrogen atoms are omitted for clarity.

Cations of (**4-7**) are less planar than those of (**4-3**), (**2-3**), and (**3-3**), with a maximum displacement of +0.220 and +0.217 Å exhibited by C1 and N1, respectively, from the mean plane. This high deviation is caused by torsion angles between the pyridine rings with values of 6.67° and 2.12°, leading to a puckering of the ligand.

There is a net of hydrogen bonds between the Pd cations, triflate anions and acetonitrile molecule. The C–H…O distances lie in the range 2.206 – 2.927 Å and the C–H…F distances lie in the range 2.562 – 2.966 Å (Figure 4.24).

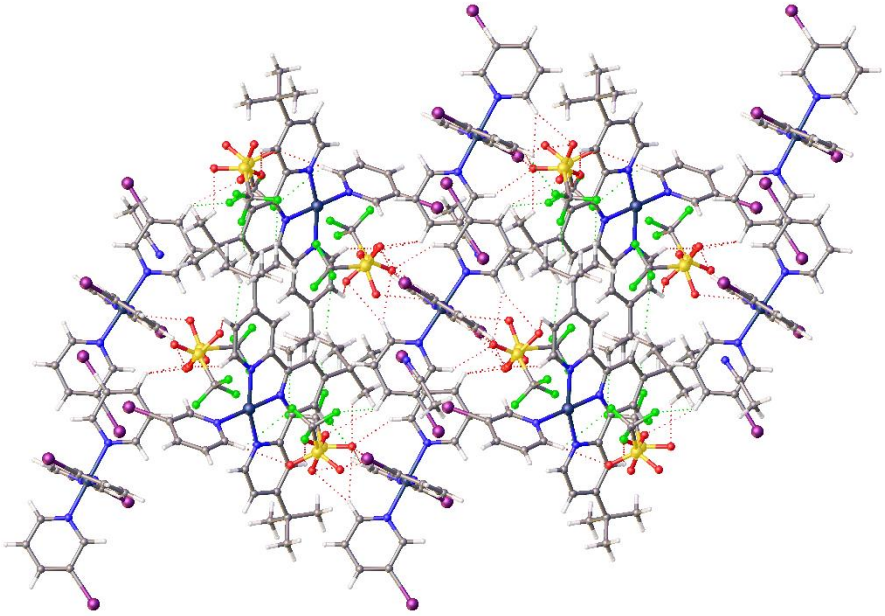


Figure 4.24: A net of hydrogen bonds links Pd cations, triflate anions and acetonitrile molecules for [Pd(*t*Bu$_3$-terpy)(3-iodopyridine)].[Pd(3-iodopyridine)$_4$](CF$_3$SO$_3$)$_4$.

4.2 Conclusions

The present work was undertaken to extend the conclusions in the previous chapters for substituted pyridines. To illustrate the influence of the pyridine ligands with different substitutions at *meta* position on the crystal structure, *meta*-substituted pyridine derivatives were used.

A series of Pd(Yterpy) (Y = H or *t*Bu$_3$) complexes have been synthesised using six *meta*-substituted pyridine derivatives. It was possible to grow crystals suitable for single crystal X-ray diffraction for all complexes. In all complexes, Pd cation adopts a distorted square planar geometry. Complexes (**4-1**), (**4-5**), (**4-6**) and (**4-7**) contain solvent acetonitrile molecules. There are no statistically significant differences in bond lengths between any of the complexes discussed here and complexes with *para*-substituted pyridine derivatives reported previously. This applies in particular for bond lengths involving the palladium

and nitrogen atoms. The bond between central nitrogen and the Pd atom is the shortest (average = 1.941(11) Å), with two longer bonds between the terminal nitrogen atoms and the Pd atom (falling in the range of 1.994(14)–2.054(11) Å). The N2–Pd1–N1 and N3–Pd1–N2 angles lie between 79.89(16) and 82.00(5)°. The N3–Pd1–N1 angle in (**4-7**) 162.30(5)° indicates the smallest deviation from the theoretical value of 180°, while (**4-6**) shows the highest deviation 161.57(17)°. The (**4-7**) cations show the highest deviation from planarity of all the complexes, while (**4-2**) is the closest to a planar geometry observed in any of the complexes. Complexes (**4-5**) and (**4-6**) exhibit the same packing in crystal structures. All of Pd(terpy) complexes in this Chapter, except (**4-3**), show π· · ·π interactions between aromatic rings. In terms of (**4-3**), the outer pyridyl ring and the central pyridyl ring of another molecule have a centroid–centroid distance of 4.452 Å, indicating π· · ·π interactions are absent. This can be attributed to the orientation of the triflate anions between the cations which hinder the formation of such interactions. All of Pd(*t*Bu$_3$-terpy) complexes do not exhibit any π· · ·π interactions.

There is a net of hydrogen bonds between the cations and the anions. The data shows that the O…C-H and F…C-H distances are within the range typical for weak hydrogen bond lengths.

Further study is still required in order to compare and contrast the effects of the *meta*-substituted pyridine ligands on the crystal structures. For example, kinetics of the complex formation of palladium(II)complexes with different *para*- and *meta*-pyridine derivatives can be studied.

4.3 Materials and Methods

All chemicals and solvents were purchased from Alfa-Aesar, Fisher Scientific, VWR International or Sigma-Aldrich and were used as received without any further purification. Reactions sensitive to air and moisture were performed using a standard Schlenk line, with nitrogen as the inert atmosphere. Glassware used was flame dried under vacuum and backfilled with nitrogen. ^{1}H and ^{13}C NMR spectra were recorded using either a Bruker AV(III)400, AV(III)500, AV400 or DPX400 spectrometer at room temperature. Mass spectroscopy was conducted using a Bruker Daltons Ultraflex MALDI- TOF with trans-2-[3-(4-*tert*-butylphenyl)-2-methyl-2-propenylidene]-malononitrile as the matrix (m/z = 250.3).

Single crystal X-ray diffraction experiments were performed on an Oxford Diffraction SuperNova CCD area detector diffractometer at 120 K using monochromated Cu Kα radiation (λ = 1.54184 Å); on Agilent GV1000 AtlasS2 or TitanS2 CCD area detector diffractometers at 120 K using monochromated CuKα radiation (λ = 1.54184 Å); or at the UK Diamond Light Source I19-1 3-circle diffractometer (λ = 0.6889 Å). Absorption 202 corrections were applied using analytical numerical methods using CrysAlisPro software [8]. The structures were solved by direct methods using either SHELXS or SHELXT and refined with SHELXL using a least squares method [9-11]. In all instances, Olex2 software was used as the solution, refinement and analysis program [12].

4.3.1 Synthesis of 2,2':6',2''-terpyridine (3-cyanopyridine) palladium triflate [Pd(terpy)(3-cyanopyridine)](CF$_3$SO$_3$)$_2$.

A mixture of 2,2':6',2''-terpyridine (72.5 mg, 0.311 mmol) and palladium chloride (50 mg, 0.282 mmol) in acetonitrile (20 mL) was stirred at room temperature for 24 h. Silver triflate (290 mg, 1.129 mmol) was added. In the absence of light, the mixture was stirred

for 48 h. After 48 h, the white precipitate (AgCl) was filtered. 3-Cyanopyridine (29 mg, 0.279 mmol) was added to the reaction solution and stirred for 3 h. The resulting pink solution was concentrated *via* rotary evaporation to remove the excess acetonitrile solvent. The resulting beige solid was washed with diethyl ether, before being dried in *vacuo*. Yield (93 mg, 45%). Single crystals suitable for X-ray diffraction were obtained by vapour diffusion of diethyl ether into an acetonitrile solution of [Pd(terpy)(3-cyanopyridine)] $(CF_3SO_3)_2$. MALDI-TOF MS (RP; m/z): 221.52 $[C_{23}H_{15}F_6N_5O_6PdS_2\text{-}2OTf]^{2+}$. ^{1}H NMR (400 MHz, $CDCl_3$) δ ppm: 8.90 (s, 1H, 2-py), 8.85 (dd, *J* = 5.0, 2.0 Hz, 1H, 6-py), 8.69 (d, *J* = 5.5 Hz, 2H, 6, 6``-terpy), 8.60 (m, 3H, 3`, 4`, 5`-terpy), 8.48 (m, 4H, 3, 4, 3``, 4``-tepry), 7.90 (m, 3H, 5, 5``-tepry, 4-py), 7.45 (t, *J* = 6.5 Hz, 1H, 5-py).

4.3.2 Synthesis of 2,2':6',2''-terpyridine (3-methylpyridine) palladium triflate [Pd(terpy)(3-methylpyridine)]$(CF_3SO_3)_2$.

A mixture of 2,2':6',2''-terpyridine (72.5 mg, 0.311 mmol) and palladium chloride (50 mg, 0.282 mmol) in acetonitrile (20 mL) was stirred at room temperature for 24 h. Silver triflate (290 mg, 1.129 mmol) was added. In the absence of light, the mixture was stirred for 48 h. After 48 h, the white precipitate (AgCl) was filtered. 3-Methylpyridine (27 μL, 0.282 mmol) was added to the reaction solution and stirred for 3 h. The resulting pink solution was concentrated *via* rotary evaporation to remove the excess acetonitrile solvent. The resulting beige solid was washed with diethyl ether, before being dried in *vacuo*. Yield (66 mg, 32%). Single crystals suitable for X-ray diffraction were obtained by vapour diffusion of diethyl ether into an acetonitrile solution of [Pd(terpy)(4-methylpyridine)]$(CF_3SO_3)_2$. MALDI-TOF MS (RP; m/z): 216.03 $[C_{23}H_{18}F_6N_4O_6PdS_2\text{-}2OTf]^{2+}$. ^{1}H NMR (400 MHz, $CDCl_3$) δ ppm: 8.80 (s, 1H, 2-py), 8.78 (m, 3H, 6, 6``-tepry, 6-py), 8.51 (m, 6H, 3, 3`, 3``, 4`, 5`-terpy, 4-py), 8.45 (td, *J*= 8.0, 1.2 Hz, 2H, 4, 4``-terpy), 7.43 (m, 3H, 5, 5``-terpy, 5-py), 2.59 (s, 3H, CH_3).

4.3.3 Synthesis of 2,2':6',2''-terpyridine (3-iodopyridine) palladium triflate [Pd(terpy)(3-iodopyridine)]$(CF_3SO_3)_2$.

A mixture of 2,2':6',2''-terpyridine (72.5 mg, 0.311 mmol) and palladium chloride (50 mg, 0.282 mmol) in acetonitrile (20 mL) was stirred at room temperature for 24 h. Silver triflate (290 mg, 1.129 mmol) was added. In the absence of light, the mixture was stirred for 48 h. After 48 h, the white precipitate (AgCl) was filtered. 3-Iodopyridine (58 mg, 0.283 mmol) was added to the reaction solution and stirred for 3 h. The resulting solution was concentrated *via* rotary evaporation to remove the excess acetonitrile solvent. The resulting beige solid was washed with diethyl ether, before being dried in *vacuo*. Yield (78 mg, 33%). Single crystals suitable for X-ray diffraction were obtained by vapour diffusion of diethyl ether into an acetonitrile solution of [Pd(terpy)(3-iodopyridine)]$(CF_3SO_3)_2$. MALDI-TOF MS (RP; m/z): 271.31 $[C_{22}H_{15}F_6IN_4O_6PdS_2\text{-}2OTf]^{2+}$. ^{1}H NMR (400 MHz, $CDCl_3$) δ ppm: 8.88 (s, 1H, 2-py), 8,75 (d, *J* = 3.8 Hz, 1H, 6-py), 8.70 (d, *J* = 5.6 Hz, 2H, 6, 6``-terpy), 8.61 (m, 6H, 3, 3`, 3``, 4`, 5`-terpy, 4-py), 8.40 (m, 2H, 4, 4``-terpy), 7.85 (td, *J* = 6.0, 1.2 Hz, 2H, 5, 5``-terpy), 7.55 (m, 1H, 5-py).

4.3.4 Synthesis of 2,2':6',2''-terpyridine (3-pyridinecarboxaldehyde) palladium triflate [Pd(terpy)(3-pyridinecarboxaldehyde)]$(CF_3SO_3)_2$.

A mixture of 2,2':6',2''-terpyridine (72.5 mg, 0.311 mmol) and palladium chloride (50 mg, 0.282 mmol) in acetonitrile (20 mL) was stirred at room temperature for 24 h. Silver triflate (290 mg, 1.129 mmol) was added. In the absence of light, the mixture was stirred for 48 h. After 48 h, the white precipitate (AgCl) was filtered. 3-Pyridinecarboxaldehyde (26 μL, 0.280 mmol) was added to the reaction solution and stirred for 3 h. The resulting solution was concentrated *via* rotary evaporation to remove the excess acetonitrile solvent. The resulting beige solid was washed with diethyl ether, before being dried in *vacuo*. Yield (56 mg, 27%). Single crystals suitable for X-ray diffraction were obtained by

vapour diffusion of diethyl ether into an acetonitrile solution of Pd(terpy)(3-pyridinecarboxaldehyde)]$(CF_3SO_3)_2$. MALDI-TOF MS (RP; m/z): 223.02 $[C_{23}H_{16}F_6N_4O_7PdS_2\text{-}2OTf]^{2+}$. ^{1}H NMR (400 MHz, CD_3CN) δ ppm: 9.18 (s, 1H, 2-py), 8.86 (d, *J* = 8.6 Hz, 1H, 6-py), 8.72 (d, *J* = 5.6 Hz, 2H, 6, 6``-terpy), 8.63 (m, 5H, 3, 3`, 3```, 4`, 5`-terpy), 8.46 (m, 3H, 4, 4``-terpy, 4-py), 7.89 (t, *J* = 6.0Hz, 2H, 5, 5``-terpy), 7.51 (t, *J* = 6.6 Hz, 1H, 5-py).

4.3.5 Synthesis of 4,4',4''-tri-*tert*-butyl-2,2':6',2''-terpyridine (3-aminopyridine) palladium triflate [Pd(*t*Bu$_3$-terpy)(3-aminopyridine)]$(CF_3SO_3)_2$.

A mixture of 4,4',4"-tri-*tert*-butyl-2,2':6',2"-terpyridine (113 mg, 0.311 mmol) and palladium chloride (50 mg, 0.282 mmol) in acetonitrile (20 mL) was stirred at room temperature for 24 h. Silver triflate (290 mg, 1.129 mmol) was added. In the absence of light, the mixture was stirred for 48 h. After 48 h, the white precipitate (AgCl) was filtered. 3-Aminopyridine (27 mg, 0.287 mmol) was added to the reaction solution and stirred for 2 h. The resulting solution was concentrated *via* rotary evaporation to remove the excess acetonitrile solvent. The resulting beige solid was washed with diethyl ether, before being dried in *vacuo*. Yield (171 mg, 68%). Single crystals suitable for X-ray diffraction were obtained by vapour diffusion of diethyl ether into an acetonitrile solution of [Pd(*t*Bu$_3$-terpy)(3-aminopyridine)]$(CF_3SO_3)_2$. MALDI-TOF MS (RP; m/z): 300.62 $[C_{34}H_{41}F_6N_5O_6PdS_2\text{-}2OTf]^{2+}$. ^{1}H NMR (400 MHz, CD_3CN) δ ppm: 8.98 (d, *J* = 6.1 Hz, 2H, 6, 6``-*t*Bu$_3$-terpy), 8.81 (s, 2H, 3`, 5`-*t*Bu$_3$-terpy), 7.83 (m, 1H, 2-py), 7.47 (m, 4H, 3, 3``-*t*Bu$_3$-terpy, 4, 6-py), 7.40 (m, 3H, 5, 5``-*t*Bu$_3$-terpy, 5-py), 4.45 (s, 2H, NH_2), 1.59 (s, 9 H, *t*Bu$_3$), 1.52(s, 18 H, *t*Bu$_3$).

4.3.6 Synthesis of 4,4',4''-tri-*tert*-butyl-2,2':6',2''-terpyridine (3-hydroxypyridine) palladium triflate [Pd(*t*Bu$_3$-terpy)(3-hydroxypyridine)](CF$_3$SO$_3$)$_2$.

A mixture of 4,4',4''-tri-*tert*-butyl-2,2':6',2''-terpyridine (113 mg, 0.311 mmol) and palladium chloride (50 mg, 0.282 mmol) in acetonitrile (20 mL) was stirred at room temperature for 24 h. Silver triflate (290 mg, 1.129 mmol) was added. In the absence of light, the mixture was stirred for 48 h. After 48 h, the white precipitate (AgCl) was filtered. 3-Hydroxypyridine (27 mg, 0.284 mmol) was added to the reaction solution and stirred for 2 h. The resulting solution was concentrated *via* rotary evaporation to remove the excess acetonitrile solvent. The resulting beige solid was washed with diethyl ether, before being dried in *vacuo*. Yield (130 mg, 51%). Single crystals suitable for X-ray diffraction were obtained by vapour diffusion of diethyl ether into an acetonitrile solution of [Pd(*t*Bu$_3$-terpy)(3-hydroxypyridine)](CF$_3$SO$_3$)$_2$. MALDI-TOF MS (RP; m/z): 301.11 [C$_{34}$H$_{40}$F$_6$N$_4$O$_7$PdS$_2$-2OTf]$^{2+}$. ^{1}H NMR (400 MHz, CDCl$_3$) δ ppm: 8.77 (m, 4H, 3, 3`, 3``, 5`-*t*Bu$_3$-terpy), 8.71 (d, *J* = 5.7 Hz, 2H, 6, 6``-*t*Bu$_3$-terpy), 8.40 (m, 2H, 2, 6-py), 7.78(m, 2H, 5-py), 7.37 (m, 3H, 5, 5``-*t*Bu$_3$-terpy, 4-py), 1.55(s, 9 H, *t*Bu$_3$), 1.49(s, 18 H, *t*Bu$_3$).

4.3.7 Synthesis of 4,4',4''-tri-*tert*-butyl-2,2':6',2''-terpyridine (3-iodopyridine) palladium triflate and palladium(3-iodopyridine)$_4$ triflate [Pd(*t*Bu$_3$-terpy)(3-iodopyridine)].[Pd(3-iodopyridine)$_4$](CF$_3$SO$_3$)$_4$.

A mixture of 4,4',4''-tri-*tert*-butyl-2,2':6',2''-terpyridine (113 mg, 0.311 mmol) and palladium chloride (50 mg, 0.282 mmol) in acetonitrile (20 mL) was stirred at room temperature for 24 h. Silver triflate (290 mg, 1.129 mmol) was added. In the absence of light, the mixture was stirred for 48 h. After 48 h, the white precipitate (AgCl) was filtered. 3-Iodopyridine (58 mg, 0.283 mmol) was added to the reaction solution and stirred for 2 h. The resulting solution was concentrated *via* rotary evaporation to remove the excess acetonitrile solvent. The resulting beige solid was washed with diethyl ether,

before being dried in *vacuo*. Yield (250 mg, 42%). Single crystals suitable for X-ray diffraction were obtained by vapour diffusion of diethyl ether into an acetonitrile solution of [Pd(*t*Bu$_3$-terpy)(3-iodopyridine)].[Pd(3-iodopyridine)$_4$](CF$_3$SO$_3$)$_4$. Elemental analysis calculated (%) for $C_{58}H_{58}F_{12}I_5N_9O_{12}Pd_2S_4$: C 30.59, H 2.57, N 5.54. Found: C 30.82, H 2.66, N 5.29.

4.3.8 Crystal data

Crystal data for (**4-1**): $C_{25}H_{18}F_6N_6O_6PdS_2$ (M + MeCN) (M =782.97 g/mol): monoclinic, space group P2$_1$/c (no. 14), a = 8.0977(3) Å, b = 19.2150(6) Å, c = 18.7132(5) Å, β = 90.763(3)°, V = 2911.47(16) Å^3, Z = 4, T = 120(2) K, μ(CuKα) = 7.316 mm^{-1}, $Dcalc$ = 1.786 g/cm^3, 11775 reflections measured (9.204° ≤ 2θ ≤ 147.31°), 5685 unique (R_{int} = 0.0391, R_{sigma} = 0.0532) which were used in all calculations. The final R_1 was 0.0412 (I > 2σ(I)) and wR_2 was 0.1237 with GOF = 0.884.

Crystal data for (**4-2**): $C_{23}H_{18}N_4O_6F_6S_2Pd$ (M =730.93 g/mol): monoclinic, space group P2$_1$/n (no. 14), a = 10.3536(7) Å, b = 9.6163(6) Å, c = 26.887(2) Å, β = 94.581(7)°, V = 2668.4(3) Å^3, Z = 1, T = 120.02(10) K, μ(CuKα) = 1.976 mm^{-1}, $Dcalc$ = 0.455 g/cm^3, 34333 reflections measured (8.932° ≤ 2θ ≤ 155.122°), 5407 unique (R_{int} = 0.0418, R_{sigma} = 0.0606) which were used in all calculations. The final R_1 was 0.0826 (I > 2σ(I)) and wR_2 was 0.1637 with GOF = 1.032.

Crystal data for (**4-3**): $C_{22}H_{15}F_6IN_4O_6PdS_2$ (M =842.80 g/mol): monoclinic, space group P2$_1$/c (no. 14), a = 8.5019(2) Å, b = 28.1389(8) Å, c = 11.4611(3) Å, β = 94.352(3)°, V = 2733.98(12) Å^3, Z = 4, T = 120(2) K, μ(CuKα) = 16.581 mm^{-1}, $Dcalc$ = 2.048 g/cm^3, 10863 reflections measured (8.35° ≤ 2θ ≤ 147.726°), 5346 unique (R_{int} = 0.0311, R_{sigma} = 0.0400) which were used in all calculations. The final R_1 was 0.0324 (I > 2σ(I)) and wR_2 was 0.1022 with GOF = 0.799.

Crystal data for (**4-4**): $C_{25}H_{19}F_6N_5O_7PdS_2$ (M + MeCN) (*M* =785.97 g/mol): triclinic, space group P-1 (no. 2), *a* = 9.0683(3) Å, *b* = 10.8301(4) Å, *c* = 15.1898(5) Å, *α* = 82.149(3)°, *β* = 77.866(3)°, *γ* = 86.079(3)°, *V* = 1443.59(9) Å^3, *Z* = 2, *T* = 120(2) K, μ(CuKα) = 7.396 mm^{-1}, *Dcalc* = 1.808 g/cm^3, 20763 reflections measured (5.998° ≤ 2θ ≤ 150.642°), 5803 unique (R_{int} = 0.0465, R_{sigma} = 0.0367) which were used in all calculations. The final R_1 was 0.0349 (I > 2σ(I)) and wR_2 was 0.1058 with GOF = 0.864.

Crystal data for (**4-5**): $C_{36}H_{44}F_6N_6O_6PdS_2$ (M + MeCN) (*M* =941.29 g/mol): monoclinic, space group $P2_1/c$ (no. 14), *a* = 11.3627(4) Å, *b* = 30.6458(9) Å, *c* = 12.0776(3) Å, *β* = 95.781(3)°, *V* = 4184.3(2) Å^3, *Z* = 4, *T* = 120(2) K, μ(CuKα) = 5.187 mm^{-1}, *Dcalc* = 1.494 g/cm^3, 26508 reflections measured (7.82° ≤ 2θ ≤ 147.86°), 8262 unique (R_{int} = 0.0405, R_{sigma} = 0.0400) which were used in all calculations. The final R_1 was 0.0368 (I > 2σ(I)) and wR_2 was 0.1203 with GOF= 0.888.

Crystal data for (**4-6**): $C_{36}H_{45}F_6N_5O_7PdS_2$ (M + MeCN) (*M* =944.29 g/mol): monoclinic, space group $P2_1/c$ (no. 14), *a* = 11.1617(3) Å, *b* = 30.4042(10) Å, *c* = 12.0108(4) Å, *β* = 93.871(3)°, *V* = 4066.7(2) Å^3, *Z* = 4, *T* = 120(2) K, μ(CuKα) = 5.349 mm^{-1}, *Dcalc* = 1.542 g/cm^3, 17610 reflections measured (7.93° ≤ 2θ ≤ 179.274°), 8050 unique (R_{int} = 0.0459, R_{sigma} = 0.0551) which were used in all calculations. The final R_1 was 0.0593 (I > 2σ(I)) and wR_2 was 0.1853 with GOF = 1.272.

Crystal data for (**4-7**): $C_{58}H_{58}F_{12}I_5N_9O_{12}Pd_2S_4$ (M + MeCN) (*M* =2276.67 g/mol): triclinic, space group P-1 (no. 2), *a* = 15.8202(11) Å, *b* = 16.0772(15) Å, *c* = 16.7333(13) Å, *α* = 78.201(7)°, *β* = 87.277(6)°, *γ* = 70.044(7)°, *V* = 3914.8(6) Å^3, *Z* = 2, *T* = 120(2) K, μ(CuKα) = 20.957 mm^{-1}, *Dcalc* = 1.931 g/cm^3, 28537 reflections measured (6.85° ≤ 2θ ≤ 150.198°), 15432 unique (R_{int} = 0.0925, R_{sigma} = 0.1330) which were used in all calculations. The final R_1 was 0.0845 (I > 2σ(I)) and wR_2 was 0.2473 with GOF = 1.112.

4.4 References

1. S. S. Hosseini, M. Bhadbhade, R. J. Clarke, P. J. Rutledge and L. M. Rendina, *Dalton Transactions*, 2011, **40**, 506-513.

2. R. Kaskafetou, M. J. Manos and A. Garoufis, *Inorganic Chemistry Communications*, 2013, **35**, 176-180.

3. Ž. D. Bugarčić, B. Petrović and E. Zangrando, *Inorganica Chimica Acta*, 2004, **357**, 2650-2656.

4. S. Coşar, M. B. Janik, M. Flock, E. Freisinger, E. Farkas and B. Lippert, *Journal of the Chemical Society, Dalton Transactions*, 1999, 2329-2336.

5. P. C. Chieh, *Journal of the Chemical Society, Dalton Transactions*, 1972, 1643-1646.

6. A. Siedle and L. Pignolet, *Inorganic Chemistry*, 1982, **21**, 135-141.

7. W. Chen, C.-M. Liu, R.-G. Xiong and X.-Z. You, *Acta Crystallographica Section C: Crystal Structure Communications*, 1997, **53**, 1218-1220.

8. CrysAlisPro, *Agilent Technologies UK Ltd., Oxford, UK*, 2013.

9. G. M. Sheldrick, *Acta Crystallographica Section A: Foundations of Crystallography*, 2008, **64**, 112-122.

10. G. M. Sheldrick, *Acta Crystallographica Section A: Foundations and Advances*, 2015, **71**, 3-8.

11. G. M. Sheldrick, *Acta Crystallographica Section C: Structural Chemistry*, 2015, **71**, 3-8.

12. O. V. Dolomanov, L. J. Bourhis, R. J. Gildea, J. A. Howard and H. Puschmann, *Journal of Applied Crystallography*, 2009, **42**, 339-341.

Chapter 5

Dinuclear Palladium (2,2':6',2''-Terpyridine) Complexes

5.1 Introduction

The synthesis of multinuclear complexes combining two or more 2,2':6',2"-terpyridine metal-binding domains is an essential step to extend the area of coordination chemistry from the molecular to the supramolecular level.

One of the most important themes in the chemistry of the terpyridine complexes $[M(Yterpy)X]^{n+}$ (M = Pt or Pd, X represents ligands occupying the fourth coordination site, Y represents substituents on the terpy ligand and *n* is the charge of the complex) is the propensity for these square-planar to "stack" with other $[M(Yterpy)X]^{n+}$ cations. The two terpyridine complexes can be linked by a bridging ligand in the X position or by terpyridine derivatives that are covalently linked. The coordination geometry of the bridging ligand can determine if $[M(Yterpy)X]^{n+}$ units adopt a stacked or un-stacked orientation. A wide range of dinuclear Pt(II) and Pd(II) complexes with short linkers such as pyrazole, diphenylformamidine, guanidine, 2-mercaptoimidazole, 1-methylcytosine, acetamide and canavanine were synthesised [1-7]. All of these complexes with shorts linkers favour π· · ·π interactions between terpyridine moieties. The crystal structure of $[\{Pt(terpy)\}_2(pz)](ClO_4)_3 .CH_3CN$ displays intramolecular π· · ·π interactions with distance of 3.432 Å (Figure 5.1) [3].

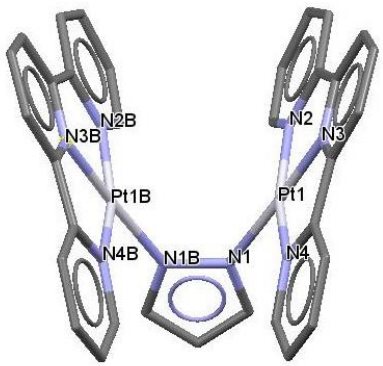


Figure 5.1: The view of the crystal structure of the dinuclear complex $[\{Pt(terpy)\}_2(pz)](ClO_4)_3 \cdot CH_3CN$ [3].

Linear bridging ligands can also form dimers with unstacked $[M(terpy)X]^+$ units. Ziessel and coworkers utilised linear diacetylene linker, consisting of 2,2'-bipyridine, to connect two Pt(II) terpyridine moieties [8]. A series of $[\{Pt(terpy)\}_2X]^{4+}$ complexes has been synthesised using pyridyl bridging ligands such as *N,N*–4,4–vinylenedipyridine, *para*-phenylenediethynyl and *para*-biphenyldiethynyl [9-11].

Many examples of Pd(II) and Pt(II) complexes have been used as building blocks to self-assemble higher ordered supramolecular architectures [12-16]. For example, molecular rectangle is in a *meso* conformation [17]. The 4,4–dipyridyl spacers are buckled in order to link the Pt^{2+} atoms, with the planes of the pyridine rings of the spacers are perpendicular to the plane of the Pt(terpy) moieties. Adjacent planes of the Pt(terpy) moieties are nearly parallel to each other at a distance of 6.9 Å (Figure 5.2).

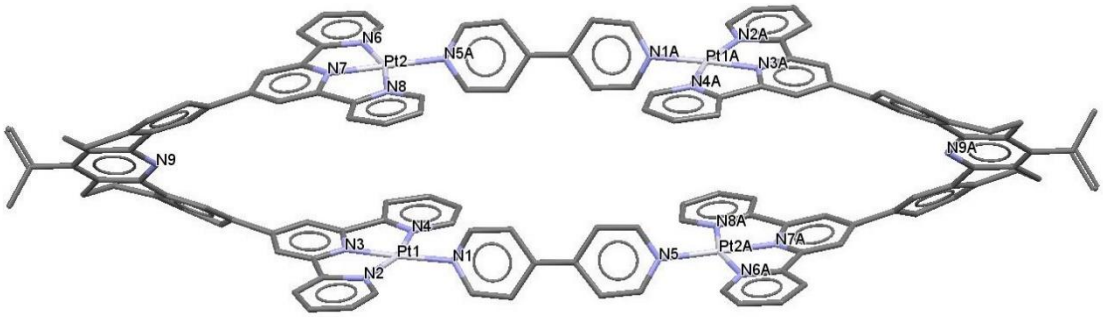


Figure 5.2: Single crystal structure of a tetranuclear Pt(II) molecular rectangle [17].

Supramolecular architectures can have molecular cavities for intercalation of different guests by π-π interactions with aromatic groups. As shown in Figure 5.3, the guest 9-methylanthracene (9-MA) lies almost fully within the molecular cleft designed by the two cofacially disposed chloro-palladium-terpyridyl moieties [18]. The other 9-MA lies outside

the cleft and is involved in π-stacking with the outer faces of the chloro-palladium-terpyridyl moieties of the two hosts in the unit cell. The crystal structure shows three different π-stacking interactions: incarceration of 9-MA in the cleft, stacking of the chloro-palladium-terpyridyl moieties of different molecules and stacking of 9-MA molecules with the outer faces of the chloro-palladium-terpyridyl moieties.

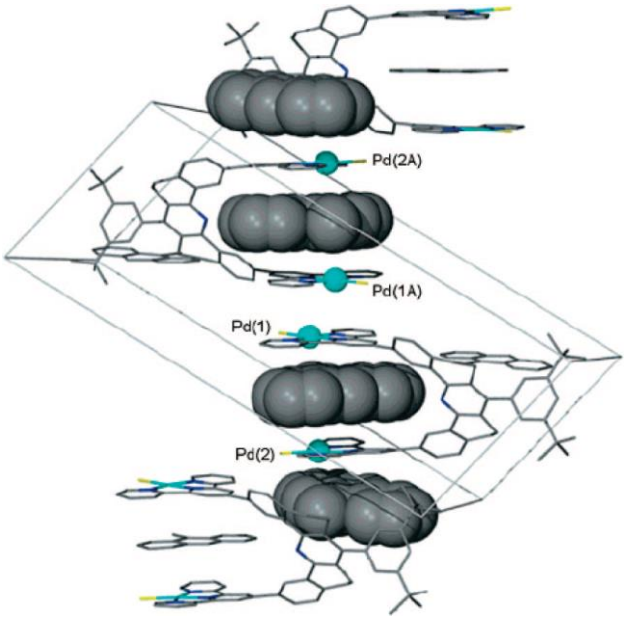
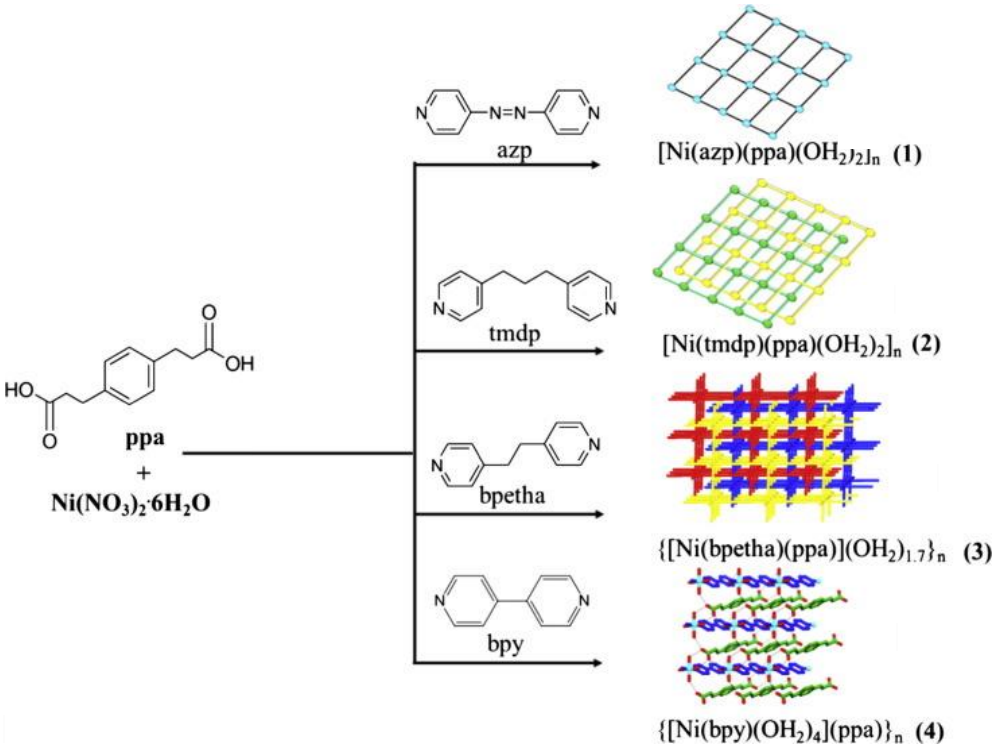


Figure 5.3: An illustration of the extended structure of dipalladium(II) complexes. 9-MA molecules of the stack are shown as space-filling models [18].

Much effort has been made to improve platinum(II)-containing drugs with an effective and non-invasive treatment for different types of cancer. *N,N*–donor ligands are used as a bridge to link two [M(terpy)] (M = Pt or Pd) components [19]. Dinuclear [M(terpy)] complexes have been reported to be more cytotoxic than their mononuclear [M(terpy)] components [20-22]. This can be attributed to their high charge and as a consequence, high affinity for DNA. Moreover, functionalisation of the ligand offers the opportunity to involve different elements that can utilise hydrogen bonding and/or van der Waals forces within the groove of DNA [23].

Many linear organic ligands terminated by pyridyl groups can be employed as effective ligands for transition metal coordination in bulk supramolecular chemistry [24-28]. It is well known that the *N,N*–donor ligands are the most common ligands in the formation of various MOFs. The main features of these ligands are the rigidity, as well as the flexibility which affect both the coordination mode and the topology of MOFs, upon which MOFs' applications depend [25–40]. Recently, four novel Ni(II)-metal–organic frameworks were synthesized and structurally characterized using different *N,N*–donor ligands (Scheme 5.1) [41].



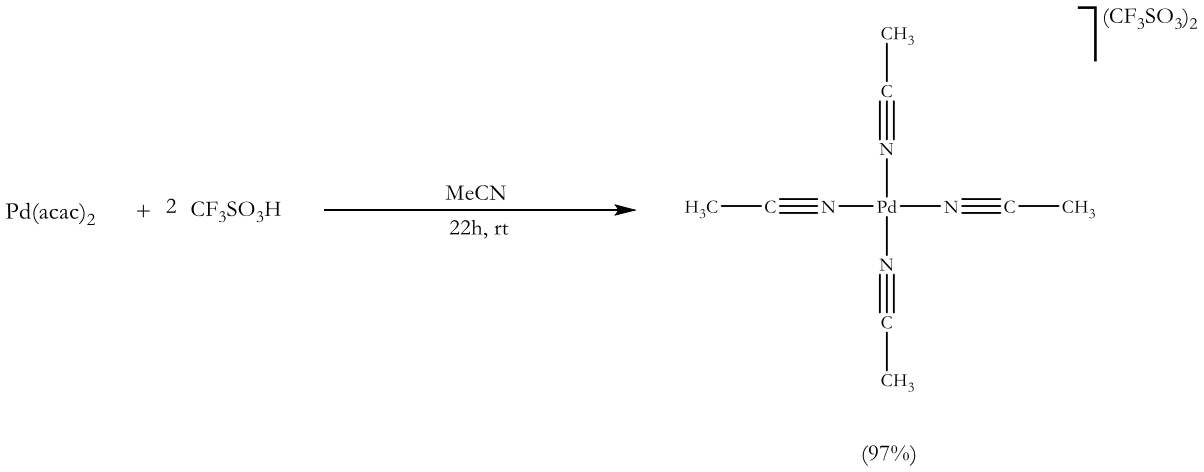
Scheme 5.1: Four Ni(II)-metal–organic frameworks using different *N,N′*–donor ligands [41].

A series of dipyridyl derivatives has been used as ligands in this work. All these ligands were chosen in order to systematically elucidate the role of the length, rigidity, flexibility and the coordination mode of ligands on the crystal structures of Pd(terpy) complexes. For the purpose of comparison related dinuclear palladium(II) *t*Bu$_3$-terpy complexes have

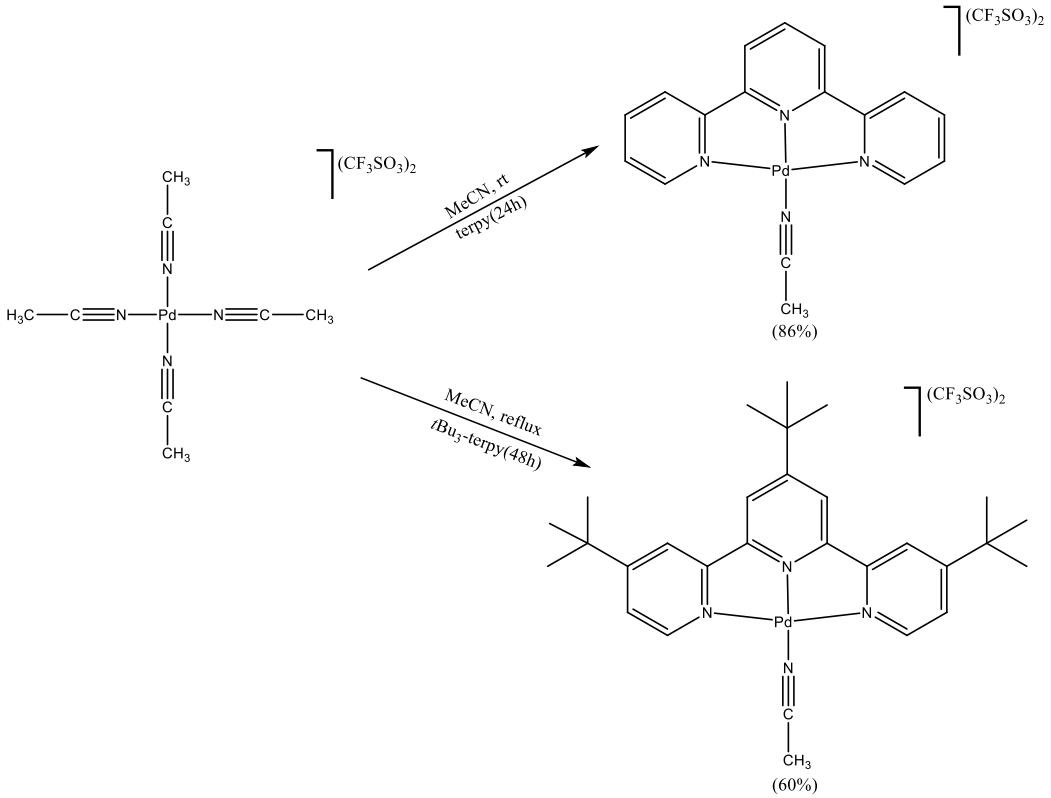
also been prepared. In addition, a porphyrin derivative has been used as a ligand to synthesise a tetranuclear Pd(terpy) complex.

5.2 Results and discussion

5.2.1 Synthesis of the precursor palladium terpyridine acetonitrile $[Pd(terpy)NCCH_3](CF_3SO_3)_2$ and palladium tBu$_3$-terpyridine acetonitrile $[Pd(t\text{Bu}_3\text{-terpy})NCCH_3](CF_3SO_3)_2$ complexes.



Scheme 5.2: Synthesis of $[Pd(NCCH_3)_4](CF_3SO_3)_2$.



Scheme 5.3: Synthesis of $[Pd(terpy)(NCCH_3)](CF_3SO_3)_2$ and $[Pd(t\text{Bu}_3\text{-terpy})(NCCH_3)](CF_3SO_3)_2$.

$[Pd(terpy)(NCCH_3)]^{2+}$ is a common precursor for novel dinuclear $[Pd(terpy)_2L]^{4+}$ complexes [42]. This precursor was obtained from a two-step process using established methods [43]. Initially, $[Pd(NCCH_3)_4](CF_3SO_3)_2$ was synthesised as an intermediate towards the desired compound $[Pd(terpy)(NCCH_3)](CF_3SO_3)_2$. $[Pd(NCCH_3)_4](CF_3SO_3)_2$ is very sensitive to moisture and must be handled under dry dinitrogen. $[Pd(NCCH_3)_4](CF_3SO_3)_2$ was synthesised in reasonable yield by the reaction of a suspension of palladium acetylacetonate in acetonitrile and triflic acid. After 24 hours, diethyl ether was added and the reaction mixture was kept in a freezer overnight. The light yellow solid formed was collected by Schlenk filtration and washed three times with diethyl ether. The terpyridine was added to an acetonitrile solution of $[Pd(NCCH_3)_4](CF_3SO_3)_2$ to afford $[Pd(terpy)(NCCH_3)]$ $(CF_3SO_3)_2$ in good yield (Scheme

5.3). The analogous *t*Bu$_3$-terpy compound was synthesised in a similar way, with the exception that reflux conditions were required for the preparation of the *t*Bu$_3$-terpy compound.

5.2.2 Synthesis of the ligands

The ligand abbreviations and associated structures are shown in (Chart 5.1). **4,4'-bipy** = 4,4'-bipyridyl, **tbpe** = trans-1,2-bis(4-pyridyl)-ethylene, **azpy** = (4,4'-azopyridine), **tmdp** = 4,4'-trimethylene dipyridine, **anbp** = 4,4'-(9,10-Anthracenediyl)bipyridine, **bpb** = 1,4-bis(4-pyridyl)benzene, **bpbp** = 4,4´-bis(4-pyridyl)biphenyl and **H$_2$T(4-Py)P** = *meso*-tetra(4-pyridyl)porphyrin. **4,4'-Bipy**, **tmdp** and **tbpe** are commercially available. All other ligands were synthesised according to literature procedures. **4,4'-Bipy** is a small and rigid ligand. **Tbpe** and **azpy** ligands differ in the replacement of –CH– with –N– and so similar was expected. **Anbp** and **bpb** have the same length, but they differ in their electronic natures. **Bpbp** is related to **anbp** and **bpb**, but with a longer Pd…Pd distance. **Tmdp** is unique amongst this series and is used as a flexible ligand. Finally, **H$_2$T(4-Py)P** can be used as a tetradentate ligand.

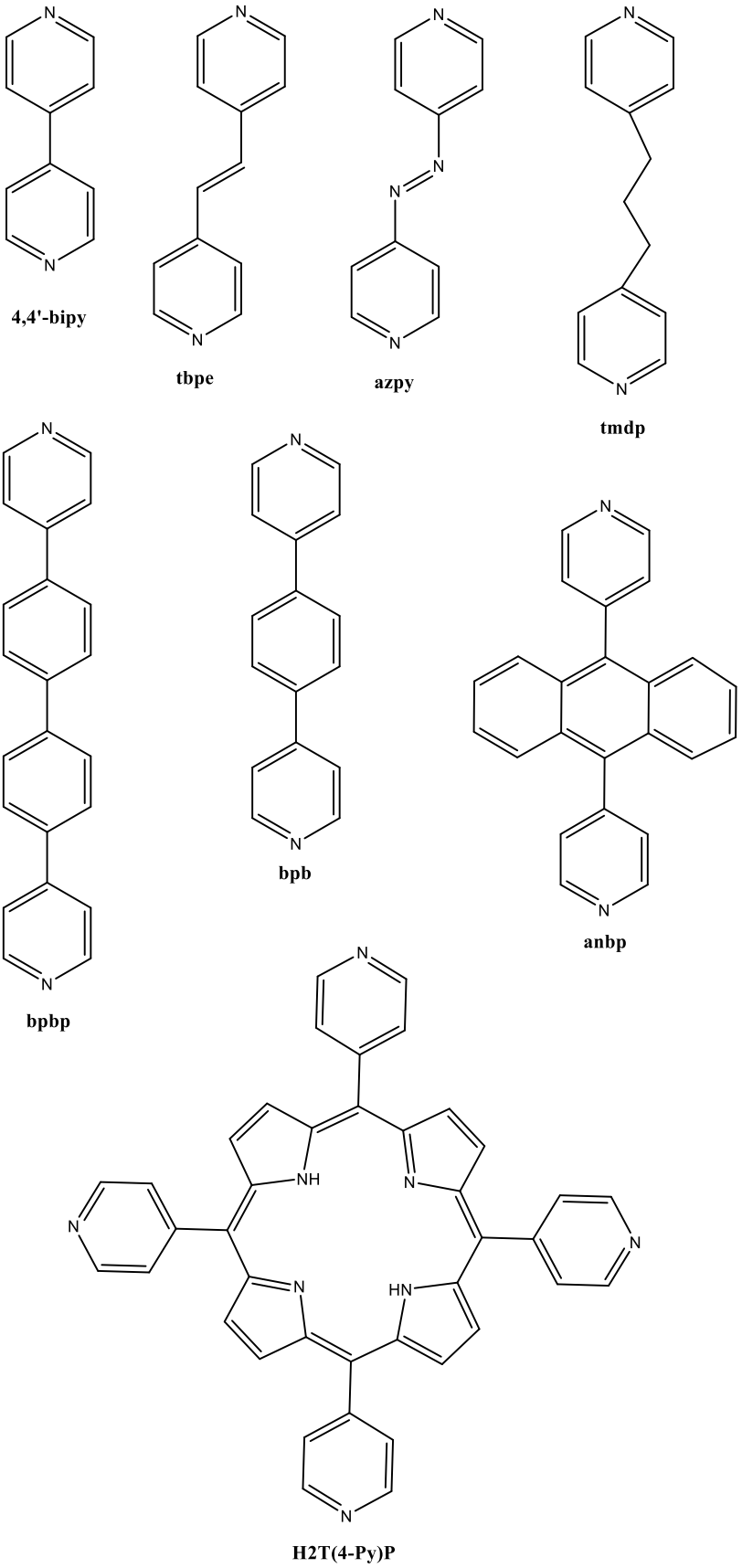
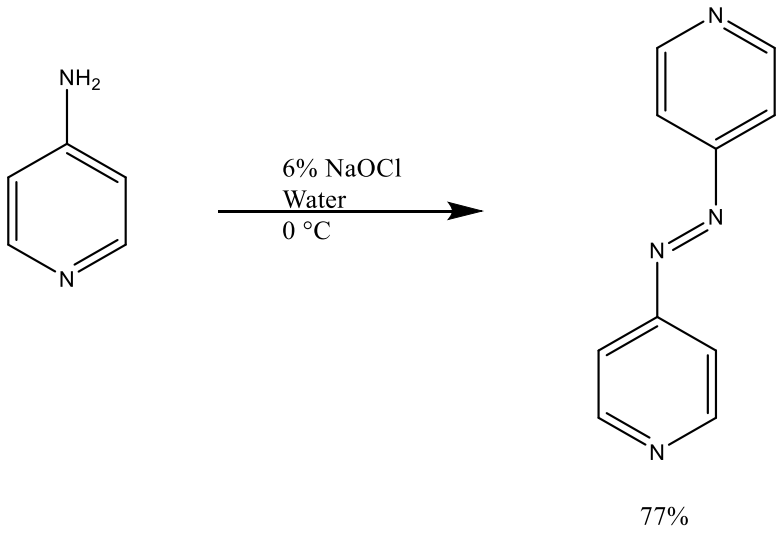


Chart 5.1: The ligand abbreviations and associated structures.

5.2.2.1 Synthesis of 4,4'-azopyridine ***(azpy)***

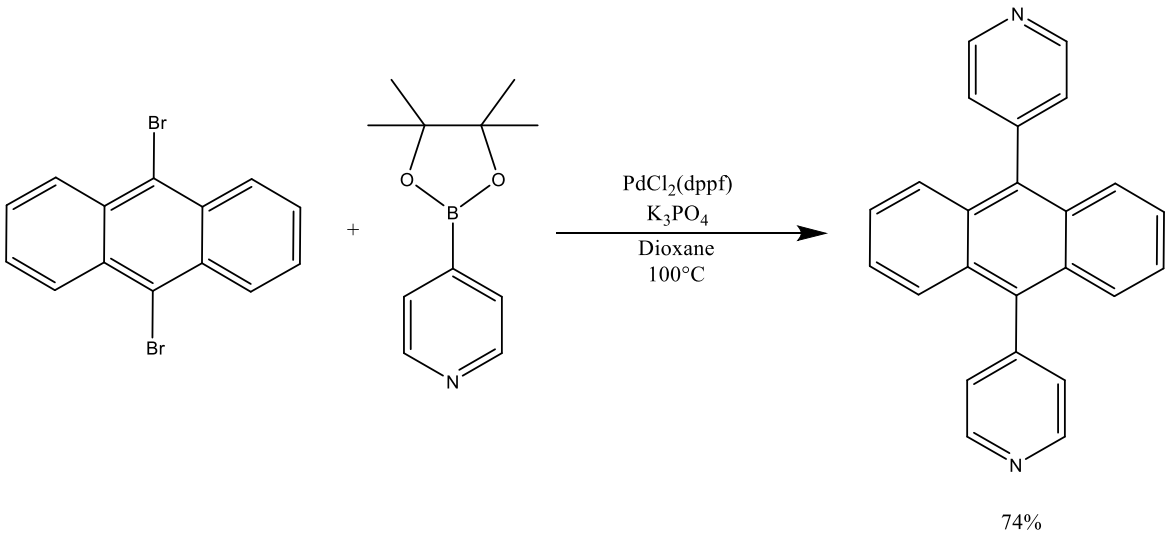


77%

Scheme 5.4: Sythesis of 4,4'-azopyridine.

4,4'-Azopyridines was simply prepared according to a literature procedure by oxidation of 4-aminopyridines with sodium hypochlorite at 0 °C. The solution was extracted with diethyl ether and the crude product was recrystallized from methanol to afford the desired compound in a good yield as long orange needles (77%) [44, 45].

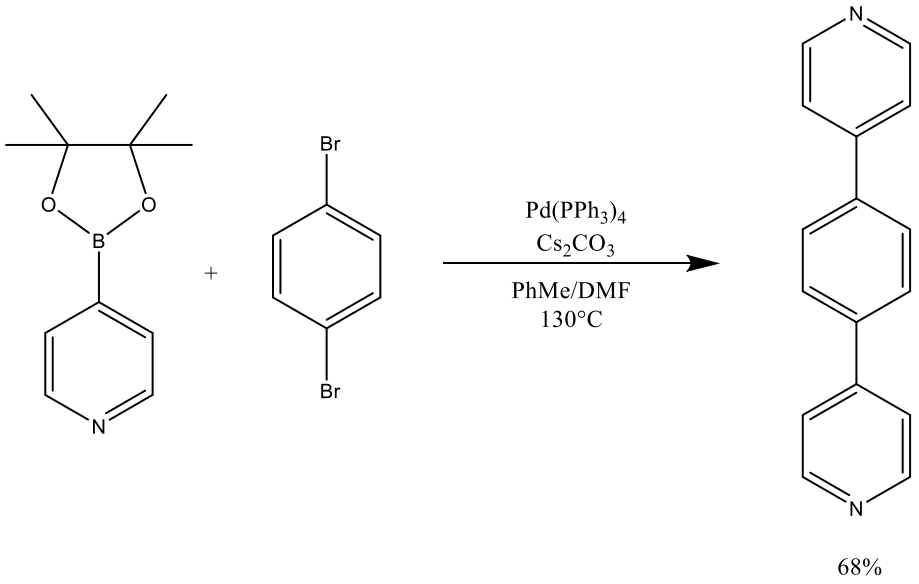
5.2.2.2 Synthesis of 4,4'-(9,10-anthracenediyl)bipyridine ***(anbp)***



Scheme 5.5: Synthesis of 4,4'-(9,10-anthracenediyl)bipyridine.

The bidentate ligand **anbp** was synthesised according to literature procedures [46, 47]. It was synthesised by Suzuki coupling of 9,10-dibromoanthracene with 4-pyridineboronic acid pinacol ester to afford the **anbp** ligand as yellow solid (46%). The **anbp** ligand is reasonably soluble in common organic solvents.

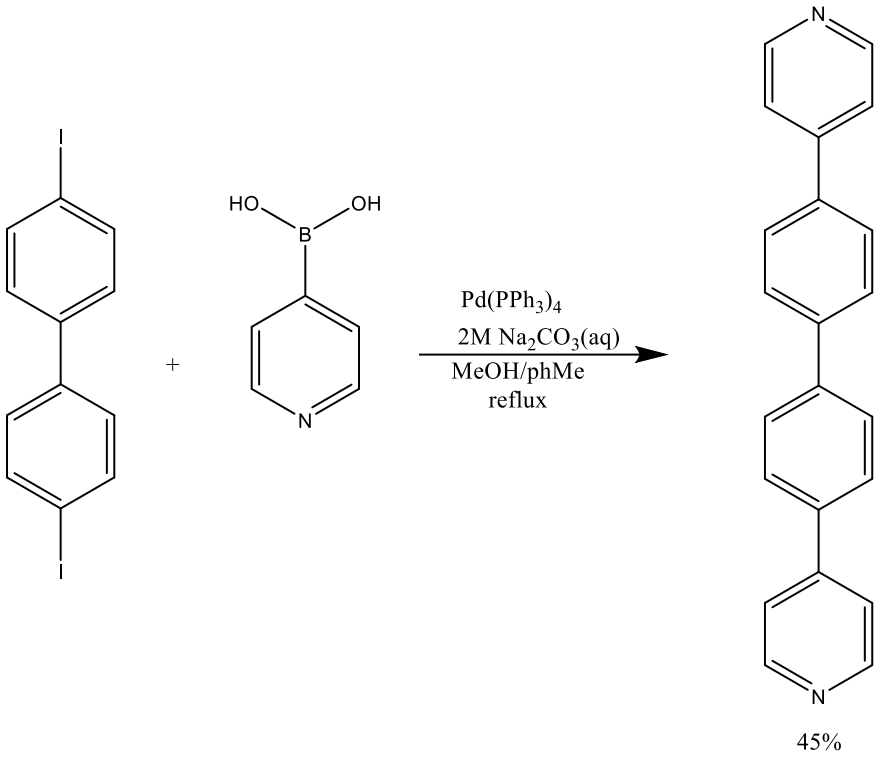
5.2.2.3 Synthesis of 1,4-bis(4-pyridyl)benzene ***(bpb)***



Scheme 5.6: Synthesis of 1,4-bis(4-pyridyl)benzene.

Synthesis of **bpb** was achieved in a single step procedure following a literature approach [48]. The reaction of pyridylboronic pinacol ester with 1,4-dibromobenzene in the presence of Cs_2CO_3 and $Pd(PPh_3)_4$ in dry PhMe/DMF (1:1) at 130 °C over 48 h afforded **bpb** as a white precipitate. As previously reported, the purification using acid-base extraction techniques is more efficient than column chromatography [49].

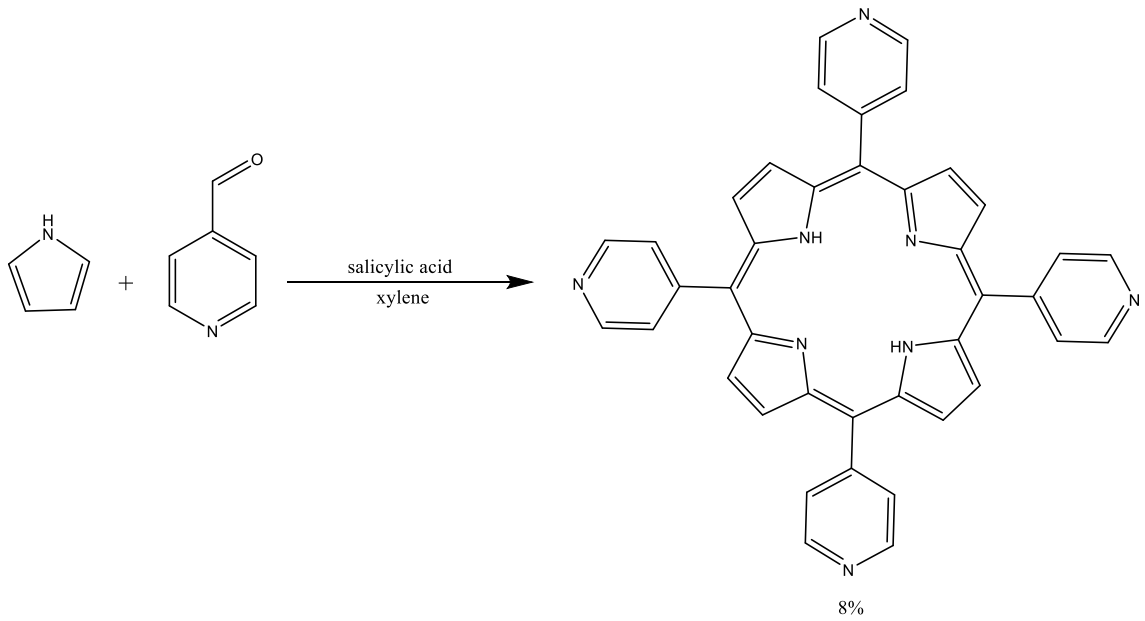
5.2.2.4 Synthesis of 4,4'-bis(4-pyridyl)biphenyl ***(bpbp)***



Scheme 5.7: Synthesis of 4,4'-bis(4-pyridyl)biphenyl.

In order to further increase the length of the bidentate ligand using **bpbp** ligand. The extended bipyridine **bpbp** was synthesized via literature procedures [50, 51]. The reaction of diiodobiphenyl with 4-pyridineboronic acid in the presence of Na_2CO_3 and $Pd(PPh_3)_4$ in dry MeOH/PhMe at reflux afforded **bpbp** as a white precipitate. The product was obtained in fair yield of sufficient purity.

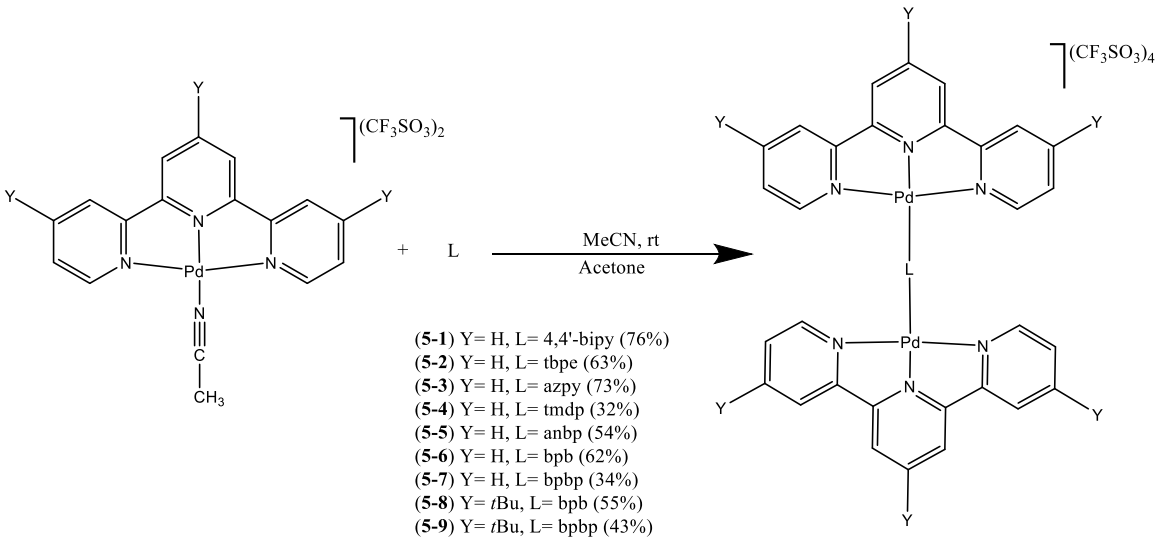
5.2.2.5 Synthesis of meso-tetra(4-pyridyl)porphyrin



Scheme 5.8: Synthesis of *meso*-tetra(4-pyridyl)porphyrin.

Porphyrins are aromatic macrocyclic molecules which consist of four pyrrole rings linked by unsaturated methylene bridges. Porphyrins are readily synthesised with multiple functionalities. The reaction of pyridine-4-carboxaldehyde with pyrrole in the presence of salicylic acid and xylene as a solvent at reflux afforded black precipitates. The resultant precipitates were washed with methanol until shining purple solids were obtained in low yield of sufficient purity [52].

5.2.3 Synthesis of dinuclear palladium terpyridine complexes

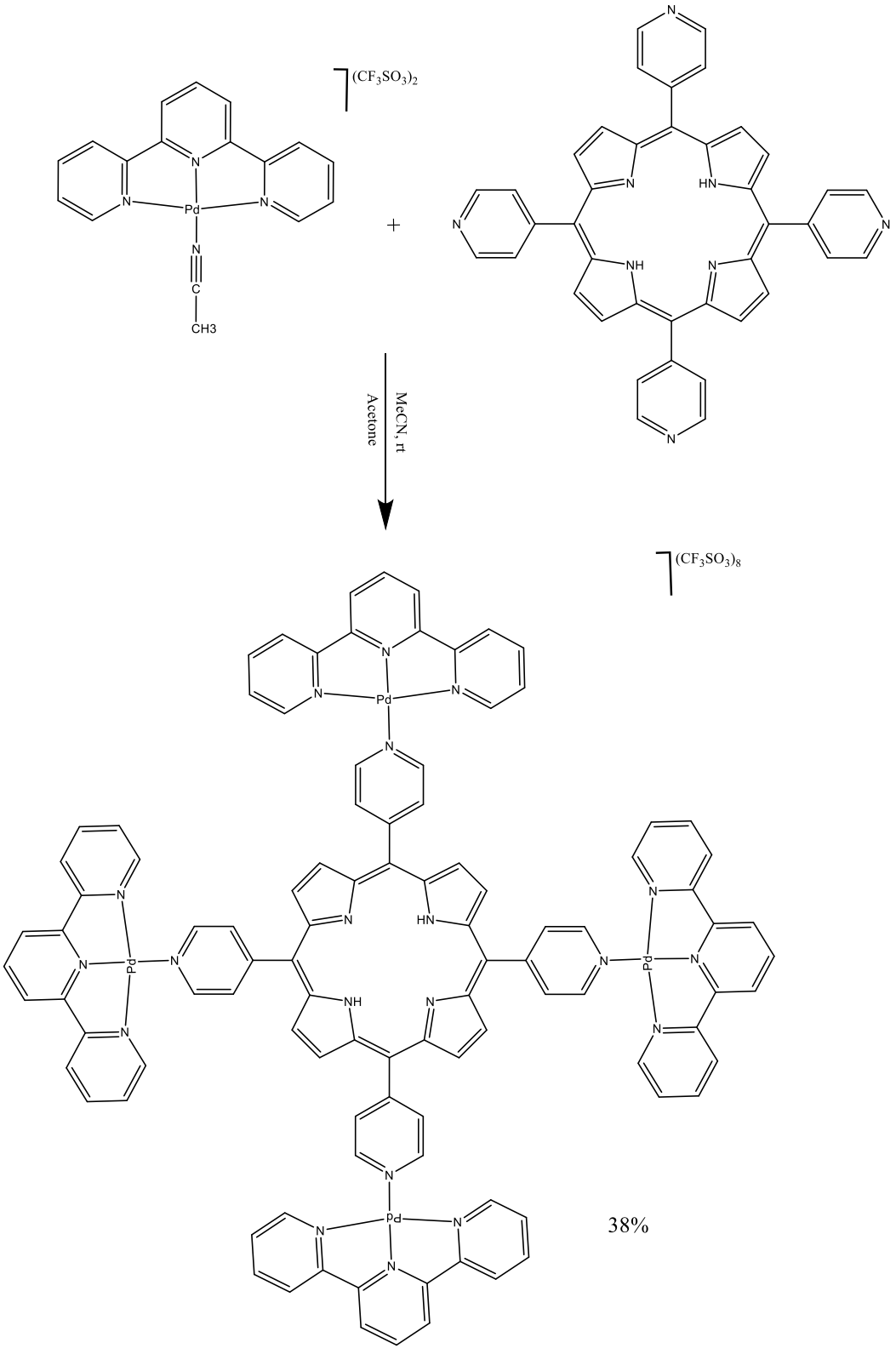


Scheme 5.9: Synthesis of dinuclear palladium terpyridine complexes.

The general formula for these complexes is $[\{Pd(Yterpy)\}_2(L)](CF_3SO_3)_4$ (Y = H or *t*Bu, L = *N,N*-bidentate ligand). The dinuclear Pd(terpy) complexes containing two Pd(terpy) moieties and bidentate ligand were obtained in fair yield by the direct reaction of the desired bispyridine ligand in acetone with $[Pd(Yterpy)NCCH_3](CF_3SO_3)_2$ in acetonitrile. The solution was stirred for 1 hour under a nitrogen atmosphere. The product was precipitated from the solution by the addition of diethyl ether–acetone 3:1 (Scheme 5.9).

5.2.4 Synthesis of tetranuclear palladium terpyridine complex

The tetranuclear Pd(terpy) complex containing four Pd(terpy) moieties and the ligand *meso*-tetra(4-pyridyl)porphyrin was prepared following the synthetic procedure mentioned above (Scheme 5.10).



Scheme 5.10: Synthesis of tetranuclear palladium terpyridine complex.

5.2.5 X-ray crystallography

Single crystals suitable for X-ray diffraction were obtained for all of the complexes reported herein. Single crystals were grown by dissolution of the product in the minimum amount of acetonitrile and diffusion of diethyl ether vapour into this solution.

*5.2.5.1 Single crystal X-ray structure of 2,2':6',2''-terpyridine (4,4'-bipyridyl) palladium triflate [{Pd(terpy)}$_2$(4,4'-bipy)](CF$_3$SO$_3$)$_4$ (**5-1**).*

Crystals of (**5-1**) were found to be colourless blocks, with the complex crystallising in the triclinic space group *P-1*. Single crystal structure of (**5-1**) indicates the formation a three component discrete assembly consisting of three $[\{Pd(terpy)\}_2(4,4'\text{-bipy})]^{4+}$ with eight triflate anions. Two of the Pd(terpy) complexes contain inversion centres of symmetry at the centres of 4,4'-bipy ligands. Table 5.1 lists important bond lengths and angles for this complex. The two Pd atoms are bridged by a single 4,4'-bipy ligand with the remaining coordination geometry completed by two terpyridine moieties. The Pd–N (central pyridyl ring) distances are similar (average 1.939(9) Å) and Pd–N (terminal pyridyl ring) distances are significantly longer (average 2.028(9) Å). The *cis* N–Pd–N angles around Pd ions are very similar and fall in the range of 81.70(4) – 80.50(6)°. The tilt angle for Pd**1A** (N2A-Pd1A-N4A = 174.0(4)°) shows the greatest deviation from the idea value 180°, while tilt angle for Pd**2A** (N5A-Pd2A-N7A = 177.40(5)°) indicates the closest value to 180°. Terpyridine of Pd**2A** shows the largest deviation from planarity with a maximum displacement of +0.170 and -0.237 Å exhibited by N5A and C39A, respectively, from the mean plane.

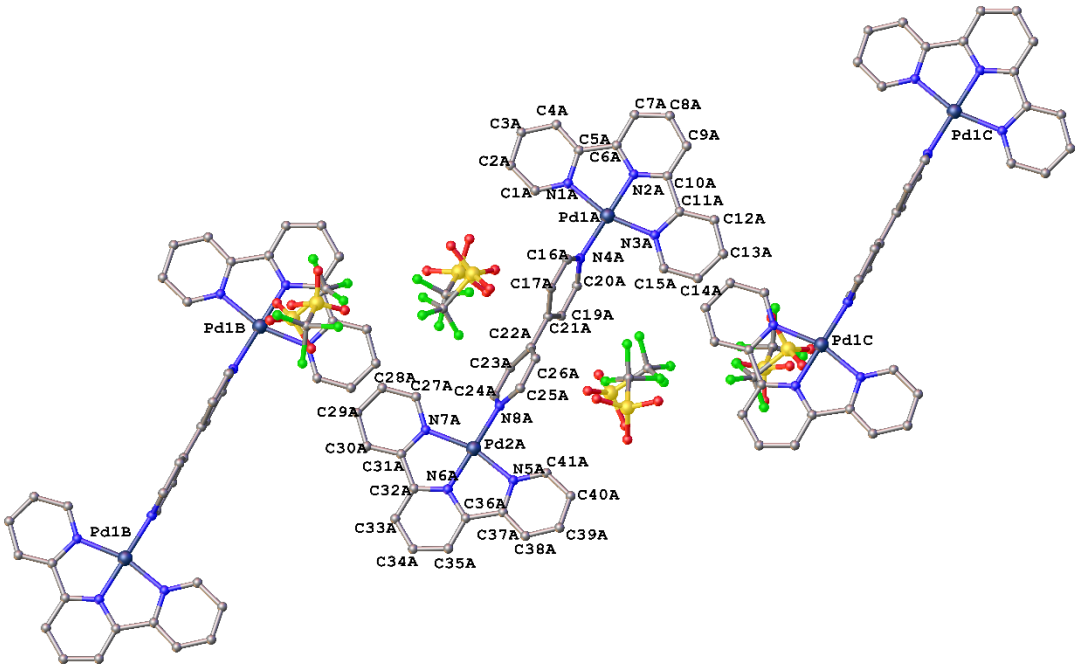


Figure 5.4: X-ray crystal structure of [{Pd(terpy)}$_2$(4,4'-bipy)](CF$_3$SO$_3$)$_4$ with crystallographically independent atom numbering scheme. Hydrogen atoms have been omitted for clarity. Atom colours - C: grey, O: red, N: blue, Pd: navy F: green and S: yellow.

Table 5.1: Selected bond lengths (Å) and angles (°) for [{Pd(terpy)}$_2$(4,4'-bipy)](CF$_3$SO$_3$)$_4$.

Pd1A-N1A	2.033(9)	N2-Pd1-N1	81.60(4)
Pd1A-N2A	1.941(9)	N2A-Pd1A-N4A	174.0(4)
Pd1A-N3A	2.017(9)	N3A-Pd1A-N1A	162.70(4)
Pd1A-N4A	2.036(9)	N3A-Pd1A-N2A	81.10(4)
Pd2A-N5A	2.050(8)	N6A-Pd2A-N7A	80.70(4)
Pd2A-N6A	1.938(9)	N5A-Pd2A-N7A	177.40(5)
Pd2A-N7A	2.025(9)	N6A-Pd2A-N8A	161.90(4)

Pd2A-N8A	2.043(9)	N7A-Pd2A-N8A	80.50(6)
Pd1B-N1B	2.015(10)	N2B-Pd1B-N1B	81.70(4)
Pd1B-N2B	1.942(10)	N2B-Pd1B-N4B	174.10(4)
Pd1B-N3B	2.030(9)	N3B-Pd1B-N1B	163.30(4)
Pd1B-N4B	2.037(11)	N3B-Pd1B-N2B	80.70(4)
Pd1C-N1C	2.031(8)	N2C-Pd1C-N1C	81.00(4)
Pd1C-N2C	1.935(9)	N2C-Pd1C-N4C	174.60(4)
Pd1C-N3C	2.026(9)	N3C-Pd1C-N1C	162.30(4)
Pd1C-N4C	2.040(9)	N3C-Pd1C-N2C	81.30(4)

The pyridyl ring of 4,4'-bipy ligand in (Pd**2A**) is significantly twisted with respect to the terpyridine plane forming a dihedral angle of 61.93(7)°. However, the corresponding angle in (Pd**1B**) (83.27(9)°) indicates that the terpyridine ring and pyridyl ring are almost perpendicular to each other.

Complex (**5-1**) packs in channels running parallel to the *a*-axis. The channels of cations are separated from each other by channels containing triflate anions (Figure 5.5). The molecules of (**5-1**) undergo a series of face-to-face π· · ·π interactions indicated by ring centroid–ring centroid separations of 3.589, 3.603, 3.653, 3.657, 3.912, 3.931, 3.954 Å (corresponding slip angles are 4.155, 4.017, 4.698, 4.230, 0.00, 8.859 and 0.00°) (Figure 5.6).

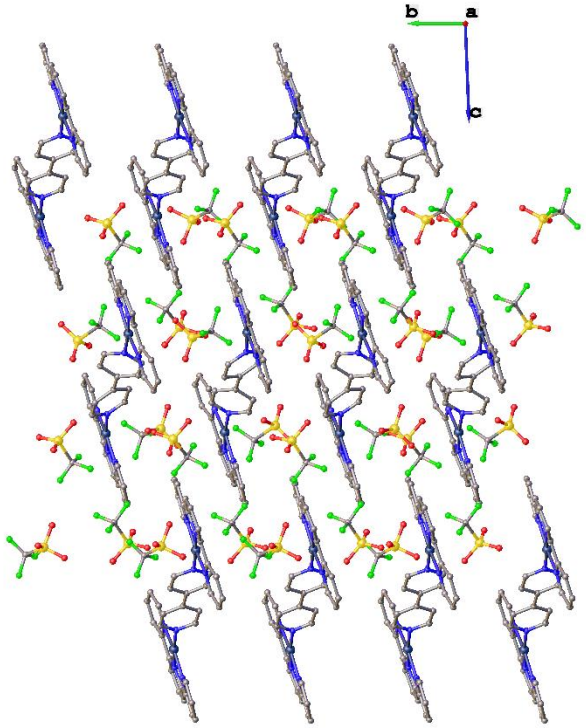


Figure 5.5: The packing diagram of [{Pd(terpy)}$_2$(4,4'-bipy)](CF$_3$SO$_3$)$_4$ along the *a*-crystal axis. Hydrogen atoms are omitted for clarity.

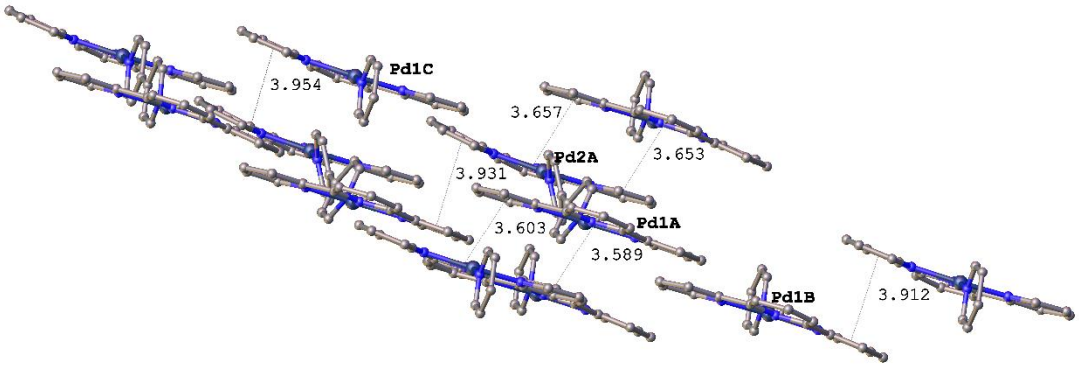


Figure 5.6: Representation of the π· · ·π interactions in [{Pd(terpy)}$_2$(4,4'-bipy)](CF$_3$SO$_3$)$_4$. Dashed lines indicate the presence of π· · ·π interactions.

A series of hydrogen bonds is observed between aromatic protons and triflate anions (Figure 5.7). The C–H…O distances lie in the range 2.221 – 2.996 Å and the C–H…F distances lie in the range 2.220 – 2.998 Å.

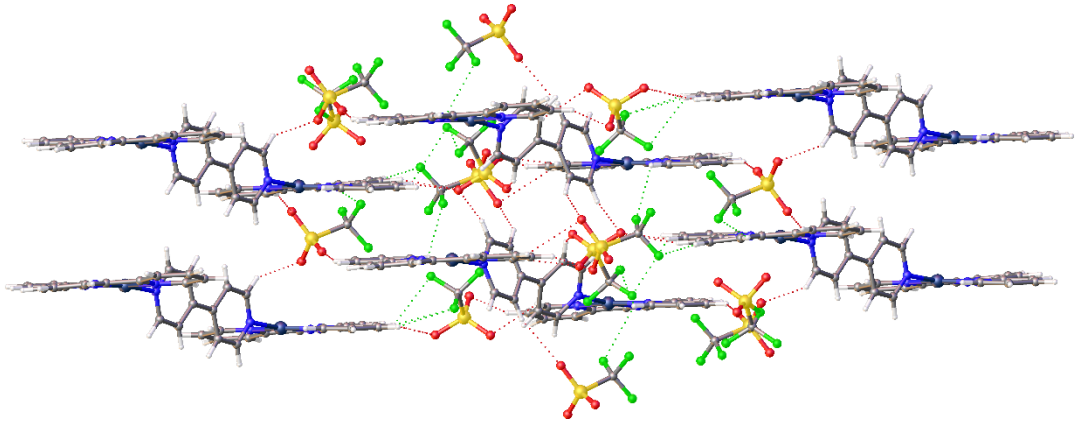


Figure 5.7: A net of hydrogen bonds links Pd cations, triflate anions and acetonitrile molecules for [{Pd(terpy)}$_2$(4,4'-bipy)](CF$_3$SO$_3$)$_4$.

*5.2.5.2 Single crystal X-ray structure of 2,2':6',2''-terpyridine (trans-1,2-bis(4-pyridyl)-ethylene) palladium triflate [{Pd(terpy)}$_2$(tbpe)](CF$_3$SO$_3$)$_4$ (**5-2**).*

Crystals of (**5-2**) were found to be colourless plates, crystallising in the monoclinic space group $P2_1/n$. The structure has high symmetry with ordered acetonitrile molecules and triflate anions, resulting in only four crystallographically distinct Pd–N bond lengths. The asymmetric unit consists of one Pd(terpy) cation, one-half tbpe ligand, two triflate anions and one acetonitrile molecule. As shown in Figure 5.8, space above and below the dinuclear Pd(terpy) cation is occupied by four triflate anions and two molecules of acetonitrile. The two Pd atoms are bridged by a single tbpe ligand with the remaining coordination geometry completed by two terpyridine moieties. The Pd…Pd separation is 13.393 Å. The coordination geometry of the palladium ion is distorted slightly from that found in the perfect square-planar Pd(II) complexes. Table 5.2 lists important bond

lengths and angles for this complex. The angles between the adjacent N atoms in the plane deviate slightly from the theoretical value of 90° (N2–Pd1–N1= 80.30(5)°, and N3–Pd1–N2 = 82.60(5)°) and N3A-Pd1A-N1A angle (162.90(5)°) is smaller than the theoretical value of 180°. The Pd–N2 (1.955(11) Å) distance to the central nitrogen atom of the terpyridine is shorter than those to the other two nitrogen atoms, Pd–N1 2.037(12) Å and Pd–N3 2.028(12) Å. A similar distorted square-planar geometry, which is a result of the geometric constraints imposed by coordination of the tridentate terpyridine molecule, also occurs in the related terpyridine complexes of palladium(II) reported previously. The terpyridine moiety is almost coplanar with a maximum displacement of +0.051 and -0.037 Å exhibited by N2 and C13, respectively, from the mean plane.

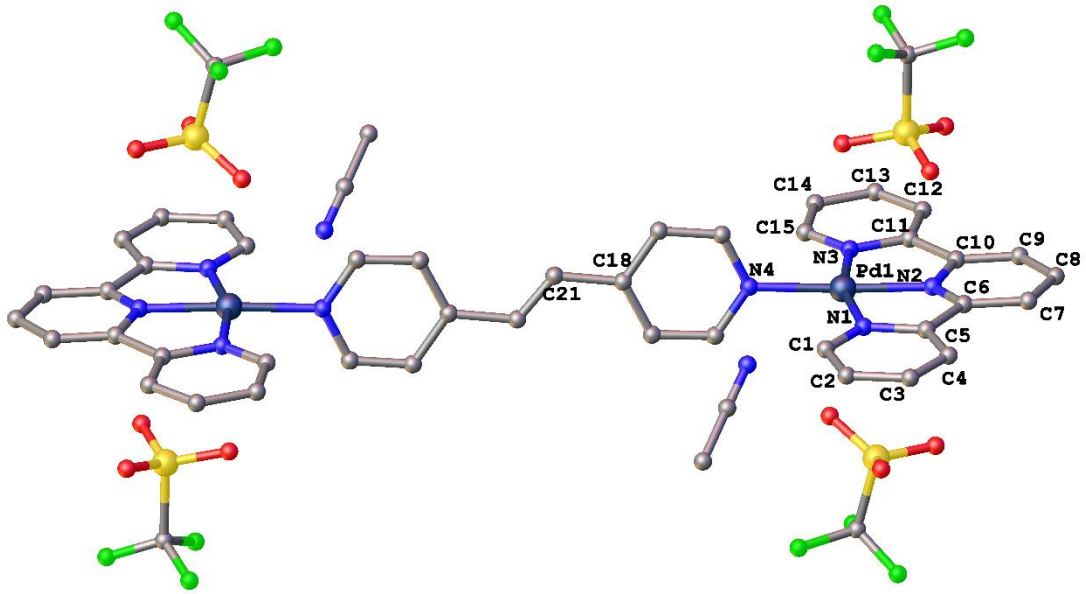


Figure 5.8: X-ray crystal structure of [{Pd(terpy)}$_2$(tbpe)](CF$_3$SO$_3$)$_4$ with crystallographically independent atom numbering scheme. Hydrogen atoms have been omitted for clarity. Atom colours - C: grey, O: red, N: blue, Pd: navy F: green and S: yellow.

Table 5.2: Selected bond lengths (Å) and angles (°) for [{Pd(terpy)}$_2$ (tbpe)](CF$_3$SO$_3$)$_4$.

Pd1-N1	2.037(12)	N2-Pd1-N1	80.30(5)
Pd1-N2	1.955(11)	N2-Pd1-N4	177.50(5)
Pd1-N3	2.028(12)	N3-Pd1-N1	162.90(5)
Pd1-N4	2.043(10)	N3-Pd1-N2	82.60(5)

The dihedral angle between the square planar coordination geometry of the Pd(terpy) moieties and the plane of tbpe is 81.79(6)°. The dihedral angle indicates that the terpyidine moieties and tbpe are almost perpendicular to each other. This geometrical feature is comparable to that observed in (Pt(terpy)(*N*-Methyl-4,4'-bipyridinium) triperchlorate monohydrate (81.7°) [50].

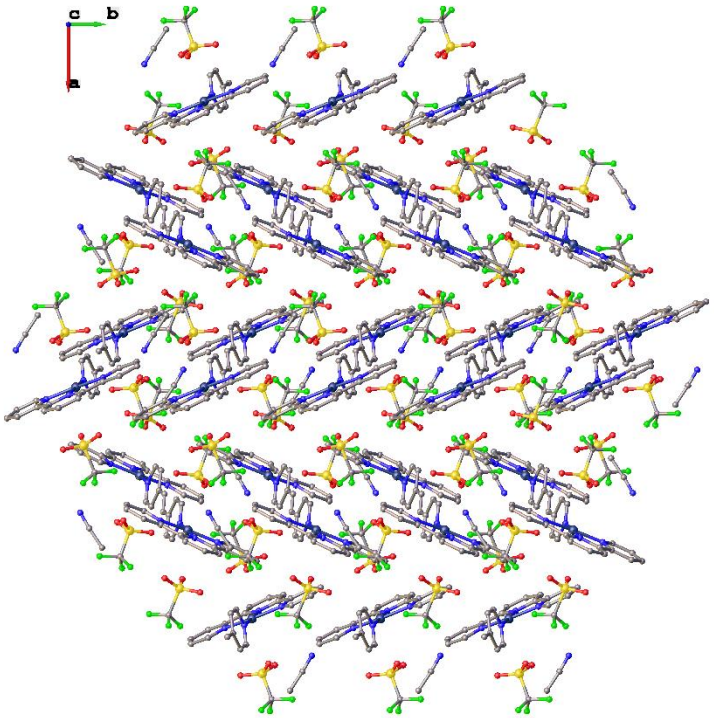


Figure 5.9: The packing diagram of [{Pd(terpy)}$_2$(tbpe)](CF$_3$SO$_3$)$_4$ along the *c*-crystal axis. Hydrogen atoms are omitted for clarity.

Analysis of packing in the crystal structure showed that the cations have herringbone stacking pattern along the *c*-axis direction, as shown in Figure 5.9. The triflate anions and acetonitrile molecules fill the space between cations.

Each molecule packs with its neighbour *via* intermolecular face-to-face π· · ·π stacking interactions with centroid-centroid separations of 3.859 Å and slip angle of 0.526° (Figure 5.10).

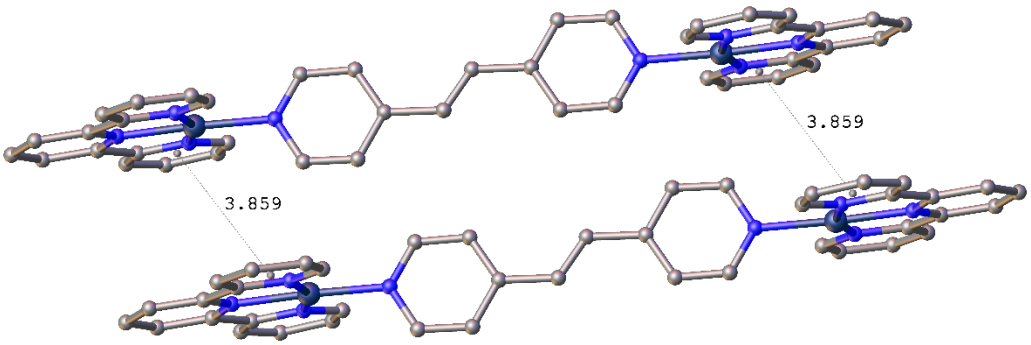


Figure 5.10: Representation of the π· · ·π interactions in [{Pd(terpy)}$_2$ (tbpe)](CF$_3$SO$_3$)$_4$. Dashed lines indicate the presence of π· · ·π interactions.

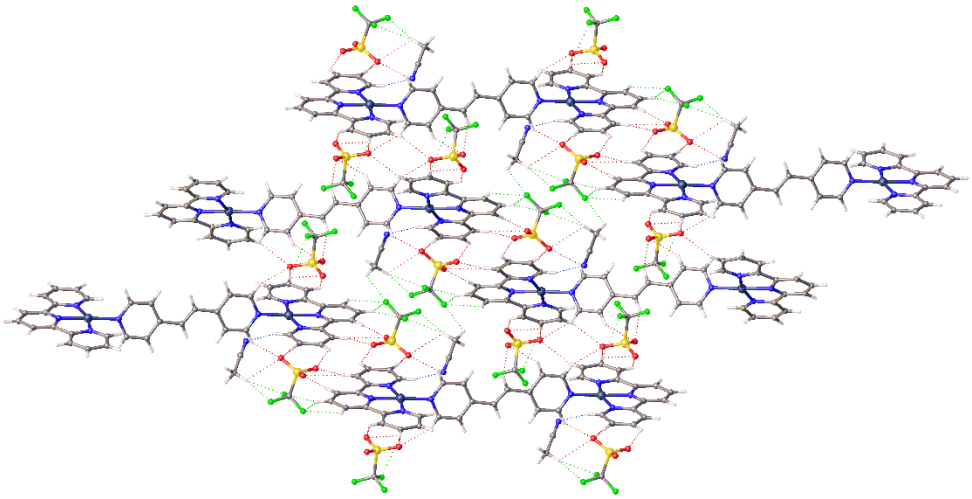


Figure 5.11: A net of hydrogen bonds links Pd cations, triflate anions and acetonitrile molecules for [{Pd(terpy)}$_2$(tbpe)](CF$_3$SO$_3$)$_4$.

There is a net of hydrogen bonds, as shown in Figure 5.11. The triflate anion acts as a hydrogen bond acceptor and forms hydrogen bonds with acetonitrile molecule, tbpe, and terpyridine. The C–H…O distances lie in the range 2.193 – 2.995 Å and the C–H…F distances lie in the range 2.500 – 2.995 Å. The C–H…N distances lie in the range 2.393 – 2.847 Å. The tbpe ligand acts as a hydrogen bond donor via four sets of C–H…O hydrogen bonds. The C16–H16…O1T, C19–H19…O5T, C20–H20…O4T and C21–H21…O5T distances are 2.193, 2.725, 2.461 and 2.485 Å, respectively.

*5.2.5.3 Single crystal X-ray structure of 2,2':6',2''-terpyridine (4,4'-azopyridine) palladium triflate [{Pd(terpy)}$_2$(azpy)](CF$_3$SO$_3$)$_4$ (**5-3**).*

The ligands 4,4'-azopyridine and trans-1,2-bis(4-pyridyl)-ethylene differ in the replacement of CH=CH with N=N and so a similarity is expected. Crystals of (**5-3**) were found to be colourless prism. The complex crystallises in the monoclinic space group $P2_1/n$. The structure has high symmetry with ordered acetonitrile molecules and triflate anions, resulting in only four crystallographically distinct Pd–N bond lengths. The asymmetric unit consists of one Pd(terpy) cation, one-half azpy ligand, two triflate anions and one acetonitrile molecule. As shown in Figure 5.12, space above and below the dinuclear Pd(terpy) cation is occupied by four triflate anions and two molecules of acetonitrile, similar to crystal structure of complex (**5-2**). The two Pd atoms are bridged by a single 4,4'-azopyridine ligand with the remaining coordination geometry completed by two terpyridine moieties. The Pd…Pd separation is 13.031 Å. The angles N2-Pd1-N1, N3-Pd1-N1 and N2-Pd1-N3 deviate from the theoretical values more than those in (**5-2**). In terms of bond lengths, they are in excellent agreement with those found in (**5-2**).

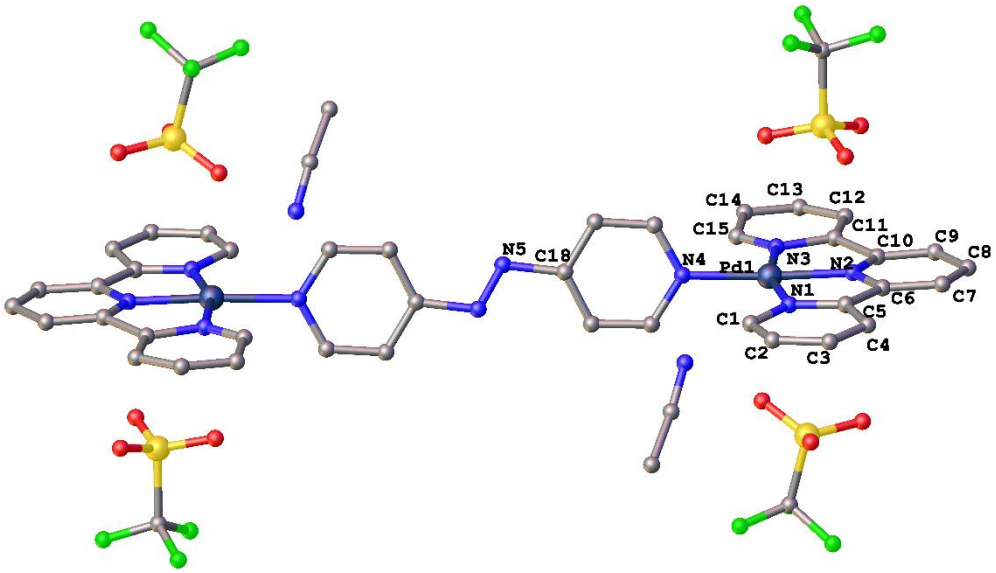


Figure 5.12: X-ray crystal structure of [{Pd(terpy)}$_2$(azpy)](CF$_3$SO$_3$)$_4$ with crystallographically independent atom numbering scheme. Hydrogen atoms have been omitted for clarity. Atom colours - C: grey, O: red, N: blue, Pd: navy F: green and S: yellow.

Table 5.3: Selected bond lengths (Å) and angles (°) for [{Pd(terpy)}$_2$(azpy)](CF$_3$SO$_3$)$_4$

Pd1-N1	2.055(14)	N2-Pd1-N1	81.50(6)
Pd1-N2	1.940(13)	N2-Pd1-N4	176.80(8)
Pd1-N3	2.097(17)	N3-Pd1-N1	162.80(5)
Pd1-N4	2.033 (12)	N3-Pd1-N2	81.30(6)

The angle between the square planar coordination geometry of the Pd(terpy) moieties and the plane of 4,4'-azopyridine is 78.74(6)°. The dihedral angle indicates that the ligand in complex (**5-3**) is bent more than that in complex (**5-2**). The tilt angle of complex (**5-3**) is 176.80(8)°, slightly smaller than that found in complex (**5-2**) 177.50(5)°. The dihedral

angle and tilt angle indicate that the replacement of CH=CH with N=N in complex (**5-3**) leads to more distortion of the square-planar geometry than complex (**5-2**).

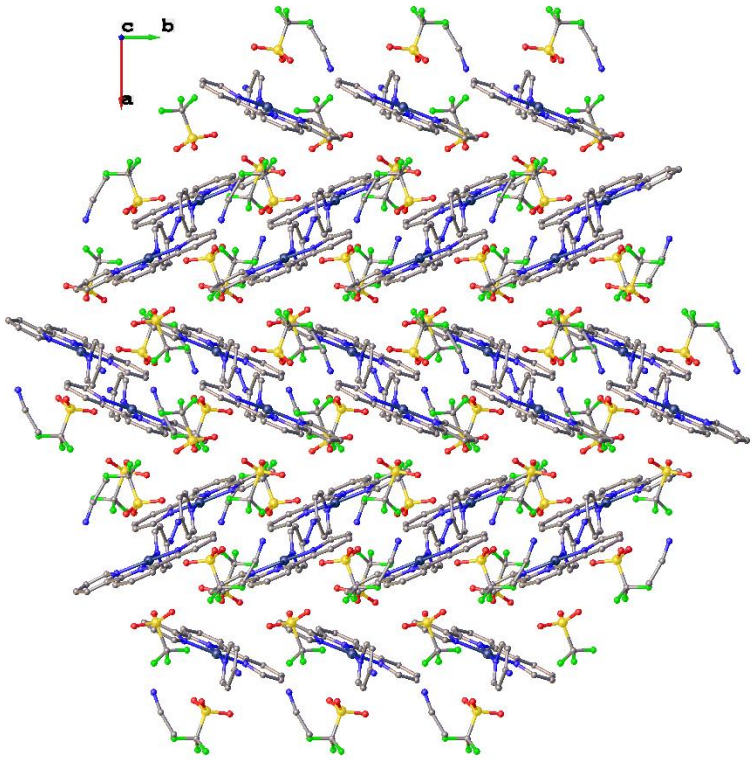


Figure 5.13: The packing diagram of [{Pd(terpy)}$_2$(azpy)](CF$_3$SO$_3$)$_4$ along the *c* crystal axis. Hydrogen atoms are omitted for clarity.

In terms of planarity, the cations of (**5-3**) are less planar than those observed in (**5-2**), with a maximum displacement of +0.072 and -0.078 Å exhibited by C5 and C10, respectively, from the mean plane.

Analysis of packing in the crystal structure showed that the cations have herringbone stacking pattern along the *c*-axis direction, similar to (**5-2**) (Figure 5.13). Each molecule packs with its neighbour *via* intermolecular face-to-face π· · ·π stacking interactions with centroid-centroid separations of 3.806 Å and slip angle of 0.535° (Figure 5.14).

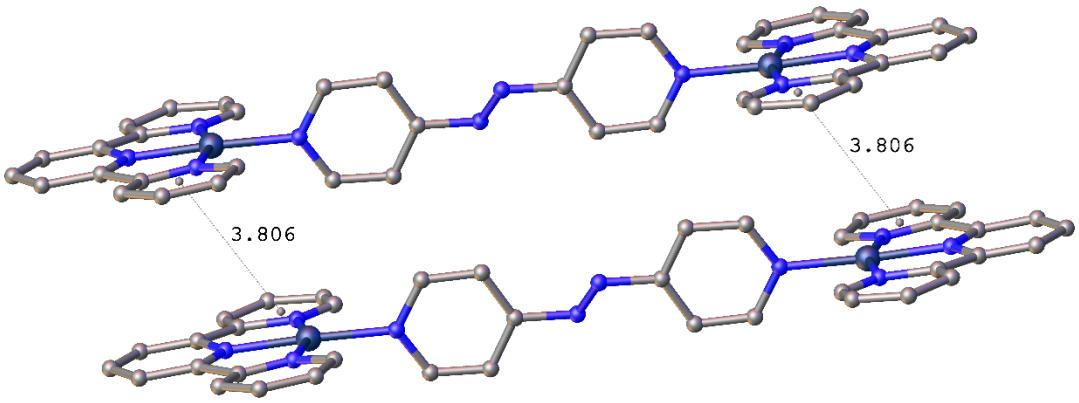


Figure 5.14: Representation of the π· · ·π interactions in [{Pd(terpy)}$_2$(azpy)](CF$_3$SO$_3$)$_4$. Dashed lines indicate the presence of π· · ·π interactions.

This arrangement is further stabilised by a series of hydrogen bonds between terpyridine, azpy ligand, acetonitrile molecule and triflate anion (Figure 5.15). The triflate anions act as hydrogen bond acceptors and form hydrogen bonds with azpy ligand, acetonitrile molecules and terpyridine moieties. The C–H…O distances lie in the range 2.321 – 2.775 Å and the C–H…F distances lie in the range 2.482 – 2.772 Å. In addition, each azpy ligand is involved in intermolecular hydrogen bonds and acts as a hydrogen bond donor through four sets of C–H…O hydrogen bonds. The C16–H16…O4T, C17–H17…O1T, C19–H19…O1T and C20–H20…O2T distances are 2.393, 2.753, 2.665, 2.470 Å, respectively.

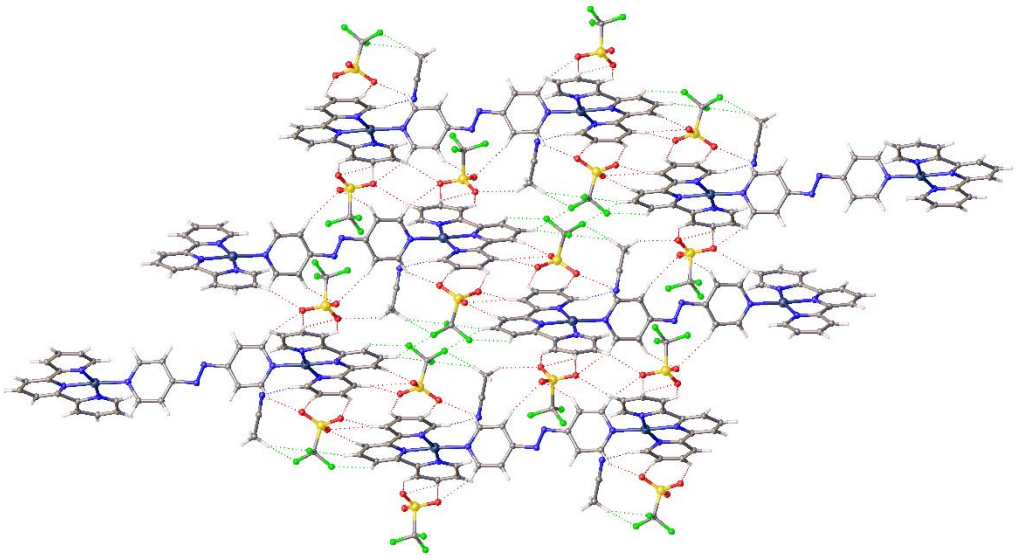


Figure 5.15: A net of hydrogen bonds links Pd cations, triflate anions and acetonitrile molecules for [{Pd(terpy)}$_2$(azpy)](CF$_3$SO$_3$)$_4$.

*5.2.5.4 Single crystal X-ray structure of 2,2':6',2''-terpyridine (4,4'-trimethylenedipyridine) palladium triflate [{Pd(terpy)}$_2$(tmdp)](CF$_3$SO$_3$)$_4$ (**5-4**).*

Crystals of (**5-4**) were found to be colourless plates. The complex crystallises in the monoclinic space group $P2_1/c$. The two Pd atoms are bridged by a single 4,4'-trimethylenedipyridine ligand with the remaining coordination geometry completed by two terpyridine moieties (Figure 5.16). There is disorder exhibited by one of the triflate anions. The Pd…Pd separation is 12.626 Å. The tmdp ligand adopts a TT (T = *trans* and G = *gauche*) conformation with an N…N separation of 9.468 Å. All Pd–N bonds are crystallographically distinct, unlike some of the other complexes in this series. Selected bond lengths and angles are summarized in Table 5.4.

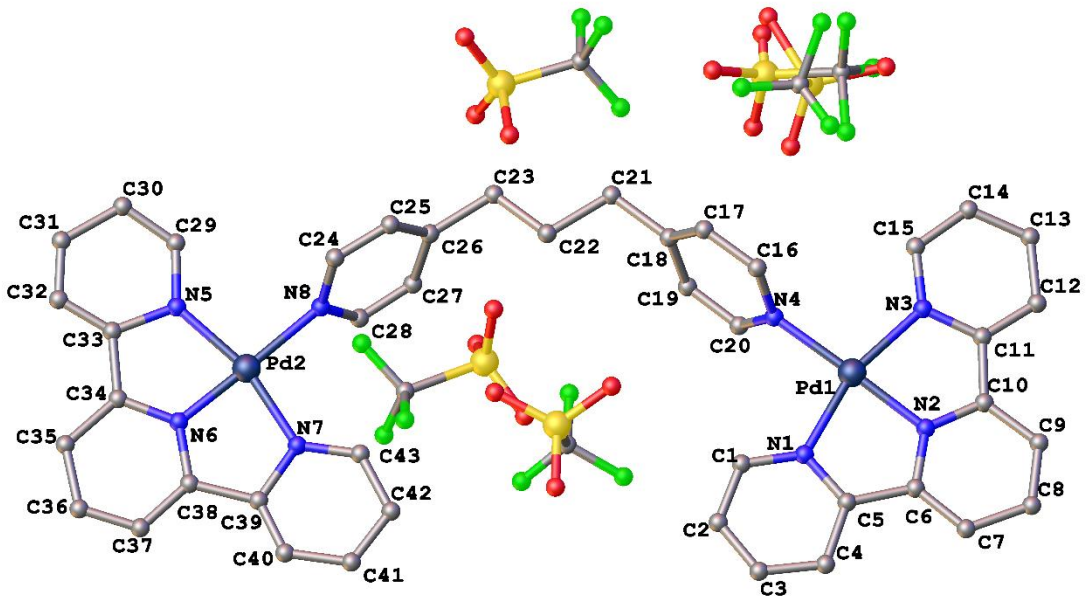


Figure 5.16: X-ray crystal structure of [{Pd(terpy)}$_2$(tmdp)](CF$_3$SO$_3$)$_4$ with crystallographically independent atom numbering scheme. Hydrogen atoms have been omitted for clarity. Atom colours - C: grey, O: red, N: blue, Pd: navy F: green and S: yellow.

Table 5.4: Selected bond lengths (Å) and angles (°) for [{Pd(terpy)}$_2$(tmdp)](CF$_3$SO$_3$)$_4$

Pd1-N1	2.054(14)	N2-Pd1-N1	81.70(6)
Pd1-N2	1.931(15)	N2-Pd1-N4	177.70(6)
Pd1-N3	2.041(17)	N3-Pd1-N1	162.80(6)
Pd1-N4	2.018(16)	N3-Pd1-N2	81.0(6)
Pd2-N5	1.970(2)	N5-Pd2-N6	81.20(9)
Pd2-N6	1.817(19)	N6-Pd2-N8	177.80(8)
Pd2-N7	1.989(19)	N5-Pd2-N7	164.20(8)
Pd2-N8	2.036(17)	N6-Pd2-N7	83.20(8)

In general, the bond lengths between N and (Pd**1**) are slightly longer than those found around (Pd**2**). However, the angles between (Pd**1**) and nitrogen atoms are slightly smaller than those around (Pd**2**). The pyridyl rings of tmdp ligand are significantly bent with respect to terpyridine planes forming dihedral angles of 75.52(6)° (Pd**1**) and 68.74(6)° (Pd**2**), respectively. Terpyridine of (Pd**2**) is less planar than that of (Pd**1**), with a displacement of +0.178 and -0.125 Å exhibited by C31and N6, respectively, from the mean plane. The terpyridine moiety of (Pd**1**) has a maximum displacement of +0.072 and -0.078 Å exhibited by C15 and C12, respectively, from the mean plane.

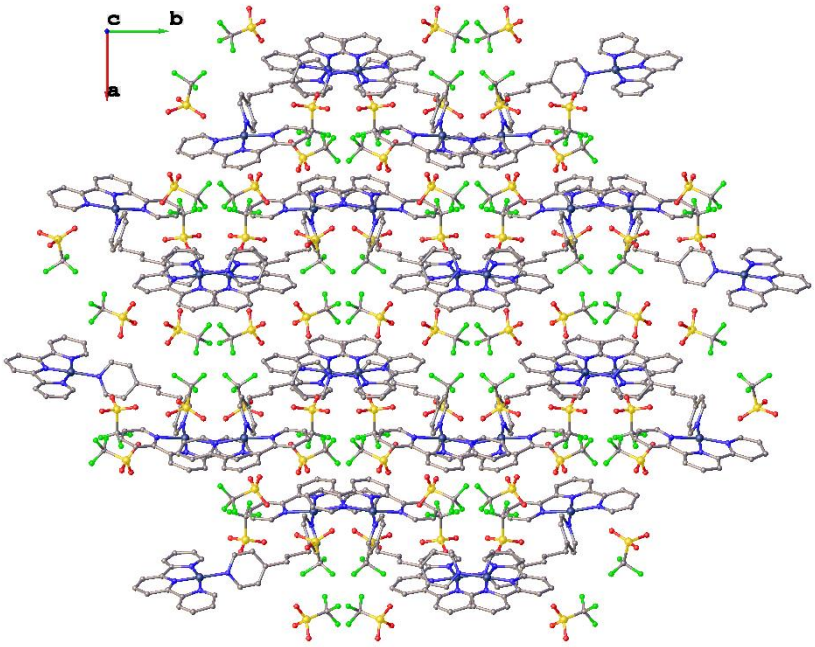


Figure 5.17: The packing diagram of [{Pd(terpy)}$_2$(tmdp)](CF$_3$SO$_3$)$_4$ along the *c* crystal axis. Hydrogen atoms are omitted for clarity.

Analysis of packing in the crystal structure showed that the rows of stacked cations are arranged in a herringbone architecture. Triflate anions occupied the channels between the cations (Figure 5.17). The π· · ·π stacking distance between two terpyridine moieties of neighbouring molecules amounts to 3.870 Å (corresponding slip angle is 12.931°) (Figure 5.18).

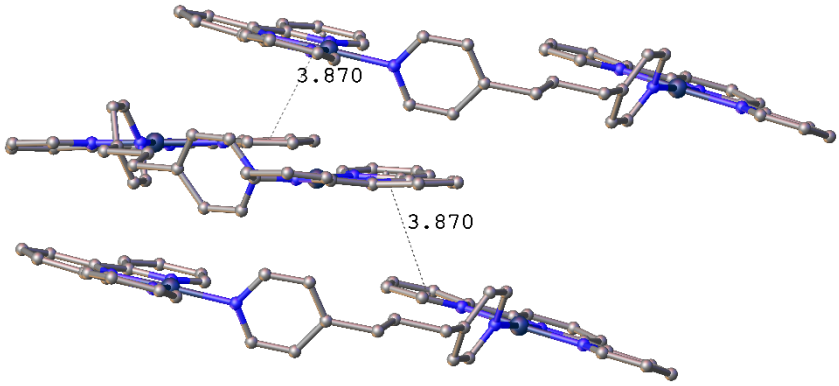


Figure 5.18: Representation of the π· · ·π interactions in [{Pd(terpy)}$_2$ (tmdp)](CF$_3$SO$_3$)$_4$. Dashed lines indicate the presence of π· · ·π interactions.

The dihedral angle between the two planes of terpyridine moieties is 4.74° (Figure 5.19).

This arrangement is further stabilised by a series of hydrogen bonds between the terpyridine, tmdp ligand and triflate anion. The triflate anions act as hydrogen bond acceptors and form hydrogen bonds with tmdp ligand and terpyridine moieties. The C–H…O distances lie in the range 2.295 – 2.770 Å and the C–H…F distances lie in the range 2.437 – 2.990 Å. In addition, tmdp ligand acts as a hydrogen bond donor through C–H…O and C–H…F hydrogen bonds via five sets each. The C–H…O distances lie in the range 2.432 – 2.744 Å and the C–H…F distances lie in the range 2.518 – 2.751 Å (Figure 5.20).

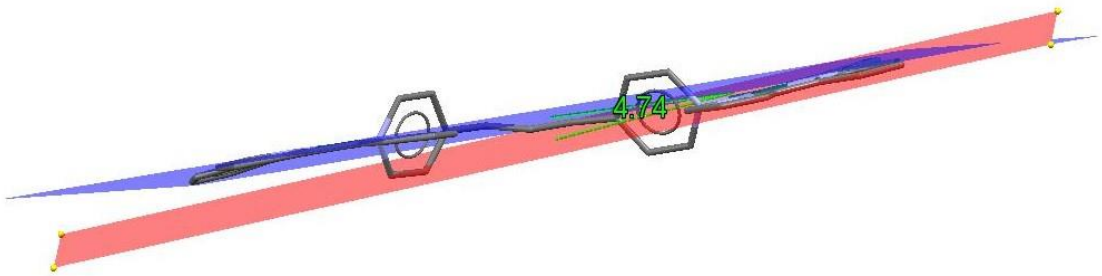


Figure 5.19: The dihedral angle between the two [Pd(trpy)] coordination planes of [{Pd(terpy)}$_2$(tmdp)](CF$_3$SO$_3$)$_4$.

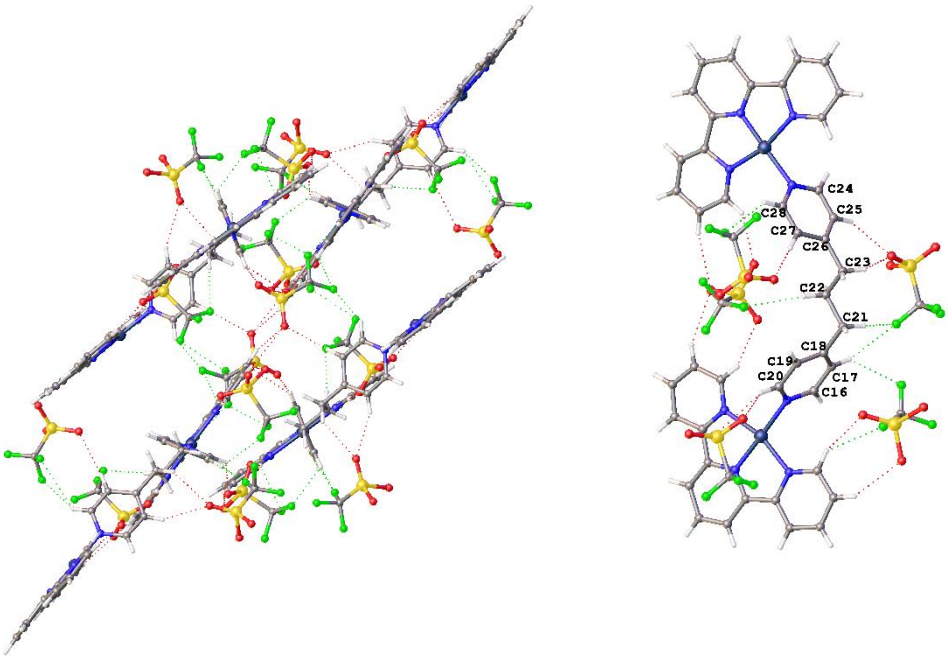


Figure 5.20: (a) A net of hydrogen bonds links Pd cations and triflate anions for [{Pd(terpy)}$_2$(tmdp)](CF$_3$SO$_3$)$_4$. (b) Hydrogen bonds formed by (tmdp) ligand.

*5.2.5.5 Single crystal X-ray structure of 2,2':6',2''-terpyridine (4,4'-(9,10-anthracenediyl)dipyridine) palladium triflate [{Pd(terpy)}$_2$(anbp)](CF$_3$SO$_3$)$_4$ (**5-5**).*

Crystals of (**5-5**) were found to be colourless plates, crystallising in the triclinic space group *P-1*. The cation has high symmetry with ordered triflate anions and one acetonitrile molecule, resulting in only four crystallographically distinct Pd–N bond lengths. There is disorder exhibited on one of the acetonitrile molecule. The asymmetric unit consists of one Pd(terpy) cation, one-half anbp ligand, two triflate anions and two acetonitrile molecules. As shown in Figure 5.21, space above and below the dinuclear Pd(terpy) cation is occupied by four triflate anions and four molecules of acetonitrile. The two Pd atoms are bridged by a single anbp ligand with the remaining coordination geometry completed by two terpyridine moieties. The Pd…Pd separation is 15.439 Å.

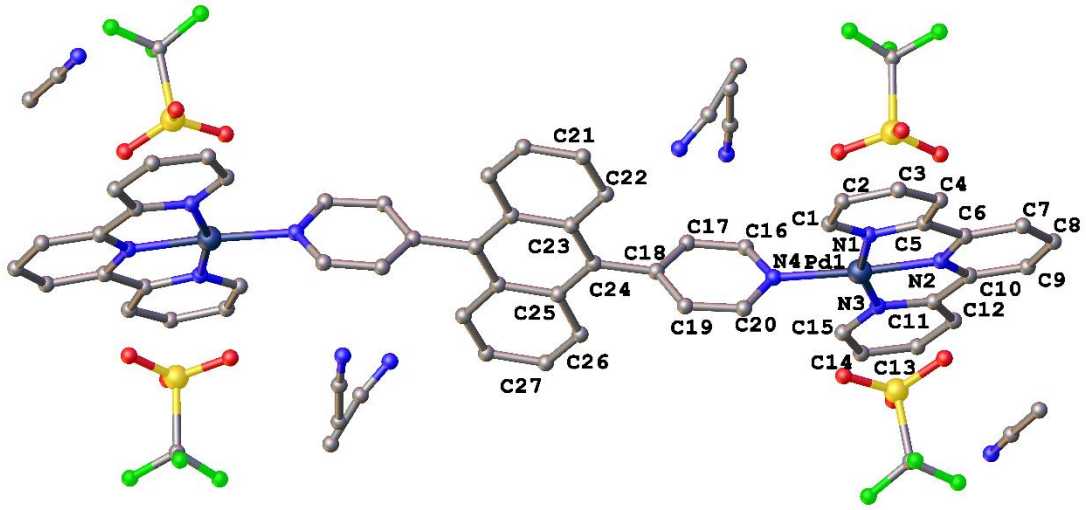


Figure 5.21: X-ray crystal structure of [{Pd(terpy)}$_2$(anbp)](CF$_3$SO$_3$)$_4$ with crystallographically independent atom numbering scheme. Hydrogen atoms have been omitted for clarity. Atom colours - C: grey, O: red, N: blue, Pd: navy F: green and S: yellow.

Table 5.5: Selected bond lengths (Å) and angles (°) for [{Pd(terpy)}$_2$ (anbp)](CF$_3$SO$_3$)$_4$

Pd1-N1	2.051(3)	N2-Pd1-N1	80.87(13)
Pd1-N2	1.936(3)	N2-Pd1-N4	175.91(12)
Pd1-N3	2.036(3)	N3-Pd1-N1	161.60(12)
Pd1-N4	2.050(3)	N3-Pd1-N2	80.79(12)

As before, Pd cation sits in a distorted square planar geometry, with two terpyridine moieties both coordinated in a tridentate fashion.

The dihedral angle between the square planar coordination geometry of the Pd(terpy) moieties and the plane of pyridyl ring of anbp ligand is 64.58(9)°. Unlike other related palladium(II) systems, no significant π· · ·π interaction is observed from the crystal

packing of (**5-5**) owing to the presence of triflate anions and acetonitrile molecules above and below the terpyridine moieties, which hinder the molecules from coming into close proximity with each other. The stacks of cations orient themselves into sheets separated by channels containing the triflate anions and acetonitrile molecules (Figure 5.22). The terpyridine moiety is almost coplanar with a maximum displacement of +0.093 and -0.087 Å exhibited by C1 and C3, respectively, from the mean plane. The two [Pd(terpy)] coordination planes are essentially parallel, as revealed by the interplanar angle of 0.00°.

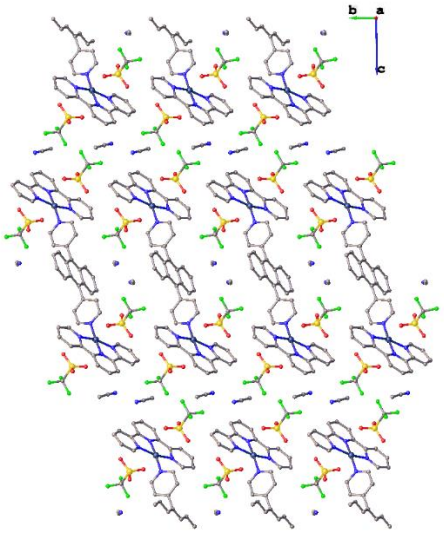


Figure 5.22: The packing diagram of [{Pd(terpy)}$_2$(anbp)](CF$_3$SO$_3$)$_4$ along the *a*-crystal axis. Hydrogen atoms are omitted for clarity.

There is a net of hydrogen bonds, as shown in Figure 5.23. The triflate anion acts as a hydrogen bond acceptor and forms hydrogen bonds with acetonitrile molecules, anbp, and terpyridine. The C–H…O distances lie in the range 2.325 – 2.882 Å and the C–H…F distances lie in the range 2.351 – 2.945 Å. The C–H…N distances lie in the range 2.459 – 2.902 Å. The anbp ligand acts as a hydrogen bond acceptor through four sets of C–H…O hydrogen bonds and two sets of C–H…N. The C16–H16…O6T, C20–H20…O3T, C26–H26…O5T and C27–H27…O6T distances are 2.531, 2.429, 2.574 and

2.543 Å, respectively. C17–H17…N2A and C21–H21…N2A distances are 2.856 and 2.814 Å, respectively.

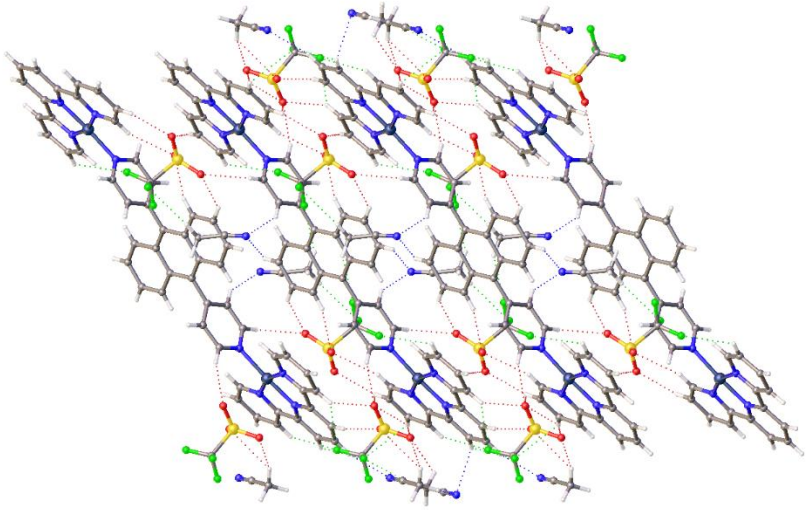


Figure 5.23: A net of hydrogen bonds links Pd cations, triflate anions and acetonitrile molecules for [{Pd(terpy)}$_2$(anbp)](CF$_3$SO$_3$)$_4$.

*5.2.5.6 Single crystal X-ray structure of 2,2':6',2''-terpyridine (1,4-bis(4-pyridyl)benzene) palladium triflate [{Pd(terpy)}$_2$(bpb)](CF$_3$SO$_3$)$_4$ (**5-6**).*

Crystals of (**5-6**) were found to be colourless blocks, crystallising in the monoclinic space group $P2_1/c$. The structure has inversion symmetry, resulting in only four crystallographically distinct Pd–N bond lengths. The asymmetric unit consists of one Pd(terpy) cation, one-half bpb ligand and two triflate anions (Figure 5.24). The bpb ligand acting as a *N,N*-bidentate bridge links the two Pd(terpy) with Pd…Pd distance of 15.388 Å. All Pd–N distances and angles are comparable to those found in the related mono and dinuclear Pd(terpy)complexes (Table 5.6).

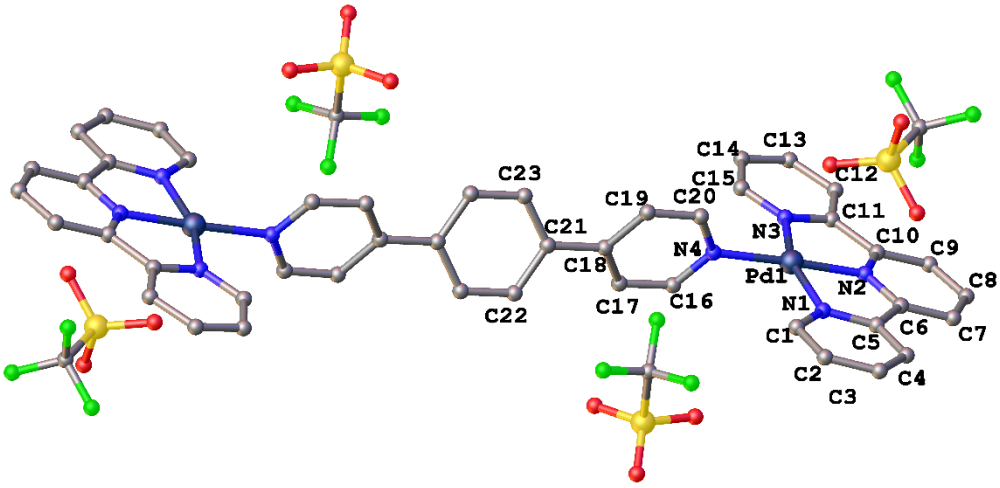


Figure 5.24: X-ray crystal structure of [{Pd(terpy)}$_2$(bpb)](CF$_3$SO$_3$)$_4$ with crystallographically independent atom numbering scheme. Hydrogen atoms have been omitted for clarity. Atom colours - C: grey, O: red, N: blue, Pd: navy F: green and S: yellow.

Table 5.6: Selected bond lengths (Å) and angles (°) for [{Pd(terpy)}$_2$ (bpb)](CF$_3$SO$_3$)$_4$

Pd1-N1	2.043(4)	N2-Pd1-N1	80.90(18)
Pd1-N2	1.930(5)	N2-Pd1-N4	177.68(10)
Pd1-N3	2.030(4)	N3-Pd1-N1	161.52(4)
Pd1-N4	2.025(6)	N3-Pd1-N2	80.53(2)

The dihedral angle between the square planar coordination geometry of the Pd(terpy) moieties and the plane of pyridyl ring of bpb ligand is 79.71(7)°. The terpyridine moiety is almost coplanar with a maximum displacement of +0.100 and -0.106 Å exhibited by C1 and C4, respectively, from the mean plane. The two [Pd(trpy)] coordination planes are parallel, as revealed by the interplanar angle of 0.00°.

Analysis of packing in the crystal structure showed that the rows of cations are arranged in a herringbone architecture. Triflate anions occupy the channels between the cations (Figure 5.25). Each molecule packs with its neighbour *via* intermolecular face-to-face π· · ·π stacking interactions with centroid-centroid separations of 3.771 Å and slip angle 0.00° (Figure 5.26).

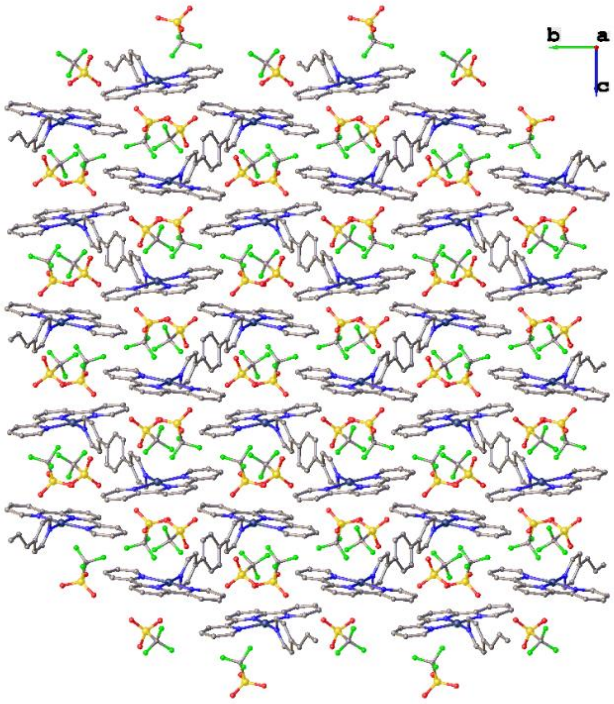


Figure 5.25: The packing diagram of [{Pd(terpy)}$_2$(bpb)](CF$_3$SO$_3$)$_4$ along the *a*-crystal axis. Hydrogen atoms are omitted for clarity.

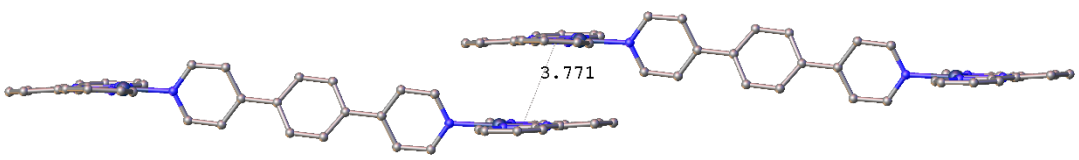


Figure 5.26: Representation of the π· · ·π interactions in [{Pd(terpy)}$_2$ (bpb)](CF$_3$SO$_3$)$_4$. Dashed lines indicate the presence of π· · ·π interactions.

A net of hydrogen bonds, as shown in Figure 5.27, is observed. The triflate anion acts as a hydrogen bond acceptor and forms hydrogen bonds with bpb ligand and terpyridine. The C–H…O distances lie in the range 2.193 – 2.995 Å and the C–H…F distances lie in the range 2.500 – 2.995 Å. The bpb ligand acts as hydrogen bond donor via four sets of C–H…O hydrogen bonds. The C16–H16…O1T, C19–H19…O5T, C20–H20…O4T and C21–H21…O5T distances are 2.193, 2.725, 2.461 and 2.485 Å, respectively.

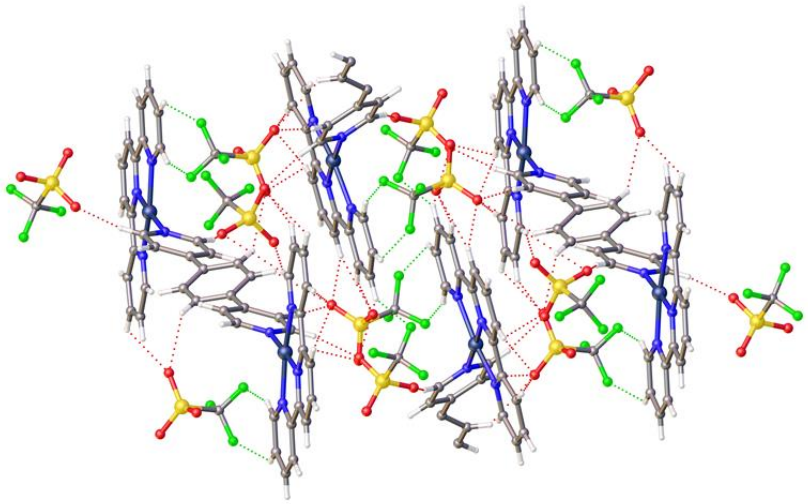


Figure 5.27: A net of hydrogen bonds links Pd cations and triflate anions for [{Pd(terpy)}$_2$(bpb)](CF$_3$SO$_3$)$_4$.

*5.2.5.7 Single crystal X-ray structure of 2,2':6',2''-terpyridine (4,4´-bis(4-pyridyl)biphenyl) palladium triflate [{Pd(terpy)}$_2$(bpbp)](CF$_3$SO$_3$)$_4$ (**5-7**).*

Crystals of (**5-7**) were found to be colourless plates, crystallising in the monoclinic space group *C2/c*. The two Pd atoms are bridged by a single 4,4'-bis(4-pyridyl)biphenyl ligand with the remaining coordination geometry completed by two terpyridine moieties (Figure 5.28). The Pd…Pd separation is 19.676 Å. All Pd–N bonds are crystallographically distinct, as shown in Table 5.7. The Pd–N2 and Pd–N7 (average ≈ 2.029(15) Å) distances to the central nitrogen atoms of the terpyridine moieties are shorter than those to the other two nitrogen atoms. The Pd–N distances for (**5-6**) and (**5-7**) are significantly

different, with those to (**5-7**) [average ≈ 2.123(6) Å] elongated compared to those for (**5-6**) [average 2.007(4) Å]. The two [Pd(terpy)] coordination planes are not coplanar, due to significant twisting of the ligand as revealed by the interplanar angle of 30.38(6)° (Figure 5.29).

The most notable feature of the structure is that the two terpyridyl moieties show different binding to the Pd ions. The bond lengths between nitrogen atoms and (Pd**1**) are slightly longer than those found around (Pd**2**). However, the angles between (Pd**1**) and nitrogen atoms are slightly smaller than those around (Pd**2**). Terpyridine of (Pd**1**) is less planar than that of (Pd**2**), with a maximum displacement of +0.074 and -0.067 Å exhibited by C7 and C12, respectively, from the mean plane. The terpyridine moiety of (Pd**2**) has a maximum displacement of +0.039 and -0.055 Å exhibited by N8 and C51, respectively, from the mean plane. However, the terpyridine moieties in (**5-7**) are more planar than those in (**5-6**).

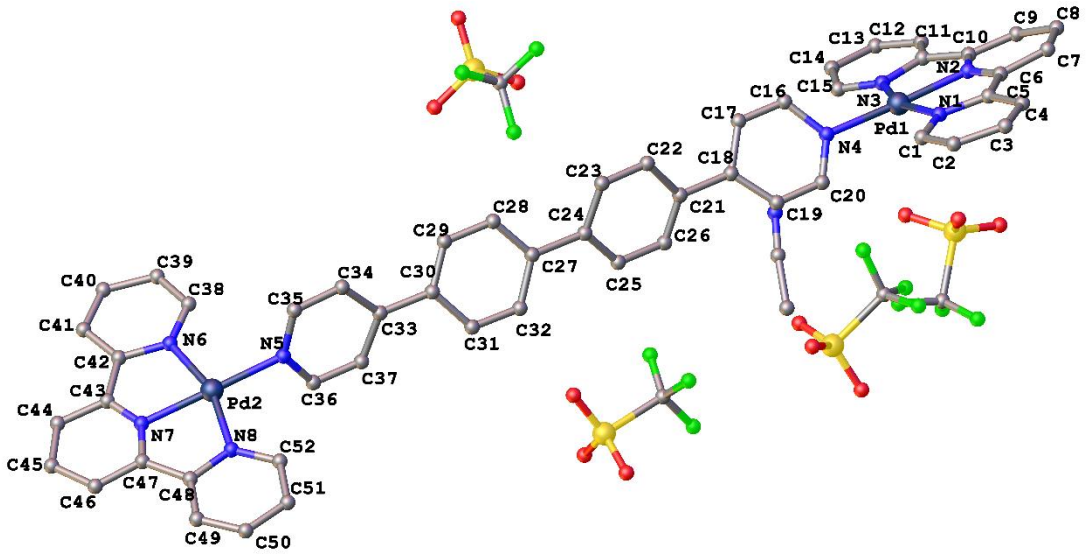


Figure 5.28: X-ray crystal structure of [{Pd(terpy)}$_2$(bpbp)](CF$_3$SO$_3$)$_4$ with crystallographically independent atom numbering scheme. Hydrogen atoms have been omitted for clarity. Atom colours - C: grey, O: red, N: blue, Pd: navy F: green and S: yellow.

Table 5.7: Selected bond lengths (Å) and angles (°) for [{Pd(terpy)}$_2$(bpbp)](CF$_3$SO$_3$)$_4$.

Pd1-N1	2.066(15)	N2-Pd1-N1	80.80(7)
Pd1-N2	2.044(16)	N2-Pd1-N4	178.00(5)
Pd1-N3	2.061(17)	N3-Pd1-N1	160.30(7)
Pd1-N4	2.080(15)	N3-Pd1-N2	79.50(7)
Pd2-N5	2.056(15)	N6-Pd2-N7	80.90(6)
Pd2-N6	2.063(14)	N5-Pd2-N7	177.40(5)
Pd2-N7	2.014(14)	N6-Pd2-N8	161.20(6)
Pd2-N8	2.051(13)	N7-Pd2-N8	80.50(6)

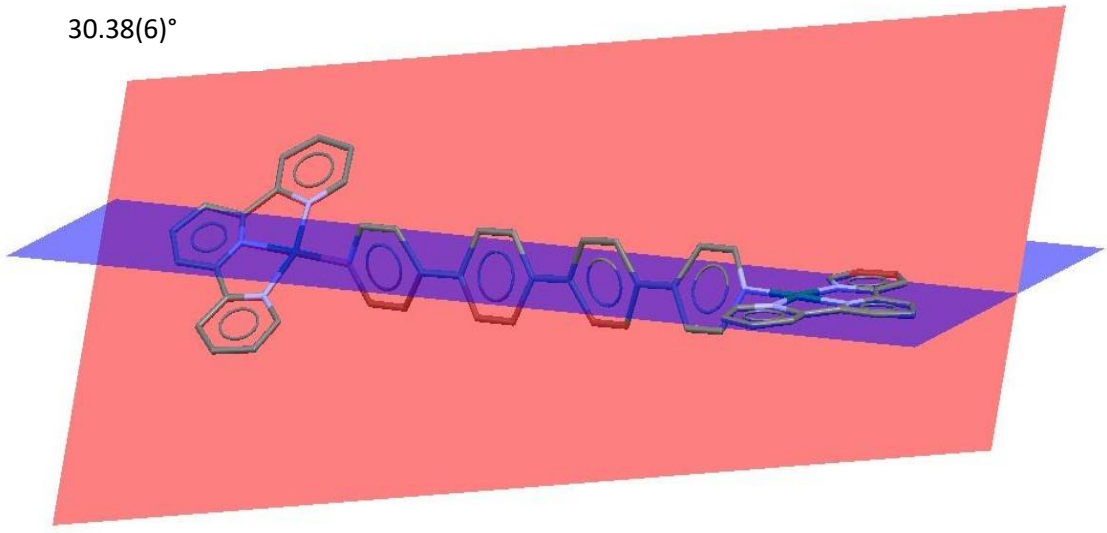


Figure 5.29: The dihedral angle between the two [Pd(terpy)] coordination planes of [{Pd(terpy)}$_2$(bpbp)](CF$_3$SO$_3$)$_4$.

The pyridyl rings of bpbp ligand are significantly bent with respect to the coordination N4 donors forming dihedral angles of 63.72(8)° (Pd**1**) and 74.51(7)° (Pd**2**), respectively. This complex packs in channels running parallel to the *b*-axis (Figure 5.30). The channels of cations are separated from each other by channels containing four triflate anions and acetonitrile molecule. As shown in Figure 5.31, the molecules of (**5-7**) undergo a series of face-to-face π· · ·π interactions indicated by ring centroid–ring centroid separations of 3.753, 3.938 and 3.753 Å (corresponding slip angles are 6.193°, 3.116° and 1.124°).

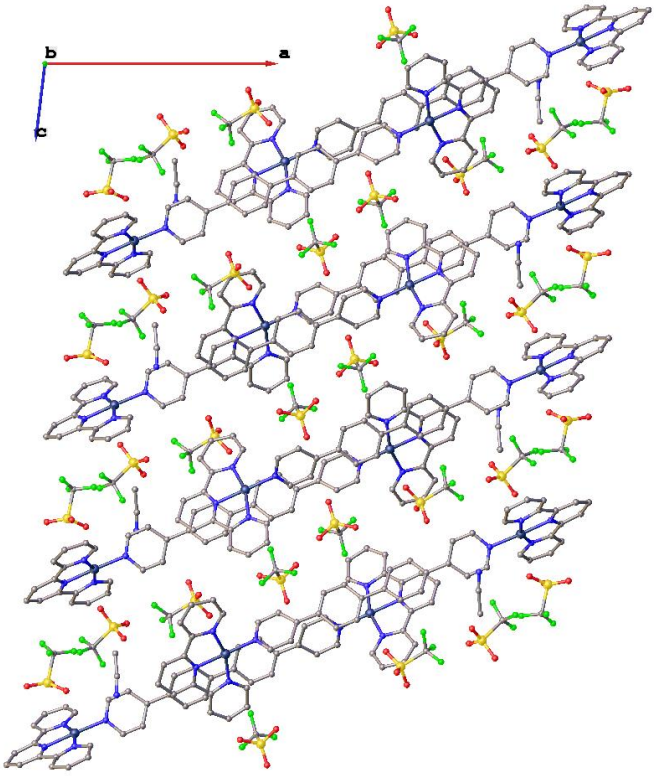


Figure 5.30: The packing diagram of [{Pd(terpy)}$_2$(bpbp)](CF$_3$SO$_3$)$_4$ along the *b*-crystal axis. Hydrogen atoms are omitted for clarity.

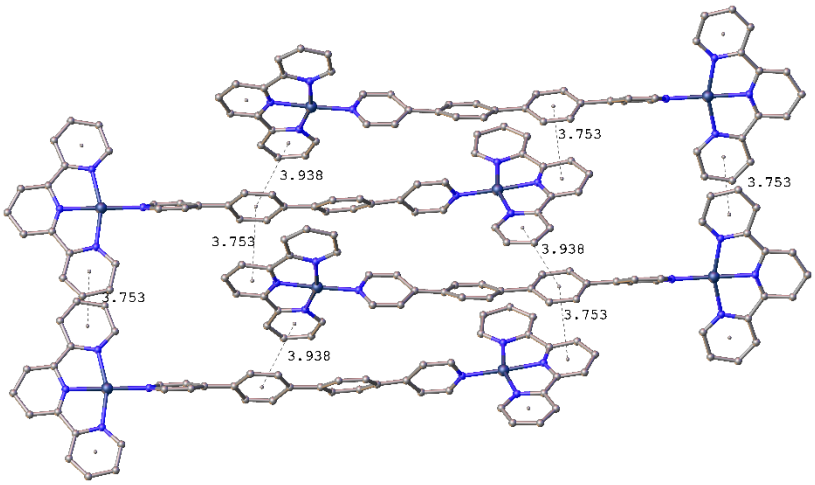


Figure 5.31: Representation of the π· · ·π interactions in [{Pd(terpy)}$_2$ (bpbp)](CF$_3$SO$_3$)$_4$. Dashed lines indicate the presence of π· · ·π interactions.

There is a series of hydrogen bonds between aromatic protons, acetonitrile molecule and triflate anions. The C–H…O distances lie in the range 2.284 – 2.918 Å and the C–H…F distances lie in the range 2.714 – 2.879 Å. The C–H…N distances lie in the range 2.703 – 2.856 Å (Figure 5.32).

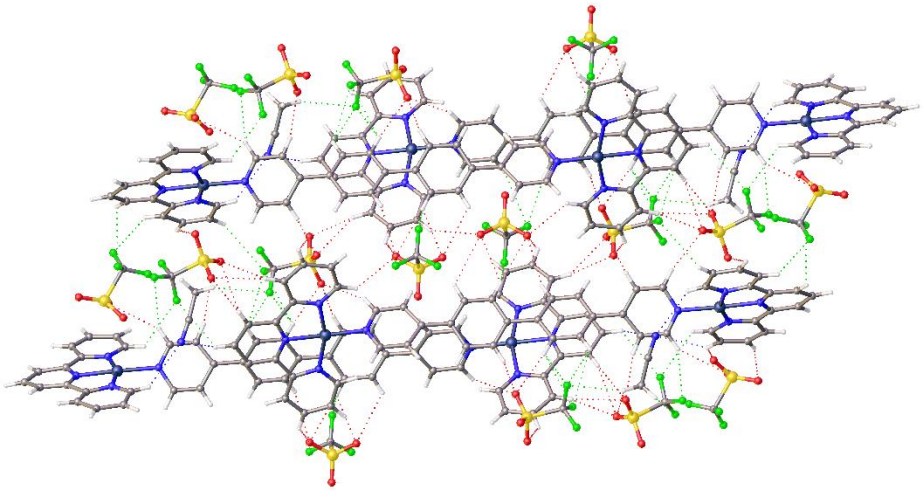


Figure 5.32: A net of hydrogen bonds links Pd cations, triflate anions and acetonitrile molecules for [{Pd(terpy)}$_2$(bpbp)](CF$_3$SO$_3$)$_4$.

*5.2.5.8 Single crystal X-ray structure of 4,4',4''-tri-tert-butyl-2,2':6',2''-terpyridine (1,4-bis(4-pyridyl)benzene) palladium triflate [{Pd(tBu$_3$-terpy)}$_2$(bpb)](CF$_3$SO$_3$)$_4$ (**5-8**).*

Crystals of (**5-8**) were found to be colourless plates, crystallising in the triclinic space group *P-1*. The structure has high symmetry with ordered triflate anions, resulting in only four crystallographically distinct Pd–N bond lengths. The asymmetric unit consists of one Pd(*t*Bu$_3$-terpy) cation, one-half bpb ligand and two triflate anions (Figure 5.33). The bpb ligand acting as a *N,N*-bidentate bridge links the two Pd(*t*Bu$_3$-terpy) with Pd…Pd distance of 15.376 Å, which is slightly shorter than that found in complex (**5-6**). All Pd–N distances in (**5-8**) are highly similar to those in (**5-6**), as are the *cis* N-Pd-N angles in (**5-8**) and (**5-6**) (Table 5.8).

Table 5.8: Selected bond lengths (Å) and angles (°) for [{Pd(*t*Bu$_3$-terpy)}$_2$ (bpb)](CF$_3$SO$_3$)$_4$.

Pd1-N1	2.039(3)	N2-Pd1-N1	80.80(13)
Pd1-N2	1.935(3)	N2-Pd1-N4	172.13(13)
Pd1-N3	2.025(3)	N3-Pd1-N1	161.62(14)
Pd1-N4	2.039(3)	N3-Pd1-N2	80.89(13)

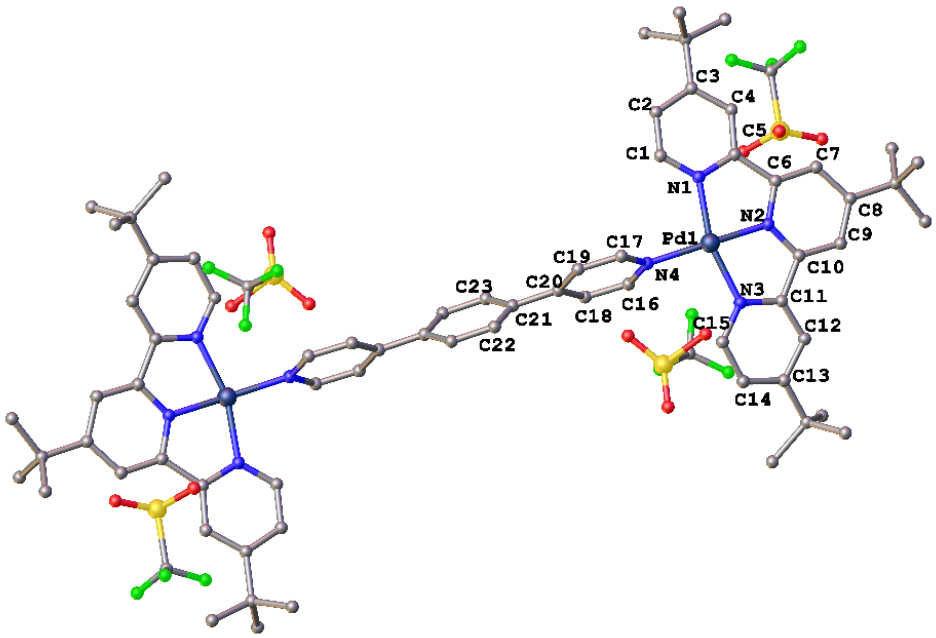


Figure 5.33: X-ray crystal structure of [{Pd(*t*Bu$_3$-terpy)}$_2$(bpb)](CF$_3$SO$_3$)$_4$ with crystallographically independent atom numbering scheme. Hydrogen atoms have been omitted for clarity. Atom colours - C: grey, O: red, N: blue, Pd: navy F: green and S: yellow.

The dihedral angle between the square planar coordination geometry of the Pd(*t*Bu$_3$-terpy) moieties and the plane of pyridyl ring of bpb ligand is 68.90(3)°. The dihedral angle indicates that bpb ligand in (**5-8**) is bent more than that in (**5-6**). The phenyl ring in bpb is twisted by 43.47(14)° relative to the pyridine ring. Cations of (**5-8**) are less planar than those of (**5-6**), with a maximum displacement of +0.530 and +0.475 Å exhibited by C15 and N3, respectively, from the mean plane.

Compound (**5-8**) packs in channels running parallel to the *a*-axis. The channels of cations are separated from each other by channels containing triflate anions (Figure 5.34). The presence of butyl groups prevents any significant π· · ·π interactions between aromatic moieties in the packing structure.

A series of hydrogen bonds between Pd cations, bpb ligand and triflate anions is observed. The C–H…O distances lie in the range 2.409 – 2.947 Å and the C–H…F distances lie in the range 2.373 – 2.985 Å (Figure 5.35).

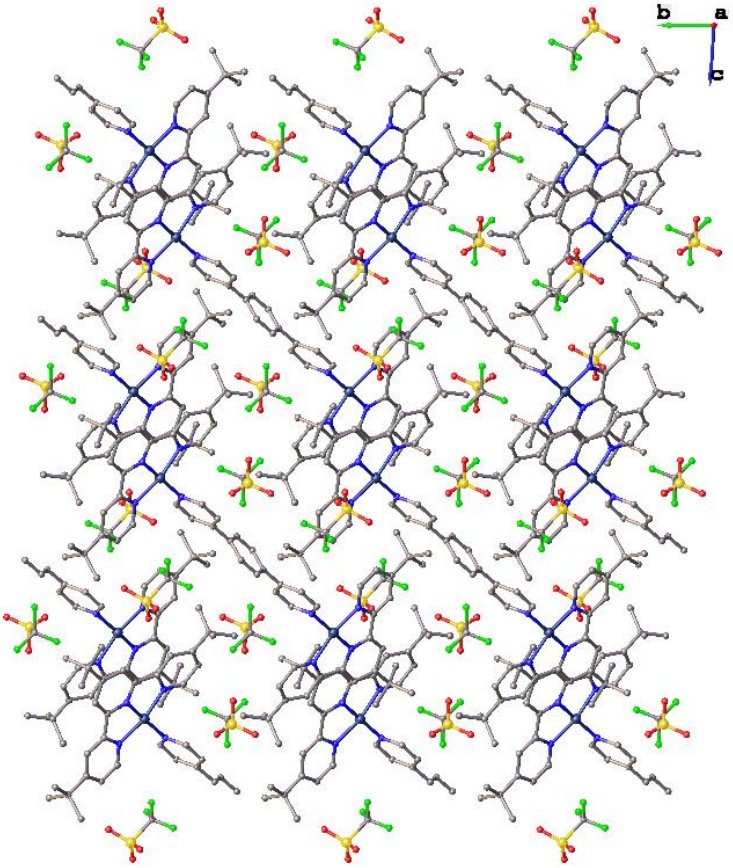


Figure 5.34: The packing diagram of [{Pd(*t*Bu$_3$-terpy)}$_2$(bpb)](CF$_3$SO$_3$)$_4$ along the *a*-crystal axis. Hydrogen atoms are omitted for clarity.

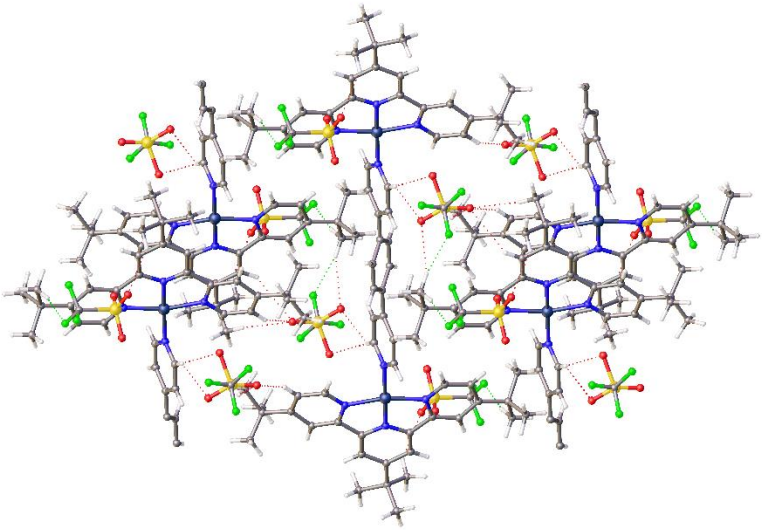


Figure 5.35: A net of hydrogen bonds links Pd cations and triflate anions for[{Pd(*t*Bu$_3$-terpy)}$_2$(bpb)](CF$_3$SO$_3$)$_4$.

*5.2.5.9 Single crystal X-ray structure of 4,4',4''-tri-tert-butyl-2,2':6',2''-terpyridine (4,4'-bis(4-pyridyl)biphenyl) palladium triflate [{Pd(tBu$_3$-terpy)}$_2$(bpbp)](CF$_3$SO$_3$)$_4$ (**5-9**).*

Crystals of (**5-9**) were found to be colourless plates, crystallising in the monoclinic space group *P2$_1$/n*. The structure displays inversion symmetry, resulting in only four crystallographically distinct Pd–N bond lengths. The asymmetric unit consists of one Pd(*t*Bu$_3$-terpy) cation, one-half bpbp ligand, two triflate anions and one acetonitrile molecule (Figure 5.36). The bpbp ligand acts as a *N,N*-bidentate bridge linking the two Pd(*t*Bu$_3$-terpy) moieties with Pd…Pd distance of 19.630 Å, slightly shorter than that found in complex(**5-7**). All Pd–N distances in (**5-9**) are significantly shorter than those in (**5-7**), while the N-Pd-N angles in (**5-9**) and (**5-7**) are similar.

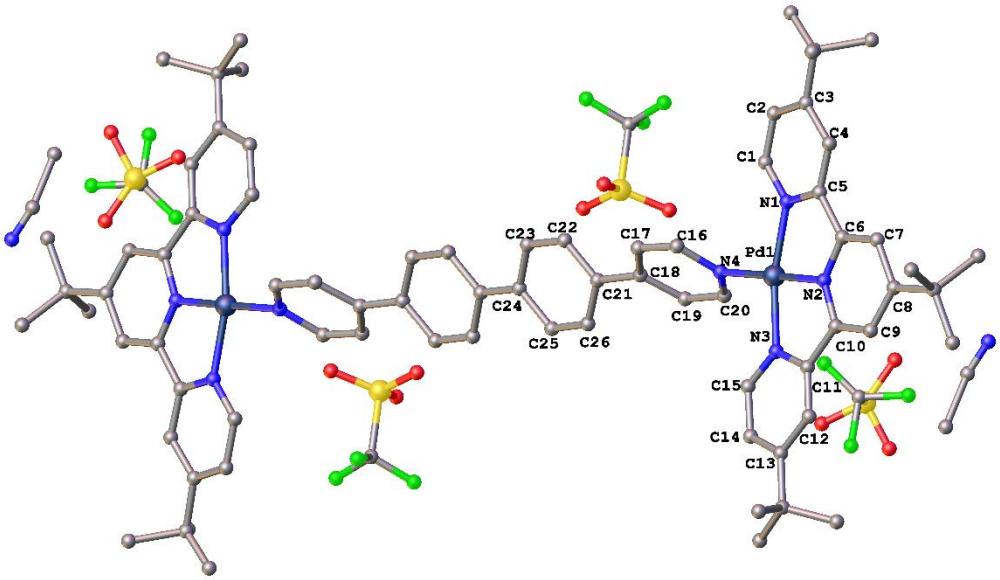


Figure 5.36: X-ray crystal structure of [{Pd(*t*Bu$_3$-terpy)}$_2$(bpbp)](CF$_3$SO$_3$)$_4$ with crystallographically independent atom numbering scheme. Hydrogen atoms have been omitted for clarity. Atom colours - C: grey, O: red, N: blue, Pd: navy F: green and S: yellow.

Table 5.9: Selected bond lengths (Å) and angles (°) for [{Pd(*t*Bu$_3$-terpy)}$_2$ (bpbp)](CF$_3$SO$_3$)$_4$.

Pd1-N1	2.025(9)	N2-Pd1-N1	80.70(3)
Pd1-N2	1.943(9)	N2-Pd1-N4	178.2(4)
Pd1-N3	2.023(9)	N3-Pd1-N1	161.50(4)
Pd1-N4	2.030(9)	N3-Pd1-N2	80.80(3)

The dihedral angle between the square planar coordination geometry of the Pd(*t*Bu$_3$-terpy) moieties and the plane of pyridyl ring of bpbp ligand is 57.78(7)°. The dihedral angle indicates that bpb ligand in (**5-9**) is bent more than that in (**5-7**), with the phenyl ring in bpbp is twisted by 36.50(10)° relative to the pyridine ring.

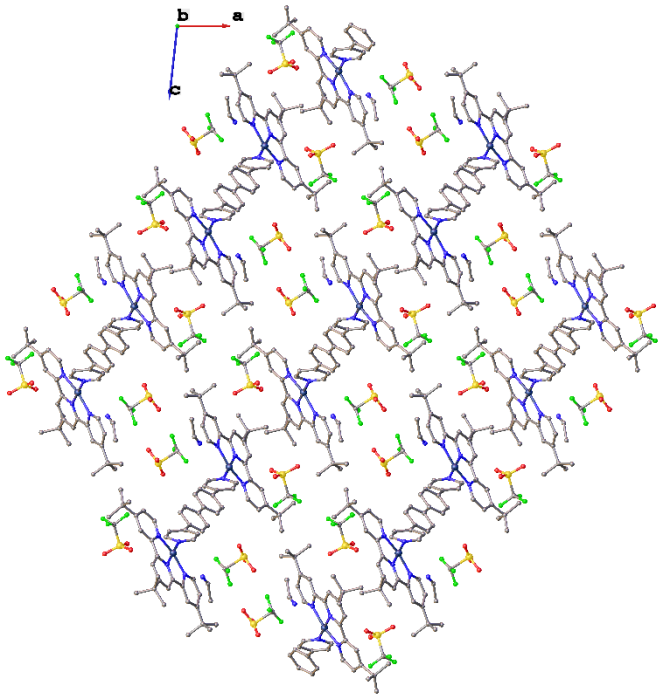


Figure 5.37: The packing diagram of [{Pd(*t*Bu$_3$-terpy)}$_2$(bpbp)](CF$_3$SO$_3$)$_4$ along the *b*-crystal axis. Hydrogen atoms are omitted for clarity.

Cations of (**5-9**) pack in channels running parallel to the *b*-axis, similar to (**5-7**). Cations of (**5-9**) are less planar than those of (**5-7**), with a maximum displacement of +0.255 and +0.238 Å exhibited by N1 and C15, respectively, from the mean plane.

There is a series of hydrogen bonds between Pd cations, bpbp ligand, triflate anions and acetonitrile molecules. The C–H…O distances lie in the range 2.323 – 2.981 Å and the C–H…F distances lie in the range 2.372 – 2.991 Å. The C–H…N distances are between 2.661 – 2.998 Å (Figure 5.38).

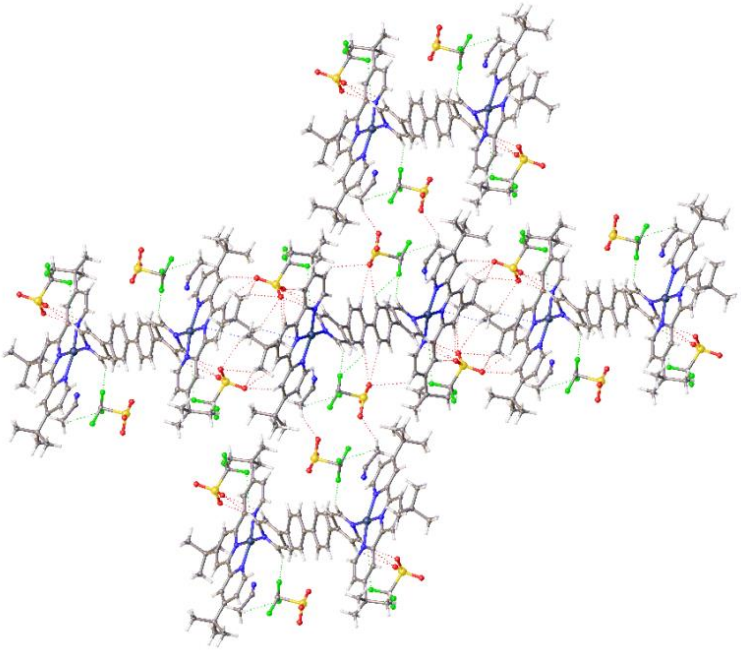


Figure 5.38: A net of hydrogen bonds links Pd cations and triflate anions for[{Pd(*t*Bu$_3$-terpy)}$_2$(bpbp)](CF$_3$SO$_3$)$_4$.

*5.2.5.10 Single crystal X-ray structure of 2,2':6',2''-terpyridine (meso-tetra(4-pyridyl)porphyrin) palladium triflate [{Pd(terpy)}$_4$(H$_2$T(4-Py)P)](CF$_3$SO$_3$)$_8$ (**5-10**).*

Crystals of (**5-10**) were found to be colourless plates. The complex crystallises in the triclinic space group *P-1*. The structure has inversion symmetry with ordered acetonitrile molecules and triflate anions, resulting in only eight crystallographically distinct Pd–N bond lengths. The asymmetric unit consists of two Pd(terpy) cations, one-half [H$_2$T(4-Py)P] ligand, four triflate anions and two acetonitrile molecules (Figure 5.39). In general, Pd–N distances of this complex are comparable to those found in the related mono and dinuclear complexes reported earlier. Table 5.10 lists important bond lengths and angles for this complex.

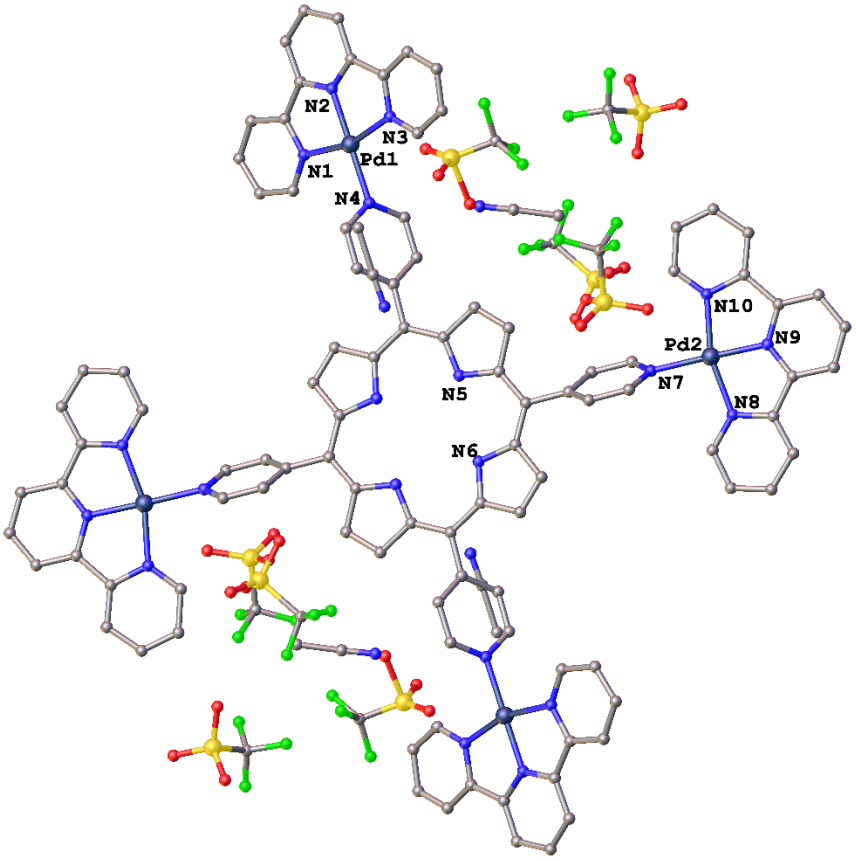


Figure 5.39: X-ray crystal structure of [{Pd(terpy)}$_4$(H2T(4-Py)P)](CF$_3$SO$_3$)$_8$ with crystallographically independent atom numbering scheme. Hydrogen atoms have been omitted for clarity. Atom colours - C: grey, O: red, N: blue, Pd: navy F: green and S: yellow.

Table 5.10: Selected bond lengths (Å) and angles (°) for [{Pd(terpy)}$_4$(H$_2$T(4-Py)P)](CF$_3$SO$_3$)$_8$.

Pd1-N1	2.051(11)	N2-Pd1-N1	81.50(5)
Pd1-N2	1.928(8)	N2-Pd1-N4	179.10(4)
Pd1-N3	2.042(10)	N3-Pd1-N1	163.10(4)
Pd1-N4	2.028(6)	N3-Pd1-N2	81.60(5)
Pd2-N7	2.025(7)	N8-Pd2-N9	81.20(3)

Pd2-N8	2.032(8)	N7-Pd2-N9	177.80(3)
Pd2-N9	1.923(7)	N8-Pd2-N10	162.90(3)
Pd2-N10	2.040(8)	N9-Pd2-N10	81.80(3)

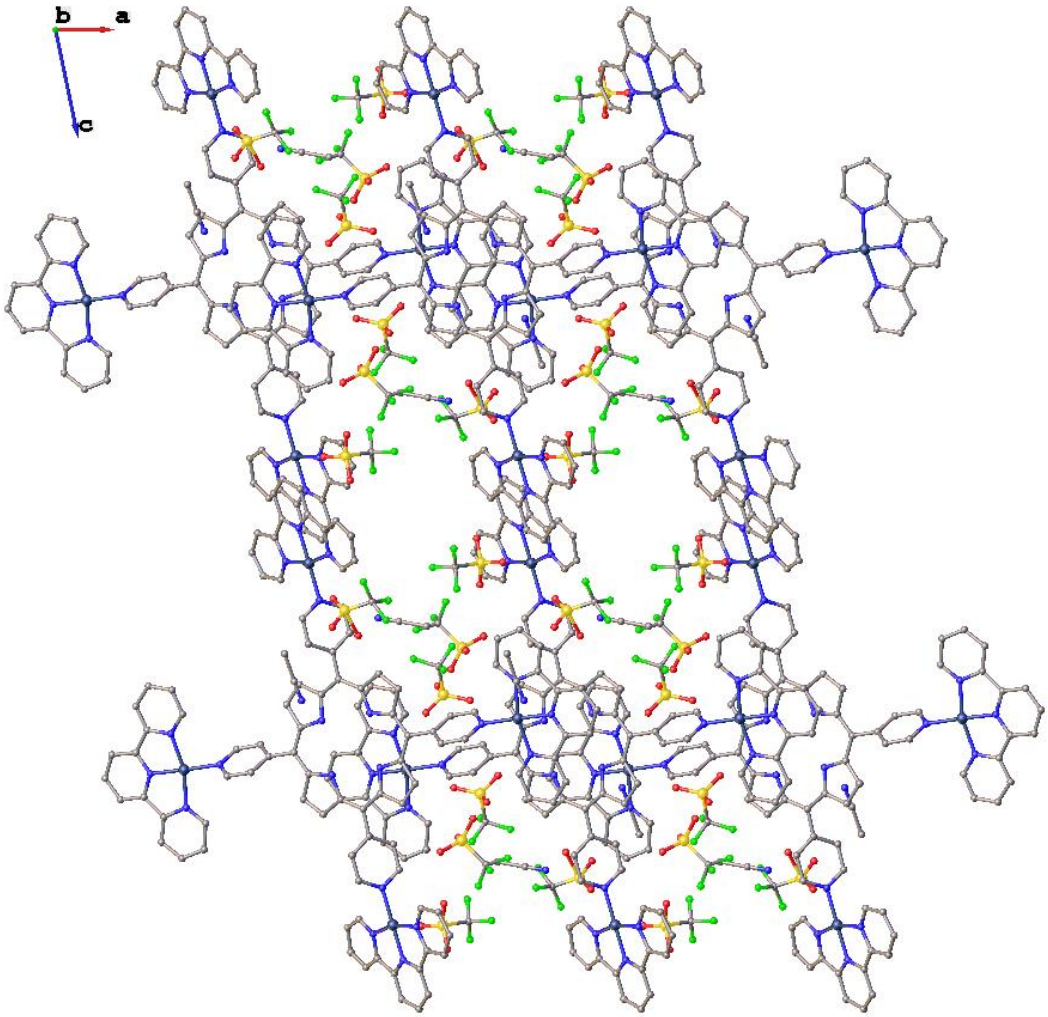


Figure 5.40: The packing diagram of [{Pd(terpy)}$_4$(H_2T(4-Py)P)](CF_3SO_3)$_8$ along the *b*-crystal axis. Hydrogen atoms are omitted for clarity.

The four Pd atoms are bridged by *meso*-tetra(4-pyridyl)porphyrin ligand with the remaining coordination geometry completed by a terpyridine ligand in each instance. The Pd1…Pd1 and Pd2…Pd2 separations are 15.509 and 15.457 Å, respectively. As before,

the coordination geometry of the palladium ion is distorted slightly from that found in perfect square-planar Pd(II) complexes. Table 5.10 lists important bond lengths and angles for this complex. In general, the bond lengths between nitrogen atoms and (Pd**1**) are slightly longer than those found around (Pd**2**). In addition, the angles between (Pd**1**) and nitrogen atoms are slightly larger than those around (Pd**2**). Terpyridine of (Pd**1**) is more planar than that of (Pd**2**), with a maximum displacement of +0.065 and -0.060 Å exhibited by N2 and C3, respectively, from the mean plane. The terpyridine moiety of (Pd**2**) has a maximum displacement of +0.135 and -0.107 Å exhibited by C50 and C47, respectively, from the mean plane. The pyridyl rings of $H_2T(4\text{-Py})P$ ligand are significantly bent with respect to terpyridine planes forming dihedral angles of 75.29(6)° (Pd**1**) and 65.63(7)° (Pd**2**).

The cavities formed by cations accommodate triflate anions and acetonitrile molecules (Figure 5.40). Each molecule packs with its neighbour *via* intermolecular face-to-face π· · ·π stacking interactions with centroid-centroid separations of 3.634 Å and slip angle of 1.007° (Figure 5.41).

There is a series of hydrogen bonds between Pd cations, $H_2T(4\text{-Py})P$ ligand, triflate anions and acetonitrile molecules. The C–H…O distances lie in the range 2.215 – 2.984 Å and the C–H…F distances lie in the range 2.521 – 2.933 Å. The C–H…N distances lie in the range 2.415 – 2.929 Å (Figure 5.42).

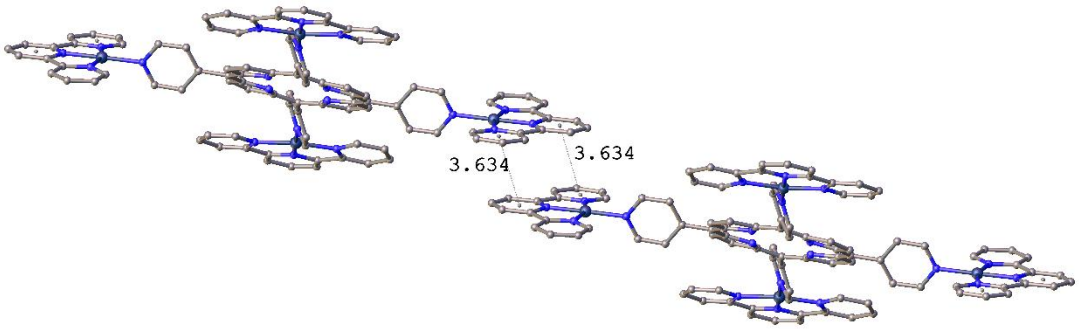


Figure 5.41: Representation of the π· · ·π interactions in [{Pd(terpy)}$_4$(H_2T(4-Py)P)](CF_3SO_3)$_8$. Dashed lines indicate the presence of π· · ·π interactions.

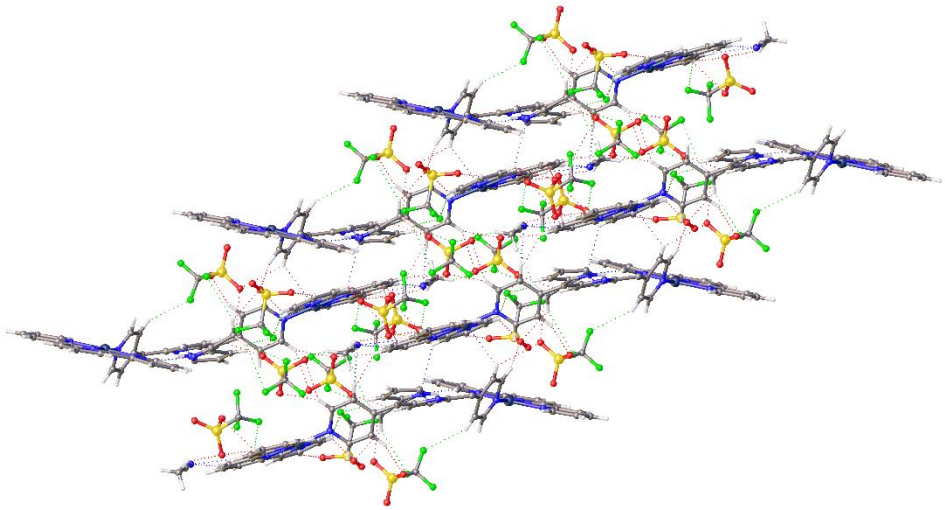


Figure 5.42: A net of hydrogen bonds links Pd cations and triflate anions for[{Pd(terpy)}$_4$(H_2T(4-Py)P)](CF_3SO_3)$_8$.

5.3 Conclusions

A series of dinuclear Pd(terpy) complexes have been synthesised using seven different *N,N*-bidentate ligands. A tetranuclear Pd(terpy) complex using *meso*-tetra(4-pyridyl)porphyrin as a bridging ligand has also been synthesised. It was possible to grow single crystals suitable for X-ray diffraction for all complexes. In all complexes, the Pd ions adopt a distorted square planar geometry. Complexes (**5-2**), (**5-3**), (**5-4**), (**5-7**), (**5-9**) and (**5-10**) contain solvent acetonitrile molecules. There are no statistically significant differences in bond lengths between any of the complexes discussed here and mononuclear Pd(terpy) complexes reported previously. The bond between the central terpy nitrogen and the Pd atom is the shortest (average = 1.936(11) Å), with two longer bonds between the terminal terpy nitrogen atoms and the Pd atom (falling in the range of 1.989(19) – 2.097(17) Å). In complex (**5-7**), however, the Pd–N distances to the central nitrogen atoms are significantly longer than 1.936(11) Å with an average = 2.029 Å. The *cis* N–Pd–N angles lie between 79.50(7) and 83.20(8)°. The N3–Pd1–N1 angle in (**5-4**) 164.20(8)° indicates the smallest deviation from the theoretical value of 180°, while (**5-7**) shows the highest deviation, 160.30(7)°.

The cations of (**5-8**) show the highest deviation from planarity of all the complexes, while (**5-2**) is the closest to a planar arrangement. In (**5-7**), the two [Pd(terpy)] coordination planes are not coplanar, due to significant twisting of the ligand as revealed by the interplanar angle of 30.38(6)°.

All complexes, except (**5-1**), (**5-4**) and (**5-7**), crystallise with half a molecule in the asymmetric unit. Complexes (**5-4**) and (**5-7**) are slightly different, having a complete molecule in the asymmetric unit. Complex (**5-1**) indicates the formation a three component discrete assembly consisting of three $[\{Pd(terpy)\}_2(4,4'\text{-bipy})]^{4+}$ cations with

eight triflate anions. Two of Pd(terpy) complexes contain inversion centres of symmetry at the centre of the 4,4'-bipy ligand.

The *meso*-(4-pyridyl)porphyrin containing four Pd(terpy) moieties attached to the peripheral pyridine groups have also been investigated, indicating that strategy can, in principle, be used to create multinuclear complexes as desired.

All complexes, except (**5-5**), (**5-8**) and (**5-9**), exhibit π· · ·π interactions between aromatic rings. No significant π· · ·π interaction is observed from the crystal packing of (**5-5**) owing to the presence of triflate anions and acetonitrile molecules above and below the terpyridine moieties, which hinder the molecules from coming into close proximity with each other. The presence of butyl groups in complexes (**5-8**) and (**5-9**) prevents any significant π· · ·π interactions between aromatic moieties in the packing structure.

A net of hydrogen bonds forms between the cations and anions and the data shows that the O…C-H and F…C-H distances are within the range typical for weak hydrogen bond lengths.

In the future, there is an aim to synthesise new aromatic thiol bidentate ligands, such as μ-4,4'-dithiolterphenylbis and μ[3-mercapto-N-(2-mercapto-ethyl)-propanamide. These ligands can used instead of *N,N*-bidentate ligands to compare the effect of varying chain length, flexibility, charge and stabilities on the crystal structures.

5.4 Materials and Methods

4,4'-Dipyridine, trans-1,2-bis(4-pyridyl)-ethylene, 4,4'-trimethylenedipyridine, 4-pyridineboronic acid pinacol ester were all purchased from Sigma Aldrich.

5.4.1 Synthesis of $[Pd(terpy)(CH_3CN)](CF_3SO_3)_2$

5.4.1.1 Synthesis of $[Pd(CH_3CN)_4](CF_3SO_3)_2$

$Pd(acac)_2$ (0.338 g, 2.192 mmol) was suspended in CH_3CN (12 mL) in a Schlenk flask. CF_3SO_3H (1.14 mL) was added to the stirred suspension. After 22 h at room temperature, diethyl ether (70 mL) was added dropwise to the yellow solution. The sealed flask was put in a freezer for 24 h. The light yellow solid was collected by Schlenk filtration, washed with diethyl ether and dried in *vacuo* to afford a light yellow solid 1.146 g (92%). ^{1}H NMR (400 MHz, CD_3NO_2) δ ppm: 2.64 (s, 12H). Elemental analysis calculated (%) for $C_{10}H_{12}F_6N_4O_6PdS_2$: C 20.54, H 2.30, N 9.12. Found: C 20.65, H 2.63, N 9.6.

5.4.1.2 Synthesis of $[Pd(terpy)(CH_3CN)](CF_3SO_3)_2$

To a dry 100 ml Schlenk flask was added $[Pd(CH_3CN)_4](CF_3SO_3)_2$ (0.802 g, 1.22 mmol) and 2,2':6',2''-terpyridine (0.312 g, 1.34 mmol) and anhydrous acetonitrile (12 mL). After stirring for 24 h, a light yellow precipitate had formed. 40 mL of anhydrous diethyl ether was added to promote further precipitation of the product. The yellow solid was filtered and washed twice with anhydrous diethyl ether (2 x 10 mL) then dried in *vacuo.* Yield (658 mg, 69%). ^{1}H NMR (400 MHz, CD_3CN) δ ppm: 8.55 (d, J = 5.6 Hz, 2H, 6, 6``), 8.50 (t, $J$ = 8.2 Hz, 1H, 4`), 8.40 (m, 2H, 3, 3``), 8.33 (d, J = 8.0 Hz, 2H, 3`, 5`), 8.25 (d, J = 8.4 Hz, 2H, 4, 4``), 7.80 (m, 2H, 5, 5``), 1.96 (s, 3H, CH_3). ^{13}C NMR (100 MHz, DMSO-d_6) δ ppm: 157.0, 155.2, 150.5, 143.5, 143.2, 129.0, 125.5, 124.7, 118.1, 1.2.

5.4.2 Synthesis of the ligands

5.4.2.1 Synthesis of 4,4'-azopyridine (azpy)

4-Aminopyridine (1.25 g, 0.013 mol) was dissolved in 20 mL water and kept cold in an ice bath. Using a dropping funnel, 6% NaOCl (25 mL, 0.0018 mol diluted in 25 mL of water) was slowly added to the pyridine solution with stirring, maintaining the temperature between 0-7 °C. The resulting mixture was stirred for 3 h. The solution was extracted into diethyl ether and the solvent was removed under reduced pressure. A small amount of hexane was added to dissolve the desired product. Any insoluble residue was filtered off. The solvent was removed under reduced pressure. The crude product was recrystallized from methanol to afford the desired product as long orange needles. Yield (950 mg, 77%). ^{1}H NMR (400 MHz, $CDCl_3$) δ ppm: 8.86 (m, 4H, 2, 6, 2`, 6`), 7.74 (m, 4H, 3, 5, 3`, 5`). ^{13}C NMR (100 MHz, $CDCl_3$) δ ppm: 155.9, 151.2, 115.9.

5.4.2.2 Synthesis of 4,4'-(9,10-anthracenediyl)dipyridine (anbp)

To a degassed mixture of 9,10-dibromoanthracene (450 mg, 1.34 mmol), 4-pyridineboronic acid pinacol ester (600 mg, 2.93 mmol), $PdCl_2(dppf).CH_2Cl_2$ and K_3PO_4 in a Schlenk flask, was added dry degassed dioxane (35 mL). The resulting mixture was heated at 100 °C for 24 h under a nitrogen atmosphere. Water was added to the reaction mixture then extracted with CH_2Cl_2. The crude product was purified by column chromatography (silica, CH_2Cl_2). Yield (37 mg, 83%). HRMS $(EI)^+$ m/z: 332.10 [$C_{24}H_{16}N_2$]. ^{1}H NMR (400 MHz, CD_3OD) δ ppm: 7.48 (m, 4H, 2, 6, 2`, 6`), 7.63 (m, 8H), 8.74 (m, 4H, 3, 5, 3`, 5`).

5.4.2.3 Synthesis of 1,4-bis(4-pyridyl)benzene (bpb)

Pyridylboronic pinacol ester (246 mg, 1.20 mmol), 1,4-dibromobenzene (95 mg, 0.40 mmol), and Cs_2CO_3 (780 mg, 2.40 mmol) were added to a dry mixture of toluene/DMF (1:1, 30 mL). The mixture was degassed for 30 minutes. $Pd(PPh_3)_4$ (46 mg, 0.04 mmol) was added to the reaction mixture and the solution heated to 130 ºC. After 48 h, the reaction mixture was cooled to room temperature and filtered. The filtrate was concentrated under vacuum to dryness to afford a solid residue, which was dissolved in CH_2Cl_2 followed by extraction with H_2O three times. The acidity of the organic layer was adjusted by adding dropwise concentrated HCl (pH 2–3). The acid encourages the desired product to precipitate from solution. The resulting precipitate was collected by filtration and then dissolved in H_2O. The water layer was made basicity (pH 8–9) by adding dropwise concentrated aq. NaOH (10 M), which caused the desired product to precipitate from solution as a white solid 63 mg (68%). HRMS $(EI)^+$ m/z: 232.04 $[C_{16}H_{12}N_2]$. ^1H NMR (300 MHz, $CDCl_3$) δ ppm: 8.73 (dd, J = 4.6, 1.5 Hz, 4H, 2, 6, 2`, 6`), 7.79 (s, 4H, 8, 9, 8`, 9`), 7.58 (dd, J = 4.6, 1.5 Hz, 4H, 3, 5, 3`, 5`). ^{13}C NMR (100 MHz, $CDCl_3$) δ ppm: 150.1, 146.5, 138.5, 126.8, 121.5.

5.4.2.4 Synthesis of 4,4'-bis(4-pyridyl)biphenyl (bpbp)

4,4'-Diiodobiphenyl (1.00 g, 2.46 mmol), 4-pyridineboronic acid (740 mg, 5.43 mmol) and $Pd(PPh_3)_4$ (285 mg, 0.246 mmol) were added to a mixture of toluene (40 mL), MeOH (20 mL) and Na_2CO_3 (2M in H_2O, 10 mL). The reaction mixture was heated under reflux. After 48 hours, the mixture was cooled to room temperature and the precipitate was filtered off. The filtrate was concentrated under vacuum to dryness to afford a solid residue. The residue was partitioned between CH_2Cl_2 (3 X 40 mL) and saturated aqueous $NaHCO_3$ (50 mL). The combined organic phases were dried over $MgSO_4$ and concentrated under vacuum. The solid residue was washed with MeOH (2 x

30 mL) to give the desired compound as a white solid (343 mg, 45%). HRMS $(EI)^+$ m/z: 309.37 $[C_{24}H_{16}N_2+H]^+$. ^1H NMR (300 MHz, $CDCl_3$) δ ppm: 8.69 (d, *J* = 6.1 Hz, 4H, 2, 6, 2`, 6`), 7.73–7.80 (m, 8H, 8, 9, 11, 12, 8`, 9`, 11`, 12`), 7.57 (d, *J* = 5.9 Hz, 4H, 3, 5, 3`, 5`). ^{13}C NMR (100 MHz, $CDCl_3$) δ ppm: 150.3, 147.6, 141.1, 137.4, 127.8, 127.6, 121.5.

5.4.2.5 Synthesis of meso-tetra(4-pyridyl)porphyrin (H_2T(4-Py)P)

The mixture of salicylic acid (4.0 g, 28 mmol) and pyridine-4-carbaldehyde (6.4 g, 60 mmol) dissolved in xylene (500 mL) was added to pyrrole (4.0 g, 60 mmol） dropwise over 40 min. The reaction mixture was stirred at reflux for 3 h under a nitrogen atmosphere. The reaction mixture was cooled to room temperature and poured into 30 mL of methanol and stood overnight. The black precipitate was washed with methanol until the bright purple solids were obtained as *meso*-tetra(4-pyridyl)porphyrin with a yield of (30 mg, 8%).^1H NMR (400 MHz, $CDCl_3$) δ ppm: 9.06 (d, *J* = 4.9 Hz, 8H, 4x(2, 6-py), 8.86 (s, 8H, 4x(3, 4-pyrrole), 8.13 (d, *J* = 5.9 Hz, 8H, 4x(3, 5-py), -2.91 (s, 2H, NH_2).

5.4.3 Synthesis of dinuclear palladium terpyridine complexes

*5.4.3.1 Synthesis of 2,2':6',2''-terpyridine (4,4'-bipyridyl) palladium triflate [{Pd(terpy)}$_2$(4,4'-bipy)][CF_3SO_3)$_4$ (**5-1**).*

The complex (**5-1**) was obtained by the direct reaction of 4,4'-bipyridyl (14 mg, 0.09 mmol) in acetone with $[Pd(terpy)NCCH_3](CF_3SO_3)_2$ (110 mg, 0.162 mmol) in acetonitrile. The solution was stirred for 1 hour under a dinitrogen atmosphere. The product was precipitated from the solution by the addition of diethyl ether–acetone 3:1. Yield (101 mg, 76%). MALDI-TOF MS (RP; m/z): 208.45 $[C_{44}H_{30}N_8O_{12}F_{12}S_4Pd_2\text{-}4OTf]^{4+}$. ^1H NMR (400 MHz, CD_3CN) δ ppm: 9.48 (d, *J* = 6.0 Hz, 4H, 2x(2,6-py)), 8.62 (t, *J* = 7.5 Hz, 2H, 2x(4`-terpy)), 8.52 (m, 16H, 2x(3, 4, 3`, 5`, 3``, 4``-terpy, 2x(3, 5-py)), 7.98 (d, *J* = 5.2 Hz, 4H, 2x(6, 6``-terpy)), 7.83 (m, 4H, 2x(5, 5``-terpy)).

*5.4.3.2 Synthesis of 2,2':6',2''-terpyridine (trans-1,2-bis(4-pyridyl)-ethylene) palladium triflate [{Pd(terpy)}$_2$(tbpe)](CF$_3$SO$_3$)$_4$ (**5-2**).*

The complex (**5-2**) was obtained by the direct reaction of trans-1,2-bis(4-pyridyl)-ethylene (17 mg, 0.094 mmol) in acetone with [Pd(terpy)NCCH$_3$](CF$_3$SO$_3$)$_2$ (116 mg, 0.171 mmol) in acetonitrile. The solution was stirred for 1 hour under a dinitrogen atmosphere. The product was precipitated from the solution by the addition of diethyl ether–acetone 3:1. Yield (86 mg, 63%). MALDI-TOF MS (RP; m/z): 215.44 [$C_{46}H_{32}F_{12}N_8O_{12}Pd_2S_4$-O4Tf]$^{4+}$. ^{1}H NMR (400 MHz, CD_3CN) δ ppm: 9.12 (d, *J* = 6.0 Hz, 4H, 2x(2, 6-py)), 8.50 (t, *J* = 8.0 Hz, 2H, 4`-terpy), 8.39 (m, 12H, 2x(3, 4, 3`, 5`, 3``, 4``-terpy), 8.09 (d, *J* = 6.4 Hz, 4H, 2x(3, 5-py)), 7.80 (m, 6H, 2x(6, 6``-terpy), CH=CH ), 7.67 (m, 4H, 2x(5, 5``-terpy)).

*5.4.3.3 Synthesis of 2,2':6',2''-terpyridine (4,4'-azopyridine) palladium triflate [{Pd(terpy)}$_2$(azpy)](CF$_3$SO$_3$)$_4$ (**5-3**).*

The complex (**5-3**) was obtained by the direct reaction of 4,4'- azopyridine (15 mg, 0.081 mmol) in acetone with [Pd(terpy)NCCH$_3$](CF$_3$SO$_3$)$_2$ (100 mg, 0.147 mmol) in acetonitrile. The solution was stirred for 1 hour under a dinitrogen atmosphere. The product was precipitated from the solution by the addition of diethyl ether–acetone 3:1. Yield (74 mg, 73%). MALDI-TOF MS (RP; m/z): 216.03 [$C_{44}H_{30}F_{12}N_{10}O_{12}Pd_2S_4$-O4Tf]$^{4+}$. ^{1}H NMR (400 MHz, CD_3CN) δ ppm: 9.15 (d, *J* = 6.2 Hz, 4H, 2x(2, 6-py)), 8.55 (m, 2H, 2x(4`-terpy)), 8.44 (m, 12H, 2x(3, 4, 3`, 5`, 3``, 4``-terpy)), 8.12 (d, 4H, *J* = 6.4 Hz, 2x(3, 5-py)), 7.88 (m, 4H, 2x(6, 6``-terpy)), 7.70 (m, 4H, 2x(5, 5``-terpy)).

*5.4.3.4 Synthesis of 2,2':6',2''-terpyridine (4,4'-trimethylenedipyridine) palladium triflate [{Pd(terpy)}$_2$(tmdp)](CF$_3$SO$_3$)$_4$ (**5-4**).*

The complex (**5-4**) was obtained by the direct reaction of 4,4'-trimethylenedipyridine (17 mg, 0.085 mmol) in acetone with [Pd(terpy)NCCH$_3$](CF$_3$SO$_3$)$_2$ (108 mg, 0.155 mmol) in

acetonitrile. The solution was stirred for 1 hour under a dinitrogen atmosphere. The product was precipitated from the solution by the addition of diethyl ether–acetone 3:1. Yield (40 mg, 32%). MALDI-TOF MS (RP; m/z): 219.29 $[C_{47}H_{36}F_{12}N_8O_{12}Pd_2S_4\text{-}4OTf]^{4+}$. ^{1}H NMR (400 MHz, CD_3CN) δ ppm: 8.96 (d, *J* = 6.3 Hz, 4H, 2x(2, 6-py)), 8.37 (t, *J* = 8.2 Hz, 2H, 2x(4`-terpy)), 8.33 (m, 12H, 2x(3, 4, 3`, 5`, 3``, 4``-terpy)), 7.80 (d, *J* = 6.2 Hz, 4H, 2x(3, 5-py)), 7.71 (d, *J* = 5.6 Hz, 4H, 2x(6, 6``-terpy)), 7.05 (m, 4H, 2x(5, 5``-terpy)), 3.04 (t, *J* = 7.7 Hz, 4H, 2x(py-CH_2)), 2.29 (m, 2H, py-CH_2-$\underline{CH_2}$).

*5.4.3.5 Synthesis 2,2':6',2''-terpyridine (4,4'-(9,10-anthracenediyl)dipyridine) palladium triflate [{Pd(terpy)}$_2$(anbp)](CF$_3$SO$_3$)$_4$ (**5-5**).*

The complex (**5-5**) was obtained by the direct reaction of 4,4'-(9,10-anthracenediyl)dipyridine (27 mg, 0.085 mmol) in acetone with $[Pd(terpy)NCCH_3](CF_3SO_3)_2$ (100 mg, 0.147 mmol) in acetonitrile. The solution was stirred for 1 hour under a dinitrogen atmosphere. The product was precipitated from the solution by the addition of diethyl ether–acetone 3:1. Yield (73 mg, 54%). MALDI-TOF MS (RP; m/z): 252.63 $[C_{58}H_{38}F_{12}N_8O_{12}Pd_2S_4\text{-}4OTf]^{4+}$. ^{1}H NMR (400 MHz, CD_3CN) δ ppm: 9.12 (m, 4H, 2x(2, 6-py)), 8.96 (m, 6H, 2x(4`-terpy), 8, 11, 8`, 11`-anbp), 8.36 (m, 12H, 2x(3, 4, 3`, 5`, 3``, 4``-terpy)), 7.95 (m, 8H, 3, 5, 3`, 5`, 9, 10, 9`, 10`-anbp)), 7.89 (m, 4H, 2x(6, 6``-terpy)), 7.75 (m, 4H, 2x(5, 5``-terpy)).

*5.4.3.6 Synthesis of 2,2':6',2''-terpyridine (1,4-bis(4-pyridyl)benzene) palladium triflate [{Pd(terpy)}$_2$(bpb)](CF$_3$SO$_3$)$_4$ (**5-6**).*

The complex (**5-6**) was obtained by the direct reaction of 1,4-bis(4-pyridyl)benzene (19 mg, 0.085 mmol) in acetone with $[Pd(terpy)NCCH_3](CF_3SO_3)_2$ (100 mg, 0.147 mmol) in acetonitrile. The solution was stirred for 1 hour under a dinitrogen atmosphere. The product was precipitated from the solution by the addition of diethyl ether–acetone 3:1.

Yield (53 mg, 62%). MALDI-TOF MS (RP; m/z): 228.05 $[C_{50}H_{34}F_{12}N_8O_{12}Pd_2S_4\text{-}4OTf]^{4+}$. ^{1}H NMR (400 MHz, CD_3CN) δ ppm: 9.09 (d, *J* = 6.2 Hz, 4H, 2x(2, 6-py)), 8.86 (t, *J* = 8.2 Hz, 2H, 2x(4`-terpy)), 8.60 (m, 12H, 2x(3, 4, 3`, 5`, 3``, 4``-terpy)), 8.34 (d, *J* = 6.4 Hz, 4H, 2x(3, 5-py)), 7.85 (s, 4H, 8, 9, 11, 12-benzene), 7.68 (m, 4H, 2x(6, 6``-terpy)), 7.52 (m, 4H, 2x(5, 5``-terpy)).

*5.4.3.7 Synthesis of 2,2':6',2''-terpyridine (4,4'-bis(4-pyridyl)biphenyl) palladium triflate [{Pd(terpy)}$_2$(bpbp)](CF$_3$SO$_3$)$_4$ (**5-7**).*

The complex (**5-7**) was obtained by the direct reaction of 4,4'-bis(4-pyridyl)biphenyl (25 mg, 0.085 mmol) in acetone with $[Pd(terpy)NCCH_3](CF_3SO_3)_2$ (100 mg, 0.147 mmol) in acetonitrile. The solution was stirred for 1 hour under a dinitrogen atmosphere. The product was precipitated from the solution by the addition of diethyl ether–acetone 3:1. Yield (46 mg, 34%). MALDI-TOF MS (RP; m/z): 246.39 $[C_{56}H_{38}F_{12}N_8O_{12}Pd_2S_4\text{-}4OTf]^{4+}$. ^{1}H NMR (400 MHz, CD_3CN) δ ppm: 9.01 (d, *J* = 5.8 Hz, 4H, 2x(2, 6-py)), 8.71 (t, *J* = 7.5 Hz, 2H, 2x(4`-terpy)), 8.45 (m, 12H, 2x(3, 4, 3`, 5`, 3``, 4``-terpy)), 7.99 (m, 4H, 2x(3, 5-py)), 7.79 (d, *J* = 5.7 Hz, 4H, 2x(6, 6``-terpy)), 7.53 (m, 4H, 2x(5, 5``-terpy)), 7.44 (m, 8H, 2x(8, 9, 11, 12-benzene)).

*5.4.3.8 Synthesis of 4,4',4''-tri-tert-butyl-2,2':6',2''-terpyridine (1,4-bis(4-pyridyl)benzene) palladium triflate [{Pd(tBu$_3$-terpy)}$_2$(bpb)](CF$_3$SO$_3$)$_4$ (**5-8**).*

The complex (**5-8**) was obtained by the direct reaction of 1,4-bis(4-pyridyl)benzene (16 mg, 0.069 mmol) in acetone with $[Pd(t\text{Bu}_3\text{-terpy})NCCH_3](CF_3SO_3)_2$ (100 mg, 0.118 mmol) in acetonitrile. The solution was stirred for 1 hour under a dinitrogen atmosphere. The product was precipitated from the solution by the addition of diethyl ether–acetone 3:1. Yield (70 mg, 55%). MALDI-TOF MS (RP; m/z): 311.98 $[C_{74}H_{82}F_{12}N_8O_{12}Pd_2S_4\text{-}4OTf]^{4+}$. ^{1}H NMR (400 MHz, CD_3CN) δ ppm: 9.03 (d, *J* = 6.5 Hz, 4H, 2x(2, 6-py)), 8.58

(m, 8H, 2x(3, 3`, 5`, 3``-*t*Bu$_3$-terpy), 8.77 (m, 4H, 2x(3, 5-py)), 7.99 (m, 4H, 2x(6, 6``-*t*Bu$_3$-terpy), 7.63 (m, 4H, 8, 9, 11, 12-benzene), 7.50 (m, 4H, 2x(5, 5``-*t*Bu$_3$-terpy), 1.55 (s, 18H, *t*Bu$_3$), 1.46 (s, 36H, *t*Bu$_3$).

*5.4.3.9 Synthesis of 4,4',4''-tri-tert-butyl-2,2':6',2''-terpyridine (4,4'-bis(4-pyridyl)biphenyl) palladium triflate [{Pd(tBu$_3$-terpy)}$_2$ (bpbp)](CF$_3$SO$_3$)$_4$ (**5-9**).*

The complex (**5-9**) was obtained by the direct reaction of 4,4'-bis(4-pyridyl)biphenyl (20 mg, 0.065 mmol) in acetone with [Pd(*t*Bu$_3$-terpy)NCCH$_3$](CF$_3$SO$_3$)$_2$ (100 mg, 0.118 mmol) in acetonitrile. The solution was stirred for 1 hour under a dinitrogen atmosphere. The product was precipitated from the solution by the addition of diethyl ether–acetone 3:1. Yield (53mg, 43%). MALDI-TOF MS (RP; m/z): 330.94 [$C_{80}H_{86}F_{12}N_8O_{12}Pd_2S_4$-4OTf]$^{4+}$. ^{1}H NMR (400 MHz, CD_3CN) δ ppm: 9.01 (d, *J* = 6.0 Hz, 4H, 2x(2, 6-py), 8.67 (m, 8H, 2x(3, 3`, 5`, 3``-*t*Bu$_3$-terpy), 8.32 (m, 4H, 2x(3, 5-py)), 8.10 (d, *J* = 6.2 Hz, 4H, 2x(6, 6``-*t*Bu$_3$-terpy), 7.41 (m, 8H, 2x(8, 9, 11, 12-benzene)), 7.49 (m, 4H, 2x(5, 5``-*t*Bu$_3$-terpy), 1.54 (s, 18H, *t*Bu$_3$), 1.47 (s, 36H, *t*Bu$_3$).

5.4.4 Synthesis of tetranuclear palladium terpyridine complex

*5.4.4.1 Synthesis of 2,2':6',2''-terpyridine (meso-tetra(4-pyridyl)porphyrin) palladium triflate [{Pd(terpy)}$_4$(H$_2$T(4-Py)P)](CF$_3$SO$_3$)$_8$ (**5-10**)*

The complex (**5-10**) was obtained by the direct reaction of *meso*-tetra(4-pyridyl)porphyrin (45 mg, 0.073 mmol) in acetone with [Pd(terpy)NCCH$_3$](CF$_3$SO$_3$)$_2$ (180 mg, 0.265 mmol) in acetonitrile. The solution was stirred for 1 hour under a dinitrogen atmosphere. The product was precipitated from the solution by the addition of diethyl ether–acetone 3:1. Yield (88 mg, 38%). MALDI-TOF MS (RP; m/z): 246.92 [$C_{108}H_{70}F_{24}N_{20}O_{24}Pd_4S_8$-8OTf]$^{8+}$. ^{1}H NMR (400 MHz, CD_3CN) δ ppm: 9.43 (m, 16H, 4x(2, 6-py), 4x(6, 6``-

terpy)), 8.82 (s, 4H, 4x(4`-terpy)), 8.52-8.25 (m, 40H, 4x(3, 4, 3`, 5`, 3``, 4``, 5, 5``-terpy), 4x(3, 5-py)), 7.95 (s, 8H, 4x(3, 5-pyrrole)), -2.86 (s, 2H, NH_2).

5.4.5 Crystal data

Crystal data for (**5-1**): $C_{44}H_{30}N_8O_{12}F_{12}S_4Pd_2$ (M =1431.80 g/mol): triclinic, space group P-1 (no. 2), a = 13.4651(6) Å, b = 14.2738(6) Å, c = 26.4571(11) Å, α = 92.127(3)°, β = 91.163(4)°, γ = 92.658(4)°, V = 5074.8(4) Å^3, Z = 4, T = 119.99(10) K, μ(CuKα) = 8.297 mm^{-1}, *Dcalc* = 1.874 g/cm^3, 38855 reflections measured (6.688° ≤ 2θ ≤ 149.486°), 20016 unique (R_{int} = 0.0394, R_{sigma} = 0.0443) which were used in all calculations. The final R_1 was 0.0264 (I > 2σ(I)) and wR_2 was 0.0384 with GOF = 0.809.

Crystal data for (**5-2**): $C_{50}H_{38}F_{12}N_{10}O_{12}Pd_2S_4$ (M + 2MeCN) (M =1539.94 g/mol): monoclinic, space group $P2_1/n$ (no. 14), a = 19.1642(9) Å, b = 8.0664(3) Å, c = 20.9733(11) Å, β = 110.372(6)°, V = 3039.4(3) Å^3, Z = 2, T = 120(2) K, μ(CuKα) = 6.985 mm^{-1}, *Dcalc* = 1.683 g/cm^3, 14951 reflections measured (7.736° ≤ 2θ ≤ 133.168°), 5358 unique (R_{int} = 0.0912, R_{sigma} = 0.0745) which were used in all calculations. The final R_1 was 0.1287 (I > 2σ(I)) and wR_2 was 0.1657 with GOF = 1.059.

Crystal data for (**5-3**): $C_{48}H_{36}F_{12}N_{12}O_{12}Pd_2S_4$ (M + 2MeCN) (M =1541.93 g/mol): monoclinic, space group $P2_1/n$ (no. 14), a = 19.465(6) Å, b = 8.0885(11) Å, c = 20.750(4) Å, β = 112.28(3)°, V = 3022.9(13) Å^3, Z = 2, T = 120(2) K, μ(CuKα) = 7.034 mm^{-1}, *Dcalc* = 1.694 g/cm^3, 19959 reflections measured (9.212° ≤ 2θ ≤ 133.2°), 5344 unique (R_{int} = 0.1081, R_{sigma} = 0.0882) which were used in all calculations. The final R_1 was 0.0671 (I > 2σ(I)) and wR_2 was 0.1901 with GOF = 1.722.

Crystal data for (**5-4**): $C_{55}H_{48}F_{12}N_{12}O_{12}Pd_2S_4$ (M =1638.09 g/mol): monoclinic, space group $P2_1/c$ (no. 14), a = 22.0500(12) Å, b = 18.2121(10) Å, c = 14.9606(11) Å, β = 103.756(7)°, V = 5835.5(6) Å^3, Z = 4, T = 120(2) K, μ(CuKα) = 7.331 mm^{-1}, *Dcalc* =

1.865 g/cm^3, 26886 reflections measured (7.784° ≤ 2θ ≤ 133.186°), 10290 unique (R_{int} = 0.0746, R_{sigma} = 0.0670) which were used in all calculations. The final R_1 was 0.1910 (I > 2σ(I)) and wR_2 was 0.2277 with GOF = 2.249.

Crystal data for (**5-5**): $C_{66}H_{50}F_{12}N_{12}O_{12}Pd_2S_4$ (M + 4MeCN) (M =1772.22 g/mol): triclinic, space group P-1 (no. 2), a = 8.0858(4) Å, b = 9.7570(5) Å, c = 23.4382(11) Å, α = 89.208(4)°, β = 85.321(4)°, γ = 69.914(5)°, V = 1730.65(15) Å^3, Z = 1, T = 120(2) K, μ(CuKα) = 6.237 mm^{-1}, *Dcalc* = 1.700 g/cm^3, 12838 reflections measured (7.57° ≤ 2θ ≤ 133.196°), 6126 unique (R_{int} = 0.0365, R_{sigma} = 0.0489) which were used in all calculations. The final R_1 was 0.0387 (I > 2σ(I)) and wR_2 was 0.0993 with GOF = 1.046.

Crystal data for (**5-6**): $C_{50}H_{34}N_8O_{12}F_{12}S_4Pd_2$ (M =1507.89 g/mol): monoclinic, space group $P2_1/c$ (no. 14), a = 13.4698(4) Å, b = 14.1350(3) Å, c = 15.5356(5) Å, β = 108.188(4)°, V = 2810.12(15) Å^3, Z = 2, T = 120.00(11) K, μ(CuKα) = 7.530 mm^{-1}, *Dcalc* = 1.782 g/cm^3, 12056 reflections measured (6.908° ≤ 2θ ≤ 147.144°), 5482 unique (R_{int} = 0.0280, R_{sigma} = 0.0323) which were used in all calculations. The final R_1 was 0.0893 (I > 2σ(I)) and wR_2 was 0.2764 with GOF = 1.275.

Crystal data for (**5-7**): $C_{58}H_{41}F_{12}N_9O_{12}Pd_2S_4$ (M + MeCN) (M =1625.04 g/mol): monoclinic, space group C2/c (no. 15), a = 68.113(6) Å, b = 8.8965(6) Å, c = 20.3855(15) Å, β = 96.903(7)°, V = 12263.4(16) Å^3, Z = 8, T = 120(2) K, μ(CuKα) = 6.961 mm^{-1}, *Dcalc* = 1.760 g/cm^3, 79463 reflections measured (7.844° ≤ 2θ ≤ 177.068°), 12971 unique (R_{int} = 0.4158, R_{sigma} = 0.2460) which were used in all calculations. The final R_1 was 0.1409 (I > 2σ(I)) and wR_2 was 0.4056 with GOF =1.083.

Crystal data for (**5-8**): $C_{74}H_{82}N_8O_{12}F_{12}Pd_2S_4$ (M =1844.51 g/mol): triclinic, space group P-1 (no. 2), a = 11.7222(3) Å, b = 12.2575(2) Å, c = 14.6339(4) Å, α = 85.268(2)°, β = 69.254(2)°, γ = 86.554(2)°, V = 1958.55(8) Å^3, Z = 1, T = 288(2) K, μ(CuKα) = 5.514

mm^{-1}, *Dcalc* = 1.564 g/cm^3, 15585 reflections measured (7.24° ≤ 2θ ≤ 147.2°), 7664 unique (R_{int} = 0.0341, R_{sigma} = 0.0391) which were used in all calculations. The final R_1 was 0.0529 (I > 2σ(I)) and wR_2 was 0.1623 with GOF = 1.319.

Crystal data for (**5-9**): $C_{84}H_{92}F_{16}N_{10}O_{16}Pd_2S_4$ (M + 2MeCN) (*M* =2132.82 g/mol): monoclinic, space group $P2_1/n$ (no. 14), *a* = 18.4010(12) Å, *b* = 9.8461(7) Å, *c* = 26.4085(15) Å, *β* = 96.274(6)°, *V* = 4756.0(5) $Å^3$, *Z* = 2, *T* = 120(2) K, μ(CuKα) = 4.641 mm^{-1}, *Dcalc* = 1.489 g/cm^3, 21652 reflections measured (9.594° ≤ 2θ ≤ 148.382°), 9321 unique (R_{int} = 0.0652, R_{sigma} = 0.0742) which were used in all calculations. The final R_1 was 0.1389 (I > 2σ(I)) and wR_2 was 0.3576 with GOF = 1.172.

Crystal data for (**5-10**): $C_{116}H_{82}F_{24}N_{24}O_{24}Pd_4S_8$ (M + 4MeCN) (*M* =3580.45 g/mol): triclinic, space group P-1 (no. 2), *a* = 11.6786(5) Å, *b* = 11.8782(5) Å, *c* = 25.2427(8) Å, *α* = 83.969(3)°, *β* = 77.874(3)°, *γ* = 85.130(3)°, *V* = 3397.5(2) $Å^3$, *Z* = 1, *T* = 120(2) K, μ(CuKα) = 6.374 mm^{-1}, *Dcalc* = 1.750 g/cm^3, 25744 reflections measured (7.5° ≤ 2θ ≤ 133.186°), 11969 unique (R_{int} = 0.0430, R_{sigma} = 0.0505) which were used in all calculations. The final R_1 was 0.0897 (I > 2σ(I)) and wR_2 was 0.2440 with GOF = 1.046.

5.5 References

1. S. Coşar, M. B. Janik, M. Flock, E. Freisinger, E. Farkas and B. Lippert, *Journal of the Chemical Society, Dalton Transactions*, 1999, 2329-2336.

2. H.-K. Yip, L.-K. Cheng, K.-K. Cheung and C.-M. Che, *Journal of the Chemical Society, Dalton Transactions*, 1993, 2933-2938.

3. J. A. Bailey, V. M. Miskowski and H. B. Gray, *Inorganic Chemistry*, 1993, **32**, 369-370.

4. J. A. Bailey, V. M. Miskowski and H. B. Gray, *Acta Crystallographica Section C: Crystal Structure Communications*, 1993, **49**, 793-796.

5. E. J. Ziolkowski, P. Turner and L. M. Rendina, *Inorganic Chemistry Communications*, 2006, **9**, 53-56.

6. K. M.-C. Wong, N. Zhu and V. W.-W. Yam, *Chemical Communications*, 2006, 3441-3443.

7. E. M. A. Ratilla, B. K. Scott, M. S. Moxness and N. M. Kostic, *Inorganic Chemistry*, 1990, **29**, 918-926.

8. V. W. W. Yam, K. M. C. Wong and N. Zhu, *Angewandte Chemie*, 2003, **115**, 1438-1441.

9. G. Lowe, A. S. Droz, T. Vilaivan, G. W. Weaver, L. Tweedale, J. M. Pratt, P. Rock, V. Yardley and S. L. Croft, *Journal of Medicinal Chemistry*, 1999, **42**, 999-1006.

10. G. Lowe, A.-S. Droz, J. J. Park and G. W. Weaver, *Bioorganic Chemistry*, 1999, **27**, 477-486.

11. G. Lowe, J. A. McCloskey, J. Ni and T. Vilaivan, *Bioorganic & Medicinal Chemistry*, 1996, **4**, 1007-1013.

12. A. J. Goshe and B. Bosnich, *Synthesis letter*, 2001, **2001**, 0941-0944.

13. A. J. Goshe, J. D. Crowley and B. Bosnich, *Helvetica Chimica Acta*, 2001, **84**, 2971-2985.

14. A. J. Goshe, I. M. Steele, C. Ceccarelli, A. L. Rheingold and B. Bosnich, *Proceedings of the National Academy of Sciences*, 2002, **99**, 4823-4829.

15. J. D. Crowley, A. J. Goshe and B. Bosnich, *Chemical Communications*, 2003, 2824-2825.

16. J. D. Crowley, A. J. Goshe and B. Bosnich, *Chemical Communications*, 2003, 392-393.

17. J. D. Crowley, I. M. Steele and B. Bosnich, *European Journal of Inorganic Chemistry*, 2005, **2005**, 3907-3917.

18. R. D. Sommer, A. L. Rheingold, A. J. Goshe and B. Bosnich, *Journal of the American Chemical Society*, 2001, **123**, 3940-3952.

19. A. Bray, D. Kelly, P. Mack, R. Martin and L. Wakelin, *Australian Journal of Chemistry*, 1990, **43**, 629-634.

20. W. D. McFadyen, L. P. Wakelin, I. A. Roos and V. A. Leopold, *Journal of Medicinal Chemistry*, 1985, **28**, 1113-1116.

21. N. J. Wheate, C. R. Brodie, J. G. Collins, S. Kemp and J. R. Aldrich-Wright, *Mini Reviews in Medicinal Chemistry*, 2007, **7**, 627-648.

22. H.-L. Chan, D.-L. Ma, M. Yang and C.-M. Che, *JBIC Journal of Biological Inorganic Chemistry*, 2003, **8**, 761-769.

23. H. L. Chan, D. L. Ma, M. Yang and C. M. Che, *ChemBioChem*, 2003, **4**, 62-68.

24. K. Biradha and M. Fujita, *Chemical Communications*, 2002, 1866-1867.

25. K. Biradha and M. Fujita, *Chemical Communications*, 2001, 15-16.

26. P. J. Steel, *Coordination Chemistry Reviews*, 1990, **106**, 227-265.

27. K. Biradha, Y. Hongo and M. Fujita, *Angewandte Chemie International Edition*, 2000, **39**, 3843-3845.

28. M. Fujita, H. Oka and K. Ogura, *Tetrahedron letters*, 1995, **36**, 5247-5250.

29. Q. Feng, M.-J. Yan, H.-H. Song and S.-K. Shi, *Inorganica Chimica Acta*, 2014, **415**, 75-80.

30. X. Chen, X. Zhang, L. Gao and H. Cui, *Inorganica Chimica Acta*, 2016, **441**, 34-41.

31. J. Zhang, J. Yang, X. Wang, H. Zhang, X. Chi, Q. Yang, Y. Chen and D. Xiao, *Inorganica Chimica Acta*, 2016, **447**, 66-76.

32. D. C. Onwudiwe, Y. B. Nthwane, A. C. Ekennia and E. Hosten, *Inorganica Chimica Acta*, 2016, **447**, 134-141.

33. W.-H. Huang, Y.-Y. Wang, Y.-N. Zhang, T. Liu, S.-Y. Liu, Y.-X. Wang, L.-Y. Pang, Y.-F. Kang and J. Li, *Inorganica Chimica Acta*, 2015, **433**, 52-62.

34. A. Saini, R. P. Sharma, S. Kumar, P. Venugopalan, P. Starynowicz and J. Jezierska, *Inorganica Chimica Acta*, 2015, **436**, 169-178.

35. R. Uhrecký, I. Svoboda, Z. Růžičková, M. Koman, Ľ. Dlháň, J. Pavlik, J. Moncol and R. Boča, *Inorganica Chimica Acta*, 2015, **425**, 134-144.

36. X.-Y. Dong, C.-D. Si, Y. Fan, D.-C. Hu, X.-Q. Yao, Y.-X. Yang and J.-C. Liu, *Crystal Growth & Design*, 2016, **16**, 2062-2073.

37. S. G. Thangavelu, R. J. Butcher and C. L. Cahill, *Crystal Growth & Design*, 2015, **15**, 3481-3492.

38. J.-X. Yang, Y.-Y. Qin, J.-K. Cheng and Y.-G. Yao, *Crystal Growth & Design*, 2014, **14**, 1047-1056.

39. L. Liu, C. Huang, X. Xue, M. Li, H. Hou and Y. Fan, *Crystal Growth & Design*, 2015, **15**, 4507-4517.

40. F.-L. Hu, W. Wu, P. Liang, Y.-Q. Gu, L.-G. Zhu, H. Wei and J.-P. Lang, *Crystal Growth & Design*, 2013, **13**, 5050-5061.

41. S. Sanram, J. Boonmak and S. Youngme, *Polyhedron*, 2016, **119**, 151-159.

42. B. W. Harper and J. R. Aldrich-Wright, *Dalton Transactions*, 2015, **44**, 87-96.

43. T. M. Pappenfus, J. R. Burney, K. A. McGee, G. G. Lee, L. R. Jarvis, D. P. Ekerholm, M. Farah, L. I. Smith, L. M. Hinkle and K. R. Mann, *Inorganica Chimica Acta*, 2010, **363**, 3214-3221.

44. N. Iranpoor, H. Firouzabadi, D. Khalili and S. Motevalli, *The Journal of Organic Chemistry*, 2008, **73**, 4882-4887.

45. C. B. Aakeröy, S. Panikkattu, B. DeHaven and J. Desper, *Crystal Engineering Communications*, 2013, **15**, 463-470.

46. C. Coudret and V. Mazenc, *Tetrahedron letters*, 1997, **38**, 5293-5296.

47. X. Cui, A. N. Khlobystov, X. Chen, D. H. Marsh, A. J. Blake, W. Lewis, N. R. Champness, C. J. Roberts and M. Schröder, *Chemistry-A European Journal*, 2009, **15**, 8861-8873.

48. J. C. Barnes, M. Juríček, N. L. Strutt, M. Frasconi, S. Sampath, M. A. Giesener, P. L. McGrier, C. J. Bruns, C. L. Stern and A. A. Sarjeant, *Journal of the American Chemical Society*, 2012, **135**, 183-192.

49. Y.-S. Su and C.-F. Chen, *Organic letters*, 2010, **12**, 1888-1891.

50. K. Sakai, M. Kurashima, N. Akiyama, N. Satoh, T. Kajiwara and T. Ito, *Acta Crystallographica Section C: Crystal Structure Communications*, 2003, **59**, m345-m349.

51. K. Uemura, K. Fukui, H. Nishikawa, S. Arai, K. Matsumoto and H. Oshio, *Angewandte Chemie International Edition*, 2005, **44**, 5459-5464.

52. Y. Liu, H.-J. Zhang, Y.-Q. Cai, H.-H. Wu, X.-L. Liu and Y. Lu, *Chemistry letters*, 2007, **36**, 848-849.

Chapter 6

Palladium 2-Phenyl-4,6-bis(2-pyridyl)-1,3,5-Triazine Complexes

6.1 Introduction

1,3,5-Triazine derivatives have found widespread applications as herbicides, drugs, catalysts or polymers [1-4]. A number of N-donor ligands involving the 1,3,5-triazine ring as the central building moiety have been used in supramolecular chemistry, both for their π· · ·π interaction capabilities and for their ability to be involved in hydrogen bond networks [5,6]. Much effort has been made to design and synthesise a wide range of multidentate ligands and their metal complexes. As described in previous Chapters, terpyridine is one of the most common ligands used in coordination chemistry. Different synthetic procedures have been developed to synthesise asymmetric tridentate ligands containing a central triazine ring instead of pyridyl ring.

1,3,5-Triazine derivatives can be 2,4,6-mono, di- or tri-substituted, symmetrical or nonsymmetrical compounds bearing different substituents. Sophisticated s-triazine derivatives can be synthesised from the inexpensive, readily available cyanuric chloride (2,4,6-trichloro-1,3,5-triazine) [7]. Each chloride atom of 2,4,6-trichloro-1,3,5-triazine can be substituted by nucleophiles (Figure 6.1).

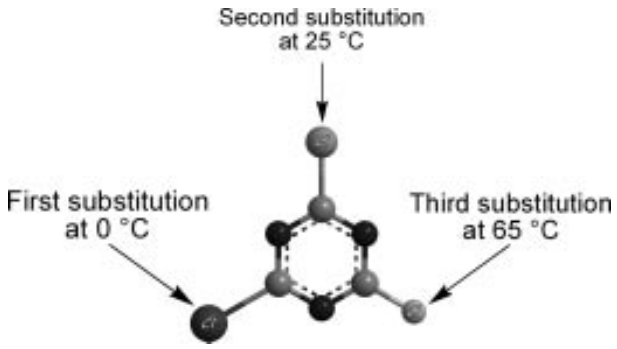


Figure 6.1: Differential reactivity 2,4,6-trichloro-1,3,5-triazine [7].

Because the first chloride substitution is exothermic, the reaction mixture must be cooled below room temperature. The second substitution can be functionalized at room temperature and the third substitution must be made at solvent reflux. Accordingly, by controlling the temperature of the reaction, 2,4,6-trisubstituted triazines can be prepared by sequential addition of different kinds of nucleophile (Figure 6.2) [8]. Many triazine derivatives have been synthesised following this synthetic procedure [9-11].

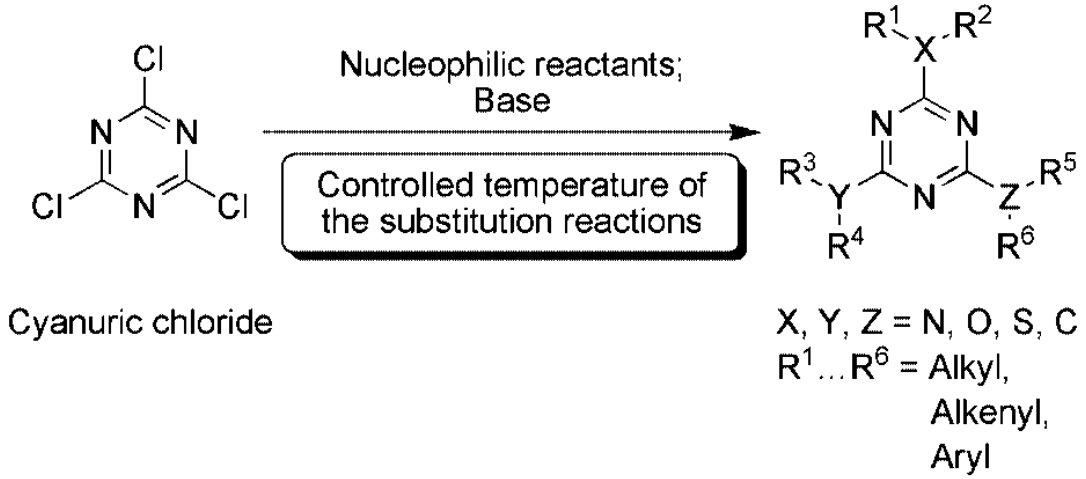


Figure 6.2: Synthesis multifunctional triazine derivatives [8].

6.1.1 Melamine derivatives as synthons for the preparation of H-bonded self-assemblies

Hydrogen bonds play an important role in supramolecular chemistry [12,13]. Whitesides and coworkers have found that melamine derivatives could be used to form remarkable aggregates [14-15]. The synthesis of H-bonded networks has been improved by using both substituted melamines and barbituric acids [15]. The reaction between 5,5-diethylbarbituric acid with 2-amino-4,6-(N-*p*-tolylamino)-1,3,5-triazine affords a linear tape (Figure 6.3 a).

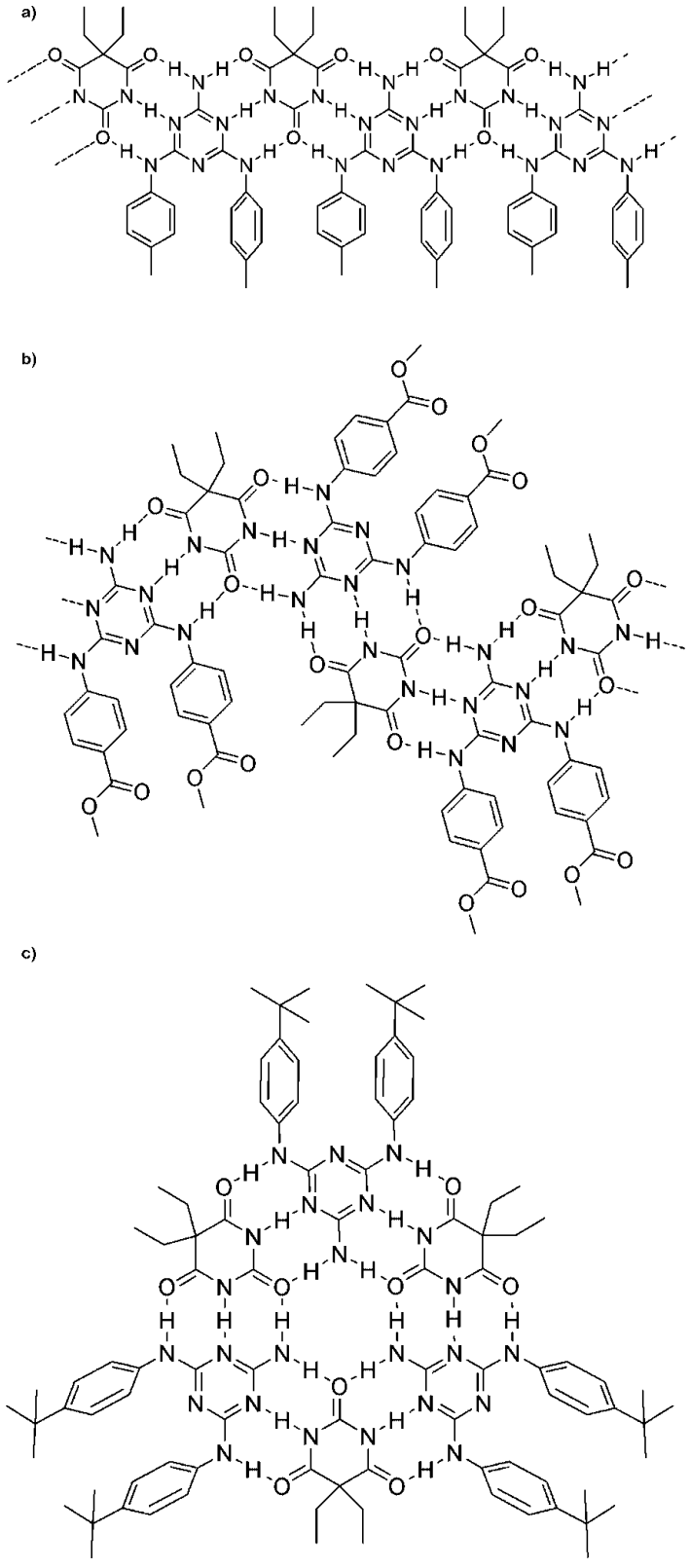


Figure 6.3: Structures of linear tape, crinkled tape, and rosette motifs [16].

However, when 2-amino-4,6-(N-p-methylbenzoatoamino)-1,3,5-triazine is reacted with 5,5- diethylbarbituric acid, a crinkled tape is achieved (Figure 6.3 b). Finally, with a bulkier substituent on the phenyl ring, i.e. *tert*-butyl, a rosette motif is obtained (Figure 6.3 c). It can be concluded that a small *para*-substituent such as a chloride or a methyl group leads to the formation of a linear tape. When the *para*-substituent is larger than a trifluoromethyl group, steric interactions between neighbouring melamines favours the crinkled motif to minimize hindrance. If this substituent is further increased, to a *tert*-butyl group for example, the steric interactions favour the rosette motif.

6.1.2 1,3,5-Triazine derivatives as ligands for the preparation of coordination self-assemblies

Over the last ten years, the interest in 1,3,5-triazine derivatives as ligands for coordination compounds has constantly grown [16-21]. This is undoubtedly due to the straightforward synthesis of polydentate ligands using simple and high-yielding reactions. 2,4,6-Tri(4-pyridyl)-1,3,5-triazine (tpt) has been exploited to obtain attractive supramolecular architectures (Figure 6.4) [22].

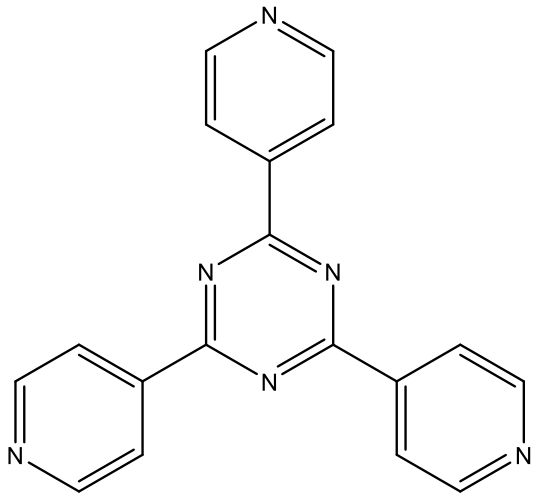


Figure 6.4: 2,4,6-Tri(4-pyridyl)-1,3,5-triazine (tpt).

An attractive system of an octahedral cage was described by Fujita and coworkers [23] (Figure 6.5). This system is based on tpt and palladium(II) nodes. This coordination cage can bind different organic guest molecules in its cavity [24-26].

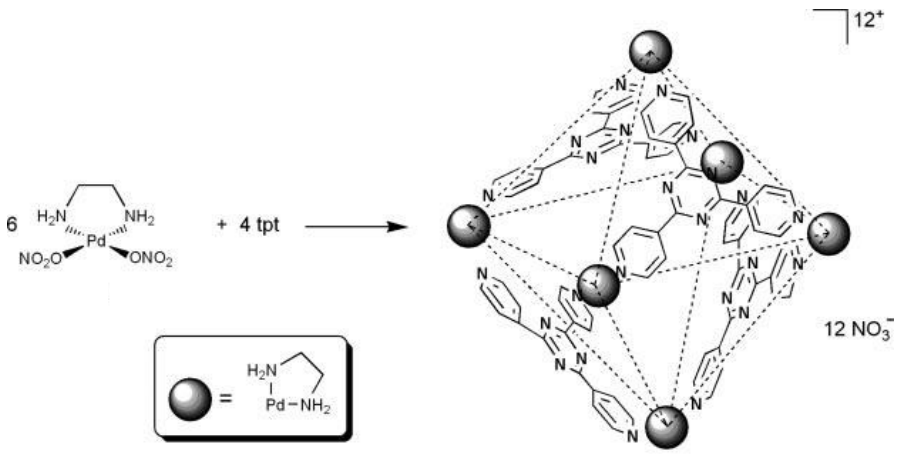


Figure 6.5: Self-assembly of an octahedral cage [23].

6.1.3 The 2-phenyl-4,6-bis(2-pyridyl)-1,3,5-triazine ligands

The tridentate N-donor ligands such as terpyridines and 1,3,5-triazine building blocks have an important role in transition metal complexation and supramolecular interactions. In 2002, Hanan and coworkers reported the synthesis of 2-phenyl-4,6-bis(2-pyridyl)-1,3,5-triazine (pbptz) [27]. 2-Phenyl-4,6-bis(2-pyridyl)-1,3,5-triazine is a polypyridyl ligand (Figure 6.6). It has received particular interest because of its straightforward synthesis, multiple coordination sites and large π systems for stabilization [28,29]. Moreover, the coplanarity of (pbptz), as opposed to the slight twist found between aromatic hydrocarbon rings in terpy analogues (4'-phenyl-terpy), could increase π-orbital overlap between the rings. With these particulars in mind, two complexes of (pbptz) with palladium (II) are reported in this chapter. The crystal structures of these two complexes with 4-cyanopyridine and 4-methyl pyridine co-ligands are discussed.

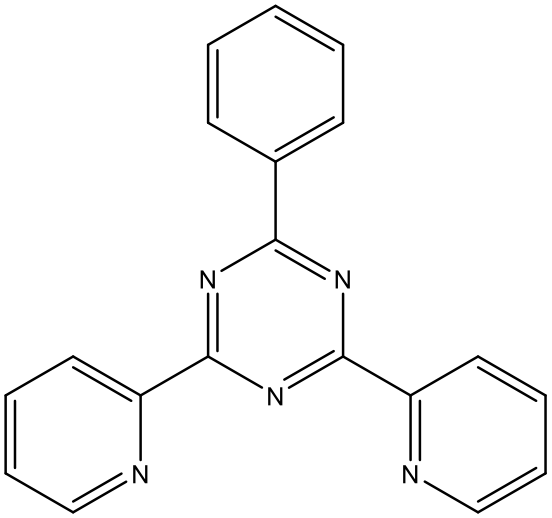
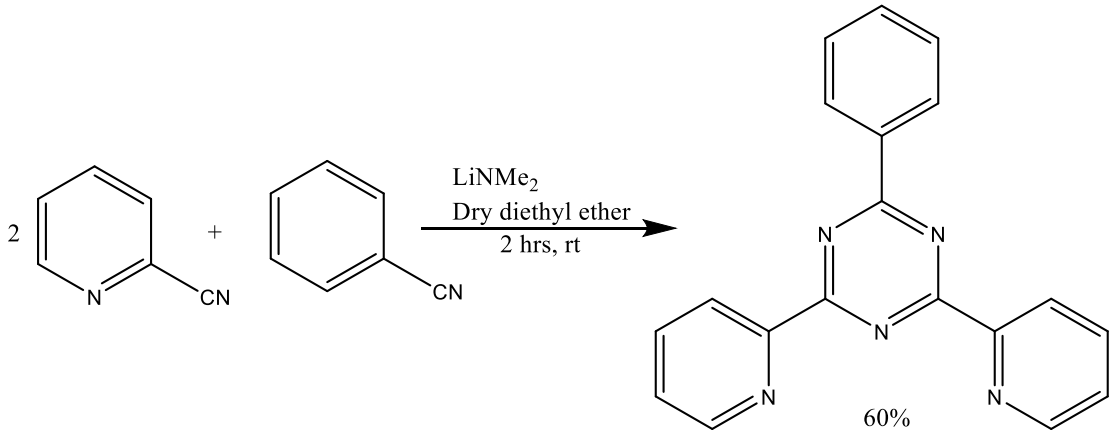


Figure 6.6: 2-Phenyl-4,6-bis(2-pyridyl)-1,3,5-triazine (pbptz).

6.2 Results and Discussion

6.2.1 Synthesis of 2-phenyl-4,6-bis(2-pyridyl)-1,3,5-triazine(pbptz).

(Pbptz) was synthesised according to the literature procedure [27]. The (pbptz) ligand consists of a triazine ring substituted with two 2-pyridyl rings and one unsubstituted phenyl ring. The reaction scheme for (pbptz) is shown below (Scheme 6.1).

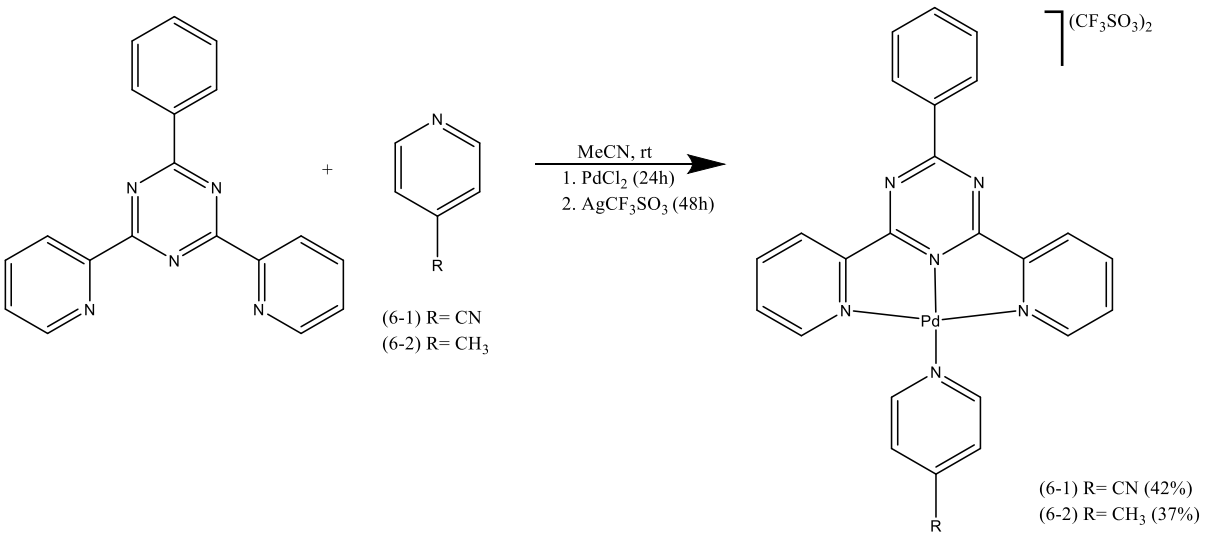


Scheme 6.1: The synthesis of 2-phenyl-4,6-bis(2-pyridyl)-1,3,5-triazine(pbptz).

Following this procedure, the target compound was obtained as a beige powder in a good yield (60%). It was characterised using standard techniques including NMR and mass spectroscopy.

6.2.2 Synthesis of palladium (2-phenyl-4,6-bis(2-pyridyl)-1,3,5-triazine) triflate complexes.

These complexes were prepared following the procedure used for Pd(terpy) analogues in previous Chapters. The reaction of one equivalent of pbptz with one equivalent of $PdCl_2$ in acetonitrile, followed by three equivalents of silver triflate and one equivalent of 4-substitiuted pyridine derivative resulted in the formation of the target palladium (2-phenyl-4,6-bis(2-pyridyl)-1,3,5-triazine) triflate complex (Scheme 6.2).



Scheme 6.2: The synthesis of palladium (2-phenyl-4,6-bis(2-pyridyl)-1,3,5-triazine) triflate complexes.

6.2.3 X-ray Crystallography

Single crystals suitable for X-ray diffraction were obtained for all of the complexes reported herein. Single crystals were grown by dissolution of the product in the minimum amount of acetonitrile and diffusion of diethyl ether vapour into this solution.

*6.2.3.1 Single crystal X-ray structure of 2-phenyl-1,4,6-bis(2-pyridyl)-1,3,5-triazine(4-cyanopyridine) palladium triflate [Pd(pbptz)(4-cyanopyridine)]$(CF_3SO_3)_2$ (**6-1**).*

Crystals of [Pd(pbptz)(4-cyanopyridine)]$(CF_3SO_3)_2$ were found to be colourless plates. The complex crystallises in the monoclinic space group $P2_1/c$. As shown in Figure 6.7, space above and below the Pd(pbptz) cation is occupied by two triflate anions and one water molecule. Similar to Pd(terpy) complexes, the triazine moiety is coordinated to palladium as a tridentate ligand and the fourth position is occupied by 4-cyanopyridine. The coordination geometry of the palladium ion is distorted slightly from that found in perfect square-planar Pd(II) complexes. Table 6.1 lists important bond lengths and angles for this complex. The angles between the adjacent nitrogen atoms in the plane (N2–Pd1–N1 = 79.45(11)° and N3–Pd1–N2 = 79.56(11)°) and N3-Pd1-N1 angle (159.01(10)°) are much smaller than those found in complexes (**2-1**) and (**3-1**). In (6-1), the Pd–N distance to the central nitrogen atom of the triazine is slightly longer than the analogous Pd–N distances in (**2-1**) and (**3-1**). Interestingly, the Pd–N distance to the central nitrogen atom of the triazine is shorter than the Pd–pyridyl distances. This is not expected as the triazine is a weaker donor than pyridyl leading to a longer Pd–N distance than the stronger pyridine donor. This complex does not follow the expected pattern due to the geometry of (pbptz) forcing the Pd–N distance to triazine ring to be the shortest. The

phenyl ring in (pbptz) is twisted by 5.68° relative to the central triazine ring. This complex shows higher distortion from an idealized square planar than (**2-1**) and (**3-1**). The most notable feature of the structure is the orientation of the 4-cyanopyridine ring with respect to the palladium square plane. The 4-cyanopyridine is twisted with respect to the coordination N4 donors forming a dihedral angle of 63.31(8)°. The dihedral angle indicates that 4-cyanopyridine in complex (**6-1**) is bent more than 4-cyanopyridine ligands in complexes (**2-1**) and (**3-1**), 84.04(7)° and 65.71(6)°, respectively.

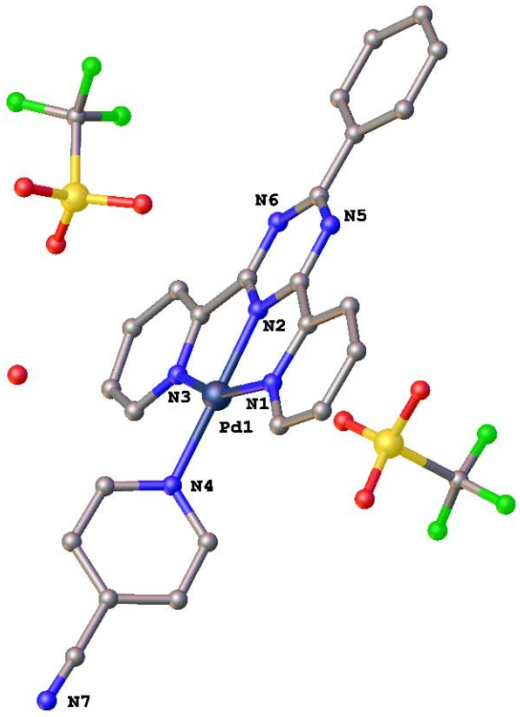


Figure 6.7: X-ray crystal structure of [Pd(pbptz)(4-cyanopyridine)]$(CF_3SO_3)_2$ with crystallographically independent atom numbering scheme. Hydrogen atoms have been omitted for clarity. Atom colours - C: grey, O: red, N: blue, Pd: navy F: green and S: yellow.

The tilt angle of complex (**6-1**) 178.08(11)° is slightly lower than those found in (**2-1**) and (**3-1**), 179.7(9)° and 179.5(2)°, respectively. Cations of (**6-1**) are more planar than those of

(**2-1**) and (**3-1**), with a maximum displacement of +0.085 and -0.041 Å exhibited by N6 and C4, respectively, from the mean plane.

Table 6.11: Selected bond lengths (Å) and angles (°) for [Pd(pbptz)(4-cyanopyridine)]$(CF_3SO_3)_2$.

Pd1-N1	2.064(3)	N2-Pd1-N1	79.45(11)
Pd1-N2	1.926(3)	N2-Pd1-N4	178.08(11)
Pd1-N3	2.065(3)	N3-Pd1-N1	159.01(10)
Pd1-N4	2.045(3)	N3-Pd1-N2	79.56(11)

Molecules of (**6-1**) pack in head to head conformation from the view along the *c*-axis. Molecules of (**6-1**) pack in channels running parallel to the *c*-axis, with two different channels for the triflate anions. One of the channels contains two triflate anions, while the other contains two triflate anions and two water molecules.

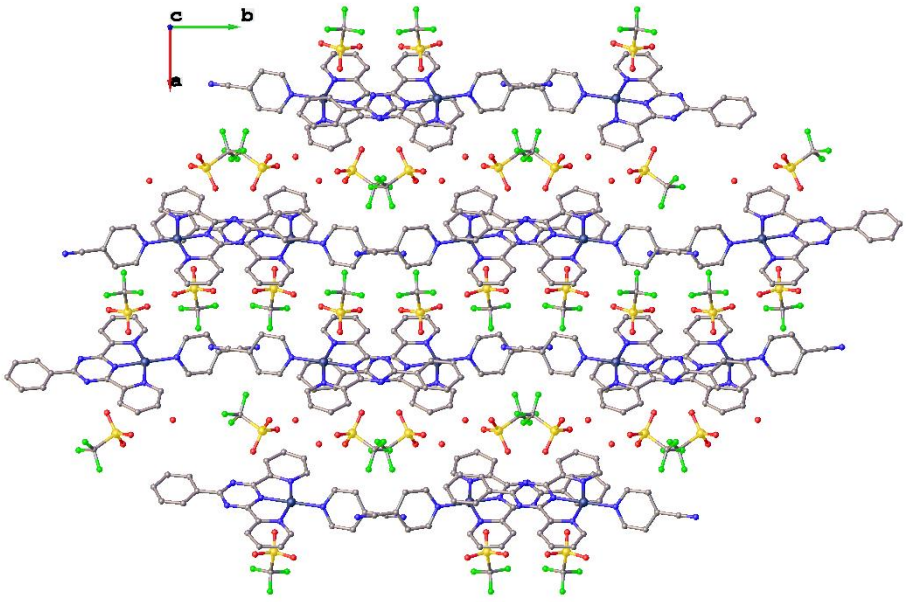


Figure 6.8: The packing diagram for [Pd(pbptz)(4-cyanopyridine)]$(CF_3SO_3)_2$ along the *c*-axis. Hydrogen atoms are omitted for clarity.

As shown in Figure 6.9, the molecules of (**6-1**) undergo a series of face-to-face π· · ·π interactions indicated by ring centroid–ring centroid separations of 3.641 and 3.636 Å (corresponding slip angles are 2.727 and 2.848°).

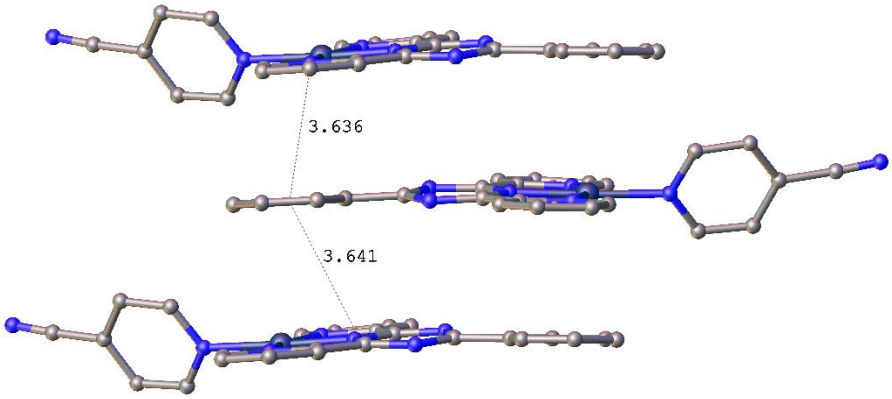


Figure 6.9: Representation of the π· · ·π interactions in [Pd(pbptz)(4-cyanopyridine)](CF_3SO_3)$_2$. Dashed lines indicate the presence of π· · ·π interactions.

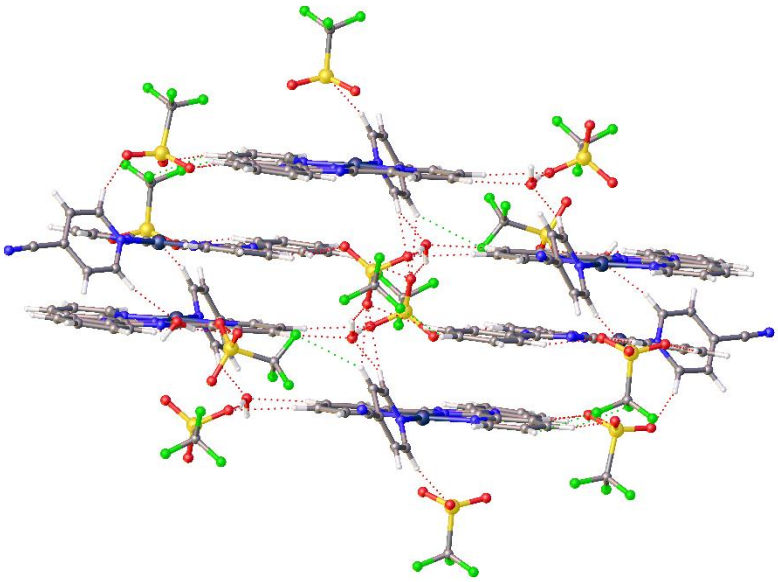


Figure 6.10: A net of hydrogen bonds links Pd(pbptz) cations, triflate anions and water molecules for [Pd(pbptz)(4-cyanopyridine)](CF_3SO_3)$_2$.

This arrangement is further stabilised by a series of hydrogen bonds between aromatic protons, water molecule and triflate anion (Figure 6.10). The C–H…O distances lie in the range 1.955 – 2.994 Å and the C–H…F distances lie in the range 2.714 – 2.879 Å. Interestingly, the cyano groups does not form any hydrogen bond, in contrast to (**2-1**) and (**3-1**).

*6.2.3.2 Single crystal X-ray structure of 2-phenyl-1,4,6-bis(2-pyridyl)-1,3,5-triazine(4-methylpyridine) palladium triflate [Pd(pbptz)(4-methylpyridine)]$(CF_3SO_3)_2$ (**6-2**).*

Crystals of [Pd(pbptz)(4-methylpyridine)]$(CF_3SO_3)_2$ were found to be colourless blocks. The complex crystallises in the monoclinic space group $P2_1/c$. As shown in Figure 6.11, space above and below the Pd(pbptz) cation is occupied by two triflate anions. The coordination geometry of the palladium ion is distorted slightly from that found in the perfect square-planar Pd(II) complexes. Table 6.2 lists important bond lengths and angles for this complex. The angles between the adjacent nitrogen atoms in the plane (N2–Pd1–N1 = 79.43(4) and N3–Pd1–N2 = 79.90(4)°) and N3-Pd1-N1 angle (159.32(6)°) are much smaller than those found in complexes (**2-2**) and (**3-2**). The Pd–N distance to the central nitrogen atom of the triazine is slightly longer than the analogous Pd–N distances in (**2-2**) and (**3-2**). The Pd–N distance to the central nitrogen atom of the triazine is shorter than the Pd–pyridyl distances. This point has already been discussed in more detail for [Pd(pbptz)(4-cyanopyridine)]$(CF_3SO_3)_2$. The phenyl ring in (pbptz) is twisted by 1.23° relative to the central triazine ring. The 4-methylpyridine is bent with respect to the coordination N4 donors forming a dihedral angle of 57.09(7)°. The dihedral angle indicates that 4-methylpyridine in complex (**6-2**) is twisted more than 4-methylpyridine ligand in complexes (**2-2**) and (**3-2**), 70.01(4)° and 61.92(11)°, respectively.

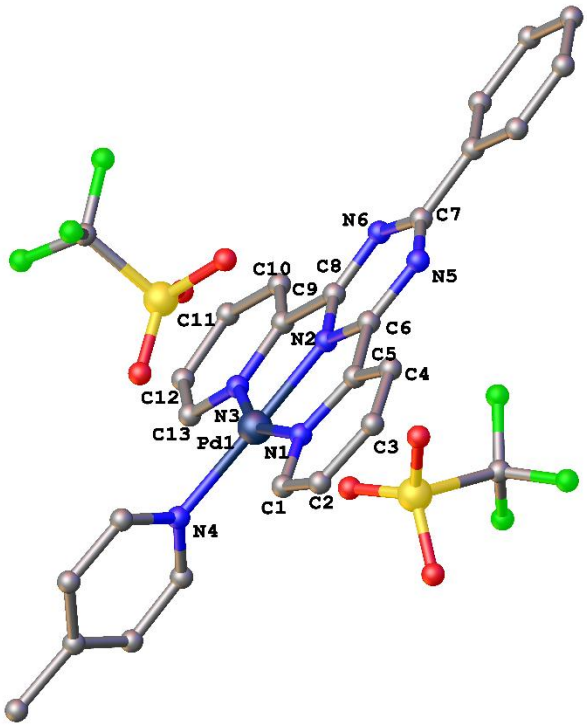


Figure 6.11: X-ray crystal structure of [Pd(pbptz)(4-methylpyridine)]$(CF_3SO_3)_2$ with crystallographically independent atom numbering scheme. Hydrogen atoms have been omitted for clarity. Atom colours - C: grey, O: red, N: blue, Pd: navy F: green and S: yellow.

Table 6.2: Selected bond lengths (Å) and angles (°) for [Pd(pbptz)(4-methylpyridine)]$(CF_3SO_3)_2$.

Pd1-N1	2.065(4)	N2-Pd1-N1	79.43(4)
Pd1-N2	1.908(4)	N2-Pd1-N4	178.72(4)
Pd1-N3	2.056(4)	N3-Pd1-N1	159.32(6)
Pd1-N4	2.018(4)	N3-Pd1-N2	79.90(4)

The tilt angle of complex (**6-2**) 178.72(4)° is slightly higher than that found in (**2-2**) and (**3-2**), 177.7(2)° and 178.0 (3)°, respectively. Cations of (**6-2**) are more planar than those of (**2-2**) and (**3-2**), with a maximum displacement of +0.027 and -0.031 Å exhibited by N2 and C9, respectively, from the mean plane.

In the solid state, the molecules of (**6-2**) are packed as shown in Figure 6.12, similar to that in the complex [Pt(terpy)(MeCN)][$(SbF_6)_2$] [30]. Complex (**6-2**) exhibits stacking of parallel sheets consisting of cations and anions.

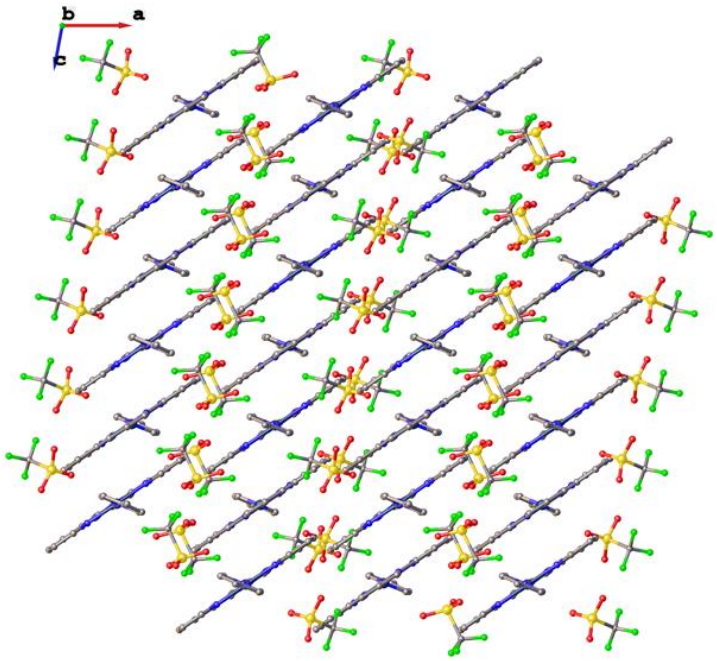


Figure 6.12: The packing diagram for [Pd(pbptz)(4-methylpyridine)]$(CF_3SO_3)_2$ along the *b*-axis. Hydrogen atoms are omitted for clarity.

As shown in Figure 6.13, the molecules of (**6-2**) undergo a series of face-to-face π· · ·π interactions indicated by ring centroid–ring centroid separations of 3.672 and 3.568 Å (corresponding slip angles are 0.565 and 2.045°, respectively). The slip angle is the angle between the ring planes.

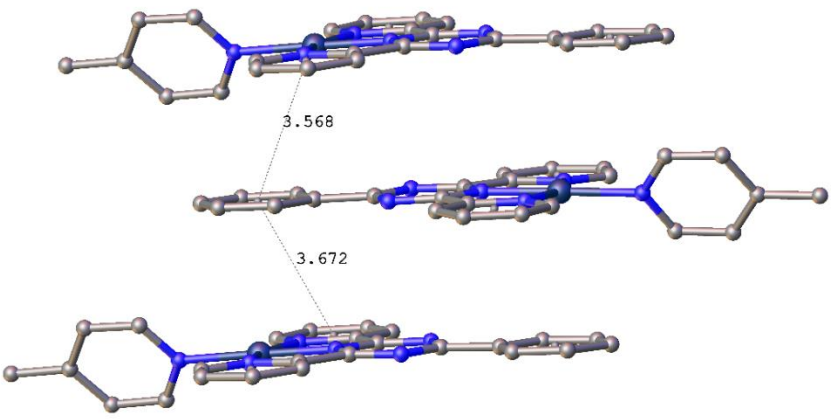


Figure 6.13: Representation of the π· · ·π interactions in [Pd(pbptz)(4-methylpyridine)](CF$_3$SO$_3$)$_2$. Dashed lines indicate the presence of π· · ·π interactions.

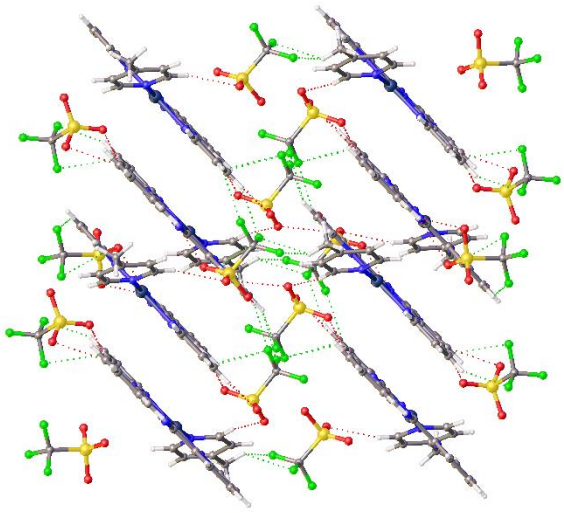


Figure 6.14: A net of hydrogen bonds links Pd(pbptz) cations and triflate anions for [Pd(pbptz)(4-methylpyridine)](CF$_3$SO$_3$)$_2$.

Within the crystal packing cations and anions are linked by a number of hydrogen bonds where the terpyridine acts as donor and triflate oxygen and fluorine atoms act as acceptor (Figure 6.14). The C–H…O distances lie in the range 2.326 – 2.971Å and the C–H…F distances lie in the range 2.358 – 2.959 Å.

6.3 Conclusions

The central pyridyl ring of terpyridine can be replaced by a triazine ring while maintaining a tridentate coordination mode. Two Pd(pbptz) complexes have been synthesised with two different *para*-substituted pyridine derivatives. It was possible to gain single crystal X-ray diffraction data for both complexes. They both crystallise in the monoclinic space group $P2_1/c$. Similar to terpyridine, triazine is coordinated to palladium as a tridentate ligand and no complex was seen to adopt and of the other potential binding modes for this ligand. The fourth position is occupied by 4-cyanopyridine (**6-1**) and 4-methylpyridine (**6-2**). The Pd atoms of each complex show distorted square planar geometries. Both complexes are similar to each other regarding their bond lengths and angles. The Pd-triazine distance is significantly shorter than either of the Pd-pyridyl distances, less than 2 Å. The *para*-substituted pyridine derivative is twisted significantly with respect to pbptz plane. The pbptz units in both complexes show small deviations from planarity, compared with Pd(tepry) analogues. The coplanarity of (pbptz) could increase π-orbital overlap between the rings. Both complexes indicate π· · ·π interactions between the terminal pyridine ring of one pbptz unit and the phenyl ring of another pbptz unit in the next layer with centroid–centroid separations 3.568 – 3.672 Å. As expected, Pd cations and triflate anions are involved in a net of hydrogen bonds.

Further investigation of the system can be done using different pyridine substitutions on triazine ring instead of phenyl ring to study the other potential binding modes for this ligand.

6.4 Materials and Methods

All chemicals and solvents were purchased from Alfa-Aesar, Fisher Scientific, VWR International or Sigma-Aldrich and were used as received without any further purification. Reactions sensitive to air and moisture were performed using a standard Schlenk line, with nitrogen as the inert atmosphere. Glassware used was flame dried under vacuum and backfilled with nitrogen. ^{1}H and 13C NMR spectra were recorded using either a Bruker AV(III)400, AV(III)500, AV400 or DPX400 machines at room temperature. Mass spectrometry was conducted using a Bruker Daltons Ultraflex MALDI- TOF with trans-2-[3-(4-*tert*,-butylphenyl)-2-methyl-2-propenylidene]-malononitrile as the matrix (m/z = 250.3).

Single crystal X-ray diffraction experiments were performed on an Oxford Diffraction SuperNova CCD area detector diffractometer at 120 K using monochromated Cu Kα radiation (λ = 1.54184 Å); on Agilent GV1000 AtlasS2 or TitanS2 CCD area detector diffractometers at 120 K using monochromated CuKα radiation (λ = 1.54184 Å); or at the UK Diamond Light Source I19-1 3-circle diffractometer (λ = 0.6889 Å). Absorption 202 corrections were applied using analytical numerical methods using CrysAlisPro software [31]. The structures were solved by direct methods using either SHELXS or SHELXT and refined with SHELXL using a least squares method [32-34]. In all instances, Olex2 software was used as the solution, refinement and analysis program [35].

6.4.1 Synthesis of 2-phenyl-4,6-bis(2-pyridyl)-1,3,5-triazine(pbptz)

2-Phenyl-4,6-bis(2-pyridyl)-1,3,5-triazine (pbptz) was synthesised according to a literature procedure [18]. Benzonitrile (0.4 mL, 3.90 mmol) was added to lithium dimethylamide (0.3 mL, 3.90 mmol) in dry diethyl ether (50 mL). The yellow suspension was stirred for 30 minutes under dinitrogen. 2-Cyanopyridine (800 mg, 7.70 mmol) was added. A dark

green precipitate formed rapidly and the resulting suspension was stirred for 2 hours. The precipitate was collected, suspended in water and acidified to *ca.* pH4. At this point, the majority of the solid dissolved and the undissolved solid was discarded. The aqueous solution was extracted with chloroform to afford a pale yellow solution. This solution was dried with Na_2SO_4, filtered and rotary evaporated to dryness. This afforded the target compound as a beige powder (730 mg, 60%). ESI-MS m/z 311 $[M]^+$, 334 $[M+Na]^+$. ^1H NMR (300 MHz, $CDCl_3$) δ ppm d=8.93 (d, *J* = 4.5 Hz, 2H, 6, 6``-py), 8.78 (m, 4H, 3, 3``-py, 2```, 6```-benzene), 7.92 (t, *J* = 7.5 Hz, 2H, 3```, 5```-benzene), 7.60 (t, *J* = 7.0 Hz, 1H, 4```-benzene), 7.56 (m, 4H, 4, 5, 4``, 5``-py). Elemental analysis calculated (%) for $C_{19}H_{13}N_5$: C 73.29, H 4.21, N 22.49; found: C 73.12, H 4.52, N 22.33.

6.4.2 Synthesis of 2-phenyl-1,4,6-bis(2-pyridyl)-1,3,5-triazine(4-cyanopyridine) palladium triflate complex [Pd(pbptz)(4-cyanopyridine)]$(CF_3SO_3)_2$.

A mixture of (pbptz) (97 mg, 0.311 mmol) and palladium chloride (50 mg, 0.282 mmol) in acetonitrile (20 mL) was stirred at room temperature for 24 h. Silver triflate (290 mg, 1.129 mmol) was added. In the absence of light, the mixture was stirred for 48 h. After 48 h, the white precipitate (AgCl) was filtered. 4-Cyanopyridine (29 mg, 0.279 mmol) was added to the reaction solution and stirred for 3 h. The resulting pink solution was concentrated *via* rotary evaporation to remove the excess acetonitrile solvent. The resulting pale yellow solid was washed with diethyl ether, before being dried in *vacuo*. Yield (96 mg, 42%). Single crystals suitable for X-ray diffraction were obtained by vapour diffusion of diethyl ether into an acetonitrile solution of [Pd(pbptz)(4-cyanopyridine)]$(CF_3SO_3)_2$. MALDI-TOF MS (RP; m/z): 260.85 $[C_{27}H_{17}F_6N_7O_6PdS_2\text{-}2OTf]^{2+}$. ^1H NMR (400 MHz, CD_3CN) δ ppm: 9.07 (m, 6H, 2,6-py, 3, 3``-py, 2```, 6```-benzene), 8.33 (t, *J* = 5.6 Hz, 2H, 4, 4``-py), 8.11 (m, 4H, 3```,5```-benzene, 3, 5-py), 7.93

(t, *J* = 5.6 Hz, 1H, 4```-benzene), 7.68 (d, *J* = 5.6 Hz, 2H, 6, 6``-py), 7.41 (m, 2H, 5, 5``-py).

6.4.3 Synthesis of 2-phenyl-1,4,6-bis(2-pyridyl)-1,3,5-triazine(4-mwthylpyridine) palladium triflate complex [Pd(pbptz)(4-methylpyridine)]$(CF_3SO_3)_2$.

A mixture of (pbptz) (97 mg, 0.311 mmol) and palladium chloride (50 mg, 0.282 mmol) in acetonitrile (20 mL) was stirred at room temperature for 24 h. Silver triflate (290 mg, 1.129 mmol) was added. In the absence of light, the mixture was stirred for 48 h. After 48 h, the white precipitate (AgCl) was filtered. 4-Methylpyridine (27 μL, 0.282 mmol) was added to the reaction solution and stirred for 3 h. The resulting pink solution was concentrated *via* rotary evaporation to remove the excess acetonitrile solvent. The resulting beige solid was washed with diethyl ether, before being dried in *vacuo*. Yield (84 mg, 37%). Single crystals suitable for X-ray diffraction were obtained by vapour diffusion of diethyl ether into an acetonitrile solution of [Pd(pbptz)(4-methylpyridine)]$(CF_3SO_3)_2$. MALDI-TOF MS (RP; m/z): 255.33 $[C_{27}H_{20}F_6N_6O_6PdS_2\text{-}OTf]^{2+}$. ^{1}H NMR (400 MHz, CD_3CN) δ ppm: 8.99 (d, *J* = 6.2 Hz, 2H, 2```, 6```-benzene), 8.83 (m, 4H, 3, 3``-py, 2, 6-py), 8.13 (m, 2H, 4, 4``-py), 7.87 (m, 3H, 3```, 4```, 5```-benzene), 7.77 (d, *J* = 6.3 Hz, 2H, 6, 6``-py), 7.45 (d, *J* = 6.3 Hz, 2H, 3, 5-py), 7.22 (m, 2H, 5, 5``-py), 2.57 (s, 3H, CH_3).

6.4.4 Crystal data

Crystal data for (**6-1**): $C_{27}H_{19}F_6N_7O_7PdS_2$ (M + H_2O) (*M* =838.01 g/mol): monoclinic, space group $P2_1/c$ (no. 14), *a* = 16.8047(3) Å, *b* = 18.4289(3) Å, *c* = 10.1500(2) Å, *β* = 99.066(2)°, *V* = 3104.11(10) Å^3, *Z* = 4, *T* = 120(2) K, μ(CuKα) = 6.947 mm^{-1}, *Dcalc* = 1.793 g/cm^3, 12963 reflections measured (7.168° ≤ 2θ ≤ 147.282°), 6087 unique (R_{int} = 0.0540, R_{sigma} = 0.0478) which were used in all calculations. The final R_1 was 0.0502 (I > 2σ(I)) and wR_2 was 0.1390 with GOF = 1.096.

Crystal data for (**6-2**): $C_{27}H_{20}N_6O_6F_6PdS_2$ (M =809.01 g/mol): monoclinic, space group $P2_1/c$ (no. 14), a = 16.1581(3) Å, b = 20.4665(4) Å, c = 9.2979(2) Å, β = 100.518(2)°, V = 3023.15(11) Å^3, Z = 4, T = 120(2) K, μ(CuKα) = 7.070 mm^{-1}, $Dcalc$ = 1.777 g/cm^3, 13559 reflections measured (7.044° ≤ 2θ ≤ 147.262°), 5920 unique (R_{int} = 0.0222, R_{sigma} = 0.0267) which were used in all calculations. The final R_1 was 0.1383 (I > 2σ(I)) and wR_2 was 0.2219 with GOF = 1.649.

6.5 References

1. S. Ronchi, D. Prosperi, F. Compostella and L. Panza, *Synlett*, 2004, **2004**, 1007-1010.

2. J. M. Oliva, M. Azenha, H. D. Burrows, R. Coimbra, J. S. Seixas de Melo, L. Canle, M. I. Fernàndez, J. A. Santaballa and L. Serrano Andrés, *ChemPhysChem*, 2005, **6**, 306-314.

3. X. P. Hu, H. L. Chen and Z. Zheng, *Advanced Synthesis & Catalysis*, 2005, **347**, 541-548.

4. L. M. Pedroso, M. M. C. Castro, P. Simões and A. Portugal, *Polymer*, 2005, **46**, 1766-1774.

5. B. F. Abrahams, S. R. Batten, H. Hamit, B. F. Hoskins and R. Robson, *Chemical Communications*, 1996, 1313-1314.

6. J. A. Zerkowski, C. T. Seto and G. M. Whitesides, *Journal of the American Chemical Society*, 1992, **114**, 5473-5475.

7. P. De Hoog, P. Gamez, W. L. Driessen and J. Reedijk, *Tetrahedron Letters*, 2002, **43**, 6783-6786.

8. P. Gamez and J. Reedijk, *European journal of Inorganic Chemistry*, 2006, **2006**, 29-42.

9. J. L. Silen, A. T. Lu, D. W. Solas, M. A. Gore, D. Maclean, N. H. Shah, J. M. Coffin, N. S. Bhinderwala,Y. W. Wang, K. T. Tsutsui, G. C. Look, D. A. Campbell, R. L. Hale, M. Navre and C. R. DelucaFlaherty, *Antimicrob. Agents Chemother.* 1998, **42**, 1447-1453.

10. T. Hayashi, A. Fujimoto, T. Kajiki, S.-i. Kondo and Y. Yano, *Chemistry Letters*, 2000, **29**, 1018-1019.

11. B. K. Saha, R. K. Jetti, L. S. Reddy, S. Aitipamula and A. Nangia, *Crystal Growth & Design*, 2005, **5**, 887-899.

12. G. A. Jeffrey and G. A. Jeffrey, *An Introduction to Hydrogen Bonding*, Oxford University Press New York, 1997.

13. C. R. Jeukens, P. Jonkheijm, F. J. Wijnen, J. C. Gielen, P. C. Christianen, A. P. Schenning, E. Meijer and J. C. Maan, *Journal of the American Chemical Society*, 2005, **127**, 8280-8281.

14. C. T. Seto and G. M. Whitesides, *Journal of the American Chemical Society*, 1990, **112**, 6409-6411.

15. G. Whiteside, J. Mathias and C. Seto, *Science*, 1991, **254**, 1312-1319.

16. R. Zibaseresht and R. M. Hartshorn, *Australian Journal of Chemistry*, 2005, **58**, 345-353.

17. R.N. Patel, N. Singh, K.K. Shukla, V.L.N. Gundla and U.K. Chauhan, *Spectrochimica Acta,* 2006, A63, 21-26.

18. M. I. Polson, E. A. Medlycott, G. S. Hanan, L. Mikelsons, N. J. Taylor, M. Watanabe, Y. Tanaka, F. Loiseau, R. Passalacqua and S. Campagna, *Chemistry-A European Journal*, 2004, **10**, 3640-3648.

19. Q.-D. Liu, W.-L. Jia, G. Wu and S. Wang, *Organometallics*, 2003, **22**, 3781-3791.

20. O. Ohmori, M. Kawano and M. Fujita, *Angewandte Chemie*, 2005, **117**, 1998-2000.

21. S. A. Barnett, A. J. Blake, N. R. Champness, J. E. Nicolson and C. Wilson, *Journal of the Chemical Society, Dalton Transactions*, 2001, 567-573.

22. G. J. Halder, S. M. Neville and C. J. Kepert, *Crystal Engineering Community*, 2005, 7, 266-268.

23. M. Fujita, D. Oguro, M. Miyazawa and H. Oka, *Nature*, 1995, **378**, 469.

24. T. Kusukawa and M. Fujita, *Journal of the American Chemical Society*, 2002, **124**, 13576-13582.

25. S. Tashiro, M. Tominaga, M. Kawano, B. Therrien, T. Ozeki and M. Fujita, *Journal of the American Chemical Society*, 2005, **127**, 4546-4547.

26. K. Nakabayashi, M. Kawano, M. Yoshizawa, S.-i. Ohkoshi and M. Fujita, *Journal of the American Chemical Society*, 2004, **126**, 16694-16695.

27. M. I. Polson, N. J. Taylor and G. S. Hanan, *Chemical Communications*, 2002, 1356-1357.

28. L. Zhang, X.-Q. Lü, Q. Zhang, C.-L. Chen and B.-S. Kang, *Transition Mmetal Chemistry*, 2005, **30**, 76-81.

29. P. Byers, G. Y. Chan, M. G. Drew, M. J. Hudson and C. Madic, *Polyhedron*, 1996, **15**, 2845-2849.

30. R. Büchner, J. S. Field, R. J. Haines, C. T. Cunningham and D. R. McMillin, *Inorganic Chemistry*, 1997, **36**, 3952-3956.

31. CrysAlisPro, *Agilent Technologies UK Ltd., Oxford, UK*, 2013.

32. G. M. Sheldrick, *Acta Crystallographica Section A: Foundations of Crystallography*, 2008, **64**, 112-122.

33. G. M. Sheldrick, *Acta Crystallographica Section A: Foundations and Advances*, 2015, **71**, 3-8.

34. G. M. Sheldrick, *Acta Crystallographica Section C: Structural Chemistry*, 2015, **71**, 3-8.

35. O. V. Dolomanov, L. J. Bourhis, R. J. Gildea, J. A. Howard and H. Puschmann, *Journal of Applied Crystallography*, 2009, **42**, 339-341.

Chapter 7

Conclusions

7.1 Conclusions

The chemistry of 2,2':6',2''-terpyridine (terpy) has been a topic of interest for many decades. The ability of (terpy) to chelate to a wide variety of metal ions has led to the synthesis of different metal-terpyridine complexes. The results illustrated within this thesis have gone some way towards exploring these complexes, as well as describing their crystal structures. The terpyridine molecule contains three nitrogen atoms and can therefore act as a tridentate ligand.

Firstly, the synthesis of a series of Pd(terpy) complexes with different *para*-substituted pyridine ligands was achieved in order to investigate the effect of the *para* substituents on the crystal structures. In addition, triflate ions ($CF_3SO_3^-$) were chosen as anions for the majority of complexes in this work, because they are ideal hydrogen bond acceptors. There are some examples using tetrafluoroborate (BF_4^-) and hexafluorophosphate (PF_6^-) instead of triflate anions, illustrating the influence of the anion on the crystal packing structure. In order to extend the experimental observations and the range of applicability of the proposed interpretation, another system involving the tridentate aromatic nitrogen donor 4,4',4''-tri-*tert*-butyl-2,2':6',2''-terpyridine (tBu$_3$-terpy) has been examined.

Chapter 4 was undertaken to extend the conclusions of the previous Chapters for substituted pyridines. To illustrate the influence of the pyridine ligands with different substitutions at *meta* position on the crystal structure, *meta*-substituted pyridine derivatives were used. A series of Pd(Yterpy) (Y = H or tBu$_3$) complexes have been synthesised using six *meta*-substituted pyridine derivatives.

The investigation was extended from mononuclear to dinuclear species. The *N,N*-bidentate ligands can be varied in length to give a wide range of Pd(terpy) complexes. All these ligands were chosen in order to systematically elucidate the role of the length, rigidity, flexibility and the coordination mode of ligands on the crystal structures of

Pd(terpy) complexes. For the purpose of comparison related dinuclear palladium(II) *t*Bu$_3$-terpy complexes have also been prepared. The reactivity of [Pd(terpy)(NCCH$_3$)](CF$_3$SO$_3$)$_2$ was investigated with a wide range of *N,N*-bidentate ligands. Substitution of the acetonitrile ligand of [Pd(terpy)(NCCH$_3$)](CF$_3$SO$_3$)$_2$ with these ligands was found to be efficient and facile with reactions occurring at room temperature. Extension of this reaction to *meso*-tetra(4-pyridyl)porphyrin results in a tetranuclear Pd(terpy) complex and affords [{Pd(terpy)}$_4$(H$_2$T(4-Py)P)](CF$_3$SO$_3$)$_8$.

The central pyridyl ring of terpyridine can be replaced by a triazine ring while maintaining a tridentate coordination mode. Two Pd(2-phenyl-4,6-bis(2-pyridyl)-1,3,5-triazine) complexes have also been synthesised with two different *para*-substituted pyridine derivatives.

In all complexes, the Pd cation adopts a distorted square planar geometry, due to the requirements of the terpyridine ligand. The bond lengths are comparable among the complexes. The bond angles exhibit the anticipated deviations from idealized geometry as are seen in Pd(terpy) and Pt(terpy) complexes. In general, the N–Pd–N bond angles within a given terpy moiety are directly tied to the Pd–N bond lengths with longer bond lengths resulting in more acute bond angles. Inspection of the body of crystallographic data for the complex cation structures reveals that the Pd–N bond to the central ring is shorter (average is 1.933(7) Å) than the Pd–N1 and Pd–N3 bonds (falling in the range of 2.097(17) – 1.970(2) Å). The distorted square planar geometry leads to a narrowing of *cis* N–M–N angles (falling in the range of 79.43(4) – 83.20(8)°). The N1–Pd–N3 bite angle ranges from 159.01(10) to 164.20(8)°. The N2–Pd–N4 tilt angle ranges from 172.13(13) to 179.70(9)°.

The asymmetric unit of the complexes (**2-3**), (**2-4**), (**2-5**), (**2-8**) and (**2-10**) contains a pair of crystallographically independent cations and four anions. All of the other mononuclear complexes have a complete molecule in the asymmetric unit, except [Pd(*t*Bu$_3$-terpy)(3-iodopyridine)](CF$_3$SO$_3$)$_2$ (**4-7**). Interestingly, this complex consists of one [Pd(*t*Bu$_3$-terpy)(3-iodopyridine)]$^{2+}$ and two [Pd(3-iodopyridine)$_4$]$^{2+}$ molecules with four triflate anions and one acetonitrile molecule. The two crystallographically independent [Pd(tetrakis(3-iodopyridine)$_4$]$^{2+}$ molecules contain inversion centres of symmetry at their Pd atom positions.

To illustrate the influence of the anion on the crystal packing structure, tetrafluoroborate and hexafluorophosphate were used instead of triflate in (**2-8**), (**2-9**) and (**2-10**). The importance of the anion is illustrated by differences between (**2-1**) and (**2-10**). The former complex packs in channels parallel to the *a*-axis and these channels of cations are separated from each other by channels of triflate anions. However, the cations of (**2-10**) form cavities which accommodate tetrafluoroborate anions and acetonitrile molecules. Analysis of packing in the crystal structure of (**2-9**) showed that the rows of cations are arranged in a zigzag architecture. Hexafluorophosphate occupied the channels between the cations. The presence of the two anions above and below Pd(terpy) unit hinders the two complex cations from coming into close proximity in the crystalline state. On the other hand, the cations of (**2-4**) have staggered orientation and the triflate anions fill the space between cations and the π· · ·π stacking distance between two terpyridine moieties of neighbouring molecules amounts to 3.907Å. Cations of complex (**2-8**) arrange in herringbone architecture and the cations of (**2-2**) pack in layers parallel to the *b*-axis. Both complexes undergo a series of face-to-face π· · ·π interactions.

Overall, there are no statistically significant differences in bond lengths and angles between any of the mononuclear complexes with *para*- or *meta*-substituted pyridine

derivatives reported in this work. The Pd(*t*Bu$_3$-terpy) complexes are less planar than the corresponding unsubstituted terpyridine analogues. In addition, the pyridine ligand in Pd(*t*Bu$_3$-terpy) complexes is bent more than that in unsubstituted terpyridine analogues. Molecules of Pd(*t*Bu$_3$-terpy) complexes pack in head to tail conformation to minimize the mutual repulsion between the sterically bulky *t*Bu$_3$-terpyridine moieties. As a consequence, the existence of the bulky *t*Bu$_3$ groups on the terpyridine moiety hinders the formation of such interactions.

In Chapter 5, the synthesis of a series of *N,N*-bidentate ligands is described. As expected, dinuclear complexes are similar to each other regarding their bond lengths and angles. All dinuclear complexes, except (**5-1**), (**5-4**) and (**5-7**), crystallise with half a molecule in the asymmetric unit. Complexes (**5-4**) and (**5-7**) have a complete molecule in the asymmetric unit. Complex (**5-1**) indicates the formation a three component discrete assembly consisting of three $[\{Pd(terpy)\}_2(4,4'\text{-bipy})]^{4+}$ with eight triflate anions. Two of Pd(terpy) complexes contain inversion centres of symmetry at their Pd atom positions. Similar to mononuclear Pd(*t*Bu$_3$-terpy) complexes, dinuclear Pd(*t*Bu$_3$-terpy) complexes are less planar than the corresponding unsubstituted terpyridine analogues. In addition, the *N,N*-bidentate ligand in Pd(*t*Bu$_3$-terpy) complexes is bent more than that in unsubstituted terpyridine analogues. In general, the bond lengths and angles in mono and dinuclear Pd(*t*Bu$_3$-terpy) complexes are largely unaffected by the electron rich *t*Bu$_3$-terpy moiety.

In Chapter 6, similarly to terpyridine, 2-phenyl-4,6-bis(2-pyridyl)-1,3,5-triazine (pbptz) is coordinated to palladium as a tridentate ligand and no complex was seen to adopt any of the other potential binding modes for this molecule. The Pd(pbptz) complexes are similar to mononuclear complexes reported in this work regarding their bond lengths and angles. The most notable feature of the structure is that the Pd-triazine distance is significantly shorter than either of the Pd-pyridyl distances, less than 2 Å. This was not expected

because the triazine is a weaker donor and it would be expected to show a longer Pd–N distance than the stronger pyridine donor. These complexes do not follow the expected pattern due to the geometry of pbptz forcing the Pd–N distance to triazine ring to be the shortest. The *para*-substituted pyridine derivative is bent significantly with respect to pbptz plane, compared with Pd(tepry) analogue. The pbptz units show small deviations from planarity, compared with Pd(tepry) analogues.

As expected, terpyridine moiety acts as a hydrogen bond donor and the anions act as hydrogen bond acceptors to form intermolecular hydrogen bonds. In addition, the pyridine ligands are involved in intermolecular hydrogen bonds. It has been found that C-H…F interactions can be as important as C-H…O and C-H…N hydrogen bonds in stabilizing crystal structures. These interactions have the characteristics of weak hydrogen bonds and they could be of utility in crystal design and engineering. In terms of π· · ·π interactions, the majority of Pd(tepry) complexes show π· · ·π interactions with acceptable centroid-centroid distance (< 4 Å and slip angle < 20°). On the other hand, all of Pd(*t*Bu$_3$-terpy) complexes do not exhibit π· · ·π interactions.

The importance of being be able to understand the influence of hydrogen bonding and π· · ·π interactions on the solid state will provide useful contributions to the field of crystal engineering by using hydrogen bonds and π· · ·π interactions as active design elements in the preparation of novel materials and extended aggregates in supramolecular chemistry.

To control structural assemblies of coordination complexes, it is important to synthesize a series of compounds of predetermined chemical structure, allowing for a comparison between assemblies with specific and controllable changes to their molecular structure. In this respect, a small change in the chemical structure of the ligand, even displacing the substituent position, can make a crucial role in controlling the supramolecular organization of molecular complexes.

While this thesis has demonstrated the synthesis of a series of Pd(terpy) complexes with different mono and dinuclear ligands, many opportunities for extending the scope of this thesis remain. The synthesis of multinuclear ligands combining three or four 2,2':6',2''-terpyridine metal-binding domains extends the area of coordination chemistry from the molecular to the supramolecular level. Several tri and tetranuclear ligands can be used to extend this work (Figure 7.1).

It is hoped that the findings presented within this thesis will prove valuable in expanding the field of coordination chemistry and in particular the use of square planar Pd(terpy) complexes.

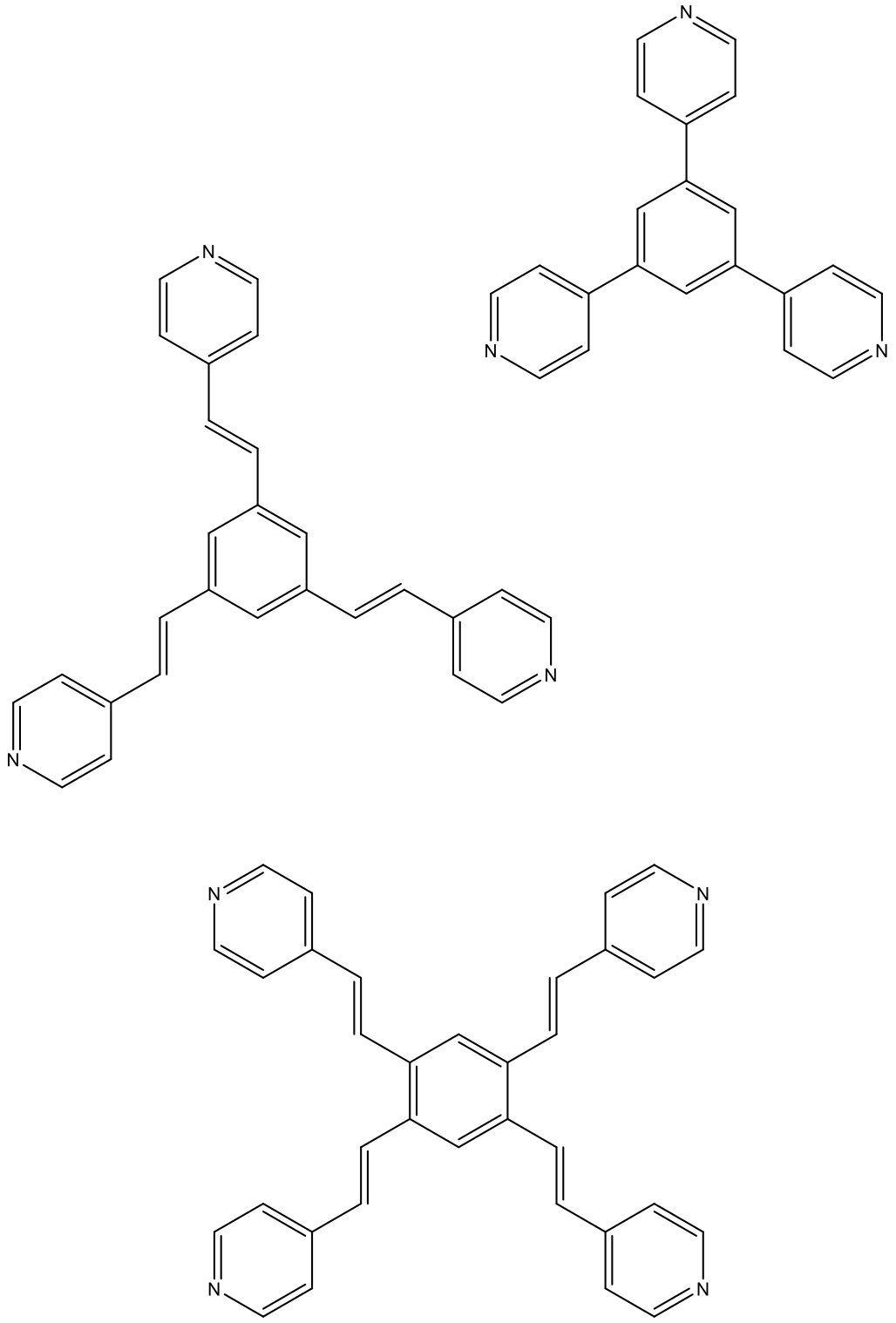


Figure 7.1: Tri and tetranuclear ligands can be used in future work.